Formulation and characterisation of conventional and 3-D printed mini-tablets and inserts for ocular use

AWIS SUKARNI BIN MOHMAD SABERE

A thesis submitted in partial fulfilment of the requirements for the degree of Doctor of Philosophy

School of Pharmacy | University College London

29 – 39 Brunswick Square

London WC1N 1AX

United Kingdom

2016

Declaration

This thesis presents my original research work conducted in the School of Pharmacy, University College London under guidance of Dr Susan Barker and Professor Duncan Craig. I declare that this work has not previously submitted and is not currently being submitted for any degree other than that of the degree of Doctor of Philosophy at the University College London. Wherever collaboration work are involved, every effort is made to indicate this clearly. I also certify that all work reported herein is that of the author with due reference to the literature or acknowledgement is made explicitly in the text.

_____ _____

Signature Date

“Those who strives shall succeed”

Abstract

This thesis describes a study into the formulation, manufacture and characterisation of mini-tablets and inserts for ocular use. Powder-based mini-tablets were formulated using the antibiotic chloramphenicol and a range of polymers. The effect of powder particle size on the quality of the products was investigated and was significant only for drug release from polyethylene oxide 8M mini-tablets. Transition temperature microscopy was used to assess drug distribution across the surface of the mini-tablets. Good contact of the nano-probe with the mini-tablet surface was the determining factor in the quality of the images created, with the residual particle shape after compaction playing a significant role.

A novel approach to the manufacture of mini-tablets using 3-D printing was investigated. The fused deposition modelling approach was unsuccessful due to the difficulty in producing extrudates of the required polymers. Stereolithography was used to prepare a range of formulations, with polyethylene glycol (PEG) diacrylate as the base material and phenylbis (2,4,6-trimethylbenzoyl) phosphine oxide as photoinitiator. The quality of the 3-D printed tablets was variable and dependent on the relative content of these two ingredients and the equipment settings. The 3-D printed mini-tablets showed a slow first-order drug release profile, which was increased by the inclusion of pore formers such as low molecular weight PEG.

The applicability of the stereolithography approach for 3-D printing of individualised ocular inserts was investigated. A cranial MRI scan of an adult male human was used, with permission, to generate a 3-D image of the eye, from which a personalised ocular insert was produced. A matching personalised flow-through dissolution chamber was constructed, in order to enable to assess the drug release profile from the

inserts. Similarly to the 3-D printed mini-tablets, the drug release followed a slow first-order profile, and was increased by the presence of pore formers in the insert.

Acknowledgements

With boundless love and appreciation, I would like to extend my heartfelt gratitude and appreciation to the people who help me bring this study into reality. I would like to extend my profound gratitude to the following:

My supervisor, Dr. Susan Anne Barker and Prof. Duncan Q.M. Craig whom expertise, consistent guidance, ample time spent and consistent advices that help me bring this study into success.

To my best friend, Juzaili Azizi, who have been by my side through thick and thin of my Ph.D journey. Without his moral support, this journey would be harder to traverse. Not to forget my fellow Ph.D friends, Goh Choon Fu, Muzamir Mahat, Norzawani Buang, Asyura Amdan, Fauzi Jalil, Hazeeq Azman and Khairunnisa Mohammed whom have been facing the same hurdle. The journey felt livelier when surrounding with friends whom understand your struggle.

To Prof. Steve Brocchini and Dr. Steve Hilton whom allow me to use their laboratories and giving their advices on my study. My sincere gratitude is extended to Dr. Matthew Penny who has been helping me with the 3D printing.

To my past and present colleagues whom have been helping me with my study, especially Dr. Fatima Pina, Dr. Chan Siok Yee and Dr. Jonathan Moffat.

Last but not least, my greatest gratitude and love to my family especially my parents, Mr. Mohmad Sabere Zakaria and Mrs. Ajar Saaid for their love, support and encouragement.

List of Contents

List of Figures

List of Tables

List of Abbreviations and Symbols

µ-TA	Micro-thermal analysis
3D	3 dimensions
AFM	Atomic force microscopy
BAPO	Phenylbis (2,4,6-trimethylbenzoyl) phosphine oxide
FDM	fused deposition modelling
HME	Hot melt extrusion
HPMC	Hydroxypropyl methylcellulose
LTA	Localised thermal analysis
MTDSC	Modulated temperature differential scanning calorimetry
Nano-TA	Nano-thermal analysis
PEG	Polyethylene glycol
PEGDA	Polyethylene glycol diacrylate
PEO	Polyethylene oxide
PVP	Polyvinylpyrrolidone
SD	Standard deviation
SEM	Scanning electron microscopy
SLA	stereolithography apparatus
SSF	Sodium stearyl fumarate
T_g	Glass transition temperature
TGA	Thermogravimetric analysis
T_m	Melting temperature
TTM	Transition temperature microscopy

Chapter 1

Introduction

Introduction

1.1 Overview

Ocular diseases have always been one of the common problems faced by patients around the world. However, relatively little research has been conducted into advanced ocular dosage forms, especially when compared to the amount of work expended on oral drug delivery. Most ocular treatments are still developed as liquids and applied as eye drops, thus accounting for 90% of the marketed ophthalmic formulations. This is because eye drops are easy to be administered and have reasonably good patient compliance (Patel et al., 2013a). However, eye drops are generally considered to be an ineffective dosage form, with a few major disadvantages such as the low ocular bioavailability of the drug due to fast drainage, reflex blinking and lacrimation (Patel et al., 2013a).

Although eye drops are still the most common ocular treatment, some novel and advanced dosage forms are being developed, which aim to deliver drugs for a longer period of time (extended release), which should enhance patient compliance by reducing administration frequency. Two possible formulation strategies that will be studied here are mini-tablets and inserts, which will be discussed later in the Chapter.

This Chapter will provide some context for the work conducted in this thesis. Initially, eye anatomy and common diseases will be considered. Following that, the manufacturing techniques used to prepare the formulations will be considered along with the analytical techniques to assess their characteristics and behaviour. Finally, the aims and objectives of the thesis will be presented.

1.1.1 Eye anatomy

In order to understand eye diseases, a knowledge of eye anatomy and functions is required. ***Figure 1.1*** shows the anatomy of human eye.

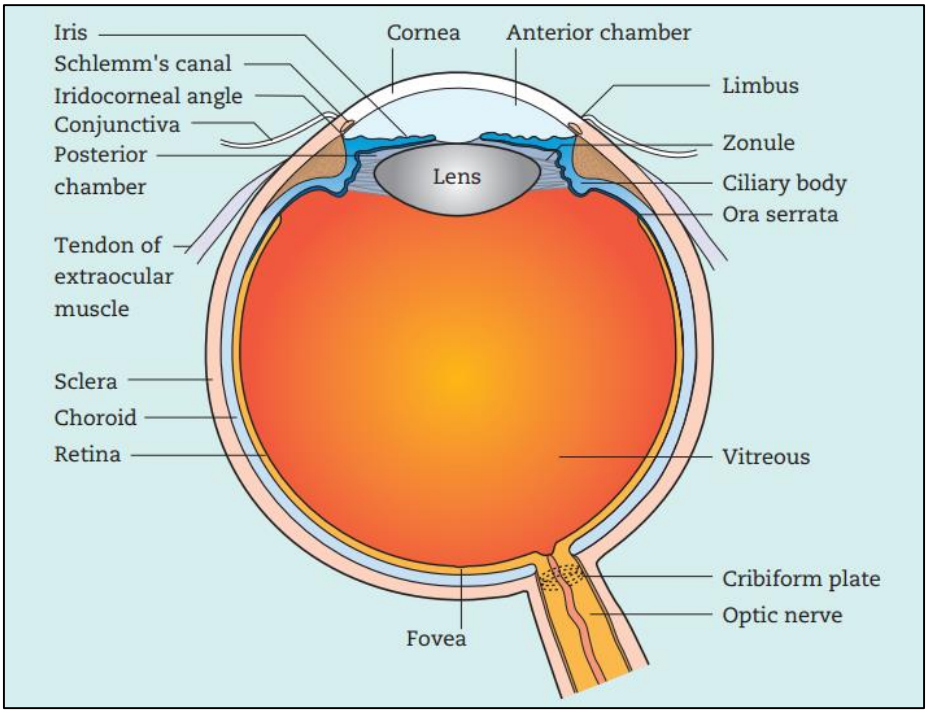

Figure 1.1 *Eye anatomy (James, 2012).*

The eye is generally regarding as being composed of two segments. The anterior segment is generally regarded as being everything forward from the lens and the posterior segment is regarded as being everything behind the lens. Within the anterior segment, there are two chambers, named the anterior and posterior chambers. The anterior is located between the cornea and the iris while the posterior is the small area between the iris, lens and ciliary body. Both chambers are filled with aqueous humour (James, 2012). This aqueous humour is partially responsible for maintaining the shape of the eyeball. It also has the functions of moisturising and providing nutrients to the anterior segment structures of the eye (Rawas-Qalaji and Williams, 2012). Meanwhile, vitreous humour (usually just called the vitreous) occupies the bulk of the posterior

segment of the eye between the lens and retina (James, 2012). The vitreous is composed of 99 % water and contains collagen fibrils and hyaluronan with a gel-like consistency (Batterbury et al., 2009). Its function is to provide physical stability to the eye, such as its function as a shock absorber, and ensure that the retina remains attached at the back of the eye.

The surrounding eye structures also comprises of three main layers which are fibrous, vascular and neural. The fibrous layer consists of the sclera and the cornea, the vascular layer consists of the choroid, the ciliary body and the iris, and neural layer consists of the retina. The sclera's functions are to give the shape of the eyeball, protect the internal structure of the eye and to provide a surface for the attachment of ocular muscles, while the cornea's function is refraction and transmission of light and protection against ingress of materials from the environment. Meanwhile, most of the eye's blood vessels are located in the vascular layer. This layer forms the blood-ocular barrier, which controls the movement of substances into the eye from the blood and vice versa. For the neural layer, the retina converts the focused light into nerve impulses and allows the individual to have sight (Rawas-Qalaji and Williams, 2012).

1.1.2 Ocular diseases

There are a large number of eye diseases in the world but only three of the common ocular diseases will be covered in this Chapter. The diseases are conjunctivitis, cataracts and glaucoma. Conjunctivitis is the most common ocular disease in the world. 15 % of ocular diseases diagnosed in United Kingdom were caused by allergic conjunctivitis, 5 % were caused by acute bacterial conjunctivitis and 20 to 30 % were caused by viral conjunctivitis (Wormald et al., 2003). Meanwhile, according to the National Eye Institute based in United States of America (USA), 2.7 million of Americans have glaucoma and another 24 million are affected by cataracts. These numbers are estimated to increase

up to 4.3 million and 38.7 million of Americans suffering from glaucoma and cataracts, respectively, by year 2030 (NEI, 2014).

1.1.2.1 Conjunctivitis

"Conjunctivitis" is defined simply as the inflammation of the conjunctiva and is usually as a result of surface infection of the conjunctiva. This then leads to dilatation of the superficial conjunctival blood vessel, resulting in hyperaemia and oedema of the conjunctiva with discharge (Leibowitz 2000), so the patient presents will a red eye and a sticky discharge. There are four different types of conjunctivitis: viral, bacterial, chlamydial and allergic conjunctivitis, as summarised in ***Table 1.1***. Conjunctivitis is treated via repeated topical applications of an anti-infective agent or an anti-allergic agent, generally applied in the form of eye drops.

Table 1.1 *Summary of four types of conjunctivitis diseases (Leibowitz 2000, James, 2012).*

Type	**Cause**	**Treatment**
Viral conjunctivitis	- Viral infection (adenovirus, Coxsackie, picornavirus).	- Self-limiting. - Topical antibiotic.
Bacterial conjunctivitis	- Bacterial infection (*Staphylococcus*, *Streptococcus*, *Pneumococcus*, *Haemophilus*).	- Self-limiting. - Topical antibiotic.
Chlamydial conjunctivitis	- *Chlamydia trachomatis.*	- Tetracycline. - Erythromycin. - Doxycycline. - Azithromycin. - Entropion (require surgical correction).

		- Trichiasis (require surgical correction).
Allergic conjunctivitis	- Pollen. - Animal dander. - Dust.	- Mast cell stabilisers (cromolyn sodium, loxodamide tromethamine, nedocromil). - Antihistamines (levocabastine hydrochloride, antazoline, pheniramine, olopatidine).

1.1.2.2 Cataracts

"Cataracts" is the term used when the lens suffers loss of clarity, which have a subsequent effect in the quality of vision. Cataracts normally occur in older patients and in this case are referred to as "age-related cataracts". However, cataracts can also be a consequence of other ocular or systemic diseases, such as trauma, uveitis, high myopia, topical medication and intraocular tumour, or inherited in an autosomal dominant fashion (Batterbury et al., 2009, James, 2012).

There are few symptoms that might indicate that the patient has cataracts, such as painless loss of vision, glare and a change in refraction. Cataracts also cause amblyopia, a failure of visual maturation, in the case of infantile cataracts. This happens because the retina is deprived of a formed image during the visual development stage (James, 2012). The only treatment currently available for cataracts is through surgery. However, a double-blind study performed by Olmedilla et al. (2003) for the period of 2 years on two dietary supplements (lutein and α-tocopherol) and placebo found that lutein supplement improved visual performance of patients with age-related cataracts. Cataracts are removed surgically, so there is no direct pharmaceutical treatment. However, post-operative antibiotic cover may be required and would be applied topically.

1.1.2.3 Glaucoma

Glaucoma is caused by the build-up of ocular pressure on the optic nerve head, which then damages the optic nerve (James, 2012). Glaucoma can be classified into four types: primary open angle, primary closed angle, secondary and congenital glaucoma. ***Table 1.2*** shows the difference between the glaucoma types. Glaucoma is treated via repeated topical applications of the appropriate agent, generally applied in the form of eye drops.

Table 1.2 *Summary of four types of glaucoma (James, 2012, Batterbury et al., 2009).*

Type	Symptom	Treatment
Primary open angle glaucoma	- Optic disc cupping. - Visual field loss. - Open anterior chamber angle. - Raised intraocular pressure.	- Topical (prostaglandin derivatives, beta-blockers, carbonic anhydrase inhibitors, alpha-agonists)
Primary closed angle glaucoma	- History of headache, blurring and coloured haloes around bright lights. - Unilateral visual loss, red eye, cloudy cornea and oval pupil.	- Systemic acetazolamide. - Topical pilocarpine. - Beta-blockers.
Secondary glaucoma	-May be open or closed angle glaucoma. - Causes are uveitis, aphakia, cataracts and retinal ischemia.	- Topical steroid.

Congenital glaucoma	- Buphthalmos (eye enlargement in infant).	- Surgical.

1.1.3 Conventional ocular drug delivery

Most ocular treatments used currently are liquids and applied as eye drops. However, there are a few other conventional ocular drug delivery systems used to treat ocular diseases, such as emulsions, ointments and suspensions. These conventional ocular drug delivery systems have their own advantages and disadvantages regarding their ease of application and the therapeutic levels of the drug achieved in the eye, as summarised in ***Table 1.3***.

Table 1.3 *Summary of advantages and disadvantages of conventional ocular drug delivery (Ghate and Edelhauser, 2006, Patel et al., 2013a).*

Ocular drug delivery system	Advantages	Disadvantages
Eye drops	- Easy to apply. - Reasonable patient compliance.	- Short precorneal residence time caused by rapid reflex blinking and increased tear secretion. - Most of the drug is removed through the lacrimal drainage system and some may be spilled onto the cheeks. - Repeated application necessary.
Emulsions	- Longer precorneal residence time.	- Causes blurred vision. - Difficulty in applying an exact

	- Sustained drug release.	dose.
Ointments	- Longer precorneal residence time. - Sustained drug release.	- Causes blurred vision. - Difficulty in applying an exact dose.
Suspensions	- Longer precorneal residence time. - Sustained drug release.	- Causes blurred vision. - Difficulty in applying an exact dose.

There are some serious issues with the current ocular formulations available for the treatment of the forward section of the eye, in that it is difficult with all formulations to know precisely what dose has been applied to the eye, because of the problems of drainage, etc. Although some improvements in retention time have been observed with making the formulations more viscous, up to the point of making an ointment, there is a consequent issue of blurred vision, which has an obvious impact on the patient's lifestyle. For anterior section treatment, implants and devices which target the drug to the back of the eye are not suitable, as the drug is delivered to the wrong site, so although a number of different devices are under development for posterior-section therapy, there are not applicable here. Hence there is a need for an improved formulation for topical treatment, which is easy to use, provides reproducible dosing, has a reliable drug release profile, preferably in a once-a-day manner. In this study, the utility of mini-tablets to provide such a formulation is investigated, with particular emphasis on the manufacturing issues concerned with this type of formulation.

1.2 Formulation and Manufacturing Processes

1.2.1 Tablets

Tablets are the most prominent pharmaceutical dosage form for drug delivery, occupying two-thirds of the global market for pharmaceutical products. They comprise a mixture of active pharmaceutical ingredients (API, drugs) and excipients, commonly pressed or compacted from a powder into a solid dose (Wu and Seville, 2009). Patients are very comfortable with taking tablets orally and they have the advantages of portability and stability, particularly when compared to liquid dosage forms.

The first tablet, which was described as a "compressed pill", was produced by William Brockeden in June 1844 (Anderson, 2005). The tablet was made by using the tablet press that he invented. The invention consisted of three parts: a base which had a central pillar with a concave upper surface, a collar that fitted over this and a punch that had a concave lower surface which fitted into the top of the collar, as shows in ***Figure 1.2***. The ingredients were placed in the space above the pillar and the punch then inserted and struck with a heavy hammer.

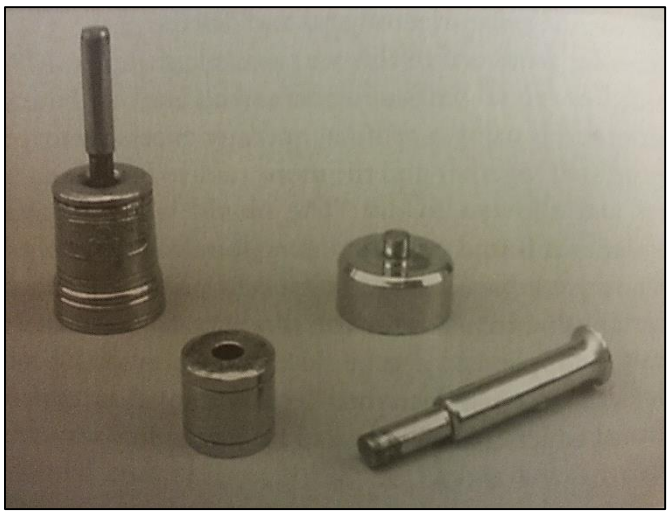

Figure 1.2 *The press patterned by William Brockeden (Anderson, 2005).*

Tablet manufacturing equipment has developed significantly since 1844, but still essentially uses the same approach of compression of a powder blend between two metal punches contained in a die.

The tabletting process is summarised in ***Figure 1.3*** below. The lower punch is fixed at a specific position in the die, leaving a void space, which is filled with the powder or granule. Pressure is applied by the punches - from the top punch only in the case of a single station press and from both punches in the case of a rotary multi-station tablet press. Pressure is removed as the top punch is lifted and then lower punch is raised to eject the tablet from the die. The weight of the tablet produced is governed by the initial position of the lower punch in the die, and the thickness and crushing strength are governed by the compression forces applied by the punches.

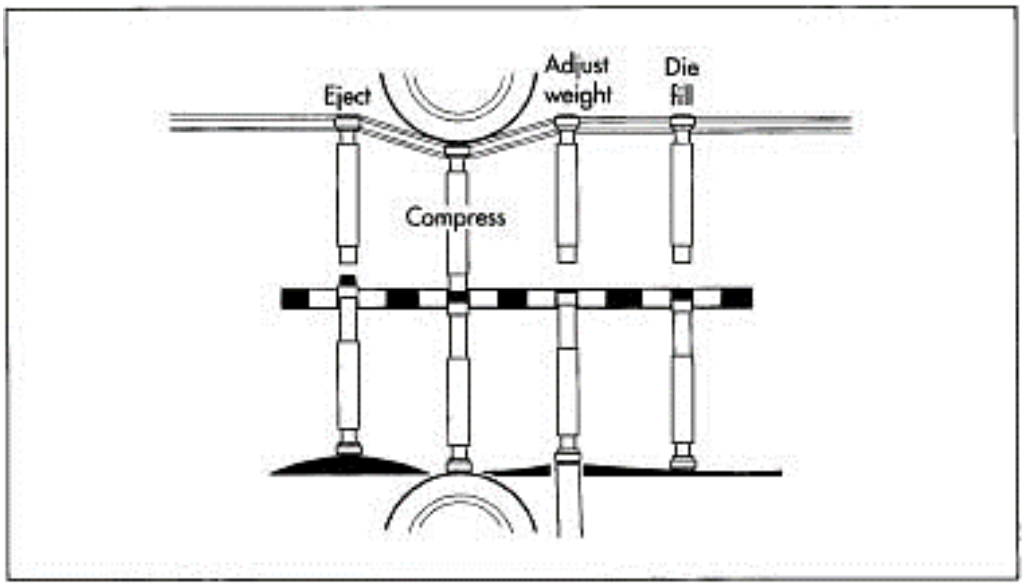

Figure 1.3 *A schematic diagram of the tabletting process.*

The quality of the powder that is used in the tabletting process is paramount. It must be adequately mixed, not subject to segregation and it must flow well to ensure that the tablets are of even weight, ensuring good content uniformity and a reproducible clinical

effect. The powder can be a simple direct mixture of ingredients or it can be processed first, most commonly by wet granulation.

Wet granulation involves the addition of a liquid (with or without binder) to the mixed powders, to form a wet mass (Agrawal and Naveen, 2011). The granulation fluid binds the powder particles into granules, with the intention of fixing the drug distribution and improves the flow characteristics of the product. Direct compression occurs when there is no wet granulation process first and the powders are simply mixed and granulated. This relies on the excipients flowing well and being compressible as they are, with no further treatment. However, direct compression offers the most expeditious method of manufacturing tablets because it required the least handling of materials, involves no drying step, and thus is the most energy-efficient method. It is also the fastest method of tablet production.

As time goes by, people are starting to be concerned about the size of tablets, especially for children. There are concerns and uncertainties about the age at which young children can safely swallow orally administered solids, such as conventional tablets and capsules (Nunn and Williams, 2005). As the result, mini-tablets have been proposed as a novel method to overcome those problems.

1.2.1.1 Mini-tablets

Conventional tablets are usually round and at least 7 mm in diameter, whilst mini-tablets are smaller with diameter equal or smaller than 2 to 3 mm (Lennartz and Mielck, 1998). These mini-tablets can be filled into hard gelatin capsules for the production of a sustained release multiple unit dosage form which has definite advantages over single unit dosage forms, such as lower risk of dose dumping, less inter- and intra- subject variability, high degree of dispersion in the digestive tract thus minimising the risks of

high local drug concentrations (Bechgaard and Nielsen, 1978, Follonier and Doelker, 1992).

Mini-tablets showed a few advantages compared to irregularly shaped units such as granules in subsequent coating steps. This is because mini-tablets can be coated reproducibly with less coating material compared to granules due to their constant surface area, smooth surface and high mechanical strength (Munday, 1994). Mini-tablets can also be an alternative for the pellets because they are easy to be manufactured, and the dimensions and weight of the mini-tablets with smooth surface can be controlled (De Brabander et al., 2000).

The preparation of mini-tablets is of rising importance in paediatrics due to new European regulatory requirements on products for paediatric use. Clinical studies have revealed that even children as young as 2 years old are able to swallow mini-tablets of 3 mm diameter (Thomson et al., 2009). Therefore, rational development of mini-tablets is of high importance with particular interest in robust mechanical properties and high drug loads.

Recently, Tissen et al. (2011) managed to prepare mini-tablets with a 1 mm diameter on a rotary tablet press using three model drugs of different compression characteristics: quinine hydrochloride, ibuprofen and spray-dried gentian extract. Depending on the individual drug substance, mini-tablets were produced by direct compression or after roll-compaction/dry granulation. They successfully produced 1 mm mini-tablets by direct compression (90% quinine hydrochloride; 90% dried gentian extract) and after roller compaction (70% ibuprofen).

Mini-tablets can either be filled into hard capsules or compacted into larger tablets. The

larger tablets will release the mini-tablets as multiple smaller individual dosage forms after disintegration. The development of multiple unit dosage forms that integrated into tablets is gaining attention compared to hard gelatin capsules because of the higher production costs of capsules (Ghebre-Selassie, 1994). Mini-tablets can maintain their structure and shape in a more reproducible way once they have been compressed into a tablet compared to normal pellets or granules. This is because of their size uniformity, regular shape, smooth surface, low porosity and high mechanical strength.

Lopes et al. (2006) have developed a biphasic oral delivery system by compressing mini-tablets into a tablet dosage form. The compressed mini-tablets showed slight deformation and no fragmentation. Because of their physical characteristics, mini-tablets tend to keep their integrity after compression, making the fracturing process of these subunits more difficult.

1.2.1.2 Ocular mini-tablets

Most of the treatments of eye involving the usage of drugs in liquid form. This is due to their easy administration. However, eye drops are considered to be a fairly primitive and ineffective dosage form with considerable disadvantages which are the low bioavailability of the eye drops due to fast drainage, reflex blinking and lacrimation. Since eye drops need to be applied frequently to maintain the therapeutic drug level, they may cause adverse effects. According to Arıcı et al. (2000), long-term use of eye drops leads to toxic side effects, cellular damage at the ocular surface and reduction in tear secretion function and it is irreversible. This is probably due to the preservatives that are used in the preparation of eye drops.

To enhance the amount of active substance reaching the target tissue or exerting a local effect in the fornix, the residence time of the drug in the tear film should be lengthened.

Various methods were investigated and developed to increase the drug bioavailability by prolonging the contact time between drug and corneal-conjunctival epithelium but most of them have disadvantages.

One of the strategies is to increase the viscosity of the vehicle by adding viscosity modifiers to the formulation. However, only a small improvement of the retention time of the drug in the fornix is usually observed (Ludwig and Van Ooteghem, 1992). Highly viscous gels and ointments on the other hand provided a sustained contact with the eye surface, but caused a sticky sensation and blurring of vision and induced reflex blinking due to their irritating properties (Sintzel et al., 1996).

A further approach to optimising ocular dosage forms was the implementation of the mucoadhesive concept. Interactions of suitable natural and synthetic polymers with mucins were evaluated (Saettone and Salminen, 1995). The use of films or inserts was proposed, to allow drug release over a long period of time. Inserts and collagen shields were very effective because of less frequent administration and absence of additives. On the contrary, insoluble inserts had to be removed manually, as they are not eliminated naturally.

To overcome these problems, ocular mini-tablets have been suggested to replace the function of eye drops. Recently, ocular ciprofloxacin-containing mini-tablets with diameter of 2 mm were developed and optimized, as shown in ***Figure 1.4*** (Weyenberg et al., 2003, Mortazavi et al., 2010).

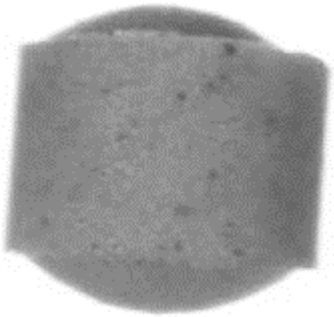

Figure 1.4 *2 mm diameter mini-tablets.*

The mini-tablet is placed in the fornix as showed in ***Figure 1.5***. After application of the mini-tablet, lacrimation occurred almost immediately. In time, the mini-tablet will be slowly dissolved and turn into viscoelastic gel that might cause blurred vision (Weyenberg et al., 2003). Compared with the use of films or inserts, there is no need to remove the mini-tablets as they will dissolve and be eliminated naturally.

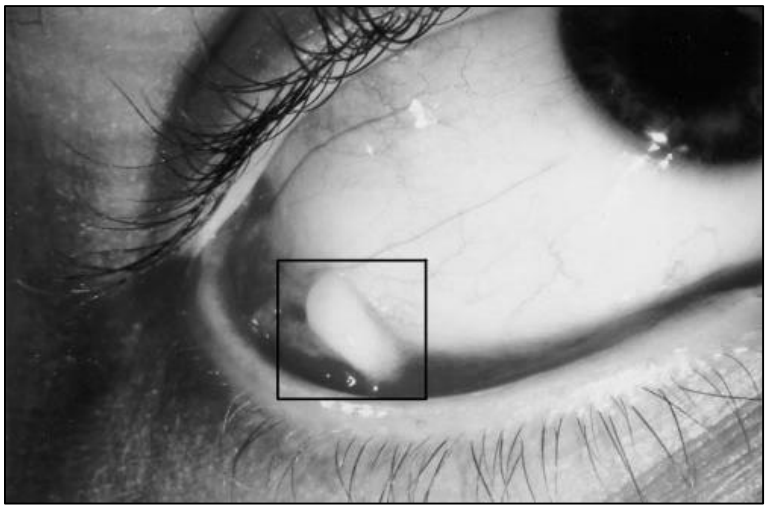

Figure 1.5 *Dissolved mini-tablets in the fornix (Weyenberg et al., 2004b).*

Since the formulation is intended for ocular use, it is important to sterilise the dosage form. In studies by Weyenberg et al. (2004a), two sterilisation techniques that are suitable for mini-tablets were compared, i.e. gamma-irradiation and dry heat sterilisation. They concluded that gamma-irradiation is the most suitable because the properties of

gamma-irradiated mini-tablets were the same as the non-sterilised tablets.

Meanwhile, El-Gawad et al. (2012) conducted a study on piroxicam-loaded ocular mini-tablets investigating the drug release profiles and the permeation across ocular membranes to distal sites. The *in-vitro* and *ex-vivo* permeation studies were conducted using Franz cells, with both biological and synthetic membranes, and porcine eyes, respectively. From the study, they concluded that mini-tablets, applied to the fornix area at the front of the eye, can be used to provide sustained delivery of the drug to posterior eye segments.

All the ocular mini-tablets manufactured in previous studies were made from combinations of biodegradable, water soluble and water insoluble excipients. However, none of the studies done using water soluble excipients only. Since the mini-tablets will be applied onto the eye, formulation using water soluble excipients only should be taken into consideration so the whole mini-tablets would dissolve after they come into contact with tears.

1.2.2 Hot Melt Extrusion

Hot melt extrusion (HME) is the process of applying heat and pressure to melt a polymer and force it through an orifice in a continuous process. This technique has been used widely in plastic, rubber and food industries since 1930s (Rauwendaal, 2001); whereas its application has only become popular in the pharmaceutical field in recent years. However, HME papers and patents issued worldwide for pharmaceutical systems have increased since early 1980s (Repka et al., 2008).

Generally, the extruders consist of single or twin rotating screw inside a stationary cylindrical barrel, as shows in ***Figure 1.6***. Single screw extruders are primarily used for

melting and conveying polymers to extrude them into continuous shapes, whereas twin screw extruders are used for melting and mixing polymers and for devolatilisation (Madan and Madan, 2012). Twin screw extruders may either be co-rotating or counter-rotating.

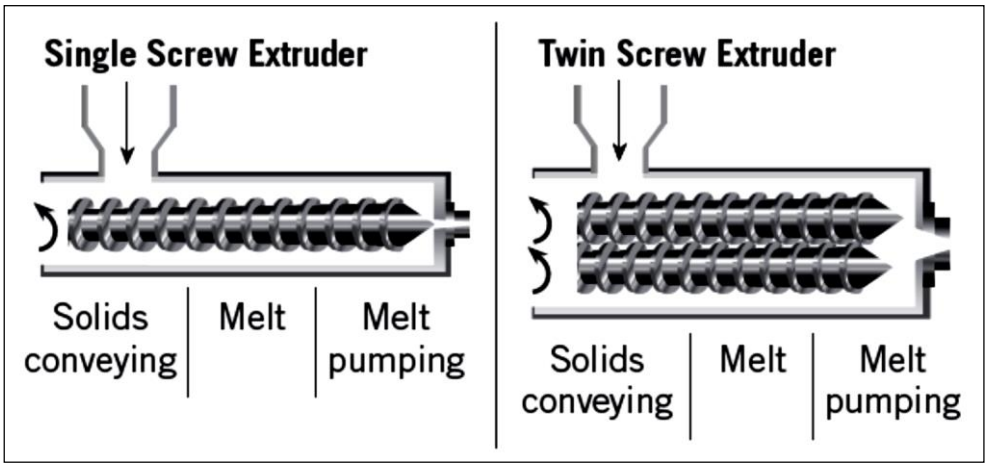

Figure 1.6 *Single and twin screw extruder barrel.*

The barrel is normally manufactured in sections, which are bolted or clamped together. A die is connected to the end of the barrel which will determines the shape of the extruded product (Chokshi and Zia, 2004). ***Figure 1.7*** shows a schematic diagram of HME twin screw process.

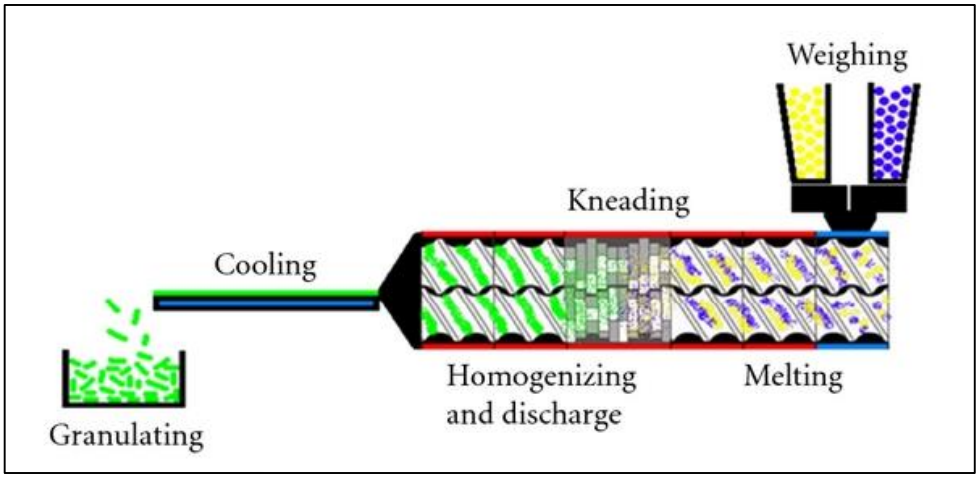

Figure 1.7 *Hot melt extrusion with twin screw process (Maniruzzaman et al., 2012).*

The polymers, with or without drug, are fed through a hopper and pumped through a die connected to the end of the barrel, by rotating screws under elevated temperature. Extruders provide extensive mixing and agitation that causes de-aggregation of the suspended particles in the molten polymer resulting in a uniform dispersion (Patel et al., 2013b).

Since the production of pharmaceutical formulations requires homogeneous and consistent mixing of multiple formulation ingredients, a twin screw is preferred as the rotation of the intermeshing screws provides better mixing to produce homogeneous solid containing finely dispersed API particles, or a solid-solution of API in polymer (Chokshi and Zia, 2004). HME offers several benefits over the conventional methods as well as some disadvantages which has been summarised in ***Table 1.4***.

Table 1.4 *Advantages and disadvantages of HME (Patel et al., 2010, Maniruzzaman et al., 2012).*

Advantage	**Disadvantage**
Increase solubility and bioavailability of water insoluble compounds.	Thermal process (drug/polymer stability).
Economic continuous process with fewer processing steps.	Flow properties of the polymer are essential to processing.
Solvent-free manufacture.	Limited number of available polymers.
High mixing efficiency which produce better content uniformity in extrudates.	
Short processing time.	
Easily controlled process parameters.	

1.2.3 3D Printing

3D-printing is a technique of making three dimensional objects from a digital file. The technique is becoming a popular research technology in pharmaceutical field, including research into tablet manufacturing (Khaled et al., 2014, Wang et al., 2016). The technique has generated interest within the pharmaceutical field because of its ability to fabricate and tailor drug delivery system accurately at a relatively low cost (Jonathan and Karim, 2016). Recently, the US Food and Drug Administration (FDA) approved the first 3D-printed tablets for the treatment of epilepsy (Szczerba, 2015). The FDA approval indicates the possibility of 3D-printing becoming one of the important manufacturing technique in pharmaceutical field.

The 3D-printing process starts with making the 3D design of the desired object. The 3D design is made using computer aided design (CAD) file using a 3D modelling application or software. There are a few free 3D modelling applications or software that are currently available such as Tinkercad, SketchUp Make, FreeCAD and many more. The 3D design can also be created using MRI image (Herrmann et al.) and 3D scanner (Arayici, 2007). The 3D design file created using those applications or software is saved in an .STL format and then uploaded to the 3D-printer for the printing process. There are several types of 3D-printer but the most commonly used are fused deposition modelling (FDM) and stereolithography apparatus (SLA) printers.

1.2.3.1 FDM printer

FDM printer is the most popular 3D-printer in the market because of its cheaper price and printing materials, compared to the SLA printers. This technique was developed and patented by Crump (1992) and commercialised in 1992 by Stratasys Inc. (Chua et al., 2003). A thermoplastic filament, such as polylactic acid (PLA) is commonly used in the printing process. The filament is heated to its melting point to extrude the filament and

ejected through the nozzle attached to the extruder. The nozzle moves in both the horizontal and vertical directions while laying down the molten filament layer by layer, to create the 3D object.

A few studies have been performed integrating FDM printing with HME. HME was used to extrude the polymer which was then used as a filament with the FDM printer (Sandler et al., 2014, Goyanes et al., 2015).

1.2.3.2 SLA printer

The SLA technique is the oldest 3D-printing technique, developed and patented by (Hull, 1986). The manufacturing of the object is based on the solidification of a liquid resin by photopolymerisation, also known as the curing process. Photopolymerisation is a process in which light initiates a chain reaction, causing monomers to form polymers. A laser is used to cure the photopolymer while shaping it into an object.

Wang et al. (2016) successfully printed tablets for oral modified-release dosage form using different grades of polyethylene glycol diacetate (PEGDA) with paracetamol and 4-amino-salicylic acid. SLA printing was also used to manufacture scaffolds for multicellular tissue (Ovsianikov et al., 2010) and aortic valve (Hockaday et al., 2012).

1.3 Analytical Techniques Used In The Study

1.3.1 Dynamic Vapour Sorption

Dynamic vapour sorption (DVS) is a gravimetric technique for measuring the rate and amount of solvent absorbed by a sample, which is crucial information in the pharmaceutical field. For pharmaceutical materials, such as excipients, drug formulations and packaging films, the propensity for absorbing moisture is recognised as a critical factor in determining their storage, stability, processing and application performance (Buckton and Darcy, 1995, Bley et al., 2009).

The DVS analyser is based on a vertical nulling microbalance in which the sample and a reference are suspended from the weighing mechanism. The humidity level of the chamber is then manipulated and the change in mass is measured. ***Figure 1.8*** showed the schematic diagram of DVS.

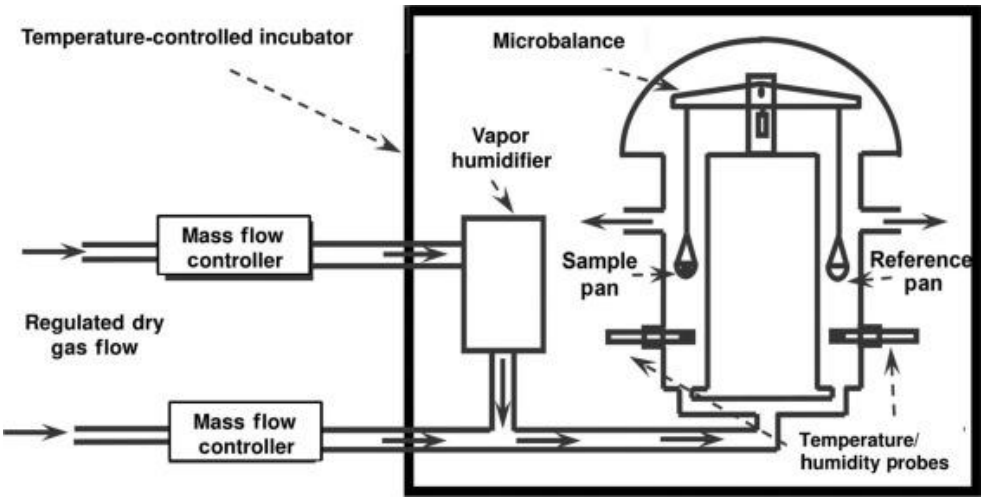

Figure 1.8 *Schematic diagram of DVS (Sheokand et al., 2014).*

1.3.2 Thermogravimetric Analysis

Thermogravimetric analysis (TGA) is one of the most common techniques used in thermal analysis, whereby changes in mass are used to determine the chemical and

physical process that happen during a reactant heating process (Craig and Reading, 2006). This technique can be applied in the pharmaceutical field to determine dehydration, water content, chemical decomposition, thermal stability and lifetime of materials (Gaisford et al., 2016, Yee, 2013).

Null-point balances are the typical type of mechanism in most of the TGA instruments. These often consist of an electromagnetically beam carrying sample and countermass which is suspended from the coil of galvanometer (Gaisford et al., 2016). An attached shutter that interrupts a light beam focused on a photocell will detect the beam movement whereby imbalance is detected. ***Figure 1.9*** summarised the TGA mechanism schematically.

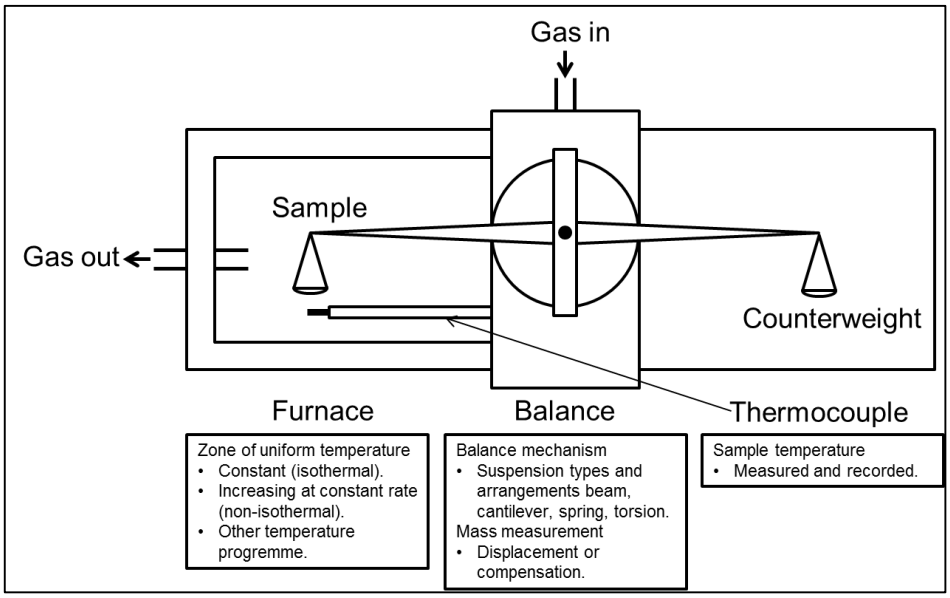

Figure 1.9 *Schematic diagram of a thermobalance (Gaisford et al., 2016; Craig and Reading, 2007).*

1.3.3 Differential Scanning Calorimetry

Differential scanning calorimetry (DSC) is the most widely used method of thermal analysis within the pharmaceutical field. It is a thermoanalytical technique in which the

difference in the amount of heat required to increase the temperature of a sample and reference is measured as a function of temperature. The technique usually involves a linear heating or cooling signal applied to the sample and the subsequent measurement of the temperature and the energy associated with a range of thermal events, such as the melting, crystallisation, glass transition and decomposition reactions (Craig and Reading, 2006). ***Figure 1.10*** shows a schematic diagram of a DSC cell.

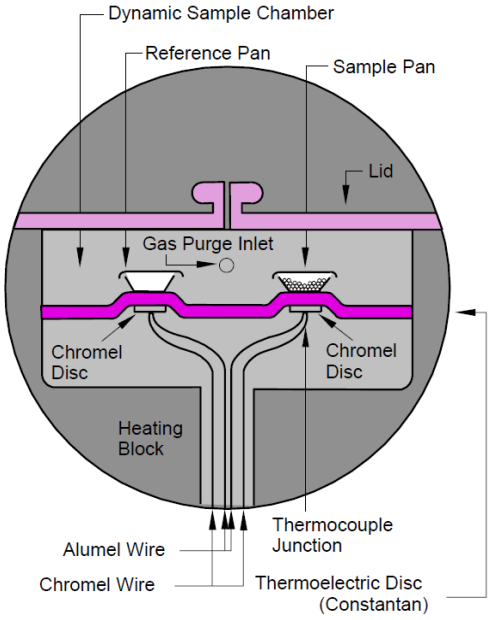

Figure 1.10 *DSC cell schematic diagram.*

The two types of DSC systems commonly in use are power-compensation and heat-flux (Nicula, 2002). In power-compensation DSC, the specimen (T_S) and reference (T_R) temperatures are controlled independently using separate (identical) ovens as showed in ***Figure 1.11***. The temperature difference between the sample and reference is maintained to zero by varying the power input to the two furnaces. This energy is then a measure of the enthalpy or heat capacity changes in the test specimen S (relative to the reference R).

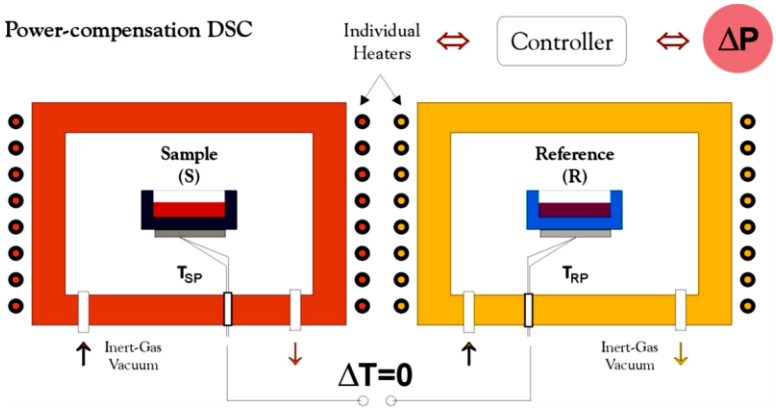

Figure 1.11 *Power-compensation DSC.*

For heat-flux DSC, the test specimen S and reference material R (usually an empty sample pan and lid) are enclosed in the same furnace together with a metallic block with high thermal conductivity that ensures a good heat-flow path between S and R (***Figure 1.12***). The enthalpy or heat capacity changes in the specimen S lead to temperature differences relative to R. These results in a certain heat-flow between S and R because of the good thermal contact between S and R. The temperature difference ΔT between S and R is recorded and further related to the enthalpy change in the specimen using calibration experiments.

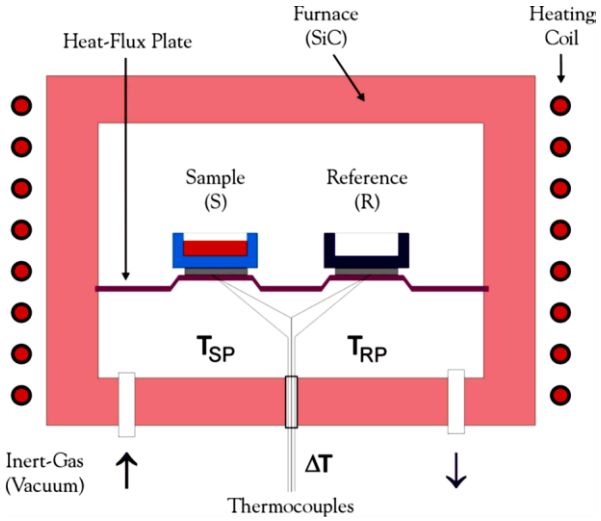

Figure 1.12 *Heat-flux DSC cell.*

The extension of DSC, known as modulated temperature DSC (MTDSC) was then introduced by Reading in the early 1990s (Craig and Reading, 2006). In essence, the technique is created by combining the application of a perturbation to the heating program of a conventional DSC with a mathematical procedure designed to separate different types of sample behaviour.

The temperature programme used in a conventional DSC experiment is based on following equation:

$$T = T_0 + \beta t \qquad \text{Eq. 1.1}$$

where T is temperature, T_0 is the start temperature, β is the heating rate and t is time (Craig and Reading, 2006). Meanwhile, for MTDSC, the separation procedure can be described as follow:

$$\frac{dQ}{dt} = C_p \cdot \frac{dT}{dt} + f(t,T) \qquad \text{Eq. 1.2}$$

where Q is the amount of heat evolved, C_p is the heat capacity, T is the absolute temperature, t is the time and $f(t,T)$ is some function of time and temperature that governs the response associated with the physical or chemical transformation (Craig and Reading, 2006).

Equation 1.2 above displays the total heat flow consisting of two contributions; one which is heating rate dependent and one which is absolute temperature dependent. The relative effect of these two contributions varies depending on the evaluated transition. Heating rate dependent contribution usually has larger transitions and the transition can be cycled by alternating heating and cooling, which is called "reversing". Meanwhile,

absolute temperature dependent contribution is considered as "non-reversing" because it cannot be reversed by the cycling process (Gill et al., 1993).

By separating the total heat flow signal into reversing and non-reversing signals, a clear transition can be observed. The reversing signal is used to analyse the melting and glass transition temperatures while relaxation, crystallisation and curing can be observed from the non-reversing signal (Gill et al., 1993, Reading et al., 1994).

1.3.4 Scanning Electron Microscopy

Scanning electron microscope (SEM) is a powerful magnification tool that utilises focussed beam of electrons to obtain information. The electrons are produced by tungsten filament, Schottky emitter or tungsten field-emission tip. The energy range of the incident electrons normally between 1 and 30 kV (Egerton, 2011).

To obtain SEM image, a finely focussed of electrons is strike on the sample surface. The beam of electrons is scanned across the sample in a raster scan by scan coils. This process is repeated until a desired surface area has been scanned. A signal is received above the surface from either analog scanning case or digital systems and stored in a computer. The signal is then converted to image (Skoog et al., 2007).

1.3.5 Transition Temperature Microscopy

In this study, transition temperature microscopy is the only thermal scanning probe microscopy technique that has been used. However, in order to understand this technique, a brief explanation about atomic force microscopy and localised thermal analysis are given.

1.3.5.1 Atomic force microscopy

Atomic force microscopy (AFM) is one of the well-established techniques in powder technology. The AFM has been used to image the surfaces of various organic crystals (Danesh et al., 2000). AFM data is matrix of data points, which enables quantitative roughness and height measurements (Luo et al., 2001). The disadvantages of AFM are the small measurement area, slow speed and the need for flat samples.

AFM provides a 3D profile of the surface on a nanoscale, by measuring forces between a sharp probe (<10 nm) and a surface at very short distance (0.2 to 10 nm probe-sample separation). The probe is supported on a flexible cantilever. The AFM tip gently touches the surface and records the small force between the probe and the surface. ***Figure 1.13*** shows AFM diagrams.

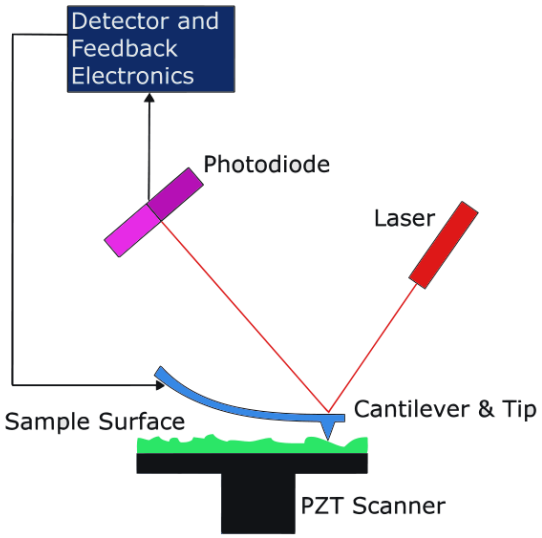

Figure 1.13 *Block diagram of AFM.*

The probe is placed on the end of a cantilever. The amount of force between the probe and sample is dependent on the spring constant (stiffness) of the cantilever and the distance between the probe and the sample surface. This force can be described using

Hooke's Law (Hubbard, 1995):

$$F = -kx \qquad \text{Eq. 1.3}$$

where F is the force, k is the spring constant and x is for cantilever deflection. If the spring constant of cantilever (typically ~ 0.1-1 N/m) is less than sample surface, the cantilever bends and the deflection is monitored.

1.3.5.2 Localised thermal analysis

*Localised thermal analysis (LTA) is a*n extension technique based on AFM principles, combined with the MTDSC principle, and was proposed by Hammiche et al. (1996) replacing the conventional AFM probe with a thermal probe. This technique allows the transition temperature of a sample surface to be locally analysed. The thermal probe used is Wollaston wire probe, consisting of 75 µm diameter silver wire containing a 5 µm platinum/rhodium core, as shows in ***Figure 1.14***. This probe was chosen because it can be used as a detector and highly localised heating source.

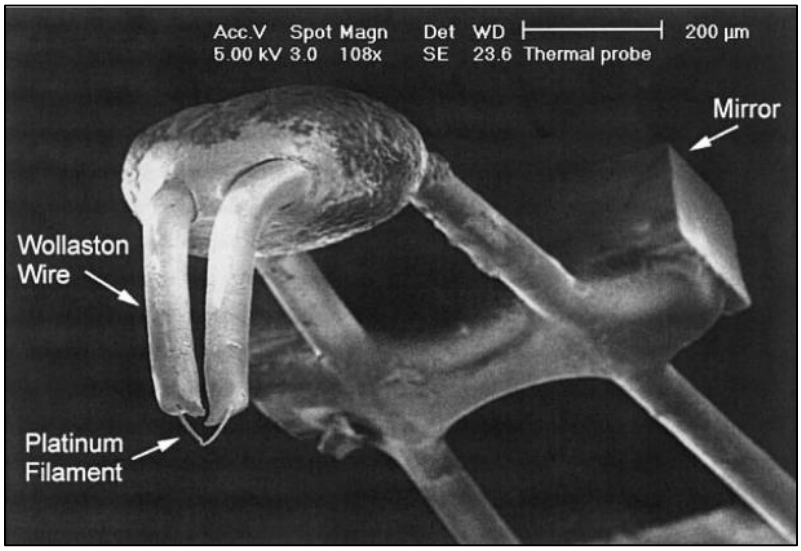

Figure 1.14 *Wollaston wire probe (Craig et al., 2002).*

An AFM image of the sample is initially obtained and then the probe is placed on the sample surface at a desired location. A voltage profile is then applied to the probe which heats up the surface of the sample locally, while the system monitors the position of the cantilever on the surface. The depth of penetration of the probe into a softened sample due to a thermal event is detected and the temperature transition is determined based on calibration measurements (Dai et al., 2012). The probe is then manually repositioned to another point on the sample's surface and a new LTA measurement made. The AFM images and thermal responses can be then correlated to understand spatial distribution of materials on a surface.

1.3.5.3 Transition temperature microscopy

Transition temperature microscopy (TTM) was invented by Kjoller et al. (2012), based on the LTA technique. In essence, it is an automated process of obtaining repeated LTA measurements in a grid (map) across a sample's surface.

For this technique, a micromachined silicon probe similar to standard AFM silicon probes but incorporating a resistive heater at the end of the cantilever is used. The probes have a tip radius of less than 30 nm and 3 to 6 µm in height. Analysis by using these probes is known as nano thermal analysis (nano-TA) since it can be conducted at the nano scale.

In TTM, a series of nano-TA measurements is performed on a sample surface over a grid pattern, generating a map of the measured transition temperatures. By using this technique, the API substances and excipients distribution on the sample's surface can thus be assessed. ***Figure 1.15*** showed the summary of TTM mechanism. Studies utilising TTM on polymer samples or films have been reported (Qi et al., 2013, Moffat et al., 2014).

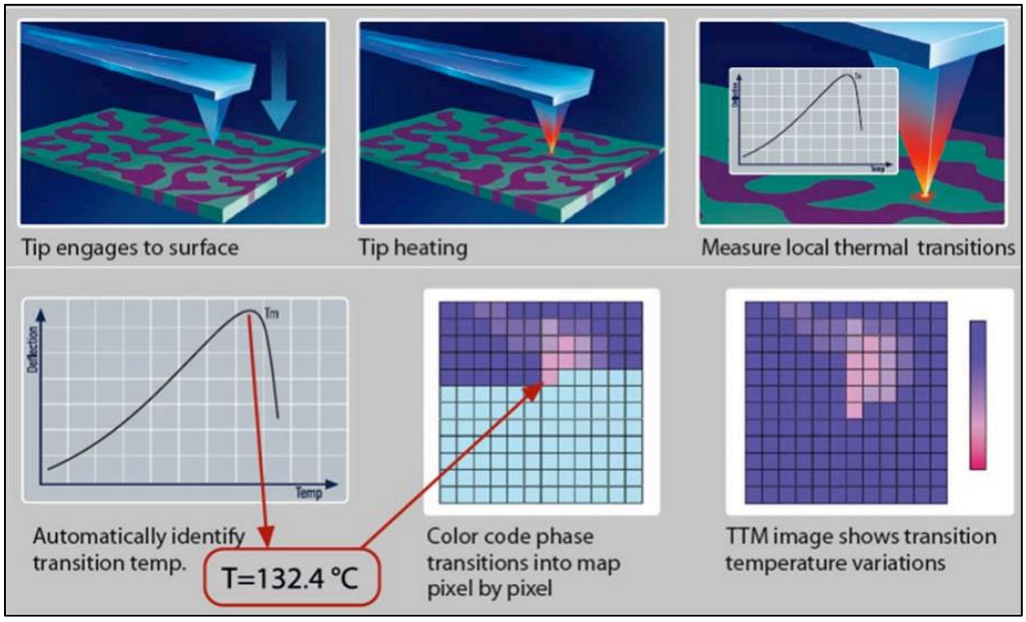

Figure 1.15 *Summary of TTM mechanism (Kjoller et al., 2010).*

1.3.6 Ultraviolet/visible Spectrophotometry

Ultraviolet/visible (UV/Vis) spectrophotometry refers to absorbance or reflectance spectroscopy in the ultraviolet (UV) and visible regions. The wavelength range of the UV region is between 200 and 400 nm, and is 400 to 800 nm for the visible region, as shows in ***Figure 1.16*** (Perkampus et al., 2013). The molecular absorbance in these regions arises from the energy transitions that involve the outer orbital or valency electrons (Cooper and Negrusz, 2013).

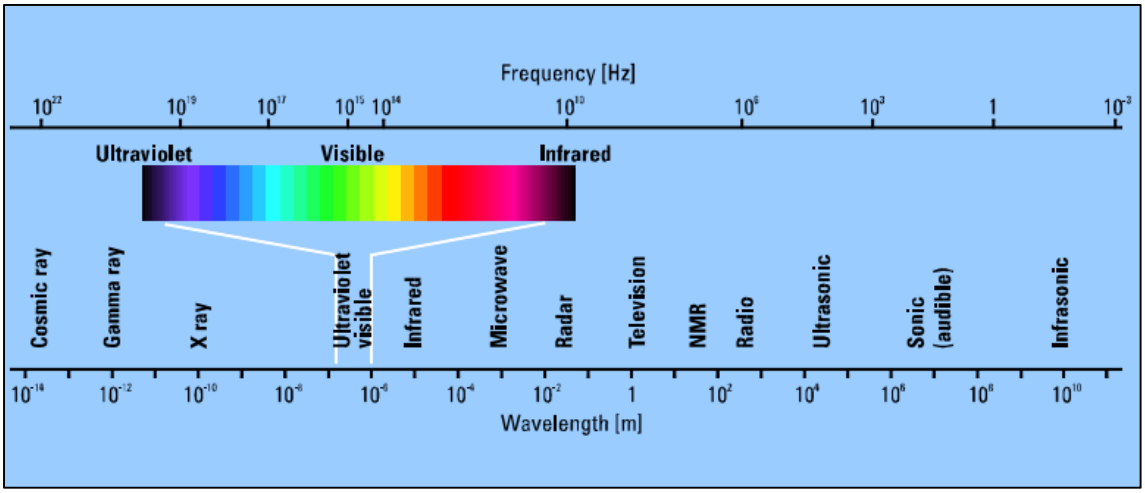

Figure 1.16 *Ultraviolet and visible spectrum (Owen, 2000).*

In general, UV/vis spectrophotometer are equipped with interchangeable tungsten and hydrogen or deuterium lamps as source of radiation. A tungsten lamp is able to emit wavelength between 350 and 2500 nm while hydrogen and deuterium lamps emitted wavelength in the range of 190 – 400 nm (Skoog et al., 2007). There are two type of UV/Vis spectrophotometer: single-beam and double-beam.

In single-beam, the light is focussed on the entrance slit of a monochromator. Monochromator will acted as filter and selectively transmit a narrow band of light. This light then will passed through the sample to the detector (Owen, 2000). The absorbance of the light is calculated by comparing the intensity of light reaching the detector between reference (blank sample) and sample. ***Figure 1.17*** shows the schematic diagram of the single-beam spectrophotometer.

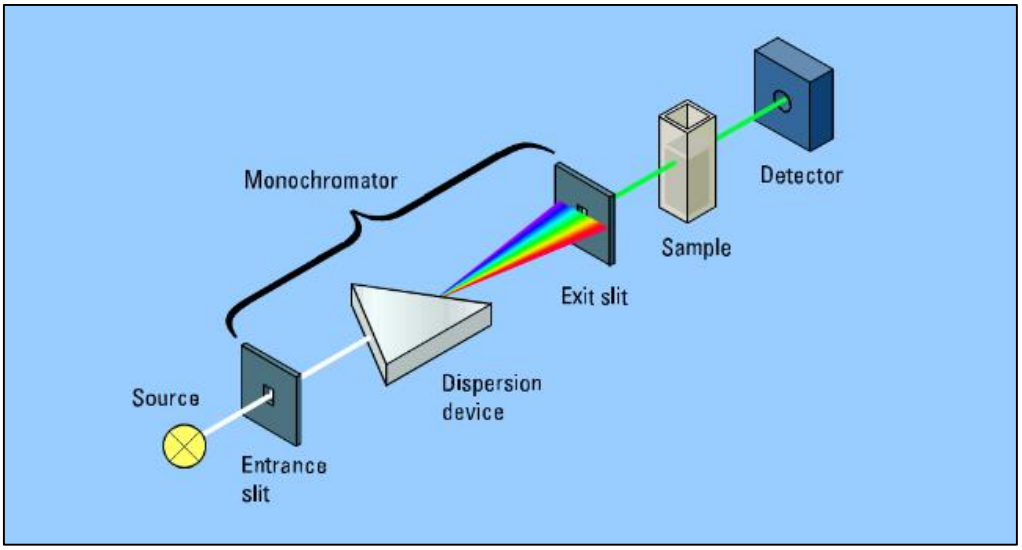

Figure 1.17 *Schematic diagram of single-beam spectrophotometer (Owen, 2000).*

For the double-beam spectrophotometer, the light is split into two beam after it passed through the monochromator. One of the beam will passed through the sample while the other will passed through the reference (Owen, 2000). ***Figure 1.18*** shows the schematic diagram of double-beam spectrophotometer.

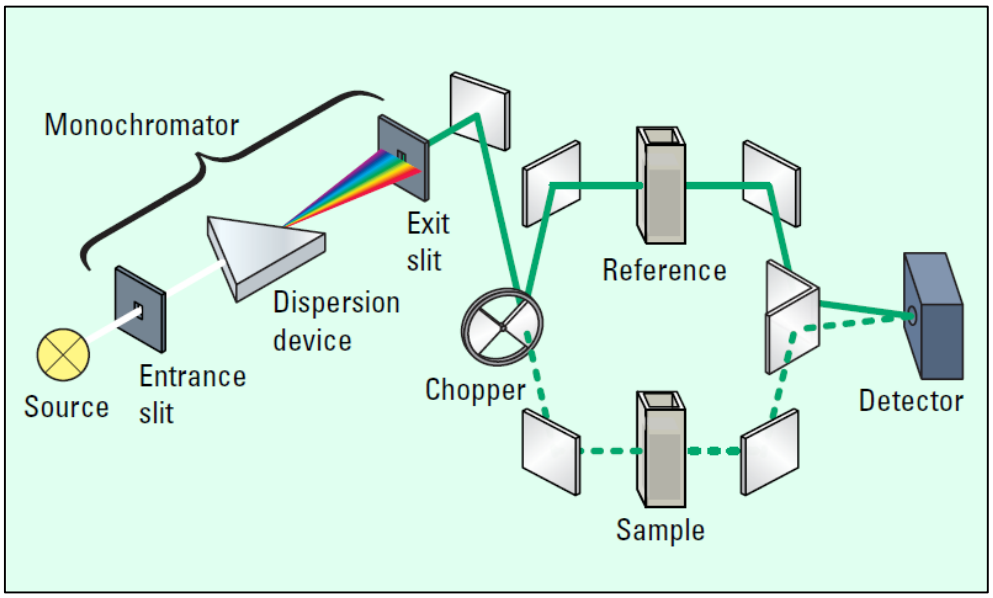

Figure 1.18 *Schematic diagram of double-beam spectrophotometer (Owen, 2000).*

The Beer-Lambert Law is used to quantify the light absorbance by the sample, which can be explained based on the following equation (Watson, 2012):

$$Absorbance\ (A) = log\frac{I_0}{I_t} = \varepsilon bc \qquad \text{Eq. 1.4}$$

where I_0 is the intensity of incident radiation, I_t is the intensity of transmitted radiation, ε is the molar absorbance coefficient of the analyte, b is the pathlength of the cell and c is the concentration of the analyte.

1.4 Aims and Objectives

The aim of this study is to investigate the formulation, manufacturing process and characterisation of the ocular mini-tablets and inserts prepared using conventional manufacturing techniques such tablet compression and unconventional manufacturing techniques such as 3D-printing.

Chloramphenicol was used as the model drug here. It is found as eye drops and ointments in the current UK market. 0.5 % (w/v) of chloramphenicol is used in eye drops with borax, boric acid, phenylmercuric nitrate and water in the formulation. The recommended dose is one drop to be applied to the infected eye every 2 hours during waking hours for the first 48 hours and then every 4 hours thereafter, with treatment continuing for 5 days. Meanwhile, for the ointments, the drug concentration used is 1.0 % (w/w) with liquid paraffin, wool fat and yellow soft paraffin as part of the formulation. The dosage regimen is to apply about 1 cm of ointment to the affected eye(s) 3 to 4 times a day for 5 days.

Using chloramphenicol eye-drops as the basis for calculation, with 8 applications per day in the first 2 days and an application volume of 50 µL, a total volume of (8 x 50 µL =) 0.4

mL per day would be applied. This equates to (0.40 mL x 0.5 %w/v =) 2 mg drug applied per day. It is usually assumed that only approximately 5 % of a topically applied dose is absorbed into the posterior segment of the eye, but in this case the site of action of the drug is much closer to the surface, so more is likely to effective, but still some drug is likely to be lost due to spillage, drainage and physical removal. A reasonable estimate may be that 25 % of the drug applied reaches its target site and has a clinical effect. Hence, of the 2 mg chloramphenicol applied per day, 0.5 mg may be assumed to have a clinical effect. For a once-a-day mini-tablet, therefore, the total dose of chloramphenicol would be 0.5 mg. If the mini-tablet weighs 10 mg, this equates to a concentration of 5 %w/w.

The target product profile will be a mini-tablet suitable for a once-daily use, with standard BP specifications for weight uniformity, content uniformity and friability. There is no BP specification for hardness, either in terms of absolute value or range, and the hardness value depends on the shape and dimensions of the product as well as the formulation and the manufacturing conditions used. However, in previous mini-tablet studies, the hardness values ranged between 0.67 N and 18.64 N (Weyenberg et al., 2003, Weyenberg et al., 2005), so it is reasonable to expect values of between 5 and 15 N to show a good balance between product resilience and drug release. There is no BP specification for thickness, either in terms of absolute value or range, as this is dependent on the diameter of the mini-tablets, their formulation and the hardness value. However, based on a 2 mm diameter mini-tablet compressed using round, normal concave punches and a weight of circa 10 mg, a thickness value of 2 mm would be expected. The drug release profile should ideally be zero-order over the full 24-hour period. This product profile is summarised in ***Table 1.5*** below.

Table 1.5 Ideal product profile of the chloramphenicol-loaded mini-tablets.

Attribute	**Specification detail**
Drug content	5 %w/w = 0.5 mg
	Meets BP specifications for content uniformity
Weight	10 mg
	Meets BP specifications for weight uniformity
Hardness	5 to 15 N
Thickness	2 mm
Friability	Meets BP specifications for friability
Dissolution profile	Zero order over 24 hours, i.e. 4.17 % per hour

The objectives of this study are:

1. To investigate the effect of particle size on the physical characterisation and drug release behaviour using the following techniques: dynamic vapour sorption (DVS), scanning electron microscopy (SEM), transition temperature microscopy (TTM), modified flow-through dissolution apparatus and UV/Vis spectrophotometer. The hypothesis is that the smaller polymer particle size will increase the drug release rate of the mini-tablets. This is presented in **Chapter 3**.
2. To evaluate the ability of TTM to cope with surface of varying smoothness using following techniques: modulated temperature differential scanning calorimetry (MTDSC), SEM and TTM. The hypothesis is that a smooth surface will give measurements of the transition temperature which are more in line with those observed by other techniques, while a rough surface is expected to give more variable results. This is presented in **Chapter 4**.
3. To formulate and manufacture 3D-printed ocular mini-tablets using following techniques: MTDSC, hot melt extrusion (HME), 3D design and modelling,

stereolithography apparatus (SLA) printer, DVS, materials microscope, SEM, TTM, modified flow-through dissolution apparatus and UV/Vis spectrophotometer. The hypothesis is that a 3D-printing technique can be used to manufacture ocular mini-tablets and possibly be considered as one of tablets manufacturing technique. This is presented in **Chapter 5**.

4. To investigate a novel approaches of modifying ocular flow-through dissolution apparatus and ocular inserts customised based on patient eye using 3D-printing techniques. This is a continuation study from **Chapter 5** using the following techniques: MTDSC, 3D design and modelling, fused deposition modelling (FDM) printer, stereolithography apparatus (SLA) printer, modified flow-through dissolution apparatus and UV/Vis spectrophotometer. The hypothesis is that a 3D-printing technique can be used to manufacture any desired shapes. Meanwhile, by designing ocular flow-through dissolution based on patient eye, a more accurate *in-vitro* study can be conducted. This is presented in **Chapter 6**.

Chapter 2

Materials and Methods

Materials and Methods

2.1 INTRODUCTION

In this study, several new approaches to ocular therapy were investigated. The products were developed, manufactured and tested using a range of techniques. For the manufacturing processes, a rotary tablet press, a hot-melt extruder (HME) and 3D-printers (fused deposition modelling (FDM) and stereolithography apparatus (SLA) printers) were used. Several tests were performed to characterise the physical properties of the products, including are weight uniformity, crushing strength, dimensional analysis, friability, vapour sorption using dynamic vapour sorption (DVS), and water content by using thermogravimetric analysis (TGA). Scanning electron microscopy (SEM) was used to capture images of the surface of the samples.

Thermal analytical studies were also conducted on selected samples to measure the melting point and/or glass transition temperature (T_g) by using modulated temperature differential scanning calorimetry (MTDSC) and transition temperature microscopy (TTM). The drug release profile from the products was assessed using a modified flow-through dissolution apparatus and spectrophotometric analysis. Mathematical modelling was performed on the dissolution profiles using zero-order, first-order and Korsmeyer-Peppas kinetics. The difference (f_1) and similarity (f_2) factors were used to determine the similarity or otherwise of the dissolution profiles.

This Chapter provides the background to the various techniques used here, as well as details on the materials used in this project.

2.2 MATERIALS

2.2.1 Chloramphenicol

In this study, chloramphenicol was chosen as the model drug. Chloramphenicol has a broad spectrum of antibiotic activity and is commonly used to treat for superficial eye infections, such as conjunctivitis. Chloramphenicol has severe side-effects, such as aplastic anaemia, when given orally, but chloramphenicol eye drops are well tolerated (BANFF, 2015).

Figure 2.1 and ***Table 2.1*** show the chemical structure and physico-chemical properties of chloramphenicol, respectively.

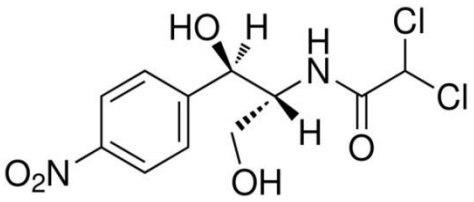

Figure 2.1 *The chemical structure of c*hloramphenicol.

Table 2.1 *Physical and chemical properties of chloramphenicol (PubChem, 2016, Laferriere and Marks, 1982).*

Properties	**Descriptions**
IUPAC name	2,2-dichloro-N-[(1R,2R)-1,3-dihydroxy-1-(4-nitrophenyl) propan-2-yl] acetamide
Molecular weight	323.13 g/mol
Molecular formula	$C_{11}H_{12}Cl_2N_2O_5$
Physical state	White to yellowish-white crystalline powder
Melting point	150.5 – 151.5 °C
Solubility	Soluble in methanol, ethanol, butanol, ethyl acetate, acetone and chloroform. Slightly soluble in water (2.5 mg/mL) and ether. Insoluble in benzene, petroleum ether and vegetable oils.
Toxicity	Induces aplastic anaemia Probably carcinogenic to human (Group 2A)

Based on the BNF (2014), the concentration of chloramphenicol in eye drops used in the UK is 0.5 % (w/v) while for the eye ointment, the concentration is 1.0 % (w/v). In this study, the concentration used in the mini-tablets was 5.0 % (w/w), with the rationale for this concentration being discussed in Chapter 1 section 1.4.

2.2.2 Polyethylene glycol

Polyethylene glycol (PEG) is polyether compound that is widely used in pharmaceutical formulations. ***Figure 2.2*** shows the structural formula of PEG.

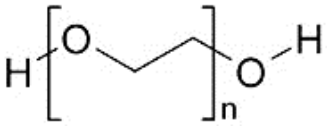

Figure 2.2 *The chemical structure of PEG.*

PEGs with molecular weights between 200 and 600 g/mol are clear colourless or slightly yellowish liquids, while for molecular weights higher than 1000 g/mol, they are solids and can be found in white waxy flakes or powders. If the molecular weight is equal to or higher than 100,000 g/mol, PEGs are often known as polyethylene oxide (PEO) rather than PEG, although chemically they remain the same (Rowe et al., 2009).

PEG (and PEO) are semi-crystalline polymers, which mean they have both crystalline and amorphous regions. They have different melting points depending on the molecular weight with the higher molecular weights having slightly higher melting points. However, there is no difference in the glass transition temperature (T_g), with all molecular weight PEGs and PEOs showing a T_g at -60 °C (Törmälä, 1974). ***Table 2.2*** summarises the physico-chemical properties of PEG. PEG 4000, PEG 6000 and PEO 8,000,000 were used for the current study.

Table 2.2 *Physical and chemical properties of PEG and PEO (Rowe et al., 2009).*

Properties	**Descriptions**
Chemical name	α-hydro-ω-hydroxypoly(oxy-1,2-ethanediyl)
Empirical formula	$HOCH_2(CH_2OCH_2)_mCH_2OH$
Physical state	PEG 200 to 600: Clear, colourless or slightly yellow-coloured liquid. PEG 1000 to >6000: White or off-white waxy flakes. PEG 6000 and above: White powder.

Melting point	PEG 4000: 40 – 48 °C. PEG 6000: 55 – 63 °C. PEO 8,000,000: 65 – 70 °C.
Solubility	Soluble in water, acetone, dichloromethane, ethanol (95 %) and methanol. Slightly soluble in aliphatic hydrocarbon and ether. Insoluble in fats, fixed oils and mineral oils.
Toxicity	Nontoxic (Included in FDA Inactive Ingredients Database for ophthalmic preparations).

PEG is often used as a component in topical formulations, as it is non-irritant topically, and cannot be absorbed by the skin (Rowe et al, 2009). Low molecular weight PEGs are commonly used as plasticisers in film formulations, with the aim of reducing the glass transition temperature (T_g) while increasing the flexibility and durability of the products (Rodríguez-Llamazares et al., 2012, Pivsa-Art et al., 2016). High molecular weight PEGs have been studied extensively as carriers in solid dispersion products, and they may improve the dissolution profile of poorly water-soluble drugs (Craig, 1990). In tabletting processes, PEG can be added into the formulation as a binder or lubricant, although this use is not common. A binder, also known as an adhesive, act as a glue to ensure that granules and tablets can be formed with the required mechanical strength. Meanwhile, lubricant is need to reduce the friction between the mixture and the die wall during tablet compression and ejection (Aulton and Taylor, 2013).

2.2.3 Microcrystalline cellulose

Microcrystalline cellulose (MCC) is one of the most widely used polymer in pharmaceutical fields. This polymer commonly used as a filler, disintegrant, binder and anti-adherent for tablets and as a binder in capsule formulations (Aulton and Taylor, 2013). ***Figure 2.3*** and ***Table 2.3*** show the chemical structure formula and physico-chemical properties of MCC,

respectively.

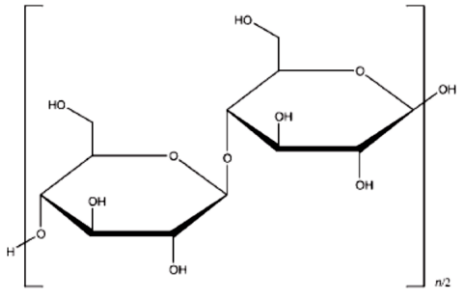

Figure 2.3 *The chemical structure formula of MCC.*

Table 2.3 *Physical and chemical properties of MCC (Rowe et al., 2009).*

Properties	**Descriptions**
Chemical name	Cellulose
Empirical formula	$(C_6H_{10}O_5)_n$
Physical state	White powder composed of porous particles.
Melting point	Char at 260 – 270 °C.
Solubility	Slightly soluble in 5% (w/v) sodium hydroxide solutions. Insoluble in water, dilute acids and most organic solvents.
Toxicity	Nontoxic (used in ocular mini-tablets study by El-Gawad et al. (2012)).

MCC is considered to be one of the most versatile polymers because of its multi-functional properties as an excipient in tabletting process. However, it cannot replace true disintegrants and lubricants in a formulation, but it may complement those properties (Thoorens et al., 2014). MCC also displays broad chemical compatibility with drugs (Çelik, 2016).

2.2.4 Hydroxypropyl methylcellulose K4M

Hydroxypropyl methylcellulose (HPMC), also known as hypromellose, is widely used in oral, ophthalmic and topical pharmaceutical formulations. In general, HPMC is an

odourless and tasteless white powder. ***Figure 2.4*** shows the structural formulas of HPMC. HPMC has a few different grades commercially available. However, in this chapter, only HPMC K4M will be discussed since this is the only HPMC grade that has been used in this work.

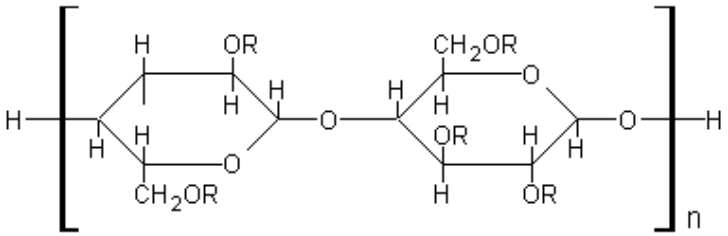

Figure 2.4 *The chemical structure formula of HPMC.*

HPMC K4M has a nominal molecular weight of 86,000 g/mol and a nominal viscosity of 4000 mPa.s for a 2 %w/w aqueous solution at 20 °C. This amorphous polymer displays a glass transition (T_g) at 186 °C (Rowe et al., 2009, Ma et al., 2013). The glass transition is very small and can be quite tricky to measure. McPhillips et al. (1999) were able to distinguish the glass transition temperature by using modulated temperature differential scanning calorimetry. ***Table 2.4*** summarises the physico-chemical properties of HPMC.

Table 2.4 *Physical and chemical properties of HPMC (Rowe et al., 2009, PubChem, 2016).*

Properties	**Descriptions**
Chemical name	Cellulose hydroxypropyl methyl ether
Empirical formula	$C_{56}H_{108}O_{30}$
Physical state	White or creamy-white fibrous or granular powder.
Melting point	Browns at 190 – 200 °C; chars at 225 – 230 °C.
	T_g at 170 – 180 °C.
Solubility	Soluble in cold water, mixtures of ethanol and dichloromethane, mixtures of methanol and dichloromethane

	and mixtures of water and alcohol. Insoluble in hot water, chloroform, ethanol (95 %), and ether.
Toxicity	Nontoxic (Included in FDA Inactive Ingredients Database for ophthalmic preparations).

HPMC is a hydrophilic polymer that can be used as a controlled-release matrix, film-coat former and binder for tablets, and a suspending and thickening agent in topical formulations (Aulton and Taylor, 2013, Rowe et al., 2009).

2.2.5 Polyvinylpyrrolidone 90F

Polyvinylpyrrolidone (PVP) is a synthetic polymer consisting of 1-vinyl-2-pyrrolidinone repeating groups, with the empirical formula of $(C_6H_9NO)_n$ (Rowe et al., 2009). PVP is commonly used as a binder in tablet formulations, either as wet or dry binder (Aulton and Taylor, 2013). PVP is a hydrophilic white powder. There are several different grades of PVP but for this study, only PVP 90F was used. ***Figure 2.5*** shows the structural formula of PVP.

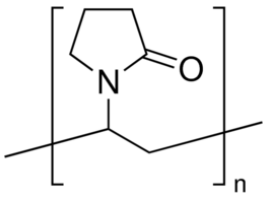

Figure 2.5 *The chemical structure of PVP*

PVP 90F has one of the highest molecular weights of the PVP grades commercially available at the moment, approximately 1,000,000 g/mol. There are several published studies using PVP 90F as part of the formulation in film coating for controlled release formulations (Fini et al., 2008, Sungthongjeen et al., 2004). This is because PVP 90F can be used as a plasticiser to increase the flexibility of the films. All PVP grades are characterised based on the relative viscosity in water at 25 °C of a 20 %w/w aqueous

solution and their *K*-value. The *K*-value for PVP 90F was 90, hence the grade name (Bühler, 2008). ***Table 2.5*** summarises the physico-chemical properties of PVP.

Table 2.5 *Physical and chemical properties of PVP (Rowe et al., 2009, Bühler, 2008).*

Properties	**Descriptions**
Chemical name	1-Ethenyl- 2-pyrrolidinone homopolymer.
Empirical formula	$(C_6H_9NO)_n$
Physical state	White or creamy-white powder.
Melting point	Soften at 150 °C.
	T_g at 170 – 180 °C.
Solubility	Soluble in water, acids, chloroform, ethanol (95 %), ketones and methanol.
	Insoluble in ether, hydrocarbons and mineral oils.
Toxicity	Nontoxic (Included in FDA Inactive Ingredients Database for ophthalmic preparations).

2.2.6 Carbopol 974P

Carbopol is commonly used in liquid and semi-solid pharmaceutical formulations as a rheology modifier. It can also be used as bioadhesive, controlled-release and emulsifying agents (Rowe et al., 2009). Carbopol 974 is the only grade used in this study. ***Figure 2.6*** shows the chemical structure formula of Carbopol.

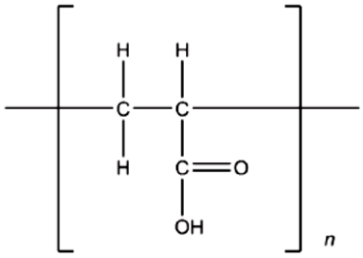

Figure 2.6 *The chemical structure formula of Carbopol.*

Carbopol is a hygroscopic polymer. The polymer can absorb moisture content between 8 and 10% (w/w) at 25 °C and 50% relative humidity. Carbopol does not dissolve in any solvents. This polymer only swell up to a certain extent due to its three-dimensionally crosslinked microgels (Rowe et al., 2009). ***Table 2.6*** shows the physico-chemical properties of Carbopol.

Table 2.6 *Physical and chemical properties of Carbopol (Rowe et al., 2009).*

Properties	**Descriptions**
Chemical name	Carbomer
Empirical formula	$(C_3H_4O_2)_n$
Physical state	White powder.
Melting point	T_g at 100 – 105 °C.
	Decomposition occurs at 260 °C within 30 minutes.
Solubility	Swellable in water, glycerin and 95% of ethanol (after neutralisation).
Toxicity	Nontoxic (Included in FDA Inactive Ingredients Database for ophthalmic preparations).

Carbopol is used pharmaceutically because it is non-toxic and non-irritant (Rowe et al., 2009). A study by Weyenberg et al. (2006) on the preparation of ocular mini-tablets by manipulating the concentration of Carbopol 974P in the formulations found that the drug release rate decreased with the increment of Carbopol 974P.

2.2.7 Sodium stearyl fumarate

Magnesium stearate is the most widely used as lubricant in tabletting and capsuling processes due to its superior lubrication properties. However, there is one drawback with magnesium stearate, which is that it is hydrophobic. (Aulton and Taylor, 2013). To overcome this problem, sodium stearyl fumarate (SSF) was used in the present work.

Figure 2.7 shows the structural formula of SSF and ***Table 2.7*** summarises its physico-chemical properties.

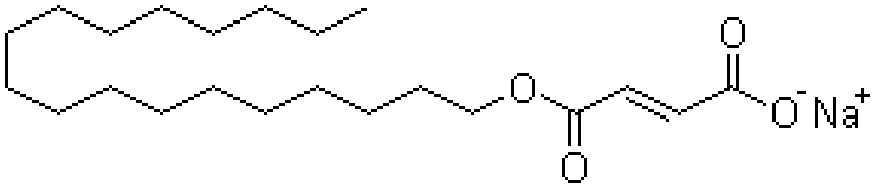

Figure 2.7 *The chemical structure of SSF.*

Tablet 2.7 *Physical and chemical properties of SSF (Rowe et al., 2009).*

Properties	**Descriptions**
Chemical name	2-butenedioic acid monooctadecyl ester.
Empirical formula	$C_{22}H_{39}NaO_4$
Physical state	White powder.
Melting point	224 – 245 °C (with decomposition).
Solubility	Soluble in water. Slightly soluble in methanol. Insoluble in acetone, chloroform and ethanol.
Toxicity	Nontoxic (used in ocular mini-tablets study by Weyenberg et al. (2006).

SSF is effective as a lubricant in tablet formulations and affect the disintegration and tensile strength of the tablets in the same fashion as magnesium stearate (Hölzer and Sjögren, 1979). As it is non-toxic, non-irritant and water soluble (Rowe et al., 2009), it is the most suitable lubricant for ocular mini-tablets, where aqueous solubility of all ingredients is desired.

2.2.8 Polyethylene glycol diacrylate 700

Polyethylene glycol diacrylate (PEGDA) is a photopolymerisable polymer that has been widely studied as a base polymer for products made using photopolymerisation process, especially hydrogels (Dana et al., 2013, Chan et al., 2010, Cuchiara et al., 2010, Nemir et al., 2010). ***Figure 2.8*** and ***Table 2.8*** show the structural formula and the physico-chemical properties of PEGDA. In this study, PEGDA 700, with a nominal molecular weight of 700 g/mol, was chosen as the base polymer for the 3D-printed mini-tablets using the stereolithography technique based on a photopolymerisation process.

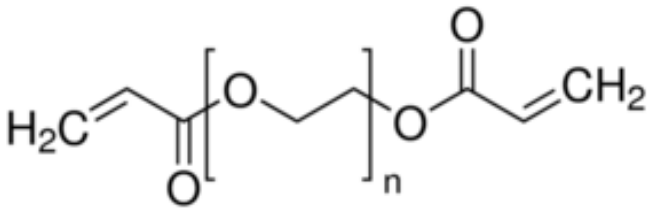

Figure 2.8 *The chemical structure of PEGDA.*

Table 2.8 *Physical and chemical properties of PEGDA (PubChem, 2016).*

Properties	**Descriptions**
Empirical formula	$H_2C=CHCO(OCH_2CH_2)_nO_2CCH=CH_2$
Physical state	Colourless liquid.
Melting point	12 – 17 °C.
Solubility	Soluble in water.
	Slightly soluble in benzene, ethanol and ligroin.
Toxicity	Nontoxic.

During the photopolymerisation process, PEGDA monomers and low molecular weight PEGDA pre-polymers are mixed with a photoinitiator and exposed to UV light. A free radical chain reaction process is induced and leads to the formation of highly crosslinked products (Allen, 1996). ***Figure 2.9*** shows the photopolymerisation process of PEGDA. The

3D-printer applies this concept by using laser light to cure the photopolymer. The 3D-printing technique will be explained later.

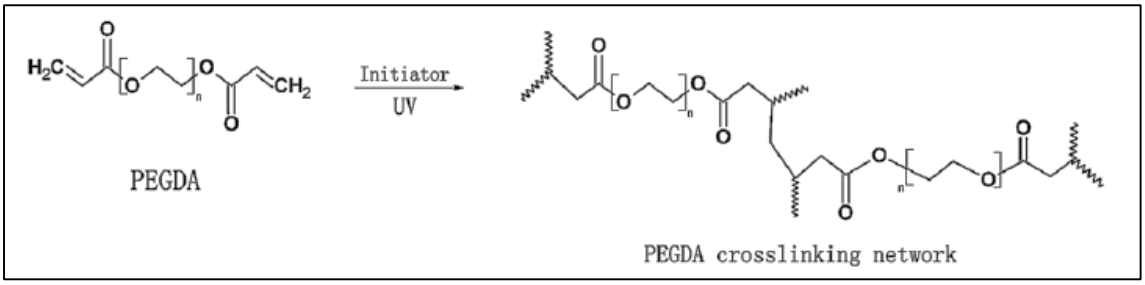

Figure 2.9 *Photopolymerisation process of PEGDA (Fei et al., 2012).*

2.2.9 Phenylbis (2,4,6-trimethylbenzoyl) phosphine oxide

Phenylbis (2,4,6-trimethylbenzoyl) phosphine oxide (BAPO) is a common photoinitiator used in photopolymerisation. Kenning et al. (2008) in their studies on photoinitiation rate comparing four different photoinitiators found that BAPO was the most efficient photoinitiator for photoinitiation in thick polymer systems. ***Figure 2.10*** and ***Table 2.9,*** respectively**,** show the structural formula and physico-chemical properties of BAPO. In this study, BAPO was used as the initiator for the photopolymerisation of PEGDA.

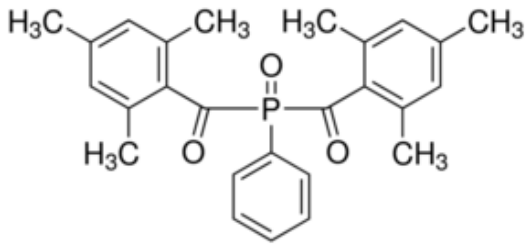

Figure 2.10 *The chemical structure of BAPO.*

Table 2.9 *Physical and chemical properties of BAPO (PubChem, 2016).*

Properties	**Descriptions**
IUPAC name	[phenyl-(2,4,6-trimethylbenzoyl) phosporyl]-(2,4,6-trimethylphenyl) methanone
Empirical formula	$C_{26}H_{27}O_3P$
Physical state	Yellowish powder.
Melting point	131 – 135 °C.
Solubility	Soluble in acetone, acetonitrile, hexanedioldiacrylate and toluene.

2.3 MANUFACTURING PROCESSES

2.3.1 Mini-tablet manufacturing

In this study, the mini-tablets were prepared by compression using a Riva Piccola rotary tablet press (Riva, Argentina) with 2 mm normal concave plain punches, supplied by Adamus (Poland), as shown in ***Figure 2.11***. This press is fitted with four B and four D stations, although the D stations were blanked off and only the B stations were used. The Piccola press was set with a 6 mm cam, allowing a fill depth in the die of approximately 5 mm. The compression force was fixed at 1.8 ± 0.2 kN for all formulations. Only one set of punches was used during the process in order to reduce variability. During the tabletting process, the feeder and turret speed were maintained at 15 rpm for the whole batch. No pre-compression force was applied in the tabletting process. All punches and die were lubricated with food grade lubricant after the tabletting process.

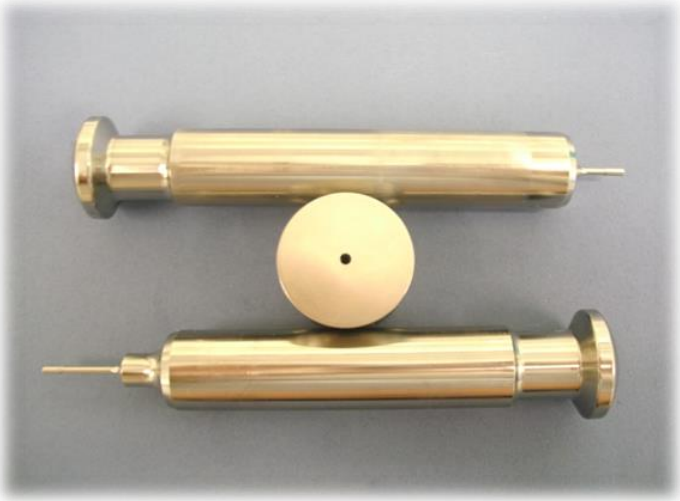

Figure 2.11 *Photograph of a set of the 2 mm normal concave tooling used in this study. Top - upper punch, middle - die and bottom - lower punch (courtesy of Dr Joanne Peacock).*

2.3.2 Hot Melt Extrusion

Hot melt extrusion (HME) is a processing technique whereby an intimate mix of materials may be obtained, generally on a molecular scale (Repka et al., 2007). It works by melting the materials and subsequent mixing them with either a single or twin screw configuration. Its use in pharmaceutics has been to prepare products with improved dissolution profiles where the drug in question has poor aqueous solubility, or to provide stabilisation for amorphous drugs.

In this study, hot melt extrusion was performed using a Process II parallel twin screw extruder (Thermo Scientific, USA) with a 2 mm nozzle. The extrusion parameters were varied, depending on the specific polymer's transition temperature. The extrusion temperature was ranged between 50 and 180 °C with a screw speed at 25 rpm. All eight heating zones were kept the same temperature for all experiments.

2.3.3 3D-Printing techniques

3D-printing can be described as the construction of in three dimensions of a material to a specific design. There are several different 3D-printing techniques available, with separate advantages and disadvantages. In this study, the fused deposition modelling (FDM) and stereolithography apparatus (SLA) approaches were both investigated and are described below.

2.3.3.1 3D model design

Before a product can be 3D-printed, it first needs to be designed. There are several software packages that can be used to design three dimensional (3D) models for 3D-printing. The one used here is Tinkercad (2015), a free browser-based 3D design and modelling application. Tinkercad allows users to create 3D models based on pre-installed

geometric shapes, letters, numbers and symbols and to share their geometric creations. ***Figures 2.12, 2.13, 2.14*** and ***2.15*** show the creation of a series of objects using the Tinkercad software.

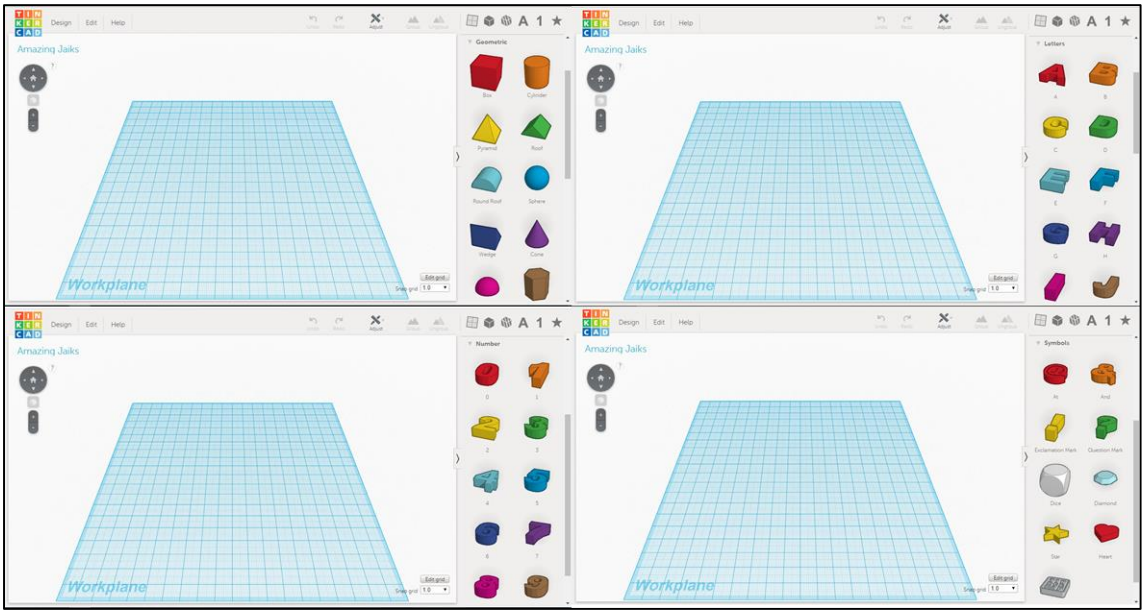

Figure 2.12 *Pre-installed geometric shapes, letters, numbers and symbols.*

Figure 2.12 shows the pre-installed basic shapes that are available. After deciding on the specific shape, it can be dragged to the workplane (the blue grid in the centre of the screen). The dimensions of the 3D object selected can be adjusted by clicking the "helpers" tab and then choosing "ruler". The object measurement will be shown once the "ruler" is used on the workplane, as indicated in ***Figure 2.13***. The object also can be rotated to a different angle by clicking the "rotate" symbol on the object and move it around.

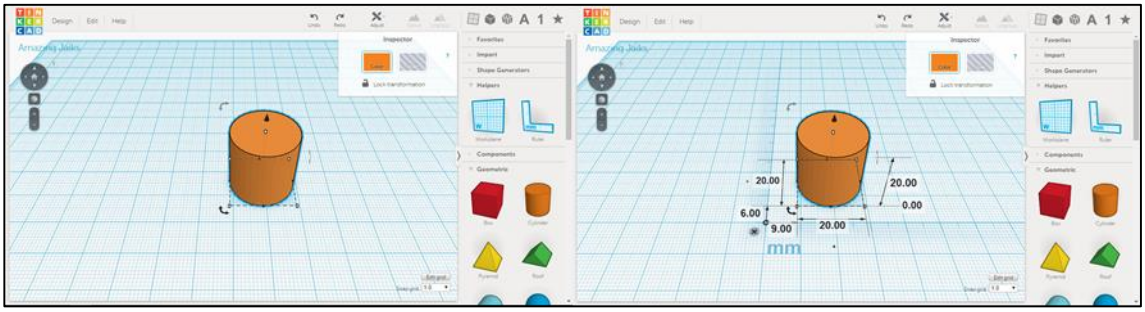

Figure 2.13 *Selected object without (left) and with (right) the "ruler".*

Two or more objects can be combined to become one object by placing them together, selecting all the objects and clicking the "group" icon, as shown in ***Figure 2.14***. The objects' colours will be changed into a single colour, indicating the object already been combined. This process can be revered and the objects separated by clicking the "ungroup" icon next to the "group" icon.

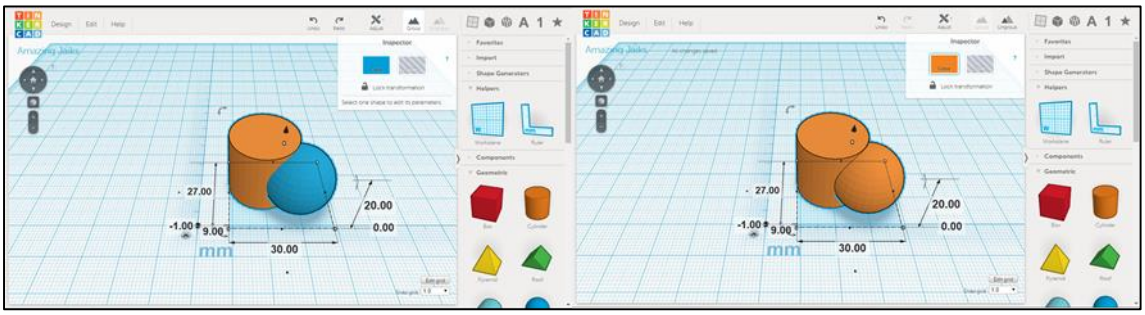

Figure 2.14 *3D objects before (left) and after (right) being combined.*

In order to make a hole in the object, the size and shape of the hole is chosen as if it were part of a second solid object and this is then overlapped with the primary object as if it was to be combined as described above. The shape is then turned into a hole once the "hole" icon on the "inspector" window is clicked as shown in ***Figure 2.15***.

Figure 2.15 *A sphere object (left) was turned into hole (right) on a cylinder.*

All the 3D-printed models used in this study were designed by applying these basic steps. The model was then saved into an .STL file format and sent to the 3D-printer to be printed.

2.3.3.2 3D model based on MRI

Magnetic resonance imaging (MRI) is a diagnostic imaging technique, commonly used in the medical field, which generates an internal image of the body by using strong magnetic fields. Since the image obtained from MRI is in 3D, it can be used to generate a model for use with a 3D printing technique. In this study, a colleague in the UCL School of Pharmacy kindly provided an MRI image of his own head and gave permission for it to be used as a model in this work.

InVesalius (2016) was used to analyse the MRI image. The MRI image used was actually a combination of several 2D images, called slices, stacked together. These slices were imported to InVesalius and a 3D image was constructed, as shown in ***Figure 2.16***. The letters in the images indicate the position of the head from different angles while the numbers at the bottom left corner indicate the slice number for the images.

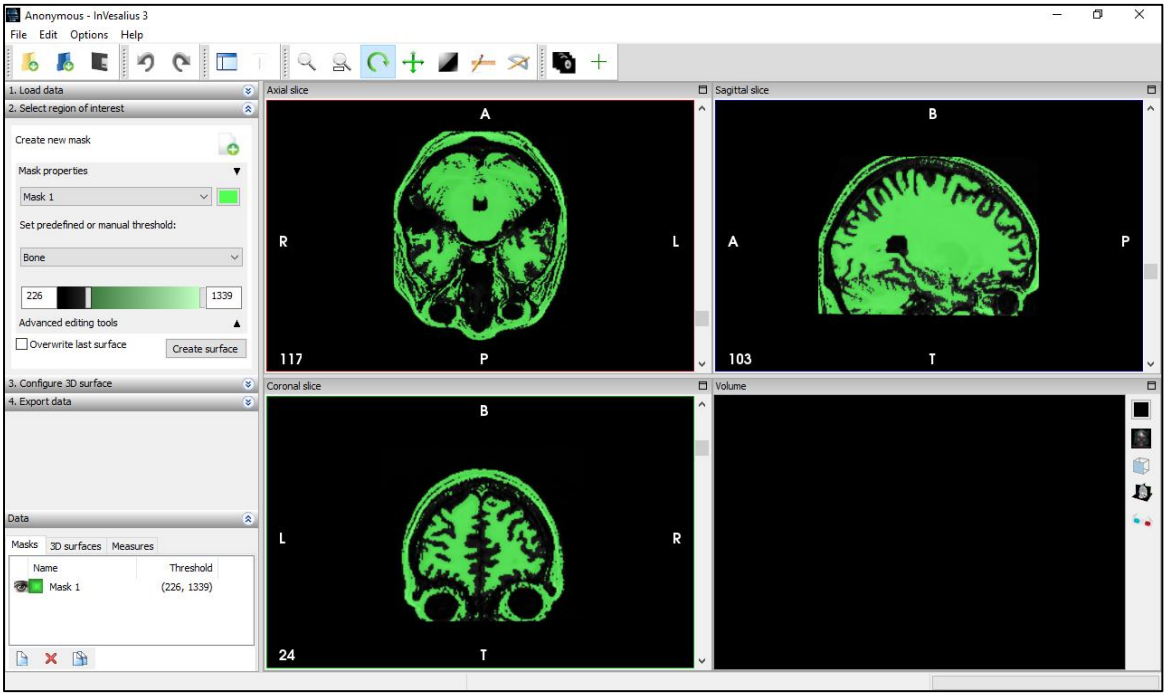

Figure 2.16 *InVesalius software with 3D images from the MRI scan.*

There are three anatomical planes that can be viewed from the MRI image: axial, sagittal and coronal as shown in ***Figure 2.17***. The axial, or transverse, images are horizontal slices through the body, beginning at the bottom and moving through to the top of the body. The sagittal images are vertical slices through the body, beginning at the left hand side and moving to the right hand side. Finally, the coronal images are vertical slices through the body, beginning at the front and moving to the back of the body.

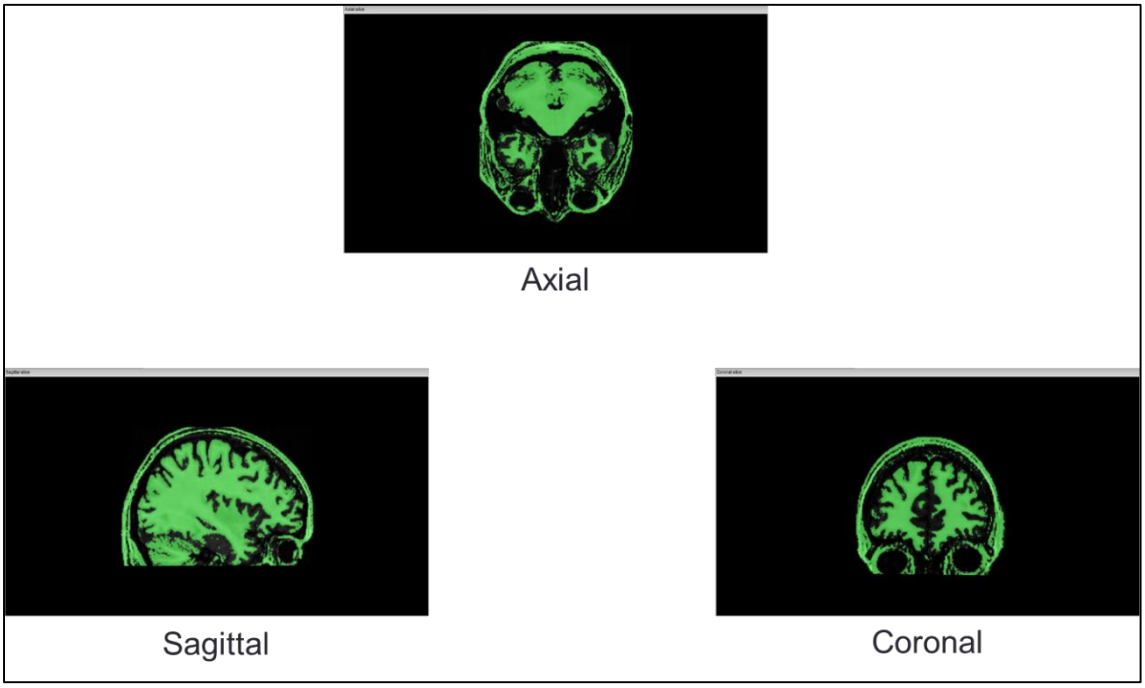

Figure 2.17 *Cross-sections of the anatomical planes through the MRI image.*

The position of the images were aligned by clicking the "slices' cross intersection" icon, as shown in ***Figure 2.18***. The red cross intersection line will appear on all images, pointing at the same position across the anatomical planes. The images from each plane were scrolled to change the slice image in order to find exactly the same position for all planes.

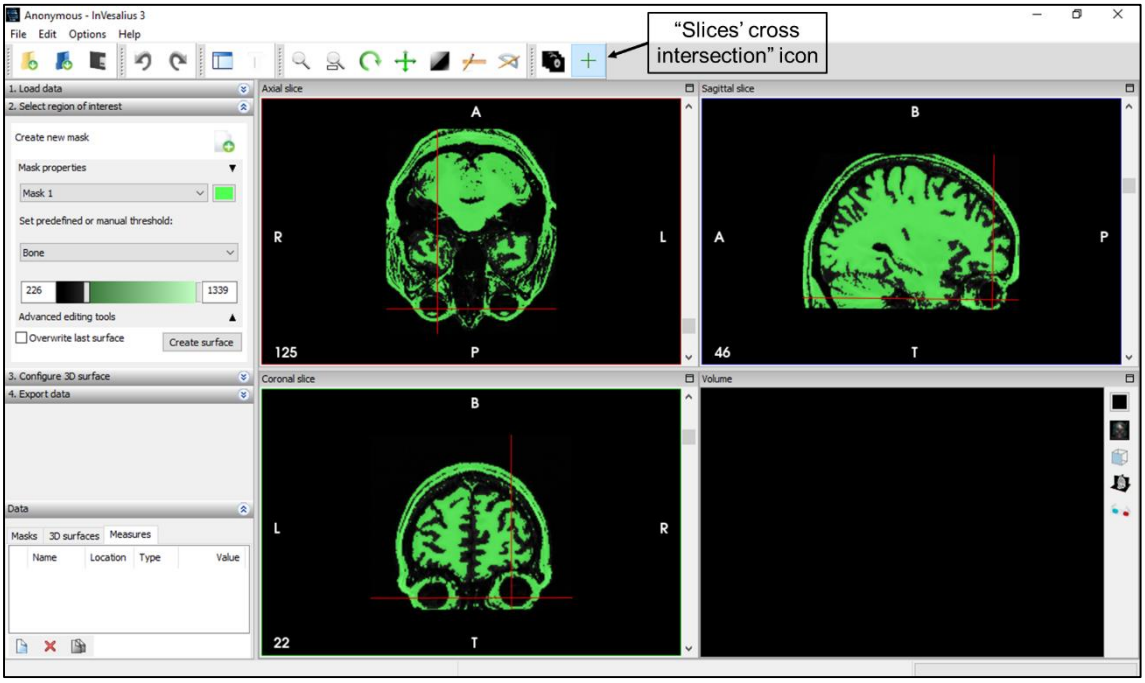

Figure 2.18 *MRI images from different anatomical planes with slices' cross intersection line.*

The dimensions of the eye across the three different planes were measured by clicking the "measure distance" icon and "clicking and dragging" the mouse across the eye. The measurements were then displayed on the images and at the bottom left corner of the software, as shown in ***Figure 2.19***. Three measurements were made for each anatomical plane. The 3D eye shape was reconstructed based on the measurements.

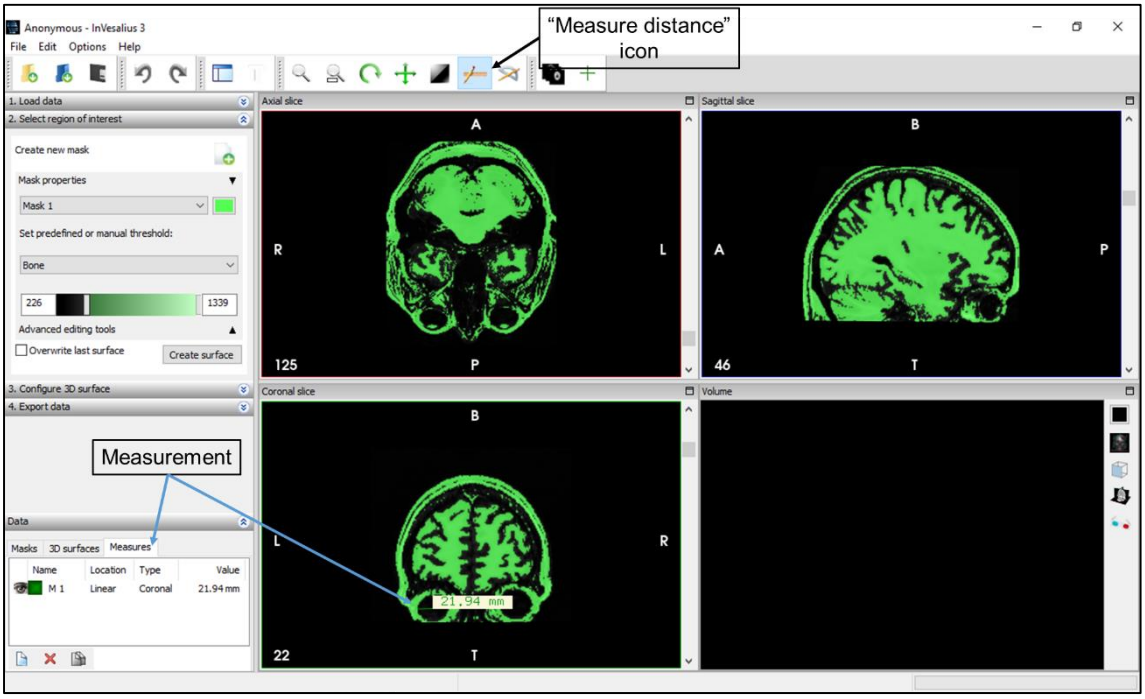

Figure 2.19 *The "Measure distance" icon and measurement of the eye.*

2.3.3.3 Printing 3D objects

There are a few types of 3D-printer available but the most popular on the market, and used in this study, are the fused deposition modelling (FDM) and stereolithography apparatus (SLA) printers.

2.3.3.3.1 Fused deposition modelling

FDM printers are the most common 3D-printers in the current market. This technique was developed and patented by Crump (1992). The FDM printer uses a thermoplastic filament which is heated to its melting point. The molten filament is then ejected as a droplet through the nozzle attached to the extruder at a specific site. Following the 3D design generated earlier, the position of the nozzle will be moved and another droplet deposited. Hence, it will be laid down layer by layer, creating the desired 3D object.

In this study, an FDM printer from MakerBot (USA) (***Figure 2.20***) was used to make prototypes of the 3D model designs before the final product design was decided. This enabled assessment of the 3D model shape after printing. An advantage of the FDM printer is that it is cheaper than the SLA, hence is useful for prototyping designs. The final product design, however, was printed by using an SLA printer because this is a more accurate printer than the FDM printer.

Figure 2.20 *The FDM printer used here (supplied by MakerBot).*

2.3.3.3.2 Stereolithography apparatus

The SLA technique is the oldest 3D printing technique, having been patented by (Hull, 1986). This technique uses the photopolymerisation concept, in which light catalyses the production of a polymer from the monomers present in solution. Here, a laser is used to cure the photopolymer while shaping it into an object.

In this study, a self-levelling platform 3D printer from Formlabs (USA) was used. This printer is from the Formlabs 1+ series, comprised of three important parts: the build platform, the resin tank and the optical system, as shown in ***Figure 2.21***.

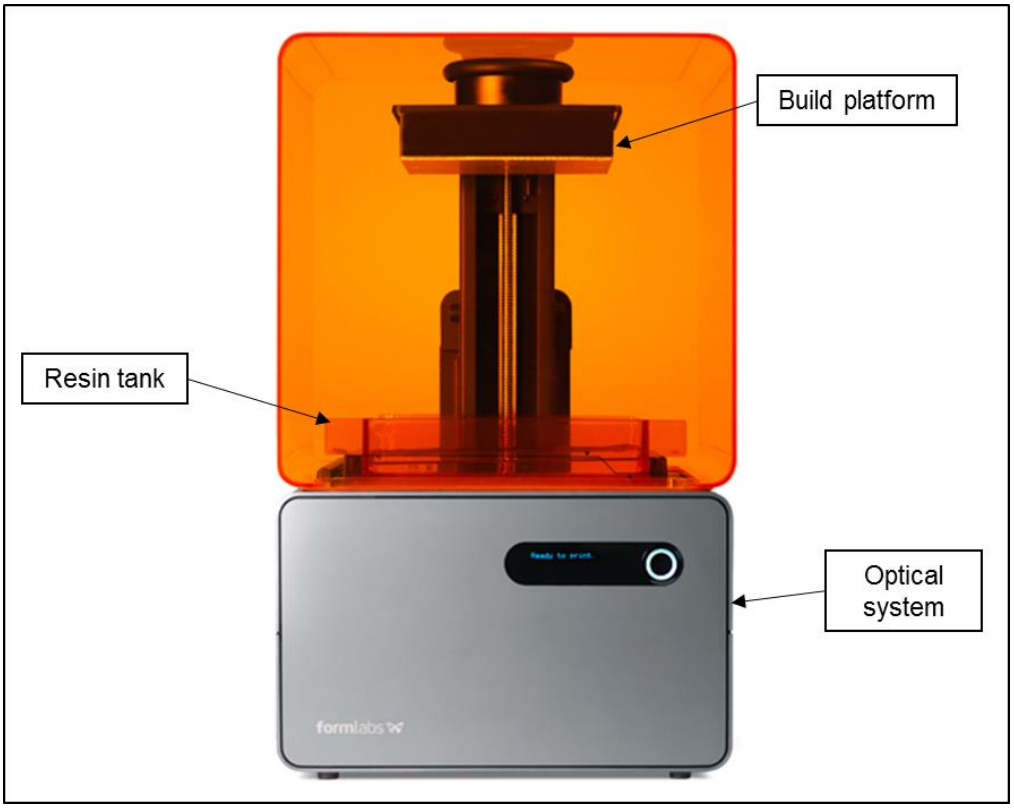

Figure 2.21 *SLA printer by Formlabs.*

Before the printing process starts, the .STL file of the required 3D designed model is uploaded to the computer connected to the printer. The model design is then opened by using PreForm software from FormLabs. On the start-up window, the software prompts the print setup window to identify the material and layer thickness (resolution) used for the printing, as shown in ***Figure 2.22***.

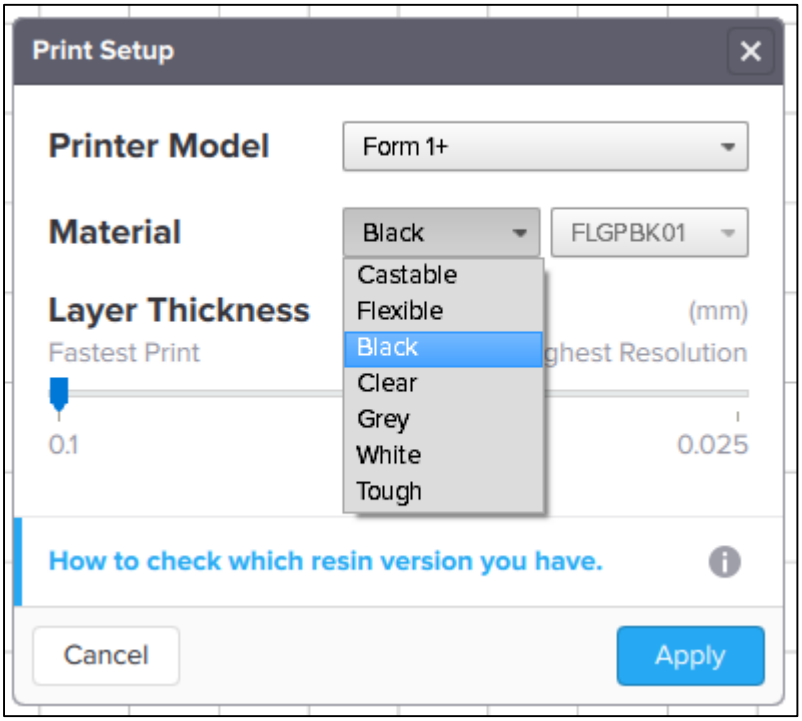

Figure 2.22 *The print setup window on the SLA printer computer.*

There are 7 types of material that can be chosen from the settings. These material types are based on resins commercially available from Formlabs (USA). Some of the materials have multiple versions that can be identified by reference to the resin bottle. If the resin used is not from Formlabs (USA), the material setting can be chosen based on the similarity of the polymer used to the properties of the commercialised resins, as summarised in ***Table 2.10***.

Table 2.10 *Materials properties summary (Formlabs, 2016).*

Material	Description
Castable	Investment casting, blue colour, slightly softer than standard resins before post-curing.
Flexible	Impact resistance, compression, great for ergonomic soft-touch grips.
Black	Highly pigmented, our most opaque, high detail resin, great for printing small, accurate features.
Clear	Transparency, polishes to near optical clarity, great for internal channels and working with light.
Grey	Neutral tone, slight opacity when thin, provides a great base colour for painting prints.
White	Neutral tone, slight opacity when thin, great for showing off surface finish, photographs easily.
Tough	Impact resistance, cyclic stress or strain, machining, snap-fits and living hinges.

After the material type and layer thickness are chosen, the main window opens. There are five icons on the left-side of the main window. The icons are, from top to bottom, "size", "orientation", "supports", "layout" and "start a print". The "size" icon is used to change the size while the "orientation" icon is used to rotate the model.

Some of the 3D models need support (essentially scaffolding) in order to print them. The "supports" function was used to create the support needed, as shows in ***Figure 2.23***. By using the support, the shape of the model can to be held in place as it is being printed.

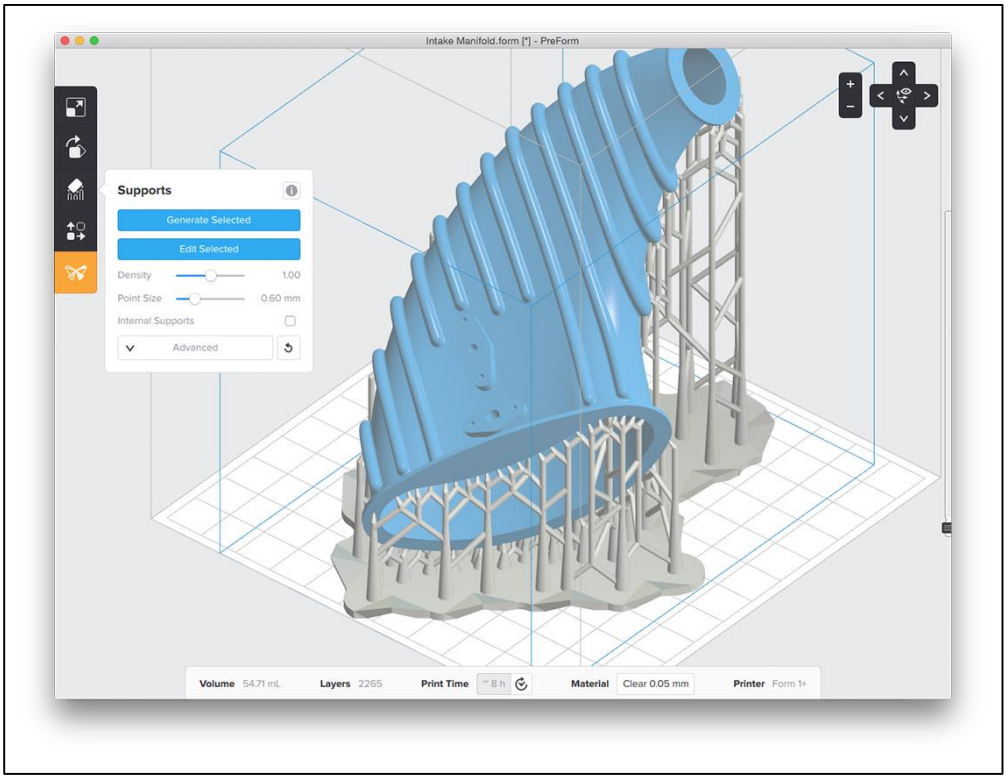

Figure 2.23 *An example of a support (grey) for the 3D model (blue).*

The "layout" function was used to align and create duplicates of the model, as shown in ***Figure 2.25***. In this mode, the model can be moved around and aligned, as required. The model can be replicated into several individual units, as long as the overall design can fit onto the build platform.

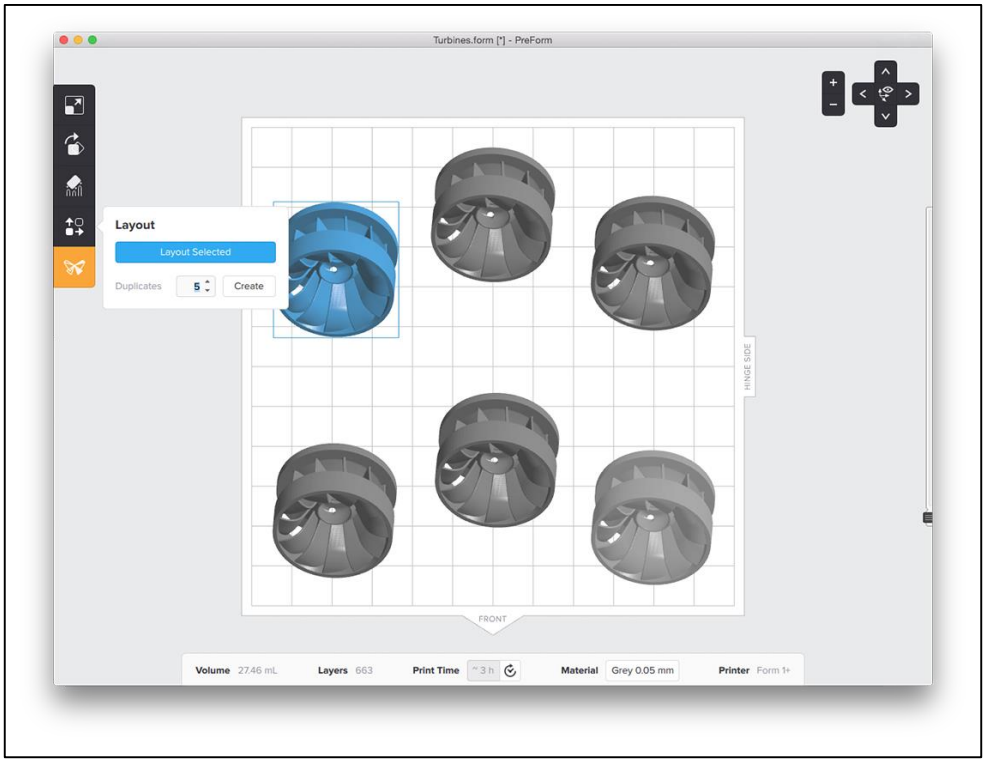

Figure 2.24 *Replicating the model.*

The "start a print" icon is clicked once the printing setting is complete. The printing setting is then sent to the printer. At this point, the printer has not started the printing process yet, as the start button needs to be pressed in order to operate the printer. Before the printing process is started, the resin needs to be filled into the resin tank.

During the printing process, the build platform is lowered down and fully submerged within the resin tank, close to the bottom surface of the tank. The laser is projected from the optical system into the resin tank, following the design of the model and cures (polymerises) the resin, layer by layer. The resin tank is lowered down by a spring-loaded tank support each time a layer is complete in order to remove the layer from the resin tank surface. This process is called "peel" (Lobovsky et al., 2014, Formlabs, 2016).

2.4 CHARACTERISATION TECHNIQUES

2.4.1 Physical Characterisation

Physical characterisation consists of several tests that are performed to determine the physical properties of the materials. The mini-tablets were evaluated for uniformity of weight, uniformity of content, crushing strength, dimensions, friability, and dissolution and swelling behaviours.

2.4.1.1 Uniformity of weight

The British Pharmacopoeia (BP) uniformity of weight test measures the weight consistency of products. Assuming that the initial powder mix is correct, the uniformity of weight is used as an initial means of determining whether the products will contain the correct dose of drug. The uniformity of weight of tablets is determined by accurately weighting 20 tablets individually, using an electrical balance. From the data, the mean weight and deviation from the mean can be obtained. Not more than 2 of the individual masses deviate from the average mass by more than the percentage deviation shown in ***Table 2.11*** and none deviate more than twice that percentage (British Pharmacopoeia, 2015).

Table 2.11 *The allowable deviation of individual weight in the BP Uniformity of weight test (British Pharmacopeia, 2015).*

Pharmaceutical Form	Average Mass	Percentage Deviation
Tablets (uncoated and film-coated)	80 mg or less	10
	More than 80 mg and less than 250 mg	7.5
	250 mg or more	5

Since the expected weight of 2 mm mini-tablets is less than 80 mg, the allowable percentage deviation is 10 %.

2.4.1.2 Uniformity of content

The British Pharmacopoeia (BP) uniformity of content test measures the content consistency of products. The uniformity of content of tablets is determined by accurately analysing 10 tablets individually, using an appropriate analytical technique. From the data, the mean drug content and deviation from the mean can be obtained. The preparation complies with the test if each individual drug content value is between 85 % and 115 % of the average content. The preparation fails to comply with the test if more than one individual content is outside these limits or if one individual content is outside the limits of 75 % to 125 % of the average content. If one individual content is outside the limits of 85 % to 115 % but within the limits of 75 % to 125 %, determine the individual contents of another 20 dosage units taken at random. The preparation complies with the test if not more than one of the individual contents of the 30 units is outside 85 % to 115 % of the average content and none is outside the limits of 75 % to 125 % of the average content (British Pharmacopoeia, 2015).

In this work, the uniformity of content was not measured directly in a "stand-alone" manner, but was inferred from the results of the dissolution assays. In this case, where the formulation had completely disintegrated and the drug completely dissolved, the total amount of drug within the formulation was calculated from the value at full release. Where the drug was not fully released from the formulation, the remaining formulation at the end of the dissolution experiment was tested for residual content and the overall total amount contained initially calculated. This method was used as some of the batch sizes, especially those of the 3D-printed products, were not large enough to allow for full testing of all parameters specified in the BP.

2.4.1.3 Mechanical strength

The mechanical strength of a tablet is associated with the resistance of the solid specimen to fracturing and attrition. This means the tablet must be able to stay intact during the manufacturing process, packaging, distribution and dispensing before it is administered by the patient. The most common tests to determine the mechanical strength of the tablet are crushing strength and friability test.

2.4.1.3.1 Crushing strength

The crushing strength of a tablet is usually determined by applying a force on the tablet diametrically and establishing the intensity of the force needed to fracture or break the tablet (Aulton and Taylor, 2013). The crushing strength depends on the composition of the tablets, the dimensions of the tablet, and the compression forces used to manufacture the tablet. Generally, increasing the compression force increases the crushing strength and decreases in friability of the tablets.

Due to the small size of the mini-tablets and the low forces that are required to crush them, conventional equipment used for larger tablets (e.g. a Schleuniger hardness tester) is not sensitive enough. El-Gawad et al (2012) developed a method using a texture analyser which allowed smaller forces to be measured accurately and that method was used here. A mini-tablet is placed on the fixed platform of the texture analyser and a probe descends vertically to the tablet, making contact and continuing to move downwards. The force required to break the mini-tablet is then recorded. A TA.XT plus Texture Analyzer (Stable Micro Systems, UK) was used with a 11.6 mm diameter Perspex cylinder probe The experimental set-up is shown in ***Figure 2.25*** and the experimental parameters listed below. Ten individual mini-tablets from each batch were tested.

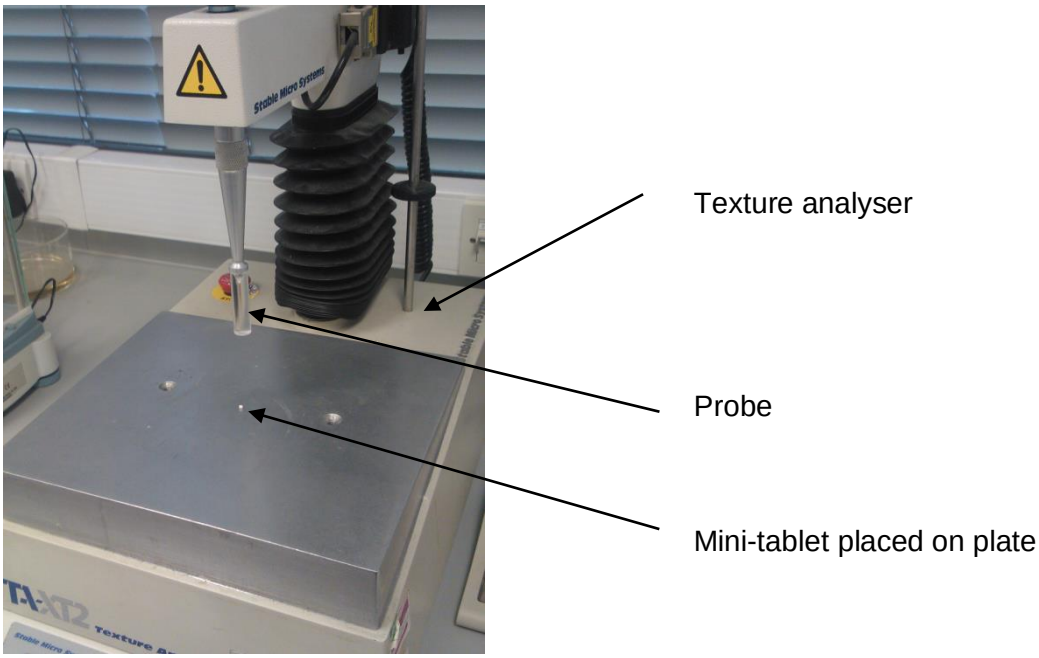

Figure 2.25 *The texture analyser set up used to measure the crushing strength of the mini-tablets (photo courtesy of Dr Joanne Peacock).*

The instrument parameters for testing the crushing strength of the mini-tablets.

Probe	11 mm diameter cylindrical Perspex probe
Pre-test speed	1 mm/s
Test speed	0.1 mm/s
Post-test speed	1 mm/s
Compression distance	1 mm
Trigger force	0.05 N

2.4.1.3.2 Friability

The reason behind the friability test is to subject the tablet to forces mimicking the conditions during handling between its production and administration, such as film-coating and packaging. It is important that the tablet is capable of resisting attrition to ensure the

correct amount of drug is administered and to maintain the tablet appearance (Aulton and Taylor, 2013).

The friability (*F*) of the mini-tablets was determined following method used by El-Gawad et al. (2012) by subjecting 10 tablets weighted together to falling shocks for 100 revolutions at 25 rpm in a friabilator. The mini-tablets are dusted off and re-weighed, and the percentage friability is calculated, using the following equation:

$$F(\%) = \left(\frac{P-P'}{P}\right) \times 100 \qquad \text{Eq. 2.1}$$

where *P* is the initial weight of 10 mini-tablets and *P'* is the final weight after the friability test (Weyenberg et al., 2003).

2.4.1.4 Sample dimensions

For the measurement of the mini-tablets dimensions, 10 mini-tablets were chosen randomly from each formulation. The dimensions of the mini-tablets were measured using a digital calliper. The mean value and standard deviation were then calculated. The digital calliper was also used to measure the inserts' dimensions. 10 inserts were randomly chosen from each formulation. The width, height, depth and thickness of the inserts were measured and the mean and standard deviation were calculated.

The surface area of the inserts was calculated using Netfabb (2016). The software is designed to be used to edit, repair and analyse .STL format files. The 3D design file for the inserts was opened using this software. The inserts' dimensions are displayed at the right bottom corner of the screen with the calculated volume and surface area values, as shows in ***Figure 2.26***.

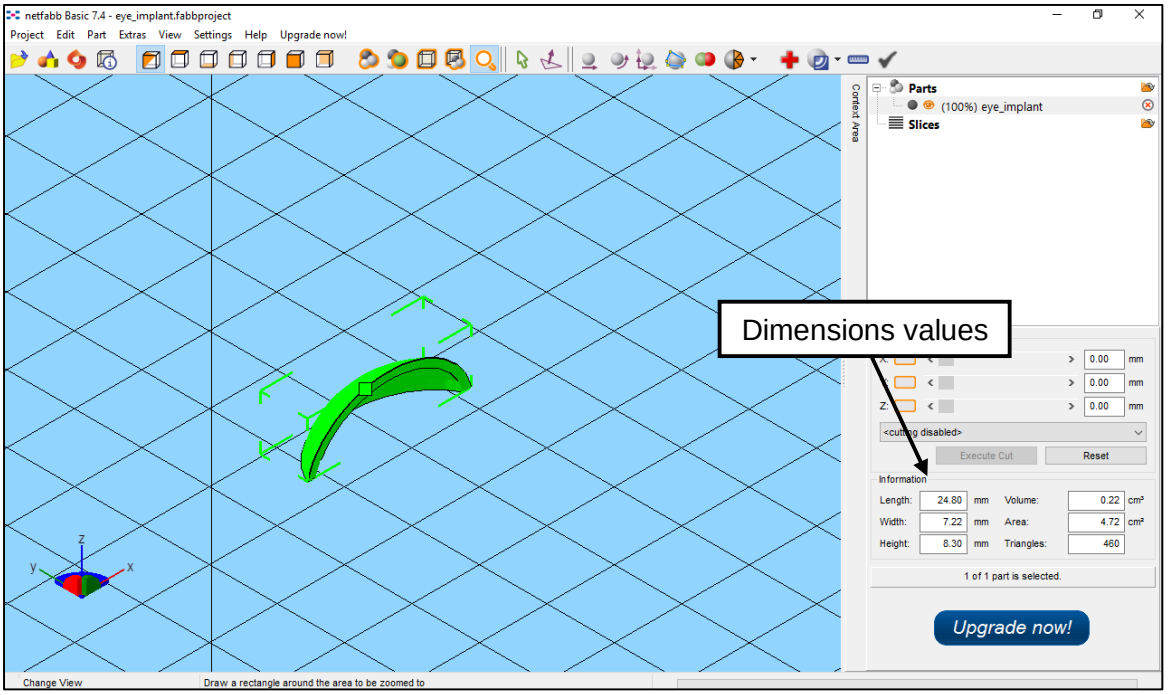

Figure 2.26 *Dimensions values on the Netfabb software.*

The surface areas of the inserts were calculated using this software, by editing the inserts' dimension based on the actual width, height and depth measurements in the "scale parts" windows. These windows are opened by clicking at the "scale parts" icon, as shown in ***Figure 2.27***. The surface area values will be automatically calculated based on the measurement values that were changed. 10 surface area measurements were recorded and the mean and standard deviation values were calculated.

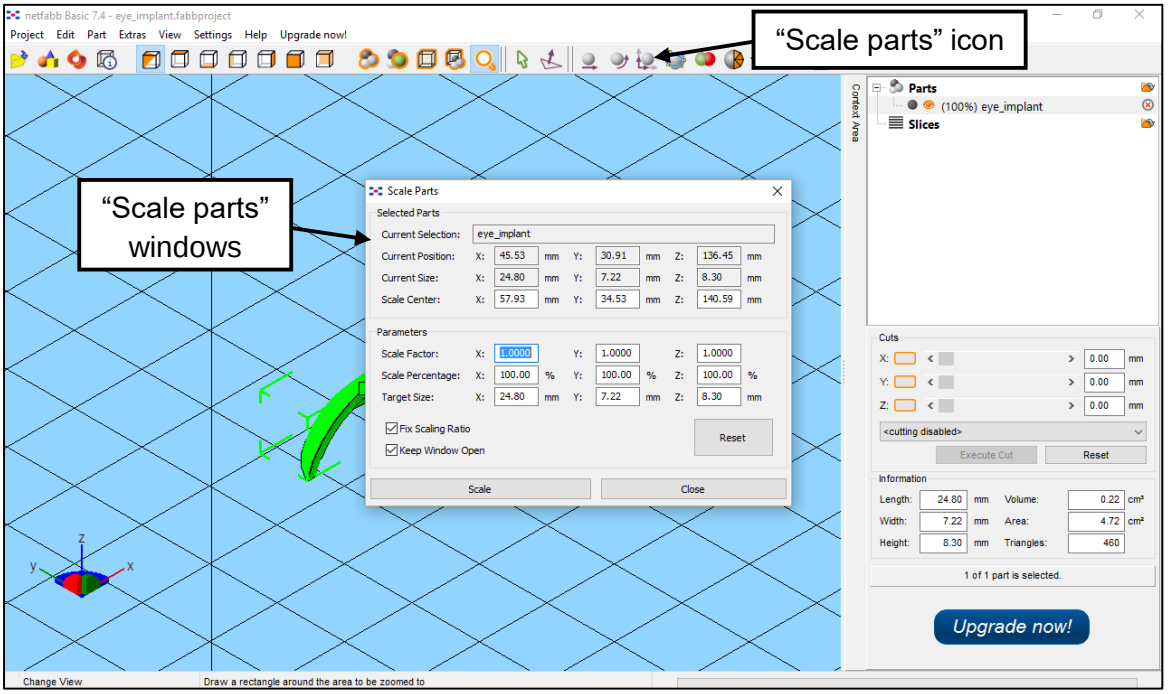

Figure 2.27 *"Scale parts" icon and windows.*

2.4.1.5 Water/moisture uptake

The amount of water uptake of the mini-tablets is determined at room temperature, gravimetrically. The weight of the mini-tablet is determined at a set of time intervals until the weight of tablet remained unchanged or even reduced. The percentage of water uptake (*W*%) is calculate using the following equation:

$$W(\%)=\left(\frac{M_w-M_d}{M_d}\right)\times 100 \qquad \text{Eq. 2.2}$$

where M_d is the initial weight of the dry mini-tablet and M_w is the final weight of the wet mini-tablet (Weyenberg et al., 2003).

The water uptake test for mini-tablets that been used previously by other researchers is performed by placing a weighed mini-tablet on top of a filter membrane connected to a

liquid reservoir on its lower side (Weyenberg et al., 2005, Mortazavi et al., 2010, El-Gawad et al., 2012). At certain time intervals, the mini-tablet is then removed, re-weighed and replaced on the membrane to continue the experiment. This process is subject to experimental errors due to the difficulty of handling the wet mini-tablets. The application of dynamic vapour sorption (DVS) was proposed to replace the previous water uptake test.

For the moisture uptake profile of the mini-tablets, the DVS was set at a fixed high humidity (95.0 ± 1.0 % RH) and left up to 24 hours. The DVS was set as half-cycle with method details as below:

dm/dt (%/min)	0.001
Incubator (°C)	32.0
Start RH (%)	95.0
dm/dt window (min)	5
Minimum stage time (min)	60
Maximum stage time (min)	1440

Water vapour was used to control the humidity level in the chamber. The temperature was set at 32 ± 1 °C based on previous set up used on the equipment. It is slightly lower than eye surface temperature (34 °C) but still closely resembles the temperature. The weight changes was recorded every minutes. The system was set to stop recording the readings after 24 hours (1440 minutes) of run or until there is no difference in weight changes for 5 minutes (dm/dt). The test was replicated three times for each formulation.

2.4.2 Thermogravimetric Analysis

Thermogravimetric analysis (TGA) is a technique whereby the weight of a sample is continually measured as it is heated. The weight loss-temperature profile can be used to assess the quantity of residual solvents, the presence of volatile materials or the chemical

reactions of the materials in air. Here, the water content in selected samples was measured by using a Hi-Res TGA 2950 (TA Instruments, USA). The TGA was equilibrated at 25 °C, heated up to 110 °C at 10 °C/min and held isothermally for 5 minutes. The percentage of water loss was then calculated based on the weight change.

2.4.3 Modulated Temperature Differential Scanning Calorimetry

Differential Scanning Calorimetry (DSC) is a common thermal analysis technique and has been used extensively to characterise pharmaceutical systems. It involves the application of a linear heating signal to a sample and a reference (generally a matched empty cell) and the measurement of the energy changes over a transition, such as melting or a glass transition. Modulated Temperature DSC (MTDSC) is an extension of the conventional DSC technique whereby a sinusoidal heating ramp is applied on top of the linear heating signal. This allows the measurement signal to be split into two components, the reversing and non-reversing signals, which then allows finer resolution of low energy transitions such as the glass transition.

In this study, MTDSC was performed using a DSC Q1000 (TA Instruments, USA) over a range of temperature, depending on the materials. The instrument was calibrated based on the manufacturer's recommendation. The temperature calibration was performed using three different materials: indium (melting point 156.6°C and heat of fusion 28.57 J/g), tin melting point 231.93°C and heat of fusion 60.6 J/g) and n-octadecane melting temperature 28.24°C and heat of fusion 238.76 J/g) (values supplied by TA instruments (USA). The cell constant was calculated using indium. The heat capacity in the modulated mode was calibrated with an aluminium oxide (sapphire) disc. The heating rate was set at 2 °C/minute, 40 seconds for modulation period and 0.212 °C for the amplitude.

The sample was weighed and sealed in a pinholed aluminium pan (Perkin Elmer). Pinholed pans were chosen in order to allow the removal of liberated moisture from the sample, which might otherwise influence the analysis, especially of the glass transition process. A purge gas and carrier gas nitrogen of was used with a flow rate of 50 mL/minute and 150 mL/minute, respectively. The sampling interval was set up at every 0.10 second per point. An oscillation amplitude of 0.212 °C with a period of 40 seconds was used with heating rate at 2 °C/minute.

2.4.4 Scanning Electron Microscopy

Scanning Electron Microscopy (SEM) is an imaging technique which is used extensively to assess the size and surface appearance of samples, both pharmaceutical and non-pharmaceutical. It is best used for solid samples that are resistant to the treatment with gold coating which is required in order to obtain a high quality image.

The surface image of mini-tablets was evaluated by using FEI™ Quanta 200F field emission scanning electron microscopy (SEM) (FEI Company, USA). The samples were attached directly on the specimen stub using double-sided tape and coated with 25 nm of gold under vacuum using a Quorum Q150T Turbo-Pumped Sputter Coater with a film thickness monitor unit. All micrographs were taken at acceleration voltage of 5 kV. Several images from difference magnifying images were recorded.

2.4.5 Transition Temperature Microscopy

Transition Temperature Microscopy (TTM) is an automated technique which measures the thermal behaviour at specific locations on the surface of a sample. A probe makes contact with the sample's surface and is heated, resulting in localised heating in the sample. When the sample goes through a thermal transition (e.g. melting or glass transition), the surface will soften and the probe will penetrate into the sample. It is this probe deflection which is measured by the equipment. By performing multiple measurements over a pre-determined

grid, a map of the transitions across the sample can be made, which can then be used to assess the distribution of materials across the sample's surface.

The probe needs to be calibrated before any measurements can be made on the sample surface. This is carried out by measurement of the transition voltage of calibration samples that are homogenous with a range of melting temperatures and exhibits sharp melting points. Polycaprolactone, polyethylene and polyethylene terephthalate with melting points of 55°C, 116°C and 235°C, respectively, were used as calibration samples. At least three measurements were taken for each sample. The calibration was analysed by using Analysis Studio software, as shows in ***Figure 2.28***. A quadratic curve was fitted to the data to quantify the voltage applied to the probe into temperature.

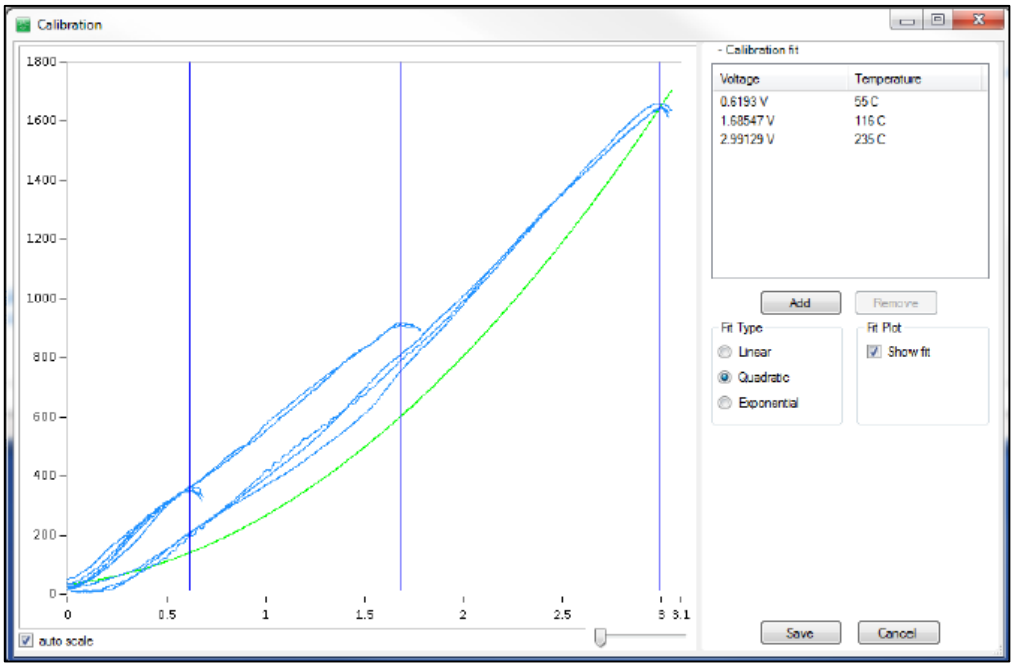

Figure 2.28 *Calibration windows from Analysis Studio software.*

After the calibration was performed, the sample was glued onto the specimen disc and placed at the centre of the platform. The TTM head was lowered down carefully and the surface image was focussed by using brightfield optical microscope. The probe tip then was aligned to the centre of the image. The measurement was carried out over an area of 100 × 100 µm with 11 × 11 grid of measurements on desired surface areas, as shows in ***Figure 2.29***.

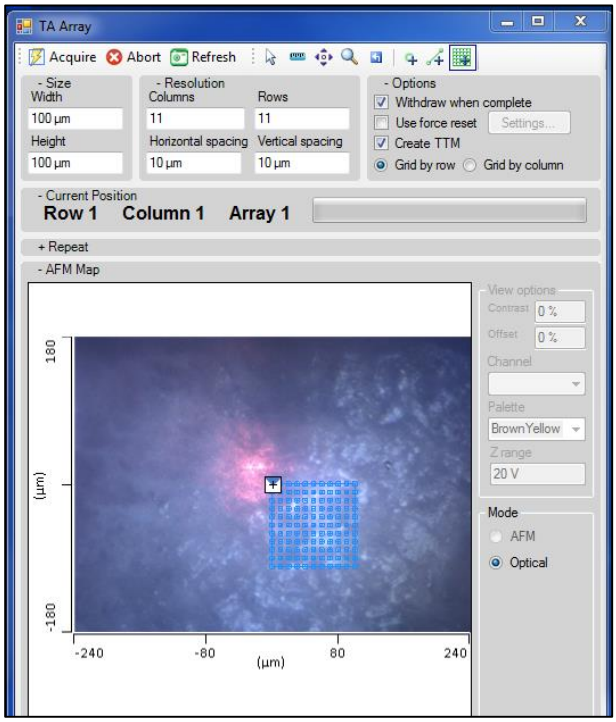

Figure 2.29 *Measurement area of 100 × 100 µm with 11 × 11 grid on the sample surface.*

2.5 DISSOLUTION STUDIES

Dissolution studies play an important role in drug development as a quality control to investigate drug release from a dosage form. Dissolution profiling is also used to predict how the formulation will perform *in-vivo* (Fotaki, 2011). There are four different types of dissolution test that have been suggested by the British Pharmacopoiea (2015) which are the basket apparatus (apparatus 1), the paddle apparatus (apparatus 2), the reciprocating cylinder (apparatus 3) and the flow-through cell (apparatus 4). In this chapter, only the flow-through cell test will be discussed as this is the only dissolution technique that been applied in this current study.

2.5.1 Dissolution Theory

Dissolution is a process where molecules or ions are transferred from a solid state into solution. This process is controlled by the relative affinity between the molecules of the solid substance and those of the solvent (Aulton and Taylor, 2013). In other words, it is the process of a solute dispersing in a solvent by forming a homogeneous dispersion at molecular-level known as a solution (Smith, 2015). There are different types of solutions based on combinations of gas, liquid and solid. However, in this chapter, only solid-in-liquid solution will be discussed as the current studies only focus on dissolution of mini-tablets (solid) in dissolution media (liquid).

In general, the solid-in-liquid dissolution is the movement from the largest form to molecularly dispersed form with no or few steps in the middle of the process as shows in ***Figure 2.30***. The intermediate process that might occur is disintegration and deaggregation process.

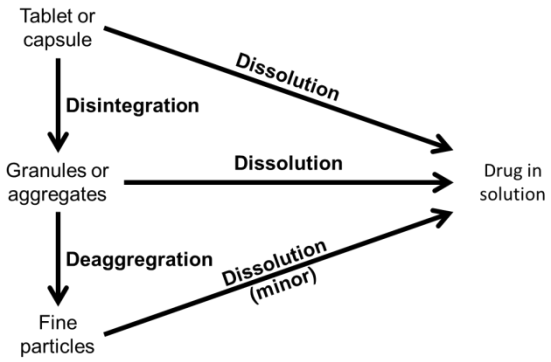

Figure 2.30 *Solid-in-liquid dissolution process (Smith, 2015).*

The rate of drug diffusion can be described by Fick's Law of Diffusion. The law states that the rate of change in concentration of dissolved material with time is directly proportional to the concentration difference between the two sides of the diffusion layer (Aulton and Taylor, 2013) as shown below:

$$\frac{dC}{dt} = k\Delta C \qquad \text{Eq. 2.3}$$

where C is the concentration of solute in solution at any point and at time (t), k is the rate constant and ΔC is the difference in concentration of solution at the solid surface and the bulk of the solution.

2.5.2 Preparation of Dissolution Media

Acidic solutions, buffers, surfactants and combination of surfactants with acid or buffers are common dissolution media used for dissolution studies. Meanwhile, for *in-vitro* and *in-vivo* correlation studies, media with bile salts and other relevant physiologically based ingredients are used (Fotaki et al., 2013). These media, also known as simulated biological fluids, are often used to give a better understanding of the release mechanisms in living organisms.

For ocular treatment, simulated tear fluid (STF) is used as the dissolution medium. This medium consists of sodium bicarbonate 0.2% (w/w), calcium chloride 0.008% (w/w) and sodium chloride 0.67% (w/w) at pH 7.4. (Marques et al., 2011). This formulation of STF is commonly used in *in-vitro* studies of drug release from ocular formulations (e.g. El-Gawad et al, 2012), and hence was used here for consistency, but it must be noted that this formulation replicates only the mineral content and pH of biological tears, and not any protein or lipid content that may be expected to be present.

2.5.3 Dissolution Method

The drug release profile of the mini-tablets was assessed by using a modified flow-through dissolution apparatus, based on the flow-through cell (apparatus 4) guideline from the British Pharmacopoiea (2015). The flow-through dissolution apparatus used was courtesy of Professor Steve Brocchini's group. A casket with a 200 µL chamber was connected to the peristaltic pump and flowed with dissolution medium at 34 °C at the rate of 50 µL/minute, as shown in ***Figure 2.31***. The samples were taken every 1 hour and filtered through a 0.45 µm membrane filter. The drug release was quantified spectrophotometrically at 278 nm. At least three replicates were made for each formulation.

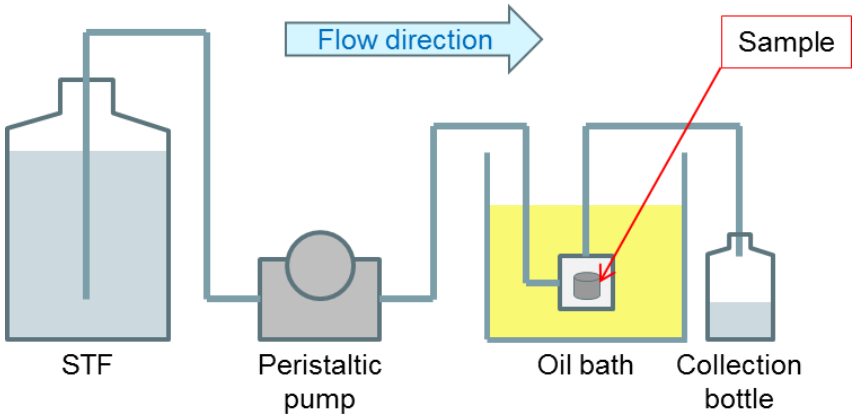

Figure 2.31 *Diagram of modified flow-through dissolution apparatus.*

2.5.4 Ultraviolet/visible Spectrophotometer

Ultraviolet/visible (UV/Vis) spectrophotometry refers to absorbance or reflectance spectroscopy in the ultraviolet (UV) and visible regions. The wavelength range of the UV region is between 200 and 400 nm, and is 400 to 800 nm for the visible region (Perkampus et al., 2013). The molecular absorbance in these regions arises from the energy transitions that involve the outer orbital or valency electrons (Cooper and Negrusz, 2013). The Beer-Lambert Law is used to quantify the light absorbance by a solution, which can be explained based on the following equation (Watson, 2012):

$$Absorbance\ (A) = log\frac{I_0}{I_t} = \varepsilon bc \qquad \text{Eq. 2.4}$$

where I_0 is the intensity of incident radiation, I_t is the intensity of transmitted radiation, ε is the molar absorbance coefficient of the analyte, b is the pathlength of the cell and c is the concentration of the analyte. A Jenway 6305 uv/vis spectrophotometer (UK) was used to quantify chloramphenicol content from the samples. Each sample was scanned at 278 nm wavelength, maximum absorbance (λ_{max}) for chloramphenicol (Tuerk et al., 2006, Hummert et al., 1995).

A calibration curve graph was constructed by plotting absorbance at 278 nm against chloramphenicol standard concentrations at 0.05, 0.025, 0.01, 0.005 and 0.001 mg/mL. The standard concentrations were prepared from a stock solution which was the highest standard concentration. The stock solution was made by accurately weighing chloramphenicol and making a solution in STF in a 100 mL volumetric flask.

The standard solutions were then prepared by diluting the stock solution into lower concentration standards solutions based on following equation:

$$M_1V_1 = M_2V_2 \qquad \text{Eq. 2.5}$$

where M_1 and M_2 indicate initial and final concentration, while V_1 and V_2 is the initial and final volume, respectively.

Three separate sets of calibration standard solutions were prepared and analysed. ***Figure 2.32*** and ***Table 2.12*** shows the data for individual replicates, and ***Figure 2.33*** and ***Table 2.13*** shows the overall mean responses.

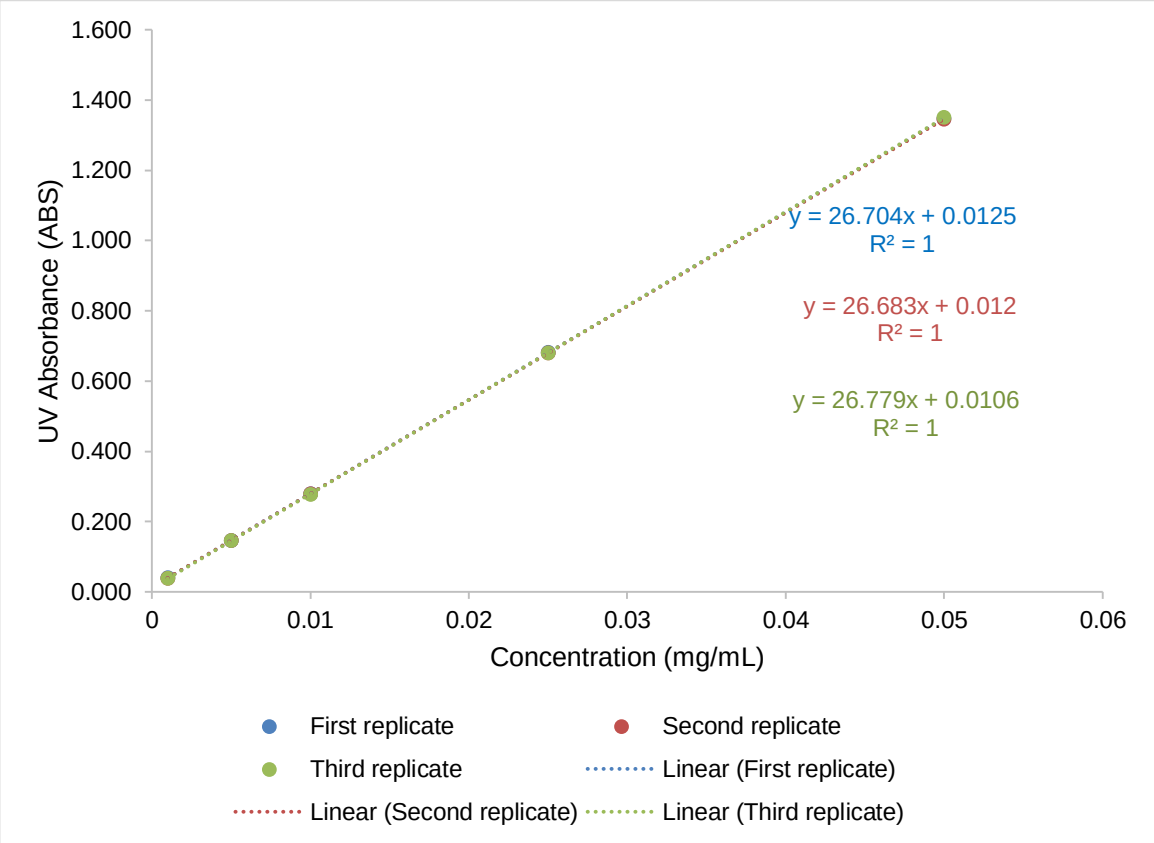

Figure 2.32 *Calibration curve of the absorbance of chloramphenicol in STF at 278 nm (mean ± SD, n=3 for each replicate set of solutions).*

Table 2.12 *Absorbance of chloramphenicol in STF at 278 nm - individual readings from the three replicate sets of standards.*

Conc. (mg/mL)	UV Absorbance (ABS)			Mean (ABS)	SD
	1	2	3		
0.05	1.347	1.347	1.348	1.347	0.001
	1.345	1.346	1.346	1.346	0.001
	1.350	1.350	1.350	1.350	0.000
0.025	0.681	0.682	0.680	0.681	0.001
	0.681	0.681	0.679	0.680	0.001
	0.679	0.680	0.680	0.680	0.001
0.01	0.279	0.279	0.278	0.279	0.001
	0.279	0.277	0.278	0.278	0.001
	0.278	0.276	0.275	0.276	0.002
0.005	0.148	0.145	0.145	0.146	0.002
	0.146	0.147	0.146	0.146	0.001
	0.146	0.144	0.145	0.145	0.001
0.001	0.040	0.038	0.040	0.039	0.001
	0.038	0.039	0.037	0.038	0.001
	0.037	0.039	0.040	0.039	0.002

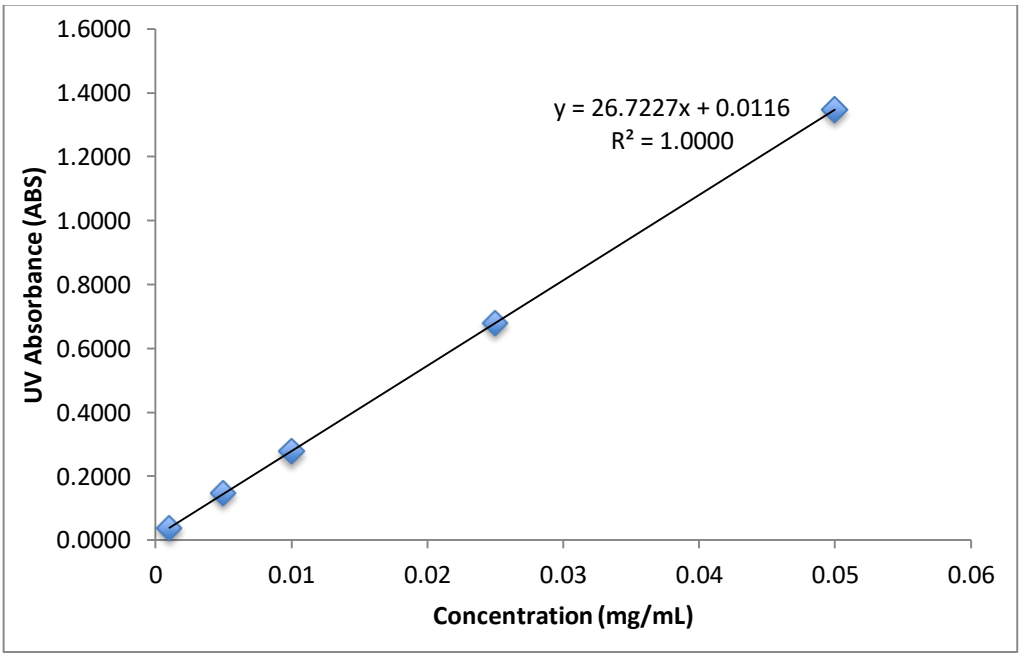

Figure 2.33 *Calibration curve of the absorbance of chloramphenicol in STF at 278 nm (overall mean ± SD, n=3).*

Table 2.13 *Absorbance of chloramphenicol in STF at 278 nm - overall mean values for each concentration.*

Conc. (mg/mL)	UV Absorbance (ABS)			Mean (ABS)	SD
	1	2	3		
0.050	1.347	1.346	1.350	1.348	0.002
0.025	0.681	0.680	0.680	0.680	0.001
0.010	0.279	0.278	0.276	0.278	0.002
0.005	0.146	0.146	0.145	0.146	0.001
0.001	0.039	0.038	0.039	0.039	0.001

The regression value (r^2) is a value between 1.0 and -1.0 where a 1.0 value indicates that all points lie on straight line with no scatter with positive gradient, while -1.0 gives the same information but negative gradient. A zero value means there is no connection between the set of data. The calibration curves for each replicate in ***Figure 2.32*** were overlapping with each other, suggesting the results are reproducible. The error bars for all graphs could not be seen because they are too small.

2.6 MATHEMATICAL MODELLING

2.6.1 Zero Order Kinetics

Zero order kinetics is the rate of a deposition, dissolution or drug release process that takes place at a constant rate independent of the reactants' concentration. This constant rate of drug release is usually the most desirable for controlled-release pharmaceutical products, as a constant input of drug into the body is achieved (Aulton and Taylor, 2013). Zero order kinetics can be calculated by using equation below:

$$Q_t = Q_0 + k_0 t \qquad \text{Eq. 2.6}$$

where Q_t is the amount of drug dissolved in time (t), Q_0 is the initial amount of drug in the

solution (usually 0 for a dissolution test) and k_0 is the release rate kinetic constant expressed in units of concentration/time. With zero order kinetics, the drug release profiles are usually analysed up to 85 % of drug release (Costa and Sousa Lobo, 2001).

2.6.2 First Order Kinetics

First order kinetics describe a process that depends on the concentration of only one reactant. Most of the drug release profiles of conventional formulations follow first order kinetics (Aulton and Taylor, 2013). First order kinetics can be expressed by using following equation:

$$ln\ C_t = ln\ C_0 + k_1 t \qquad \text{Eq. 2.7}$$

For first-order release kinetics, C_0 is the amount of drug in the formulation at the start of the dissolution experiment (usually taken to be 100 %), C_t is the amount of drug remaining in the formulation at time t during the dissolution experiment, and k_1 is the first-order release rate kinetic constant expressed in units of time^{-1}. As with zero order, first order processes are usually analysed up to 85 % of drug release (Costa and Sousa Lobo, 2001).

2.6.3 Korsmeyer-Peppas Model

The Korsmeyer-Peppas Model was developed by Korsmeyer et al. (1983) to statistically determine the mechanisms of solute release from porous hydrophilic polymers. The model can be used to analyse Fickian and non-Fickian release profile. Below is the Korsmeyer-Peppas model equation:

$$\frac{M_t}{M_\infty} = k_{KP} t^n \qquad \text{Eq. 2.8}$$

where M_t / M_∞ is the fraction of drug release at time t, k_{KP} is a kinetic constant characteristic

of the drug/polymer system, *t* is the release time and *n* is an exponent which characterizes the mechanism of release.

The values were analysed from the first 60 % of the fractional release. This is because the fractional release profile is nearly constant within this period (Korsmeyer et al., 1983, Ritger and Peppas, 1987). Korsmeyer et al. (1983) suggested that the *n* value can be used to characterise the different release mechanisms; *n* equal to 0.5 for Fickian diffusion, higher than 0.5 but lower than 1.0 for anomalous (non-Fickian) diffusion and equal to 1.0 for Case II transport (zero order release). However, according to Ritger and Peppas (1987), in case of a cylindrical swellable polymer, *n* value should be 0.45 instead of 0.5 and 0.89 instead of 1.0. ***Table 2.13*** showed the summary of diffusional exponent mechanisms for cylindrical sample.

Table 2.14 *Diffusional exponent mechanism for cylindrical sample (Ritger and Peppas, 1987, Costa and Sousa Lobo, 2001).*

Diffusional exponent (*n*)	**Drug release mechanism**	**Time-dependence of solute release rate**
0.45	Fickian diffusion	$t^{-0.5}$
$0.45 < n < 0.89$	Anomalous (non-Fickian) diffusion	t^{n-1}
0.89	Case II transport	Zero order release
$n > 0.89$	Super Case II transport	t^{n-1}

2.6.4 Fit Factors

Fit factors were determined by using two equations to compare the dissolution profiles between two formulations. These equations were proposed by Moore and Flanner (1996). The equations were difference factor (f_1) and similarity factor (f_2).

The difference factor (f_1) measures the percentage error between two curves over all time points:

$$f_1 = \frac{\sum_{j=1}^{n} |R_j - T_j|}{\sum_{j=1}^{n} R_j} \times 100 \qquad \text{Eq. 2.9}$$

where n is the sampling number, Rj and T_j are the percentage dissolved of the reference and test products respectively at each time point j. The percentage error is zero when the test and drug reference profiles are identical and increases proportionally with the dissimilarity between the two dissolution profiles.

Similarity between two drug products can be defined by f_2 taking values between 50 and 100, where f_2 equals 100 for identical dissolution profiles. The similarity factor f_2 is defined as a logarithmic reciprocal square root transformation of one plus the average squared differences of drug percentage dissolved between the test and the reference products. An average difference of 10% at all measured time point results in f_2 value of 50 (Anderson et al., 1998, Khan et al., 2013). The value of f_2 can be calculated as follows:

$$f_2 = 50 \times \log\left\{\left[1 + \frac{1}{n}\sum_{j=1}^{n} w_j |R_j - T_j|^2\right]^{-0.5}\right\} \times 100 \qquad \text{Eq. 2.10}$$

where Rj and T_j represent the average percentage of drug dissolved from the mini-tablets measured at the j^{th} time point of the reference and the test preparations respectively. n is the number of the time points tested (n is considered in the calculations as not more than one measurement after 85% of drug released in the preparation) and w_j is an optional weight factor.

Chapter 3

The Effect of Particle Size on the Physical Characteristics and Drug-release Behaviour of Chloramphenicol-loaded Mini-tablets for Ocular Use

The Effect of Particle Size on the Physical Characteristics and Drug-release Behaviour of Chloramphenicol-loaded Mini-tablets for Ocular Use

3.1 INTRODUCTION

Ocular drug delivery is challenging because of the inherent difficulty of accessing the target sites, especially those in the posterior segment of the eye. The natural defense mechanisms, such as the constant turnover of the tear film on the surface of the eye and the blink reflex, reduce the amount of drug that is therapeutically available after surface administration. Eye drops have continued to be used as the main vehicle for ocular therapy due to their perceived patient acceptance, despite the disadvantages of fast removal and low overall drug bioavailability.

One of the potential methods of improving the retention time at the site of administration and hence promoting the efficiency of drug therapy is ocular mini-tablets. Mini-tablets have a diameter of around 2 to 3 mm or smaller (Lennartz and Mielck, 1998) and a total weight of circa 6 to 21 mg in range (Stoltenberg and Breitkreutz, 2011, Thomson et al., 2009). They can be inserted into the eye fornix, where they will hydrate and release the drug into the surface ocular fluid (Weyenberg et al., 2006).

Formulation and production of mini-tablets is similar to conventionally-sized tablets, but there are specific issues related to the control of the particle size distribution of the component powders that are much more significant for mini-tablets than larger tablets. During the manufacturing process, if the particle size is too large, only a few particles can fit in the die, which is likely to result in uneven mini-tablet weight and consequently poor content uniformity of the active drug. However, if the particle size is too small, the powder will pass through the gap between the die and punch, as shown in ***Figure 3.1***. In most tablet formulations the drug has the smallest particle size compared to the excipients and

therefore is more likely to be lost in this way, resulting in low drug loading in the final product.

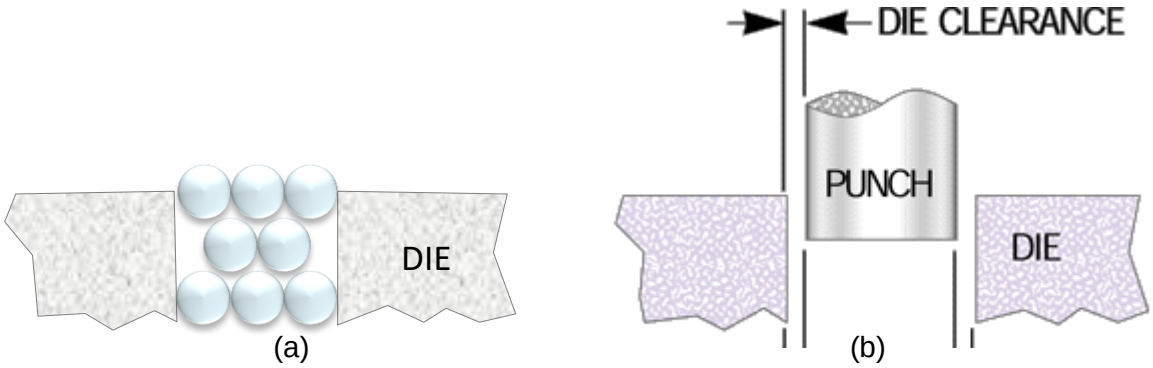

Figure 3.1 *Schematic of (a) large particles in the die; and (b) the gap between the punch and the die (die clearance).*

Particle size is also inversely correlated with surface area, in that the smaller the particle size of the drug, the larger the total surface area and vice versa. Depending on the aqueous solubility of the drug, altering the particle size distribution may subsequently affect the drug release profile of the mini-tablets. Less attention is usually focused on the effect on the overall product behaviour of the particle size distribution of the excipients used, such as their mixing and flow properties.

This work investigates the effect of excipient particle size on the physical behaviour and drug release characteristics of mini-tablets for intended for ocular use. Chloramphenicol, an antibiotic routinely used to treat surface ocular infections, was used here as the model drug. The formulations studied were direct compression mixtures in order to ensure that it was the primary particle size distribution that was being studied.

3.2 METHODOLOGY

3.2.1 Materials

Hydroxypropyl methylcellulose K4M (HPMC) was obtained from The DOW Chemical Company, USA. Polyethylene glycol 6000 (PEG 6K) was obtained from Clariant GmbH, Germany. Microcrystalline cellulose (Avicel PH101™) (MCC) was provided by FMC BioPolymer, UK. Polyvinylpyrrolidone 90F (Kollidon 90F™) (PVP 90F) was provided by BASF The Chemical Company, Germany. Polyethylene oxide 8,000,000 (PEO 8M), chloramphenicol, sodium bicarbonate and calcium chloride were obtained from Sigma Aldrich, U.K. Sodium chloride was obtained from Fluka Chemie GmbH, Germany. Sodium stearyl fumarate (SSF) was obtained from Tokyo Chemical Industry, Japan. Carbopol 974P was provided by Lubrizol, USA.

3.2.2 Methods

3.2.2.1 Manufacture of the mini-tablets

A range of mini-tablets was prepared using two general formulae. ***Formula 1*** consisted of chloramphenicol 5 %w/w, Carbopol 974P 15 %w/w, SSF 2 %w/w and polymer 78 %w/w. For ***Formula 2***, chloramphenicol 5 %w/w, SSF 2 %w/w and polymer 93 %w/w were used. For ***Formula 1***, HPMC, PEG 6K and MCC were used. These polymers were selected to give a range of dissolution profiles in the final formulations. The addition of Carbopol 974P in the formulation was to increase the viscosity of the dissolving mini-tablets in the dissolution medium and possibly influence the dispersion of MCC which is a water insoluble polymer. 5 %w/w of chloramphenicol was used in the formulation, as explained in Chapter 1, because the ocular mini-tablets is a slow-release system that needs to be applied once a day, unlike eye drops that need to be reapplied several times a day. The

Carbopol 974P percentage (15 %) was chosen based on a previous study done by Weyenberg et al. (2006). The percentage of SSF (2 %) in the formulation is commonly used in tableting process (Aulton and Taylor, 2013). Meanwhile, HPMC, PEG 6K, PVP 90F and PEO 8M were used for ***Formula 2***. Carbopol 974P was removed because all polymers used in the in this formulation were water soluble polymers. For each polymer, two sieve fractions were assessed: 125 to 180 µm and 180 to 250 µm. The powders (except the lubricant) were mixed using a Turbula mixer for 10 minutes, and then lubricated with SSF in the same mixer for another 5 minutes. Mini-tablets were prepared by compression using an instrumented 4 station Riva Piccola rotary tablet press (Riva, Argentina) with 2 mm normal concave plain punches (B tooling) at a compression force of 1.8 ± 0.2 kN. Only one set of tooling was used during the process. For each formulation, one batch of circa 100 mini-tablets was manufactured.

3.2.2.2 Physical characterisation of the mini-tablets

3.2.2.2.1 Weight uniformity

The weight uniformity of the mini-tablets was assessed following the British Pharmacopoiea (2015) method. Twenty tablets from each formulation were weighed individually and the mean and standard deviation were determined.

3.2.2.2.2 Measurement of mini-tablet dimensions

Ten tablets were selected randomly from each batch and their thickness (curved surface to curved surface) was measured using a digital calliper (Mitotoyo, Japan). The diameter was assumed to be constant at 2 mm, as this was determined by the use of the 2 mm punches.

3.2.2.2.3 Friability

The friability or *F(%)* of the mini-tablets were assessed as described in Chapter 2. Ten

tablets were weighed as a unit and placed in the drum of a friability tester (Copley Scientific, UK). The drum was rotated for 100 revolutions at 25 rpm. Any loose dust from the tablets was removed and the tablets then re-weighed as a unit to calculate the % friability using following equation:

$$F(\%)=\left(\frac{P-P'}{P}\right)\times 100 \qquad \text{Eq. 3.1}$$

where *P* is the initial weight and *P'* is the final weight of the tablets.

3.2.2.2.4 Crushing strength

The crushing strength of ten randomly-selected mini-tablets was assessed using a TA.TX2 texture analyser (Stable Microsystems Ltd, UK) following the method of El-Gawad et al. (2012) and as described in detail in **Chapter 2**.

3.2.2.2.5 Moisture uptake

The moisture uptake profile of the mini-tablets was measured over 24 hours using a dynamic vapour sorption (DVS) method (Surface Measurement Systems, UK) at fixed high humidity (95 ± 1 % RH) as described in detail in **Chapter 2**. This method was proposed to replace water uptake tests that have been used previously by other researchers (Weyenberg et al., 2005, Mortazavi et al., 2010, El-Gawad et al., 2012). The test was replicated at least three times for each formulation.

3.2.2.2.6 Surface analysis

The surface quality of the mini-tablets was evaluated by using FEI™ Quanta 200F field emission scanning electron microscopy (SEM) (FEI Company, USA). The samples were coated with 25 nm of gold under vacuum condition using a Quorum Q150T Turbo-Pumped

Sputter Coater with a film thickness monitor unit, as explained in more detail in **Chapter 2**.

The transition temperature of the mini-tablet's surface was mapped by using a VESTA instrument supplied by Anasys Instruments (USA), which is equipped with an AN-200 Therma-Lever™ micromachined silicon probe. The measurement was carried out over an area of 100 × 100 µm with 11 × 11 grid of measurements. Further details on this technique are explained in **Chapter 2**.

3.2.2.3 Drug release profile

The drug release profile of the mini-tablets was assessed using a modified flow-through dissolution apparatus with chamber size 200 µL and flow rate 50 µL/minute as described fully in **Chapter 2**. The dissolution medium used was simulated tear fluid (STF), consisting of an aqueous solution of sodium bicarbonate 0.2 %w/w, calcium chloride 0.008 %w/w and sodium chloride 0.67 %w/w at pH 7.4 (Marques et al., 2011). The outflow of the apparatus was collected in 1-hour time blocks, such that 3 mL of sample was available for analysis at each time point. The drug content in these samples was quantified spectrophotometrically at 278 nm. The study continued for 9 hours, measuring the amount released every hour. For samples which had reached maximum drug release at 9 hours, no further analysis was performed and the 9-hour cumulative amount released was taken to be the 100 % level and used to calculate the percentage drug release at each of the earlier timepoints. However, for those samples whereby drug release was not complete at 9 hours, the total amount of drug in the mini-tablet was estimated by reference to the drug content of a random sample of mini-tablets from the same batch. This was measured by dissolving a mini-tablet in STF and making the solution up to 10 mL with STF, and measuring the drug content spectrophotometrically at 278 nm. It was not possible to collect the residual tablet from the flow-through dissolution chamber in order to assess the undissolved drug content, as it had formed a viscous gel during the dissolution process,

making extraction and quantification difficult. At least three replicates were performed for each formulation.

3.2.2.4 Mathematical modelling of the dissolution profiles

The dissolution profiles generated in this study were analysed by fitting them to the zero order, first order and Korsmeyer-Peppas kinetic equations. Additionally, the dissolution profiles were compared holistically using the f_1 difference and f_2 similarity factors. The mathematical analysis is described in **Chapter 2**.

3.3. RESULTS AND DISCUSSION

3.3.1 Physical characterisation of *Formula 1* mini-tablets

The purpose of physical characterisation is to determine the physical properties of the mini-tablets and, in this case, to assess whether there was any systematic variation in these properties with the sieve fraction of the predominant polymer used in the formulation. ***Table 3.1*** shows a summary of all the physical characterisation data except the moisture uptake profile.

Table 3.1 *Summary of physical properties of* ***Formula 1*** *mini-tablets (mean ± SD).*

Polymer	Sieve Fraction (µm)	Weight (mg) (n=20)	Thickness (mm) (n=10)	Friability (%) (n=3)	Crushing Strength (N) (n=10)
HPMC	125-180	8.85 ± 1.26	2.59 ± 0.18	0.04 ± 0.07	35.2 ± 18.6
HPMC	180-250	9.22 ± 0.59	2.66 ± 0.21	0.04 ± 0.07	38.4 ± 15.6
PEG 6K	125-180	9.65 ± 0.67	2.70 ± 0.08	n/a	26.6 ± 2.6
PEG 6K	180-250	11.10 ± 0.62	3.04 ± 0.19	n/a	27.6 ± 1.2
MCC	125-180	8.70 ± 1.41	2.21 ± 0.49	0.30 ± 0.27	18.7 ± 15.2
MCC	180-250	8.34 ± 1.15	2.23 ± 0.44	0.41 ± 0.10	24.2 ± 20.7

* n/a = Not applicable.

The details of the studies regarding the physical characterisations are discussed in following sections.

3.3.1.1 Weight uniformity

The weight of the mini-tablets ranged between 8.34 ± 1.15 mg for the HPMC 125-180 µm sieve fraction and 11.10 ± 0.62 mg for the PG 6K 180-250 µm sieve fraction as shown in

Table 3.1. The British Pharmacopoeia (2015) specification for weight variation for solid products with nominal weight less than 80 mg is that a maximum of two of the twenty tablets tested have weights which are more than 10 % different from the mean value and that no tablets have weights that deviate by more than 20 % from the mean. Additionally, the BP specifies that for products with weights less than 40 mg, the test for weight uniformity does not apply and the test for content uniformity should apply instead. However, as the product weight variability is a good measure of the effectiveness of a formulation and a process in combination, this test was used here with the above specifications being applied. ***Table 3.2*** shows the weight measurements of twenty mini-tablets randomly chosen from each formulation. Black type denotes tablets that directly passed the above specification (i.e. tablets with weights showing less than 10 % deviation from the mean), red type denotes tablets that show between 10 and 20 % deviation from the mean value, and blue type denotes tablets that show greater than 20 % deviation from the mean value.

Inspection of the data shows that only the batch of mini-tablets based on the PEG 6K 180-250 µm sieve fraction passed the weight uniformity test, with 1 tablet showing greater than 10 % deviation from the mean. Its counterpart batch failed, with 3 tablets showing between 10 and 20 % deviation from the mean. These two batches of mini-tablets were also statistically different in terms of actual weight ($p < 0.05$). Mini-tablet batches made from the other two polymers were inherently more variable in terms of the individual tablets' weights, but showed no statistical difference in weight between sieve fractions ($p > 0.05$). Overall, for all three polymers, mini-tablets made from the smaller particle size powders showed greater variability than those from the larger particle size powders, as demonstrated by the RSD values.

Table 3.2 *Weight uniformity data for* ***Formula 1*** *mini-tablets.*

Mini-tablets	HPMC 125-180 µm (mg)	HPMC 180-250 µm (mg)	PEG 6K 125-180 µm (mg)	PEG 6K 180-250 µm (mg)	MCC 125-180 µm (mg)	MCC 180-250 µm (mg)
1	7.64	9.03	9.87	11.70	8.88	9.61
2	9.98	9.84	9.24	11.87	11.46	7.99
3	7.02	8.60	10.15	11.62	7.70	9.00
4	8.18	9.07	10.58	11.71	9.30	9.30
5	9.82	10.10	9.99	10.67	7.35	9.39
6	7.13	8.96	10.00	10.89	8.21	8.47
7	8.14	8.99	10.76	11.40	7.89	8.62
8	9.21	8.09	9.29	10.81	8.18	8.22
9	8.00	9.33	9.55	10.78	11.20	10.42
10	8.56	10.14	10.27	11.60	8.20	7.88
11	9.70	8.73	9.92	11.75	7.30	6.07
12	7.71	9.21	9.16	10.87	9.83	9.59
13	10.21	9.52	8.49	10.96	8.50	6.81
14	11.15	8.98	8.38	10.00	8.14	8.77
15	7.97	8.23	10.26	10.79	7.65	6.36
16	7.12	8.96	9.09	11.18	11.35	8.26
17	10.42	9.59	9.44	12.00	6.33	7.71
18	10.44	9.31	10.29	11.17	9.74	7.96
19	9.42	9.49	9.41	9.70	7.77	9.23
20	9.20	10.22	8.79	10.47	9.12	7.09
Mean (mg)	8.85	9.22	9.65	11.10	8.71	8.34
SD (mg)	1.26	0.59	0.67	0.62	1.41	1.14
RSD (%)	14.26	6.35	6.95	5.60	16.24	13.73

3.3.1.2 Thickness

There are no pharmacopoeial specifications for the thickness of tablets, either the actual value or its uniformity. However, it is a vital attribute to control as it can potentially affect the accuracy of packing of tablets into blisters or tubes. It is also indirectly related to the crushing strength of a tablet. ***Table 3.3*** shows the thickness measurements of ten mini-tablets randomly chosen from each formulation.

Table 3.3 *Thickness data for* ***Formula 1*** *mini-tablets.*

Mini-tablets	HPMC 125-180 µm (mm)	HPMC 180-250 µm (mm)	PEG 6K 125-180 µm (mm)	PEG 6K 180-250 µm (mm)	MCC 125-180 µm (mm)	MCC 180-250 µm (mm)
1	2.62	2.70	2.75	3.39	2.83	2.88
2	2.67	2.67	2.77	3.00	2.87	1.85
3	2.81	2.78	2.83	3.08	2.32	2.09
4	2.63	2.95	2.66	3.02	1.88	2.02
5	2.62	2.44	2.67	2.62	1.87	2.83
6	2.64	2.83	2.63	3.13	2.94	1.94
7	2.86	2.95	2.64	3.00	1.71	2.14
8	2.34	2.45	2.79	3.11	1.88	2.85
9	2.33	2.44	2.65	3.06	1.90	1.87
10	2.42	2.43	2.63	2.96	1.85	1.86
Mean (mm)	2.59	2.66	2.70	3.04	2.21	2.23
SD (mm)	0.18	0.21	0.08	0.19	0.49	0.44
RSD (%)	6.95	7.98	2.78	6.25	22.29	19.65

The measured thickness values ranged from 2.21 ± 0.49 mm for the MCC 125-180 µm sieve fraction to 3.04 ± 0.19 mm for the PG 6K 180-250 µm sieve fraction. No difference was observed in the thickness of the tablets based on the two sieve fractions of MCC nor

of HPMC ($p > 0.05$). A statistically significant difference ($p < 0.05$) was observed between the mini-tablets based on the two sieve fractions of PEG 6K. The variation within each batch was quite considerable and far greater than would be expected for tablets of conventional size, where an RSD value for thickness of 1 to 2 % is normal. As thickness is also directly related to the weight of the tablet, if the compression force is kept constant, these results are not surprising, given the weight variability results described above.

3.3.1.3 Crushing strength

In common with tablet thickness, there are no specific pharmacopoeial specifications for the values of the crushing strength of tablets and the measured value is dependent on the size and shape of the tablet as well as the formulation and the compression parameters used. However, it is vital that a correct value of the crushing strength is obtained: too low and the tablet will be very delicate and unable to withstand further processing or transport; too high and the dissolution profile may be adversely affected. In previous studies, the hardness values ranged between 0.67 N and 18.64 N (Weyenberg et al., 2003, Weyenberg et al., 2005), so 5 to 15 N was chosen as a target value here, as described in Chapter 1. ***Table 3.4*** shows the crushing strength measurements of ten mini-tablets randomly picked from each formulation.

HPMC mini-tablets showed the highest crushing strength values followed by PEG 6K and MCC mini-tablets respectively, for both sieve fractions. However, HPMC and MCC mini-tablets displayed great variability in their crushing strength. Although crushing strength values tend to be more variable than those of other physical characteristics (such as weight variability or thickness), this high variability is unacceptable for any pharmaceutical formulation because tablets show consistent behaviour in all aspects (Aulton and Taylor, 2013). A difference in the crushing strength may also affect the drug release profile, in that the higher the crushing strength, generally the slower the drug release (Weyenberg et al.,

2005), although the relationship should be established for each individual formulation. Typically, RSD values for tablet weights are in the order of 1 to 2 %, whereas those for thickness tend to be less than 1 % and RSD values for the hardness measurements of the same tablets tend to be in the order of 10 %. Several of the individual hardness results for the HPMC and MCC mini-tablets were extremely low. Although the individual tablet weights were not recorded prior to the crushing strength test, the tablets with the lowest crushing strength values were observed to be smaller than some of their counterparts from the same batch, so are likely to have lower resistance to crushing. This observation, taken together with the overall variability of the results for these batches of mini-tablets, suggested that these individual results were somewhat anomalous, so although they did not meet the usual statistical requirements for assessment of outliers (where the individual values should be more than 3 standard deviations from the mean), the summary data were re-calculated without these data points. If the very low results (less than 10 N) are removed from the calculations, the results are more consistent, with greater similarities seen between the two batches made from the same material.

Table 3.4 *Crushing strength data for* ***Formula 1*** *mini-tablets.*

Mini-tablets	HPMC 125-180 µm (N)	HPMC 180-250 µm (N)	PEG 6K 125-180 µm (N)	PEG 6K 180-250 µm (N)	MCC 125-180 µm (N)	MCC 180-250 µm (N)
1	3.3	58.2	24.5	27.3	15.2	29.8
2	47.6	24.9	30.6	28.4	5.4	54.6
3	25.2	20.7	26.4	28.7	9.2	28.9
4	46.7	34.7	22.4	25.0	29.7	2.5
5	50.4	48.5	25.8	27.0	37.9	2.6
6	4.2	58.2	23.8	29.3	39.1	37.9
7	56.5	26.1	29.3	28.3	4.7	56.8
8	35.5	28.3	27.9	27.3	3.6	10.3
9	40.5	26.2	26.1	27.2	6.0	3.8
10	42.4	58.2	29.0	28.0	36.2	15.0
Mean (N)	35.2	38.4	26.6	27.6	18.7	24.2
SD (N)	18.6	15.6	2.6	1.2	15.2	20.7
RSD (%)	52.88	40.62	9.85	4.36	81.23	85.50
Mean (N)	43.1	38.4	26.6	27.6	31.6	33.3
SD (N)	9.7	15.6	2.62	1.2	9.9	17.9
RSD (%)	22.4	40.6	9.85	4.36	31.2	53.7

NB The very low results were removed from the calculations in the second set of summary statistics.

3.3.1.4 Friability

For the friability test, the maximum loss of mass after the test should not exceed 1.0 % of the initial mass (British Pharmacopoeia, 2015). The friability values were all well within the acceptable range as shown in ***Table 3.5***.

Table 3.5 *Friability data for* ***Formula 1*** *mini-tablets.*

Mini-tablets	Initial (mg)	Final (mg)	Difference (mg)	Difference (%)	Mean (%)	SD
HPMC	80.3	80.3	0.0	0.00	0.04	0.07
125-180 µm	81.8	81.8	0.0	0.00		
	77.6	77.5	0.1	0.13		
HPMC	88.1	88.1	0.0	0.00	0.04	0.07
180-250 µm	96.2	96.2	0.0	0.00		
	86.6	86.5	0.1	0.12		
PEG 6K	97.8	97.8	0.0	0.00	0.00	0.00
125-180 µm	98.6	98.6	0.0	0.00		
	99.3	99.3	0.0	0.00		
PEG 6K	113.5	113.5	0.0	0.00	0.00	0.00
180-250 µm	114.0	114.0	0.0	0.00		
	107.1	107.1	0.0	0.00		
MCC	60.7	60.6	0.1	0.16	0.30	0.27
125-180 µm	76.8	76.6	0.1	0.13		
	65.5	65.1	0.4	0.61		
MCC	67.4	67.2	0.2	0.30	0.41	0.10
180-250 µm	65.2	64.9	0.3	0.46		
	63.6	63.3	0.3	0.48		

HPMC and PEG 6K mini-tablets showed very similar friability profiles for both their component sieve fractions. However, there was a notable difference in the values for MCC mini-tablets between the sieve fractions, with MCC mini-tablets prepared from the smaller sieve fraction displaying a higher friability compared to their counterparts.

3.3.1.5 Moisture uptake

The most common method used in the literature for assessing moisture/water uptake is by placing the mini-tablet on top of a membrane or glass filter which is connected on the lower side to a reservoir and then measuring the weight gain of the mini-tablets over time (Weyenberg et al., 2005, Mortazavi et al., 2010, El-Gawad et al., 2012). This technique has a drawback which is that the mini-tablet needs to be repeatedly removed from the membrane for it to be re-weighed and replaced again on top of the membrane. During the transferring process, some of the mini-tablet part might stick on the forceps which will reduce the actual weight and make the test less accurate. Additionally, as the water uptake increases over time, the mini-tablets can become less rigid and so more difficult to manipulate, again introducing errors into the measurement. By using DVS, these drawbacks can be prevented since the mini-tablet will stay in the chamber and the weight change data will be collected automatically by the computer.

Figure 3.2 illustrates the moisture uptake of the mini-tablets over a 24-hour period. PEG 6K mini-tablets absorbed moisture the most followed by the HPMC and MCC mini-tablets respectively. From the graph, it can be concluded that the mini-tablets made from the larger sieve fractions of PEG 6K and HPMC absorbed more moisture compared with their counterparts. There was no difference in the behaviour of the two batches of mini-tablets prepared from MCC.

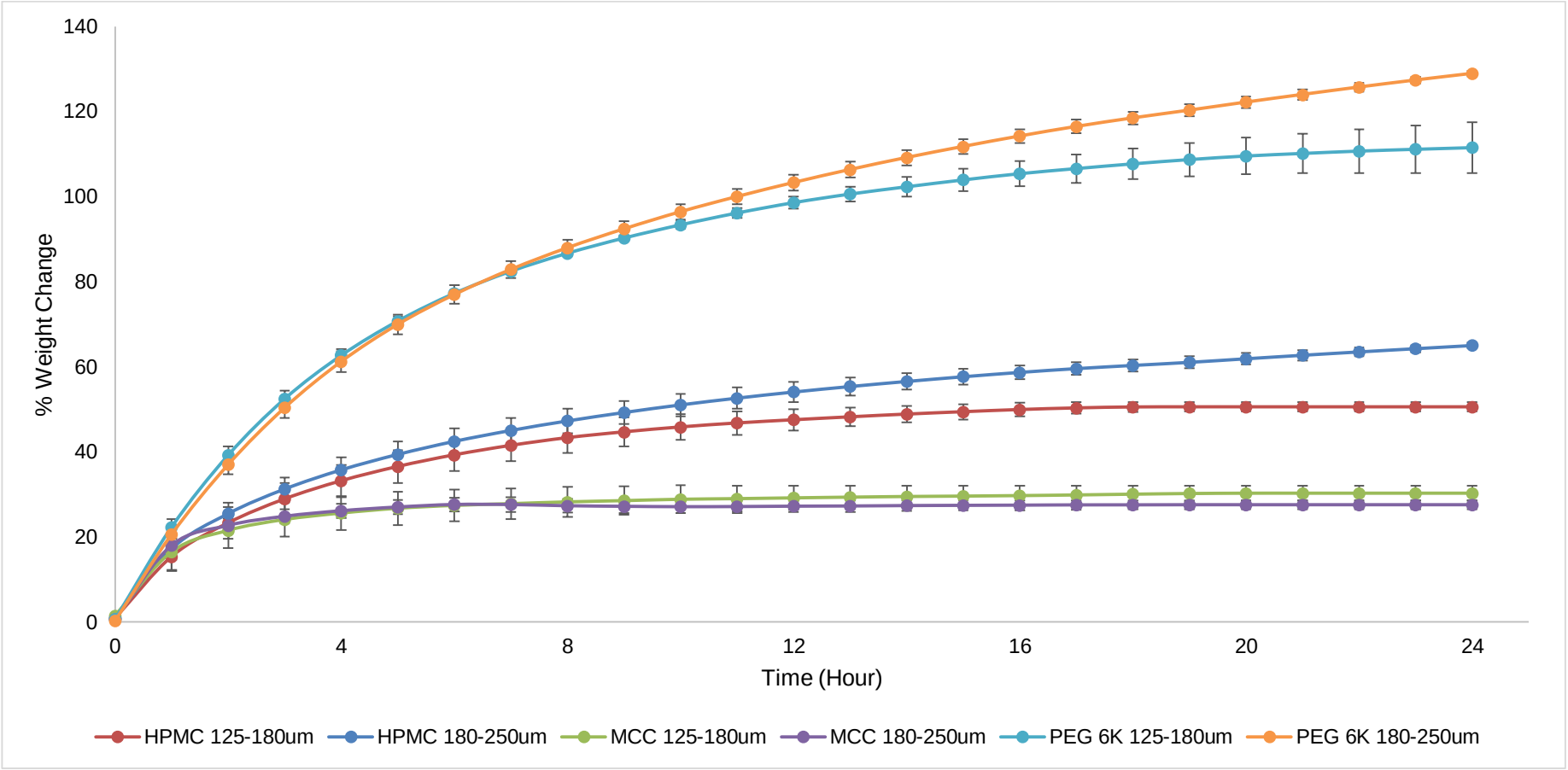

Figure 3.2 *Moisture uptake profiles of* ***Formula 1*** *mini-tablets (mean ± SD, n=3).*

MCC mini-tablets showed smaller weight changes and identical profiles for both sieve fractions because MCC is not a water-soluble or hydrophilic polymer, so it does not absorb much moisture/water. HPMC and PEG 6K mini-tablets (both sieve fractions) were completely dissolved at the end of the studies. However, MCC mini-tablets were still intact because of their hydrophobic properties.

*3.3.1.6 General discussion for the **Formula 1** mini-tablets*

There was a high degree of variability in the weight of the mini-tablets produced from ***Formula 1*** as shown in ***Table 3.2*** above. This variability probably hides any difference that may exist between the two particle size distributions of the polymers. However, the extent of this variability was unexpected and so was further investigated. Ultimately, the cause of the observed variable weight of the mini-tablets was not an intrinsic property of the powders, but the lowering cam equipped on the tablet press as shown in ***Figure 3.3.***

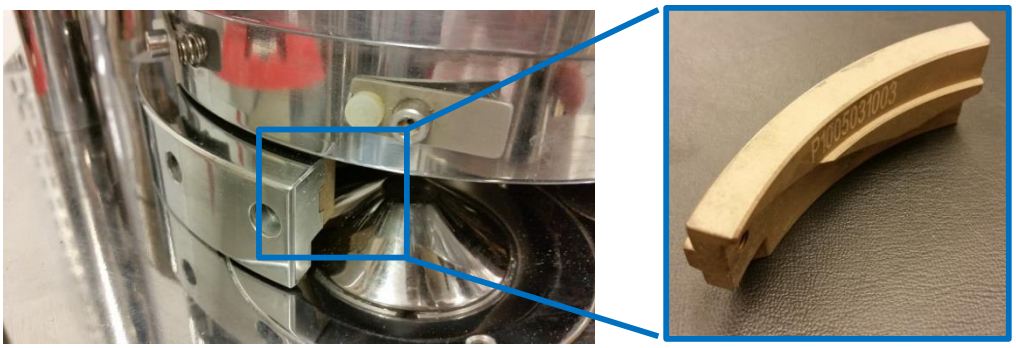

Figure 3.3 *The lowering cam from the tablet press.*

During the tableting process, after the die is filled with the powder at the feeder section, the lower punch will be drawn down by the lowering cam, creating a gap at the top of the die, with the intention of preventing the powder in the die from spillage on rotation. Due to this action, some of the powder slipped downwards through the gap that was then created between the die and the punch, reducing the amount of powder in the die. This problem only occurs with dies with small diameter cores (e.g. 2 mm), reflecting smaller diameter

tablets, due to their shape. The smaller-diameter dies are not symmetrical and have wider openings at the bottom side than the top side (shown in ***Figure 3.4***) while for the dies with larger diameter cores (e.g. 7 mm), the opening is the same size on both sides. In the case of the punches with the 2 mm diameter cores, the width of the gap on the underside is 10 mm.

(a) (b)

Figure 3.4 *(a) Top and (b) bottom opening of 2 mm diameter die.*

During the tabletting operation, when the punch is drawn down as described above, a 2 mm diameter punch tip will slide down from the 2 mm diameter opening to the 10 mm diameter opening, creating a gap into which particle will fall, causing the powder loss which ultimately results in tablet weights which are lower and more variable than would be expected. Logically, smaller particles would be expected to show greater movement through the gaps, and indeed the smaller particle size powders produced greater variability in tablet weight than their larger particle size counterparts, as indicated by the relevant RSD values. To overcome the problem, the lowering cam was removed from the tablet press machine, so that the lower punch was not pulled down during the compression cycle and powder was not lost in the gap between the lower punch and the die.

Further tests for mini-tablets from ***Formula 1*** were not conducted as most of the mini-tablets did not pass the physical characterisation tests, only the PEG 6K mini-tablets.

Formula 2 was suggested to replace ***Formula 1*** where MCC is replaced with PVP 90F and PEO 8M, and Carbopol 974P is removed from formulation. MCC is replaced with other polymers because it did not dissolve in water. And since all the polymers chosen for ***Formula 2*** are water soluble, there was no need to add Carbopol 974P in the formulation since this polymer was initially added to ***Formula 1*** formulations to act as a viscosity-raising agent which can increase the water sorption and prolong drug release, as suggested by Weyenberg et al. (2006).

3.3.2 Physical characterisation of *Formula 2* mini-tablets

Table 3.6 summarises all the physical characterisation data for the ***Formula 2*** mini-tablets except vapour sorption, performed as described for the ***Formula 1*** mini-tablets.

Table 3.6 *Summary of the physical properties of* ***Formula 2*** *mini-tablets (mean ± SD)*

Polymer	Sieve Fraction (µm)	Weight (mg) (n=20)	Thickness (mm) (n=10)	Friability (%) (n=3)	Crushing Strength (N) (n=10)
HPMC	125-180	6.26 ± 0.34	1.89 ± 0.03	0.22 ± 0.01	12.43 ± 1.74
HPMC	180-250	6.20 ± 0.21	1.91 ± 0.04	0.16 ± 0.06	17.11 ± 2.55
PEG 6K	125-180	5.50 ± 0.35	1.58 ± 0.04	0.48 ± 0.04	8.24 ± 1.29
PEG 6K	180-250	9.75 ± 0.29	2.79 ± 0.04	0.34 ± 0.07	12.10 ± 1.38
PEO 8M	125-180	6.97 ± 0.08	2.22 ± 0.01	0.03 ± 0.01	43.18 ± 1.44
PEO 8M	180-250	7.40 ± 0.09	2.33 ± 0.02	0.05 ± 0.02	40.07 ± 2.06
PVP 90F	125-180	7.84 ± 0.07	2.43 ± 0.01	1.44 ± 0.25	5.84 ± 0.59
PVP 90F	180-250	7.43 ± 0.10	2.34 ± 0.02	9.92 ± 0.69	5.64 ± 0.99

Each of the characterisation studies is discussed in detail in the following sections.

3.3.2.1 Weight uniformity

The weight of the mini-tablets ranged between 5.50 ± 0.35 mg for the PEG 6K 125-180 µm sieve fraction and 9.75 ± 0.29 mg for the PG 6K 180-250 µm sieve fraction, as shown in ***Table 3.6***. ***Table 3.7*** shows the weight measurements of twenty mini-tablets randomly chosen from each formulation. As before, black type denotes tablets that directly passed the BP specification, red type denotes tablets that show between 10 and 20 % deviation from the mean value, and blue type denotes tablets that show greater than 20 % deviation from the mean value.

Both mini-tablet batches based on PVP 90F and both mini-tablets batches based on PEO 8M directly passed the BP specification, with all individual readings being within 10 % of the relevant mean value. All four of these batches showed excellent reproducibility, with very low RSD values of circa 1 %. For both polymers, there was a slight but statistically significant difference ($p < 0.05$) in the mean weight between the two sieve fractions: the PEO 8M mini-tablets showed a higher weight with the larger size fraction, whereas the PVP 90F showed the opposite effect. The HPMC-based mini-tablets passed the BP specifications, the larger size fraction batch directly with all values being within 10 % of the mean value, and the smaller size fraction batch with one value being approximately 83 % of the mean value. There was no difference between the weights of the mini-tablets from the two sieve fractions of HPMC ($p > 0.05$). The PEG 6K mini-tablets showed the greatest difference in weight between the size fractions, which was surprisingly large compared to the other results.

The variability of the mini-tablets from the smaller particle size powder was much greater than from the larger particle size polymer, and included one tablet which fell outside of the limits of the 20 % deviation from the mean. The HPMC and PEG 6K mini-tablets in ***Formula 2*** were lower compared to both mini-tablets in ***Formula 1***. This is possibly because of the removal of Carbopol 974P from the formulation. These results suggest that

the removal of the lowering cam on the tablet press had an overall beneficial effect on the reproducibility of the tablet weight, but there was an additional small effect attributable to the powders themselves.

Table 3.7 *Weight uniformity data for* ***Formula 2*** *mini-tablets.*

Mini-tablets	HPMC (125-180 µm) (mg)	HPMC (180-250 µm) (mg)	PEG 6K (125-180 µm) (mg)	PEG 6K (180-250 µm) (mg)	PEO 8M (125-180 µm) (mg)	PEO 8M (180-250 µm) (mg)	PVP 90F (125-180 µm) (mg)	PVP 90F (180-250 µm) (mg)
1	6.59	6.06	6.10	9.79	7.16	7.35	7.71	7.38
2	6.73	6.55	5.70	9.96	6.93	7.32	7.73	7.28
3	6.20	6.41	5.49	9.84	6.97	7.44	7.72	7.22
4	6.31	6.22	5.12	9.53	6.95	7.58	7.76	7.34
5	6.25	6.08	5.63	8.97	6.93	7.42	7.87	7.57
6	5.22	6.18	5.64	10.09	7.00	7.28	7.86	7.41
7	6.33	6.34	5.24	9.74	7.02	7.29	7.74	7.31
8	6.42	6.28	5.43	9.97	6.98	7.34	7.84	7.49
9	6.05	6.00	4.67	9.54	7.02	7.41	7.86	7.35
10	6.31	6.03	5.40	9.74	6.97	7.39	7.89	7.49
11	6.46	6.12	5.61	9.87	7.03	7.40	7.83	7.58
12	6.55	6.19	5.91	9.89	6.95	7.55	7.91	7.55
13	6.30	6.07	5.65	9.89	7.02	7.52	7.86	7.43
14	6.64	6.11	6.04	9.95	7.01	7.36	7.83	7.50
15	6.36	6.14	5.15	10.08	6.86	7.56	7.82	7.46
16	5.95	5.71	5.43	9.79	7.02	7.37	7.85	7.42
17	5.80	6.26	5.71	9.76	7.03	7.37	7.96	7.42
18	6.30	6.68	5.36	9.68	6.92	7.42	7.85	7.36
19	5.98	6.41	4.98	9.09	6.85	7.42	7.92	7.49
20	6.46	6.09	5.76	9.91	6.80	7.23	7.89	7.57
Mean (mg)	6.26	6.20	5.50	9.75	6.97	7.40	7.84	7.43

SD (mg)	0.34	0.21	0.35	0.29	0.08	0.09	0.07	0.10
RSD (%)	5.44	3.44	6.43	2.96	1.13	1.27	0.89	1.37

3.3.2.2 Thickness

The thickness data are shown in ***Table 3.8***. The measured thickness values ranged from 1.89 ± 0.03 mg for the HPMC 125-180 µm sieve fraction to 2.79 ± 0.19 mg for the PEG 6K 180-250 µm sieve fraction.

Table 3.8 *Thickness data for* ***Formula 2*** *mini-tablets.*

Mini-tablets	**HPMC (125-180 µm) (mm)**	**HPMC (180-250 µm) (mm)**	**PEG 6K (125-180 µm) (mm)**	**PEG 6K (180-250 µm) (mm)**	**PEO 8M (125-180 µm) (mm)**	**PEO 8M (180-250 µm) (mm)**	**PVP 90F (125-180 µm) (mm)**	**PVP 90F (180-250 µm) (mm)**
1	1.90	1.95	1.60	2.81	2.20	2.34	2.42	2.32
2	1.93	1.90	1.54	2.73	2.21	2.35	2.45	2.33
3	1.84	1.85	1.61	2.82	2.21	2.34	2.43	2.34
4	1.86	1.88	1.53	2.72	2.20	2.33	2.44	2.34
5	1.86	1.87	1.54	2.82	2.24	2.30	2.45	2.36
6	1.90	1.90	1.63	2.78	2.23	2.32	2.43	2.36
7	1.91	1.91	1.63	2.77	2.20	2.32	2.42	2.33
8	1.93	1.94	1.57	2.80	2.22	2.31	2.44	2.37
9	1.88	1.96	1.60	2.81	2.23	2.30	2.43	2.34
10	1.91	1.89	1.52	2.82	2.22	2.34	2.43	2.33
Mean (mm)	1.89	1.91	1.58	2.79	2.22	2.33	2.43	2.34
SD (mm)	0.03	0.04	0.04	0.04	0.01	0.02	0.01	0.02
RSD (%)	1.63	1.87	2.67	1.34	0.65	0.77	0.44	0.69

All batches showed an acceptable (in some cases, very acceptable) level of variation as

demonstrated by the RSD values, although the variability for the PEG 6K 180-250 µm sieve fraction was a little on the high side, with an RSD of 2.67 %. No difference was observed in the thickness of the tablets based on the two sieve fractions of HPMC. A statistically significant difference ($p < 0.05$) was observed between the mini-tablets based on the two sieve fractions of PEO 8M and PVP 90F. Mini-tablets based on PEG 6K appeared to be anomalous here, with the larger particle size of the polymer giving rise to much thicker tablets than the smaller particle size.

3.3.2.3 Crushing strength

The crushing strength results showed a very wide range of values from 5.64 ± 0.99 N to 43.18 ± 1.44 N, as shown in ***Table 3.9***. The lowest value of crushing strength was from PVP 90F mini-tablets (from both sieve fractions) followed by the PEG 6K, HPMC and PEO 8M mini-tablets, in that order. Previous published studies on mini-tablets showed values of hardness ranging between 0.67 N and 18.64 N (Weyenberg et al., 2003, Weyenberg et al., 2005).

PEO 8M mini-tablets from both sieve fractions have the highest crushing strength and showed very different behaviour compared to the rest of the mini-tablets, because they were just deformed instead of breaking. However, the endpoint recorded was actually the force registered at the end of the probe's fixed-distance travel, rather than the force at breaking as for the other mini-tablets. Hence, although the measurements for the PEO mini-tablets were consistent with low RSD values at 3.34 % and 5.14 % for the smaller and larger sieve fractions, respectively, the data should not be over-interpreted.

The rest of mini-tablets showed conventional breaking behaviour. No difference ($P > 0.05$) was observed in the crushing strength of the two PVP 90F batches, but the mini-tablet batches based on HPMC and PEG 6K both showed statistically significant differences (p

< 0.01), with the larger particle size fraction leading to increased crushing strength. This is counter-intuitive, as it would be expected that the smaller particle size fraction would lead to increased contact between the particles, hence increased binding and greater resistance to crushing. All of these batches displayed crushing strength RSD values higher than 10 %. Even though there is no standard suggested by the British Pharmacopoeia, and values of this magnitude are reasonably common among tablet formulations, the crushing strength should be kept consistent to avoid any change in the dissolution behaviour of the tablets.

Table 3.9 *Crushing strength data of* ***Formula 2*** *mini-tablets.*

Mini-tablets	HPMC (125-180 µm) (N)	HPMC (180-250 µm) (N)	PEG 6K (125-180 µm) (N)	PEG 6K (180-250 µm) (N)	PEO 8M (125-180 µm) (N)	PEO 8M (180-250 µm) (N)	PVP 90F (125-180 µm) (N)	PVP 90F (180-250 µm) (N)
1	10.64	14.31	8.93	11.96	44.50	36.29	5.85	4.90
2	16.36	20.94	8.15	11.46	43.96	39.03	6.21	7.40
3	12.76	16.13	7.67	12.15	42.56	38.93	5.33	5.89
4	10.90	17.56	7.56	15.00	46.34	41.06	5.77	4.98
5	11.15	19.95	7.01	11.32	41.41	40.13	5.82	6.10
6	13.97	14.29	7.99	12.09	43.35	43.06	6.57	5.54
7	12.97	15.68	10.09	12.86	42.06	41.15	6.53	4.69
8	11.91	14.19	8.47	10.38	42.05	39.82	5.71	4.62
9	11.13	19.79	6.18	10.48	42.82	42.81	6.06	5.12
10	12.55	18.23	10.35	13.33	42.77	38.38	4.55	7.15
Mean (N)	12.43	17.11	8.24	12.10	43.18	40.07	5.84	5.64
SD (N)	1.74	2.55	1.29	1.38	1.44	2.06	0.59	0.99
RSD (%)	14.03	14.93	15.67	11.38	3.34	5.14	10.09	17.58

* Red = Values relating to deformation rather than breaking.

3.3.2.4 Friability

The friability data are shown in ***Table 3.10***.

Table 3.10 *Friability data for* ***Formula 2*** *mini-tablets.*

Polymer	Initial (mg)	Final (mg)	Difference (mg)	Difference (%)	Mean (%)	SD
HPMC	65.34	65.19	0.15	0.23	0.22	0.01
125-180 µm	63.26	63.13	0.13	0.21		
	65.04	64.89	0.15	0.23		
HPMC	61.19	61.13	0.06	0.10	0.16	0.06
180-250 µm	63.95	63.85	0.1	0.16		
	62.60	62.46	0.14	0.22		
PEG 6K	54.16	53.92	0.24	0.44	0.48	0.04
125-180 µm	53.35	53.10	0.25	0.47		
	53.53	53.25	0.28	0.52		
PEG 6K	98.36	97.95	0.41	0.42	0.34	0.07
180-250 µm	97.93	97.65	0.28	0.29		
	97.38	97.08	0.3	0.31		
PEO 8M	69.55	69.53	0.02	0.03	0.03	0.01
125-180 µm	69.79	69.76	0.03	0.04		
	69.09	69.08	0.01	0.01		
PEO 8M	73.70	73.66	0.04	0.05	0.05	0.02
180-250 µm	73.45	73.41	0.04	0.05		
	73.74	73.72	0.02	0.03		
PVP 90F	84.23	83.21	1.02	1.21	1.44	0.25
125-180 µm	83.65	82.22	1.43	1.71		
	84.13	82.94	1.19	1.41		

PVP 90F	77.15	69.97	7.18	9.31	9.92	0.69
180-250 µm	79.78	71.97	7.81	9.79		
	79.19	70.74	8.45	10.67		

For this friability test, a higher accuracy balance was used, compared to the previous study. The balance used in this study can measure up to 5 decimal points in grams (equal to 2 decimal points in milligrams) while the balance used in previous study could measure only up to 4 decimal points in grams. With this balance, smaller changes in weight could be determined more accurately. From ***Table 3.9***, it can be seen that all of the mini-tablets pass the friability test specification except PVP 90F mini-tablets for both sieve fractions. The percentage losses of PVP 90F (125-180 µm) and PVP 90F (180-250 µm) were 1.44 ± 0.25 % and 9.92 ± 0.69 %, respectively, higher that the limit set by British Pharmacopoiea (2015), which is not more than 1.0 % weight loss.

As would be expected, there was a general relationship between the crushing strength data and the friability results, in that a higher crushing strength results in a lower friability. The mini-tablets need to be able to withstand handling and transport from the manufacturing process to administration by patient. If the weight of the mini-tablets decreases during that period, the dose of the drug taken by the patient will be decreased commensurately, which might affect the therapeutic outcome (Aulton and Taylor, 2013).

3.3.2.5 Moisture uptake

Figure 3.5 illustrates the moisture uptake of the mini-tablets over a 24-hour period. The highest weight change after 24 hours was for the PEO 8M (125-150 µm) mini-tablets at approximately 130 % weight increase from the initial weight while the lowest weight gain was for the PVP 90F (180-250 µm) mini-tablets at approximately 40 % weight increase from the initial weight. PEG 6K and PEO 8M mini-tablets were completely dissolved at the

end of the studies while mini-tablets based on HPMC and PVP 90F absorbed water and swelled.

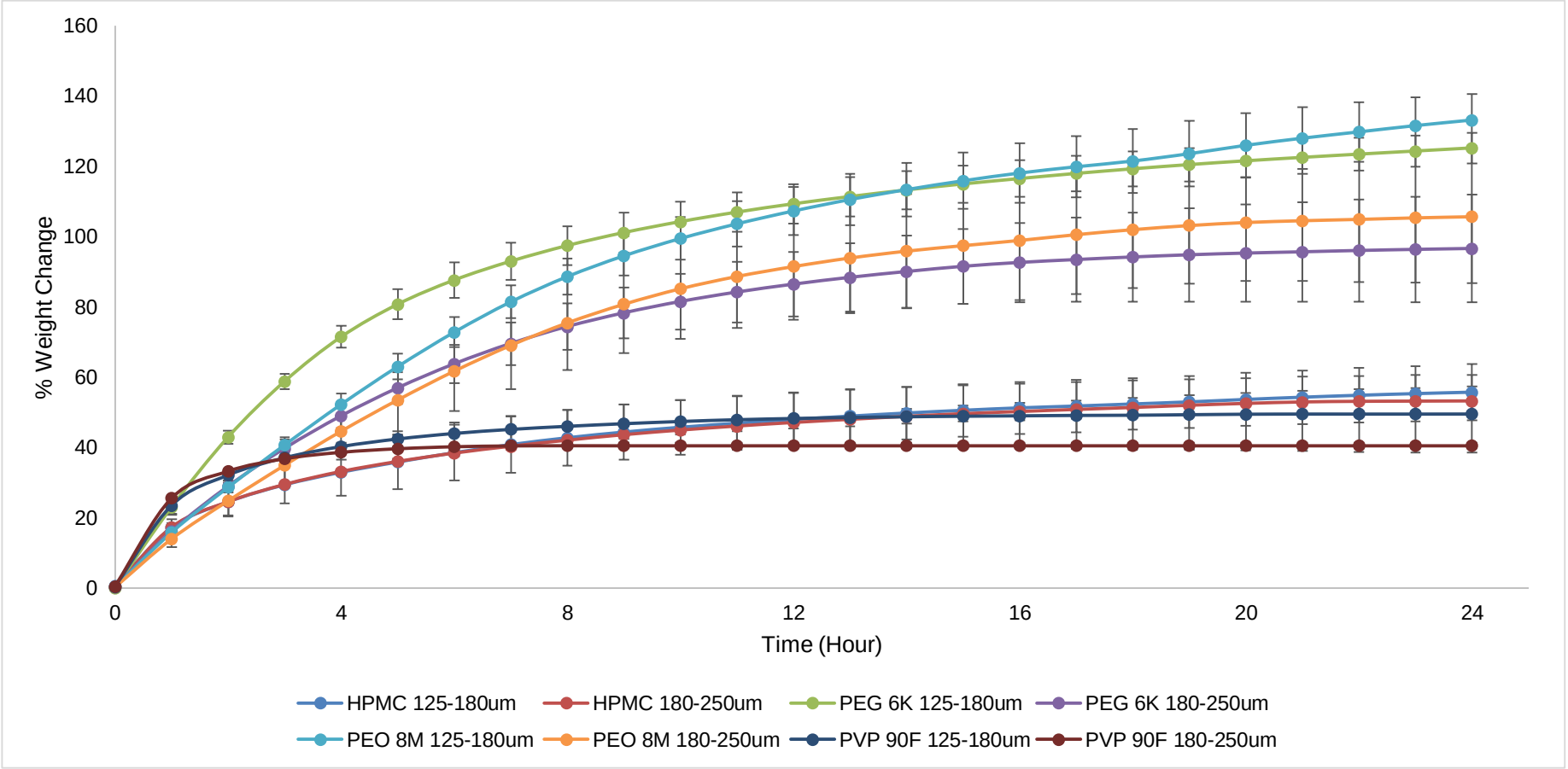

Figure 3.5 *Moisture uptake of* ***Formula 2*** *mini-tablets (mean ± SD, n=3).*

For the HPMC and PVP 90F formulations, there are only limited differences in the weight changes between the two size fractions. All of these batches absorbed between 40 and 50 % of moisture compared to their initial weights, with the bulk of the weight changes occurring within the first 3 hours and plateauing thereafter. However, for PEG 6K and PEO 8M formulations, the differences in moisture uptake are obvious where smaller sieve fraction mini-tablets are able to absorb more moisture compared to the larger sieve fraction mini-tablets. For both these polymers, the smaller sieve fractions absorbed circa 130 % of moisture compared to their initial weights while for the larger sieve fraction, they only absorbed circa 100 % moisture. Interestingly, the larger particle size batches appeared to be reaching a plateau at the end of the experiment after 24 hours study, whereas the smaller particle size batches still seem to be gaining moisture and had not yet reached a plateau when the experiment was terminated after 24 hours.

3.3.2.6 Scanning electron microscopy

All mini-tablets were smooth and shiny to the naked eye, but were scanned with SEM to observe the surface topography in more detail. The SEM images are shown in ***Figure 3.6***. There was no obvious difference in the microscopic appearance of the mini-tablets prepared from the two sieve fractions of the same polymer, although there were some differences between formulations using different polymers. PEG 6K mini-tablets showed the smoothest surface compared with the other mini-tablets while PEO 8M and HPMC mini-tablets' surfaces were relatively smooth with visible cracks. PVP 90F mini-tablets, however, showed very rough surfaces and looked very fragile. These images help to explain the reason why PVP 90F mini-tablets did not pass the friability test and have low crushing strength values.

Figure 3.6 *SEM images of* ***Formula 2*** *mini-tablets.*

Mini-tablet	**125-180 µm**	**180-250 µm**
PEG 6K	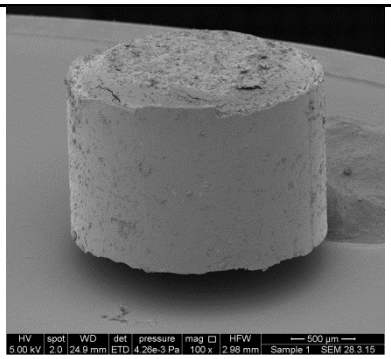	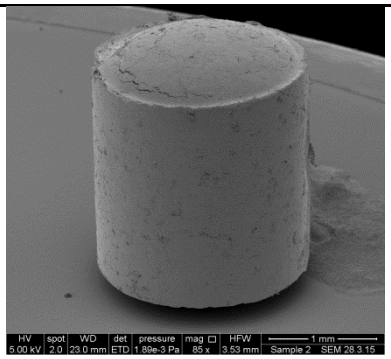
PEO 8M	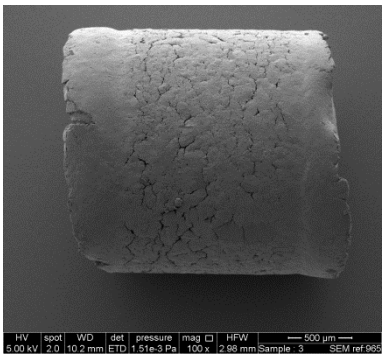	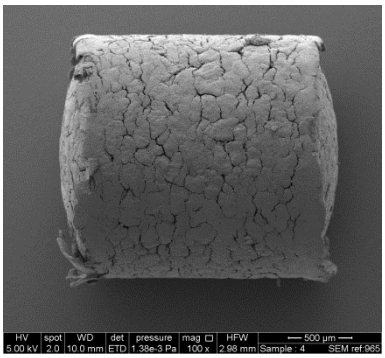
HPMC	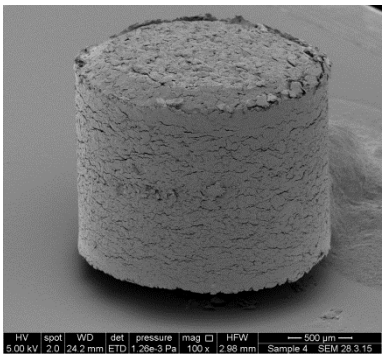	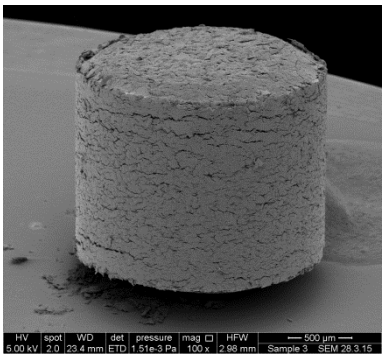
PVP 90F	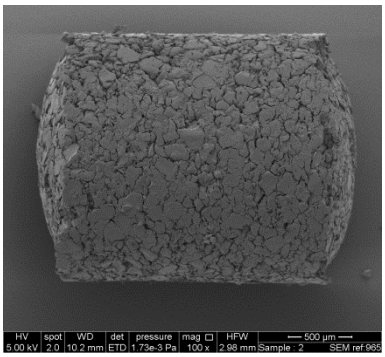	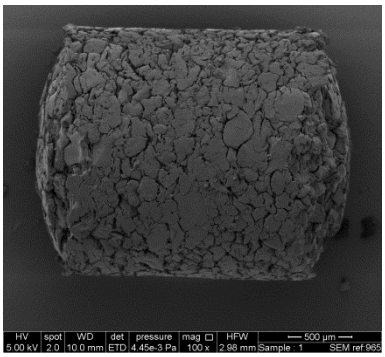

3.3.2.7 Transition temperature microscopy

The surface of the mini-tablets was analysed by using temperature transition microscopy (TTM). This technique is effectively an automated gathering of multiple local thermal analytical measurements taken over a grid pattern, measuring the thermal transition at each point. TTM is useful in assessing the distribution of materials across a surface. In this case, the selected area was 100 × 100 µm with 11 × 11 grid points. The background to the TTM technique is described in **Chapter 2**.

During the TTM study on the mini-tablets' surface, a few things captured the attention. Other than the PEG 6K mini-tablets, the mini-tablets displayed irregular results where they did not show the expected transition temperature behaviour. Further investigations into this phenomenon were conducted and are discussed in **Chapter 4**.

*3.3.2.8 General discussion for the **Formula 2** mini-tablets*

From the physical characterisation tests, it can be concluded that most of the ***Formula 2*** mini-tablet formulations complied with the standards that have been specified by BP for the weight uniformity and friability, the exception being the PVP 90F mini-tablets for both sieve fractions. PVP 90F mini-tablets did not pass the friability test as they exceeded the maximum limit which is 1.0 % of total weight loss (1.44 % for 125-180 µm sieve fraction and 9.92 % for 180-250 µm sieve fraction). The SEM images of these mini-tablets indicate that the PVP 90F mini-tablets are fairly loosely compacted which would lead to weak tablets. This problem could possibly be overcome by increasing the compression force during manufacture to provide a tougher tablet. However, the maximum force that can be applied using the 2 mm mini-tablet punches is 2.0 kN (in order to prevent damage to the punches themselves) and that was already within the force range which was used in this study (1.8 ± 0.2 kN). To exceed that compression force, larger punches would be needed, as the maximum tolerated force increases with increasing punch diameter, in a more than linear fashion. However, the larger punches would obviously produce larger tablets, which

would not be useful as ocular drug delivery systems. Overall, this means that the PVP 90F-based mini-tablet formulation cannot be included as potential formulation for ocular mini-tablets for this study. However, the dissolution test for this formulation was still performed so as to see the release profile by all the mini-tablets.

3.3.3 Drug release profile

For the dissolution studies, a modified flow-through dissolution apparatus was used, as described in **Chapter 2**. This was following the suggestion put forward by Brown et al. (2011) on dissolution methodology suitable for granules, since the size of the mini-tablets made here is approximately the same as the size of granules. The mini-tablet was inserted into a 200 µL chamber of the flow-through dissolution apparatus and ran with STF at a rate of 50 µL/minute. Samples were taken every hour up to 9 hours and spectrophotometrically quantified at 278 nm. ***Figure 3.7*** showed the release profiles of all the mini-tablets.

Chloramphenicol in the mini-tablets prepared from both sieve fractions of PVP 90F and PEG 6K was completely released within 8 hours. At the end of the dissolution experiment, all of these tablets had completely dissolved leaving no residue. More than 85 % of the chloramphenicol contained in HPMC mini-tablets (both sieve fractions) and PEO 8M (180-250 µm sieve fraction) mini-tablets had been released when the dissolution experiment was terminated after 9 hours. However, only 60% of the chloramphenicol in PEO 8M (125-180 µm sieve fraction) mini-tablets had been released at the 9 hours timepoint.

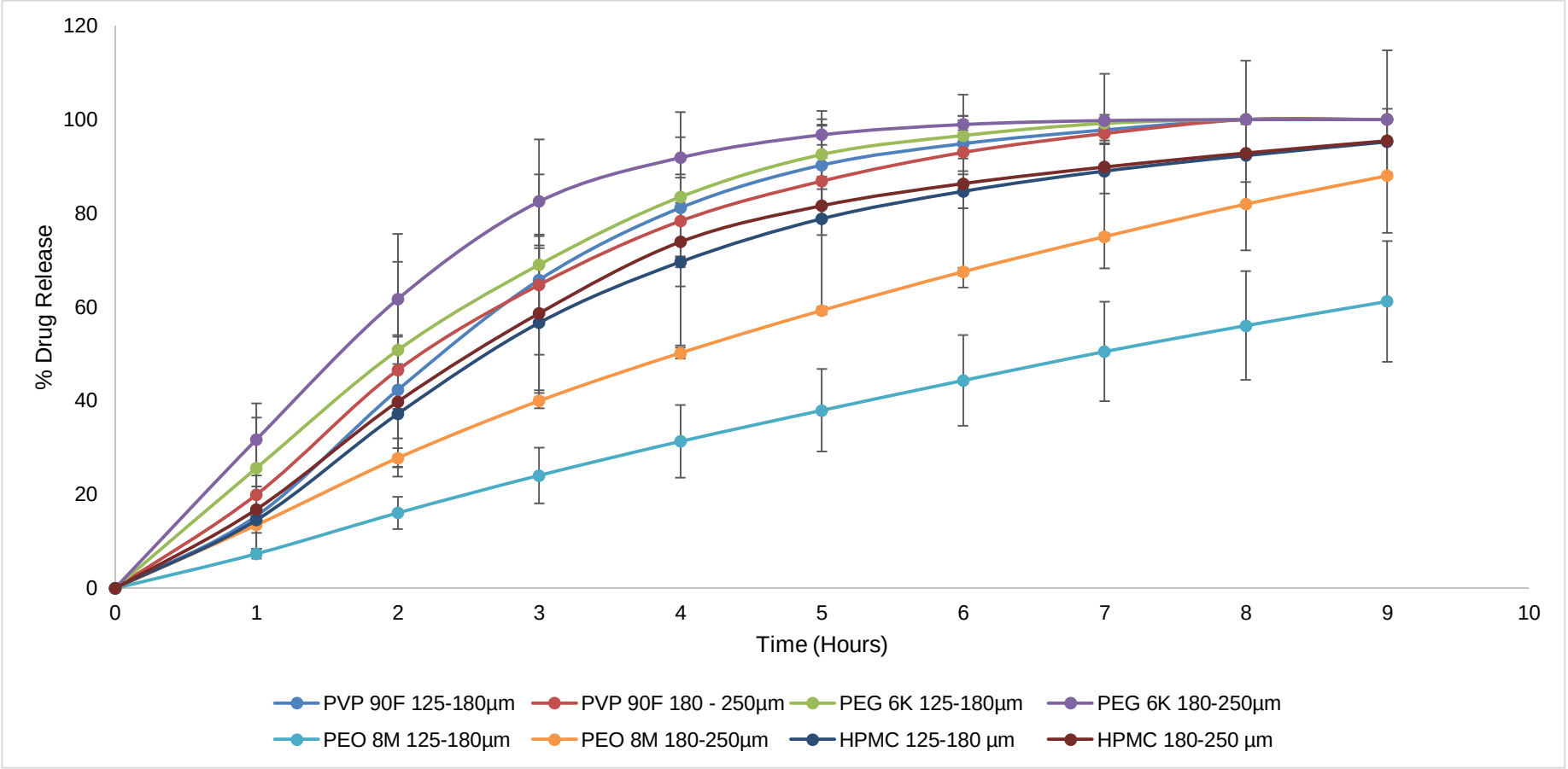

Figure 3.7 *Drug release profiles of chloramphenicol-loaded* ***Formula 2*** *mini-tablets (mean ± SD, n=3).*

From ***Figure 3.7***, the drug release rate for all formulations can be described as in the following descending order: PEG 6K 180-250 µm > PEG 6K 125-180 µm = PVP 90F 125-180 µm = PVP 90F 180-250 µm > HPMC 125-180 µm = HPMC 180-250 µm > PEO 8M 180-250 µm > PEO 8M 125-180 µm. The graph also suggests that all formulations displayed nearly identical drug release profiles compared to their counterpart sieve fraction, except for PEO 8M formulation which showed distinctly different release profiles. This observation will be investigated by using the fit factors.

3.3.3.1 Mathematical modelling of the release profiles

Three mathematical models were applied to analyse the drug release profiles of mini-tablets. The models are zero order kinetics, first order kinetics and the Korsmeyer-Peppas equation. Zero order and first order kinetics were analysed up to approximately 85 % drug release profile while the Korsmeyer-Peppas equation was analysed up to approximately 60 % of drug release. ***Table 3.11*** shows the coefficient of determination (r^2), the release rate constants (k_0, k_1 *and* k_{KP}) and the diffusional exponent (n) values for the release profiles. The best fit to the data is highlighted in green text.

Based on the fitting results, PEG 6K and PVP 90F mini-tablets (both sieve fractions) showed a better fit to zero order kinetics (green text) than first order kinetics, although the r^2 values are still quite low and indicate an imperfect fit to the profile. These mini-tablets could not be analysed with the Korsmeyer-Peppas equation because only 2 values were under 60 % of fractional drug release. This is because their release rates were too fast at the early timepoints of the dissolution test. Meanwhile HPMC and PEO 8M mini-tablets displayed better fits to the Korsmeyer-Peppas equation. However, HPMC mini-tablets for both sieve fractions were analysed with only 3 values since only these values were under 60 % of fractional release. Zero order kinetics was the second best fit for HPMC mini-

Table 3.11 Mathematical modelling parameters for drug release from chloramphenicol-loaded ***Formula 2*** mini-tablets.

Polymer	**Sieve Fraction (μm)**	**Zero order**		**First order**		**Korsmeyer-Peppas**		
		r^2	k_0	r^2	k_1	r^2	k_{KP}	n
HPMC	125-180	0.9908	17.9140	0.9966	0.1686	0.9864	10.0543	1.2064
HPMC	180-250	0.9959	18.9290	0.9887	0.2574	0.9752	12.3320	1.2154
PEG 6K	125-180	0.9930	23.8810	0.9214	0.5667	0.9957	26.0157	0.9109
PEG 6K	180-250	0.9895	29.7600	0.9409	0.7524	0.9948	32.2140	0.8793
PEO 8M	125-180	0.9908	7.1756	0.9939	0.1026	0.9951	7.9741	0.9533
PEO 8M	180-250	0.9840	11.989	0.9663	0.2063	0.9913	14.8070	0.8412
PVP 90F	125-180	0.9902	20.7380	0.9491	0.4805	0.9848	16.4233	1.2180
PVP 90F	180-250	0.9869	20.6930	0.9565	0.4386	0.9730	21.8784	0.9200

-tablets if the Korsmeyer-Peppas equation is disregarded from the results because the lack of points to be analysed. PEO 8M mini-tablets on the other hand can be fit with zero order kinetics as well since the r^2 values for both sieve fractions are close to 1.0 (0.9936 and 0.9847 for smaller and larger sieve fraction, respectively).

Although it is generally recommended that the Korsmeyer-Peppas equation is only used for the first 60 % of drug release (Korsmeyer et al., 1983, Ritger and Peppas, 1987) and there are only two or three data points in the mean values with less than 60 % drug release, if higher release quotients are studied, then the data suggest that the Korsmeyer-Peppas model is a better fit for the dissolution profile for most of these mini-tablet formulations. If the exponent n is then considered, then either it is very close to 1 (e.g. for the PEO mini-tablets), which is effectively zero-order kinetics, or it is greater than 1, which indicates a Super Case II transport situation, which is usually due to erosion. For the specific formulations and dissolution test procedure studied here, approximate zero-order kinetics may be expected for the PVP, PEG and PEO formulations as these are water-soluble polymers and would be expected to dissolve over time releasing the drug. The zero-order control factor would be the constant flow rate of the STF over the tablet surface in the dissolution chamber, effectively providing a constant sink for dissolution of the polymer. For the HPMC mini-tablets, the conditions would be slightly different, as larger HPMC tablets (e.g. 10 mm diameter) are known to release the drug via a combination of hydration, gel formation, erosion and diffusion. A similar process here would result in the dissolution profiles seen in the current study.

3.3.3.2 Fit factors

The fit factors were used to determine the difference or similarity between two drug release profiles from the same formulation but manufactured using different sieve fractions of the polymer. The two factors that are commonly used are the difference factor (f_1) and similarity factor (f_2), as described in **Chapter 2**. ***Table 3.12*** shows the difference factor and

similarity factor of drug release profiles for chloramphenicol-loaded ***Formula 2*** mini-tablets.

Table 3.12 *Difference factor and similarity factor for drug release profiles between sieve fractions of* ***Formula 2*** *mini-tablets.*

Formulation	Difference Factor (f_1)	Similarity Factor (f_2)
HPMC	4	78
PVP 90F	5	72
PEG 6K	13	52
PEO 8M	53	34

Drug release profiles are considered identical if the value of the difference factor is close to 0. Meanwhile, for the similarity factor, the drug release profiles are generally considered identical if the values are between 50 and 100 (Anderson et al., 1998). HPMC and PVP 90F mini-tablet formulations showed very low difference factor values of 5 or less and similarity factor values of greater than 50. These values indicated that drug release profiles between the two sieve fractions from those formulations can be considered to be identical. Based on the similarity factor value, drug release profiles for the PEG 6K mini-tablet formulations would be considered as identical ($f_2 = 52$). However, this value of f_2 just barely passes the benchmark for similarity and therefore it would be better to consider this result as inconclusive or borderline. For the PEO mini-tablets formulation, the fit factors clearly indicate that the drug release profiles are different between the sieve fractions.

3.3.3.3 Content uniformity assessment

The total release values (100 % release) of the drug from the mini-tablets were used to estimate the content uniformity of the mini-tablets, as shown in ***Table 3.13***. The mean drug content in the mini-tablets ranged between 0.25 and 0.56 µg with a loading average of 3.41 to 6.30 %, calculated using the mean mini-tablet weight. The target values for these

attributes were 0.5 mg and 5 %, respectively. According to BP specifications, the formulations would be considered uniform if not more than 1 individual drug content value were outside the limit of 85 to 115 % and none outside 70 to 130 % of the average content, although this specification relates to data from a greater number (10) of tablets tested than was the case here (3). The red type indicates the values that deviated outside the range of 85 to 115 % but within the 70 to 130 % range compared to the average for both the actual content and drug loading. Blue type indicates the values that deviated outside of the range of 70 to 130 %. Based on the limited data available, all mini-tablets based on HPMC, PEG 6K and PVP would pass the BP specification when compared to the mean value of the actual drug content, as all measured values were within the 85 to 115 % range. Mini-tablets based on PEO 8M showed greater variability and would most likely fail the BP content uniformity test, as several values fell into the secondary range, i.e. outside 85 to 115 % but within 70 to 130 %.

In terms of the drug loading, the target value was 5 % w/w, and only three batches of mini-tablets were close to this: PEO 8M both sieve fractions, although the variability discussed above must be remembered, and PVP 125 to 180 µm sieve fraction. The PVP 180 to 250 µm sieve fraction mini-tablets were sub-potent and the mini-tablets based on HPMC and PEG 6K were super-potent. These results probably reflect mixing and segregation issues.

Table 3.13 *Content uniformity of chloramphenicol-loaded* ***Formula 2*** *mini-tablets based on the weight and percentage of drug in mini-tablets.*

Polymer	Weight (µg) (Mean ± SD)	Drug content (µg)	Mean (µg)	SD (µg)	Drug content (%)	Mean (%)	SD (%)
HPMC	6.26 ± 0.34	0.39	0.39	0.02	6.23	6.18	0.24
125-180 µm		0.37			5.91		
		0.40			6.39		
HPMC	6.20 ± 0.21	0.41	0.38	0.03	6.61	6.18	0.49
180-250 µm		0.35			5.65		
		0.39			6.29		
PEG 6000	5.50 ± 0.35	0.38	0.35	0.03	6.91	6.30	0.56
125-180 µm		0.32			5.82		
		0.34			6.18		
PEG 6000	9.75 ± 0.29	0.57	0.56	0.03	5.84	5.78	0.31
180-250 µm		0.53			5.44		
		0.59			6.05		
PEO 8M	6.97 ± 0.08	0.40	0.38	0.09	5.74	5.40	1.25
125-180 µm		0.28			4.02		
		0.45			6.46		
PEO 8M	7.40 ± 0.09	0.42	0.38	0.06	5.68	5.18	0.74
180-250 µm		0.32			4.32		
		0.41			5.54		

PVP 90F	7.84 ± 0.07	0.37	0.39	0.02	4.72	5.02	0.27
125-180 µm		0.41			5.23		
		0.40			5.10		
PVP 90F	7.43 ± 0.10	0.24	0.25	0.03	3.23	3.41	0.43
180-250 µm		0.23			3.10		
		0.29			3.90		

3.3.3.4 Correlation between drug release and vapour sorption

The drug release and vapour sorption profiles displayed similar patterns. This suggested that there might be a correlation between these two profiles which could help explain the drug release patterns. To verify this hypothesis, a correlation graph was plotted to determine if there is any relationship between these two profiles (***Figure 3.8***). The correlation graph was plotted out using the same time points up to 9 hours in both percentage of weight changes in the vapour sorption profiles and drug release in the dissolution profiles, or until to the point where either weight changes plateaued or the release profile reached 90 % of maximum.

All *p* values obtained are smaller than 0.05. According to Seltman (2015), there are significant correlation between two profiles if the *p* value is smaller than 0.05. It can be deduced that the more water/vapour been absorbed, the greater the amount of drug been released. The vapour sorption-drug release correlation graphs give some indication into the potential drug release mechanisms from the mini-tablets. There is a clear linear relationship between water uptake and drug release from the PEO and PEG-based mini-tablets, beginning at the start of the experiments. The gradient of these correlation graphs reflects the ease and speed of dissolution of the polymer, i.e. the lower molecular weight PEG will dissolve faster than the higher molecular weight PEO (the chemistry of these two materials is the same), leading to faster drug dissolution. Both PVP-based and HPMC-based mini-tablets also show a linear relationship between water absorption and drug release, but both appeared to require a lag period, where the outer layer of the mini-tablet is hydrated, before drug release starts. This is well-known for larger HPMC matrix tablets, where the external surface forms a gel into which the drug will dissolve and through which the drug will diffuse to be released into the bulk external phase. It would be interesting to repeat this experiment, but measuring the drug release at much earlier timepoints, to fully investigate this hydration phenomenon. The vapour sorption-drug release correlation graphs show very little difference between mini-tablets made from the

two sieve fractions of HPMC and PVP 90F, slight differences for the PEG 6K formulations and greater differences between the PEO 8M formulations, which agrees with the results of the fit factor analysis above.

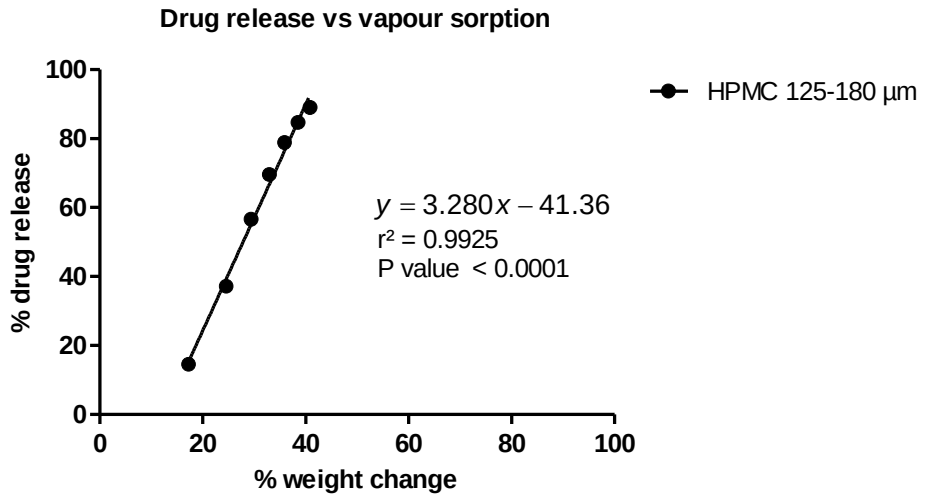
Drug release vs vapour sorption
% drug release
% weight change
HPMC 125-180 µm
y = 3.280x – 41.36
r² = 0.9925
P value < 0.0001

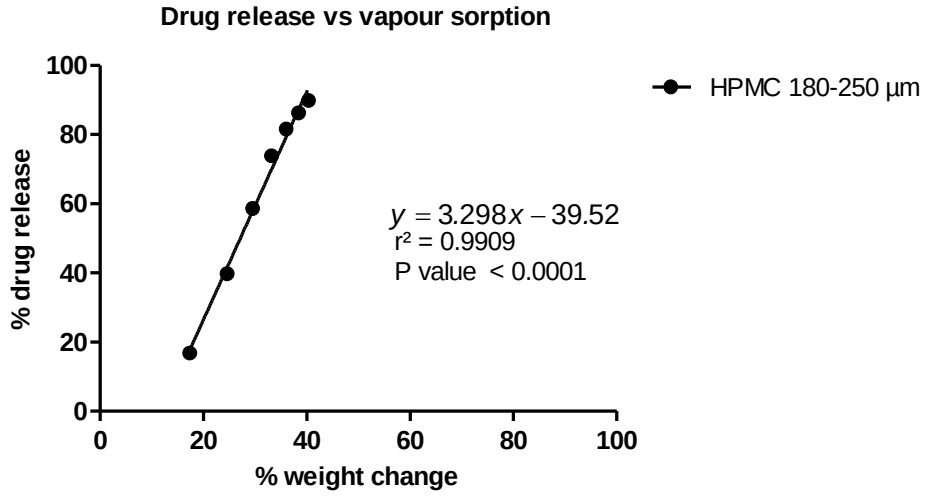
Drug release vs vapour sorption
% drug release
% weight change
HPMC 180-250 µm
y = 3.298x – 39.52
r² = 0.9909
P value < 0.0001

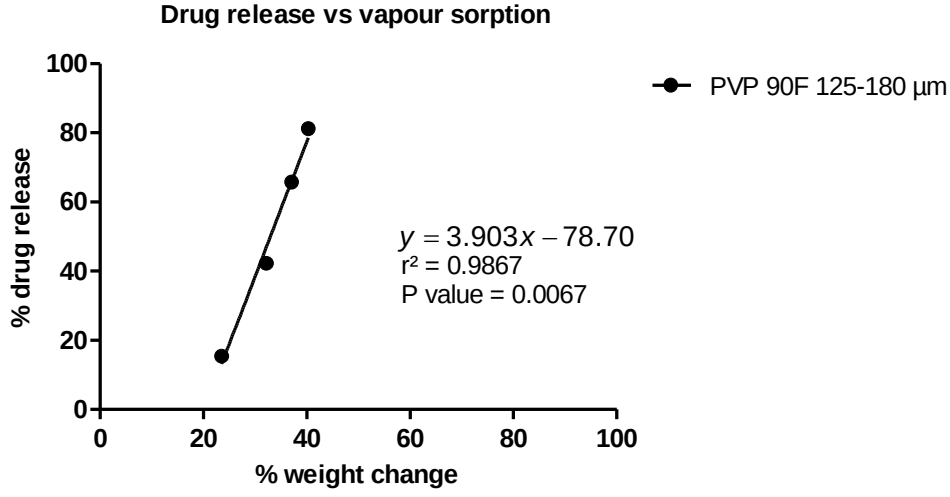
Drug release vs vapour sorption
% drug release
% weight change
PVP 90F 125-180 µm
y = 3.903x – 78.70
r² = 0.9867
P value = 0.0067

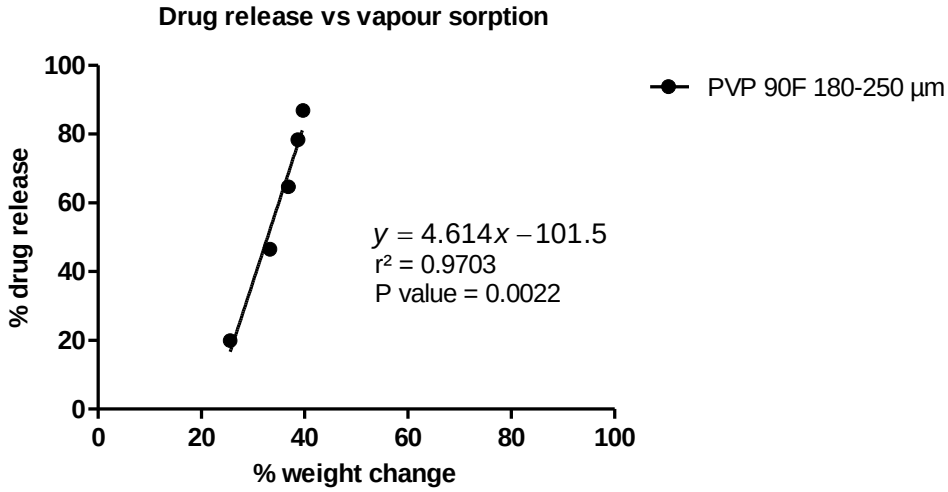
Drug release vs vapour sorption
% drug release
% weight change
y = 4.614x – 101.5
r² = 0.9703
P value = 0.0022
PVP 90F 180-250 µm

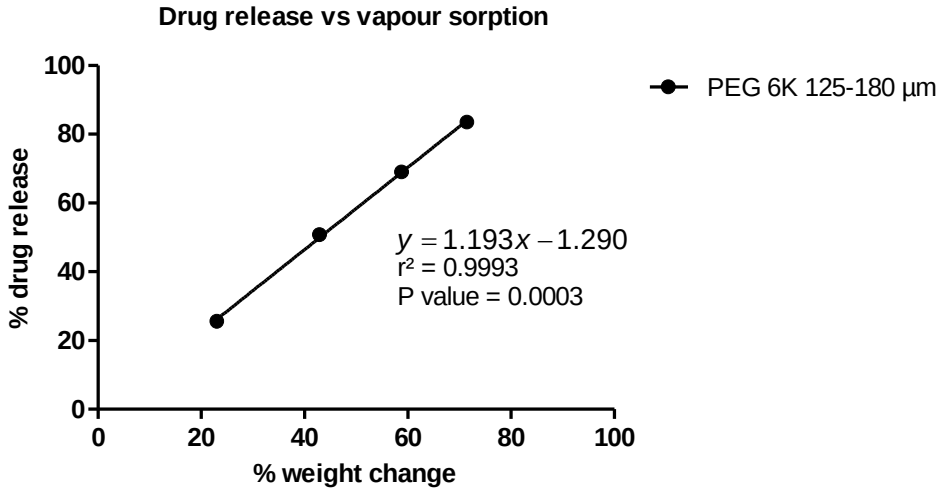
Drug release vs vapour sorption
% drug release
% weight change
y = 1.193x – 1.290
r² = 0.9993
P value = 0.0003
PEG 6K 125-180 µm

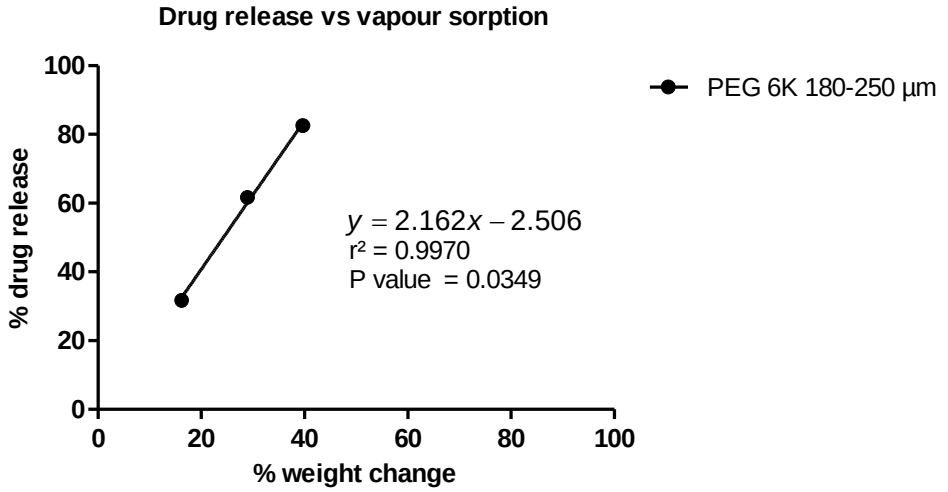
Drug release vs vapour sorption
% drug release
% weight change
y = 2.162x – 2.506
r² = 0.9970
P value = 0.0349
PEG 6K 180-250 µm

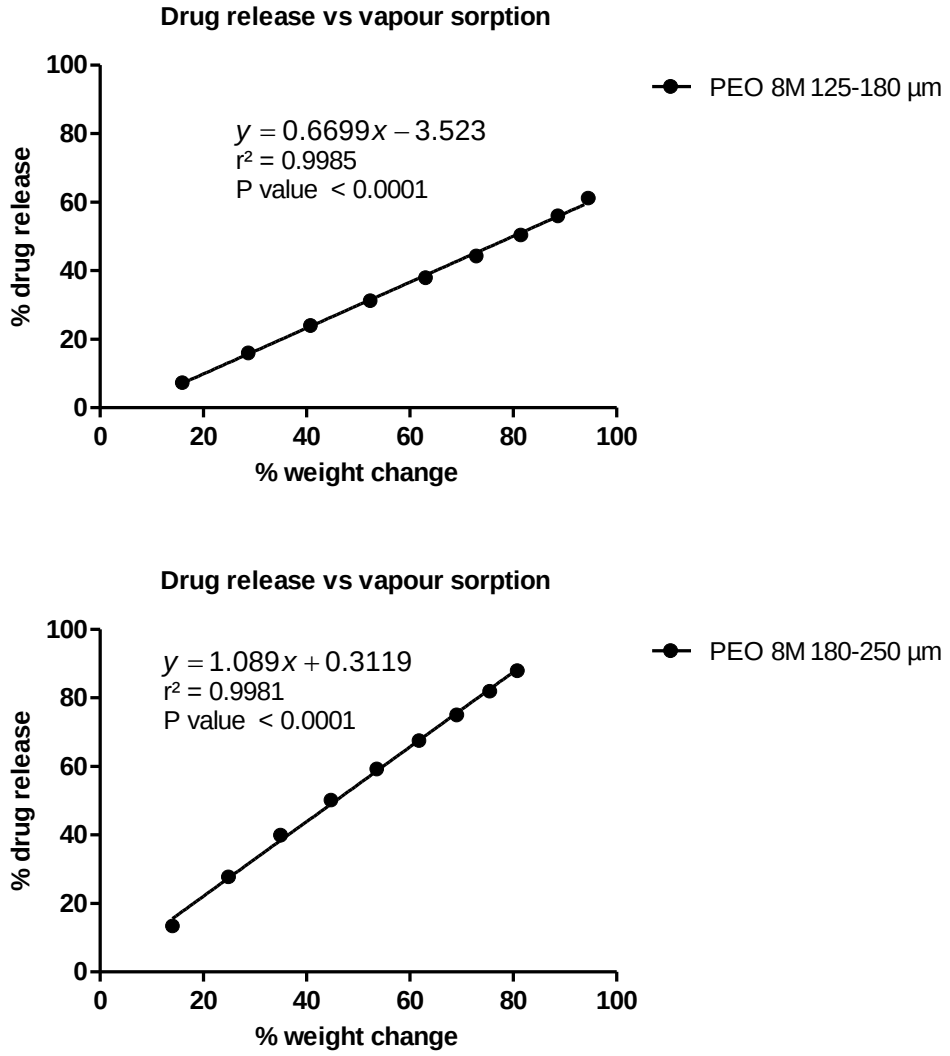

Figure 3.8 *Correlation graphs between drug release and vapour sorption.*

3.4 GENERAL DISCUSSION

The purpose of this study was to examine the influence of particle size of the predominant formulation ingredient on the behaviour of mini-tablets, in terms of ease of manufacture, pharmaceutical quality of the product and drug release behaviour. The mini-tablets here were specifically designed to be used in ocular drug delivery to provide a sustained release of the drug locally after administration. Hence, the dissolution profile required here was one of prolonged release, rather than an immediate release profile as would be the case for oral drug delivery. All other parameters describing the quality of a pharmaceutical product, such as weight uniformity and physical strength, would be the same irrespective of the route of delivery and desired drug release rate.

It was possible to make mini-tablets of all the various formulations studied here. It is important to note that the tablet tooling used here has a slightly different configuration for very small diameter punches and die cores, which can lead to loss of small particle size powder during compression, which consequent effects on product quality attributes such as weight uniformity and crushing strength. The small diameter punches are very delicate, with their maximum tolerated compression pressure being very low at 2 kN, which potentially leads to issues with materials that do not compact very well and would normally require a higher compression force. In this study, ***Formula 2*** mini-tablets based on PVP 90F were very fragile and this polymer would not be recommended as the main component of a direct compression mini-tablet formulation for this reason. PVP is usually used in tablet formulations as a binder in wet granulation processes, rather than as a diluent or compression aid. The three other polymers (i.e. PEG 6K, PEO 8M and HPMC) all produced high quality mini-tablets from both sieve fractions. The most obvious difference between the mini-tablets made from the different polymers was in the crushing strength values, with the PEO 8M-based mini-tablets showing the highest values and a different deformation / fracture behaviour to the other formulations. Although there were

differences in the weight, thickness and friability values between the batches, these differences are more subtle than the crushing strength values. Similarly, some differences were observed between matching pairs of mini-tablet formulations, which although statistically significant, would be controllable by manipulation of the settings on the tablet press. The most significant quality issue was the weight difference between the mini-tablets based on the two sieve fractions of PEG 6K, which was unexpected.

The various formulations showed quite different water absorption and drug release profiles. In terms of water absorption, the mini-tablets based on PEG 6K and PEO 8M behaved similarly, as would be expected as they are chemically similar, with only the molecular weight of the polymer being different. Conversely, the mini-tablets based on HPMC and PVP 90F behaved similarly, with less total water uptake than the PEG 6K or PEO 8M formulations. Drug release seemed to be directly correlated with water uptake for all formulations, with some subtle differences being observed in the necessity of a lag phase for hydration of the polymer before drug release started, as in the case of the HPMC-based mini-tablets, or the dissolution appearing to start as soon as the experiment begun, as in the case with the PEG 6K formulations. In most cases, at least 85 % of chloramphenicol was released from the formulation when the dissolution experiment was terminated after 9 hours, the one exception being the mini-tablets based on PEO 8M 125-180 µm. During the dissolution process, it was observed that the samples collected from PEO 8M mini-tablets formulations were highly viscous solutions. According to (Cheong et al. (1992)), the higher the solution viscosity, the more resistant it is to diffusion of drugs and a high viscosity solution surrounding a drug-loaded matrix will retard the drug release from that matrix. This is the most likely explanation for why the PEO 8M mini-tablets release profiles were the slowest. The differences between the mini-tablets based on PEO 8M is interesting to note that the smaller sieve fraction mini-tablets showed a slower profile than the larger particle size mini-tablets. The dissolution profiles of the PEO mini-tablets were best described by zero-order kinetics, supporting

the hypothesis that the dissolution is controlled by diffusion through the external viscous solution, whereas the other mini-tablets were better described by either a first order process or the Korsmeyer-Peppas model, the correlation values (r^2) being very similar in most cases. However, the Korsmeyer-Peppas model only uses the first 60 % (approximately) of drug release, and most drug release profiles look zero-order if only a few points are studied, so there is a danger of misinterpreting the data if the kinetic models are followed too slavishly, rather than observing the whole of the drug release profile. Based on the calculated difference factor (f_1) and similarity factor (f_2) values, it appears that all the mini-tablets formulations have similar drug release profiles for both sieve fractions, except the PEO 8M mini-tablets formulations which were quite different. However, PEG 6K just barely passed the benchmark for the similarity factor, so it would be better to regard this as a borderline case.

Table 3.14 below summarises whether the Formula 2 mini-tablet batches would pass the initial target specifications presented in Chapter 1 and whether they would be considered for further development.

Table 3.14 *Summary of the analytical tests of* ***Formula 2*** *mini-tablets in comparison to the initial target values.*

Attribute	**Target**	**HPMC**		**PEG 6K**		**PEO 8M**		**PVP 90F**	
		125-180 (µm)	180-250 (µm)	125-180 (µm)	180-250 (µm)	125-180 (µm)	180-250 (µm)	125-180 (µm)	180-250 (µm)
Drug content	5 %w/w = 0.5 mg	No	No	No	No	Possibly	Possibly	No	Yes
	Meets BP specifications for content uniformity	Yes	Yes	Yes	Yes	No	No	Yes	Yes
Weight	10 mg	No	No	No	Yes	No	No	No	No
	Meets BP specifications for weight uniformity	Yes	Yes	No	Yes	Yes	Yes	Yes	Yes
Hardness	5 to 15 N	Yes	No	Yes	Yes	No	No	No	No
Thickness	2 mm	Yes	Yes	No	No	No	No	No	No
Friability	Meets BP specifications for friability	Yes	Yes	Yes	Yes	Yes	Yes	No	No

Dissolution profile	Zero order	No	No	Yes	Yes	No	No	Yes	Yes
	24 hours release, i.e. 4.17 % per hour	No	No	No	No	No	No	No	No
Development potential		Possibly	Possibly	Possibly	Possibly	No	No	Possibly	Possibly
Comments		Dissolution profile needs to be altered. Drug loading needs to be increased to account for low weight.	Dissolution profile needs to be altered. Drug loading needs to be increased to account for low weight.	Dissolution profile needs to be extended. Drug loading needs to be increased to account for low weight.	Dissolution profile needs to be extended. Drug loading needs to be increased to account for low weight.			Dissolution profile needs to be extended. Hardness needs to be improved.	Dissolution profile needs to be extended. Hardness needs to be improved.

3.5 CONCLUSIONS

This study investigated the effect of polymer particle size on the physical behaviour and drug release characteristics of slow-release mini-tablets for ocular use. As this study was exploratory only, it was performed with one batch of each formulation of mini-tablets only. PVP 90F was found to be unsuitable as the major component in such a formulation, as the product was too friable, whereas all other formulations produced high quality mini-tablets. Mini-tablets composed of PEG 6K and PEO 8M, which have similar structural formulae, showed intriguing results. For both polymers, mini-tablets based on the smaller particle size absorbed more moisture and released the drug slower than their counterparts, with the similarity and difference factors clearly showing that the two batches of PEO 8M mini-tablets were significantly different in their dissolution profiles and the two batches of PEG 6K mini-tablets being of marginal similarity. HPMC and PVP 90F mini-tablets, on the other hand, did not show any significant differences in term of moisture uptake and drug release profiles between the formulations based on the two particle sizes.

Overall, the results suggest that the particle size of the polymer used to prepare the mini-tablets has limited effect on the physical quality of the product, but may have a significant effect on its drug dissolution profile as suggested by PEO 8M mini-tablets. This feature needs to be borne in mind when designing mini-tablet formulations using a direct compression method.

Chapter 4

Nano-scale Surface Analysis of Direct Compression Mini-tablets Using Transition Temperature Microscopy

Nano-scale Surface Analysis of Direct Compression Mini-tablets Using Transition Temperature Microscopy

4.1 INTRODUCTION

In the pharmaceutical field, it is important to ascertain the distribution of materials within a product, in order to understand its behaviour. In tabletting, distribution of materials can potentially affect the uniformity of content, mechanical strength, disintegration speed, and the drug release profile of the tablets. It could be argued that these potential effects are more pronounced or important for tablets with break-bars, as the quality control attributes such as content uniformity and dissolution profile are tested at the level of the split tablet as well as on the whole tablet. Similarly, any issue with distribution is likely to be more significant with mini-tablets than conventional-sized tablets, as fewer particles are required for each individual mini-tablet.

Scanning electron microscopy (SEM) is commonly used to analyse the surface of pharmaceutical products, including mini-tablets (Weyenberg et al., 2006, El-Gawad et al., 2012). However, this technique is capable only of providing topographical images of the surface and, while this is important and can provide evidence of distribution of materials across a surface, such as crystals on the surface of a film, it does not allow investigation of the chemical state of the drug, i.e. whether it is amorphous or crystalline or exists as a particular polymorph. On the other hand, bulk thermal analysis such as differential scanning calorimetry (DSC) and thermogravimetric analysis (TGA), which are able to measure thermal transitions and therefore to distinguish different physical states, analyse an entire sample and therefore provide only an overall average evaluation of the product, rather than allowing assessment of the distribution of particular materials through or across the sample.(Craig and Reading, 2006).

To overcome the limitation of the techniques described above, Hammiche et al. (1996) proposed a combination technique called localised thermal analysis (LTA). By heating the sample locally with a thermal probe, any thermal transitions at that point can be measured and associated with a particular component. Moving the probe and performing the experiment at a different location can give information on the spatial distribution of materials across a sample's surface. In LTA, the probe is made of a 75 µm diameter silver wire containing a platinum/rhodium core about 5 µm in diameter. Due to the (relatively) large size of the probe, resolution is possible only on the several micron scale and hence analysis using these probes is known as micro-thermal analysis (µTA). More recently, a much smaller micromachined silicon probe was developed, which is made of highly doped silicon that has a high electrical resistance just above the tips. This allows the probe to be heated when an electrical current is applied (Dai et al., 2012). Analysis by using these probes is known as nano-thermal analysis (nano-TA) since it can be performed at the nano scale.

An extension of the LTA technique is known as transition temperature microscopy (TTM). In TTM, a series of nano-TA measurements is performed on a sample surface over a grid pattern, generating a map of the measured transition temperatures. By using this technique, the distribution of materials on the sample's surface can be assessed. Studies utilising TTM on polymer samples or films have been reported in the literature. For example, Qi et al. (2013) prepared films using a spin-coating technique to evaluate the properties of the films under different humidity levels. Meanwhile Moffat et al. (2014) produced flat extrudates using a hot melt extrusion (HME) technique to study phase separation in HME drug dispersions. Both studies utilised TTM to analyse the materials distribution on the surface of the samples. All of the samples used in these studies have an inherently smooth and flat surface.

In **Chapter 3**, TTM was used in an attempt to examine the distribution of the drug chloramphenicol across the sample of the mini-tablets. However, the results were inconclusive, variable and did not appear to follow the expected pattern and one possible explanation is that the surface of the sample is too rough. Here, the surface of the compressed powder mini-tablets similar to those prepared in **Chapter 3** is investigated to assess the ability of TTM to cope with surfaces of varying smoothness. A range of mono-component mini-tablets was prepared using the following polymers: hydroxypropyl methylcellulose (HPMC), polyethylene glycol (PEG) 6000 and polyvinylpyrrolidone 90F (Kollidon 90F™), each with two sieve fractions: 125 to 180 µm and 180 to 250 µm.

4.2 METHODOLOGY

4.2.1 Materials

Hydroxypropyl methylcellulose K4M (HPMC) was purchased from The DOW Chemical Company, USA. Polyethylene glycol 6000 (PEG 6K) was purchased from Clariant GmbH, Germany. Polyvinylpyrrolidone 90F (Kollidon 90F™) (PVP 90F) was provided by BASF The Chemical Company, Germany.

4.2.2 Methods

4.2.2.1 Manufacture of mini-tablets

Mono-component mini-tablets of three different polymers (HPMC, PEG 6K and PVP 90F), were prepared by compression using an instrumented 4 station on a Riva Piccola rotary tablet press (Riva, Argentina) fitted with 2 mm normal concave tooling (B tooling) at a compression force of 1.8 ± 0.2 kN. Only one set of punches was used during the process. For each polymer, two sieve fractions were assessed: 125 to 180 µm and 180 to 250 µm.

4.2.2.2 Modulated temperature differential scanning calorimetry

Modulated temperature differential scanning calorimetry (MTDSC) was performed using a DSC Q1000 (TA Instruments, USA). Calibration was performed as explained in **Chapter 2**. Powder polymers samples of between 4 and 6 mg were weighed and sealed in pinholed aluminium pans (supplied by Perkin-Elmer). Nitrogen was used as both carrier and purge gas, with flow rates of 140 and 50 mL/minute, respectively. The temperature was equilibrated at 0 °C and held isothermally for 1 minute. The sampling interval was 0.10 second per point. An oscillation amplitude of 0.212 °C with a period of 40 seconds was used with an underlying heating rate at 2 °C/minute. The end point

temperatures for HPMC, PEG 6K and PVP 90F were 225 °C, 100 °C and 200 °C respectively. All studies were repeated at least three times.

4.2.2.3 Film preparation

2 g of each of the polymers used in 4.2.2.1 were dissolved in 10 mL distilled water and allowed to stand until a clear gel was formed. This gel was then spread on a Petri dish and allowed to evaporate at 60 °C. The thin film formed was then used for the surface analysis.

4.2.2.4 Scanning electron microscopy

Surface images of the mini-tablets and films were acquired using an FEI™ Quanta 200F field emission scanning electron microscopy (SEM) (FEI Company, USA). The samples were coated with 25 nm of gold under vacuum using a Quorum Q150T Turbo-Pumped Sputter Coater with a film thickness monitor unit. More details are given in **Chapter 2**.

4.2.2.5 Transition temperature microscopy mapping

The transition temperature at specific sites on the mini-tablet's and film's surfaces was mapped by using a VESTA instrument supplied by Anasys Instruments (USA), which is equipped with an AN-200 Therma-Lever™ micromachined silicon probe. The measurement was carried out over an area of 100 × 100 µm with an 11 × 11 grid of readings. A temperature ramp of 10 °C/second was used over a temperature range of 25 °C to 250 °C or until the equipment detected that the probe had penetrated through the sample. Further details on this technique are given in **Chapter 2**.

4.3 RESULTS AND DISCUSSION

4.3.1 MTDSC analysis

MTDSC was used to measure the thermal behaviour, i.e. the melting point and/or glass transition temperature (T_g), of the specific batches of all three polymers studied here.

4.3.1.1 HPMC

A representative MTDSC trace for HPMC is shown in ***Figure 4.1***. The large endotherm centred around 80 °C is thought to be due to loss of adsorbed water. A similar finding was also reported by McPhillips et al. (1999) in their study on HPMC E4M premium.

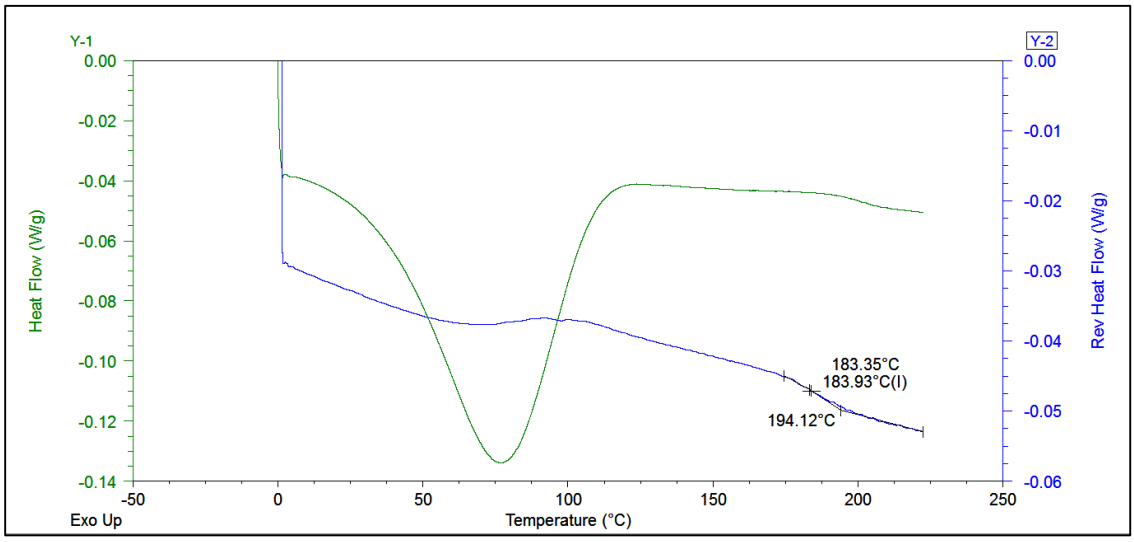

Figure 4.1 *A representative MTDSC trace of HPMC.*

The current MTDSC data suggest that HPMC's glass transition temperature (T_g) is 189.47 ± 4.80 °C. This result is slightly higher that reported by Siepmann and Peppas (2001) at 184 °C for the same grade (HPMC K4M) and significantly higher than reported by McPhillips et al. (1999), which was at 161.9 °C for HPMC E4M premium. According to Rowe et al. (2009), the T_g values for HPMC of all grades were generally between 170 °C

and 190 °C. The current MTDSC runs also indicate that HPMC has a subtle and low energy glass transition, making detection difficult, in agreement with the results of McPhillips et al. (1999).

4.3.1.2 PVP 90F

A representative MTDSC trace for PVP 90F is shown in ***Figure 4.2***. The large endotherm centred around 80 °C, similar to that observed with HPMC, is also probably due to loss of adsorbed water.

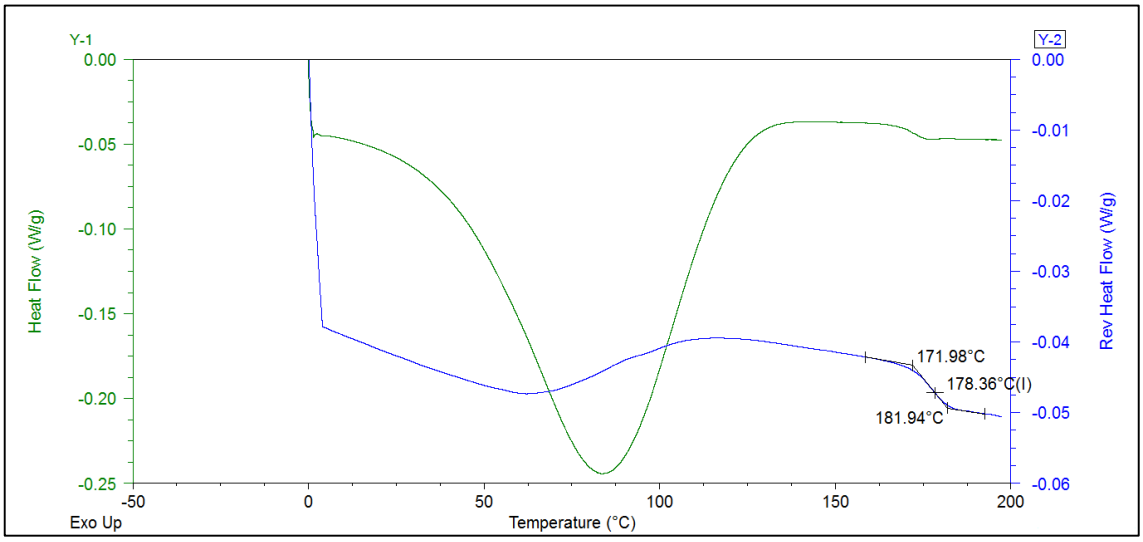

Figure 4.2 *A representative MTDSC trace of PVP 90F.*

Unlike HPMC, PVP 90F displayed a distinct glass transition. The MTDSC data suggested that the T_g is 178.35 ± 0.15 °C, in agreement with data from BASF, the manufacturer of this polymer who quoted a value of 178 °C. (Bühler, 2008).

4.3.1.3 PEG 6K

PEG 6K is a semi-crystalline polymer, which mean it contains both amorphous and crystalline regions. Since the reported T_g of PEG 6K is 259 K (-14.15 °C) (Verhoeven et al., 1989), the glass transition behaviour of PEG 6K was not analysed here. As the T_g of

PEG 6K is below room temperature, the temperature at which the surface analysis is conducted, the polymer will already have passed through the glass transition and will be in the rubbery state when these experiments will be performed.

A representative MTDSC trace for PEG 6K is shown in ***Figure 4.3***. According to Rowe et al. (2009), the melting point of PEG 6K is within the range of 55 to 63 °C, which agrees with the results obtained here of 59.30 ± 1.38 °C.

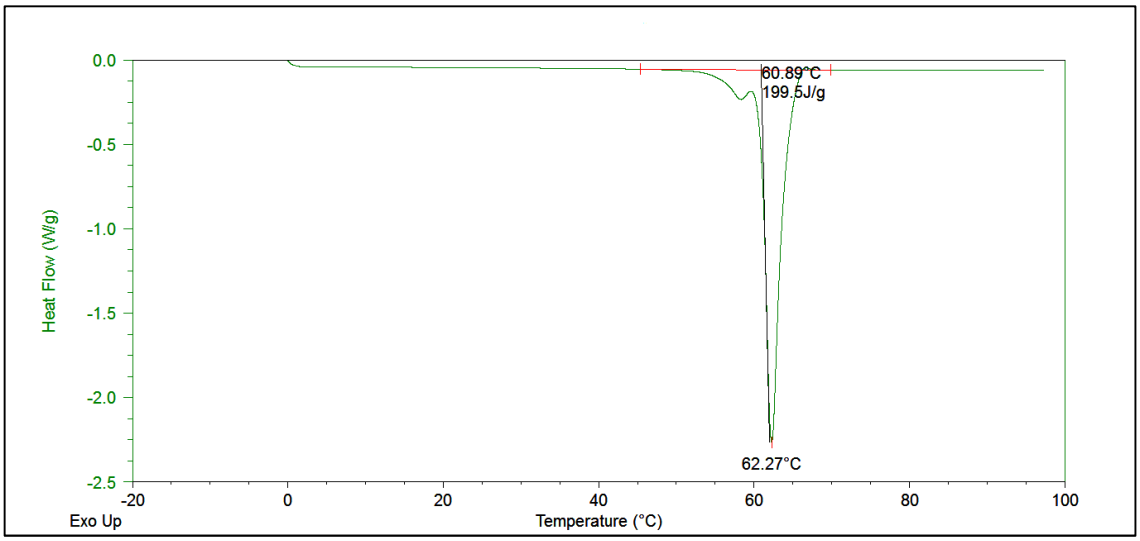

Figure 4.3 *A representative MTDSC trace of PEG 6K.*

Double melting peaks were also clearly observed in ***Figure 4.3*** and all repetition runs. It is recognised that cooling molten PEG at different rates will lead to differences in the relative amorphous / crystalline balance and the presence of different crystalline folded states, all of which will lead to different observed melting behaviours (Craig and Newton, 1991). The double melting peak observed here is probably a consequence of the original manufacturing method used to prepare this sample of PEG 6K.

4.3.2 SEM images of mini-tablets

The top (cap) and side (band) surfaces of representative samples of each mini-tablet formulation (made from both sieve fractions of the polymers) were scanned with SEM to obtain topographical images and allow comparison with the matching TTM maps.

4.3.2.1 SEM images of HPMC mini-tablets

Figure 4.4 shows representative SEM images of HPMC mini-tablets. From the SEM images, it can be seen that the top (cap) surfaces of HPMC mini-tablets are generally smooth for both sieve fractions. Individual particles were not clearly visible on any surface.

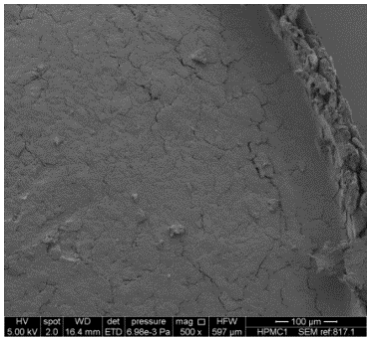

1(a)

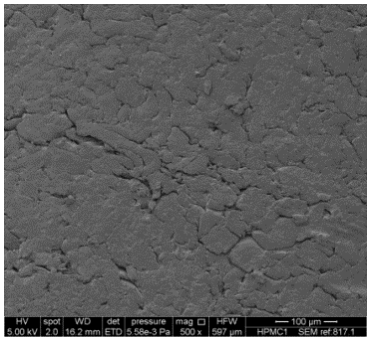

1(b)

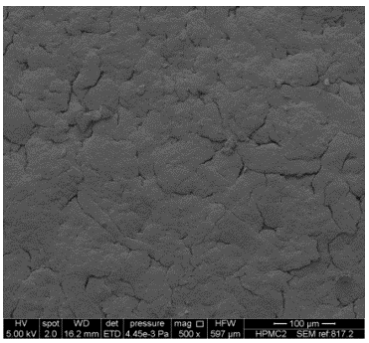

2(a)

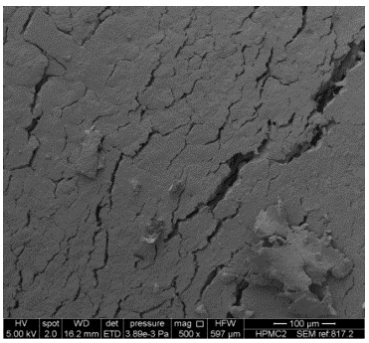

2(b)

Figure 4.4 *SEM images of (1) HPMC 125-180 µm mini-tablet and (2) HPMC 180-250 µm mini-tablet taken on the cap (a) and the band (b).*

The side (band) of the mini-tablets appeared to be more layered instead of compressed. This is because the compression force from the punches is applied on the top and bottom of the mini-tablet while there is no force applied from the side of the mini-tablet. Due to this, the surface of the tablet's cap is slightly smoother than that of the band. There are visible cracks that can be observed in the band of the mini-tablets made from both particle sizes of the polymer. These cracks can be up to a few hundred µm long and approximately 30 µm wide and were particularly apparent for the mini-tablets made with the larger particle size polymer.

4.3.2.2 SEM images of PVP 90F mini-tablets

SEM images for PVP 90F mini-tablets suggested that their surfaces were the roughest and most cracked compared to the mini-tablets prepared from the other polymers, as shown in ***Figure 4.5***. In contrast to the HPMC mini-tablets, individual particles are clearly visible in all images of the PVP 90F mini-tablets, indicating that the particles did not completely fuse during compression. There was no obvious difference in the images of the mini-tablets prepared from the two particle size distributions of the polymer.

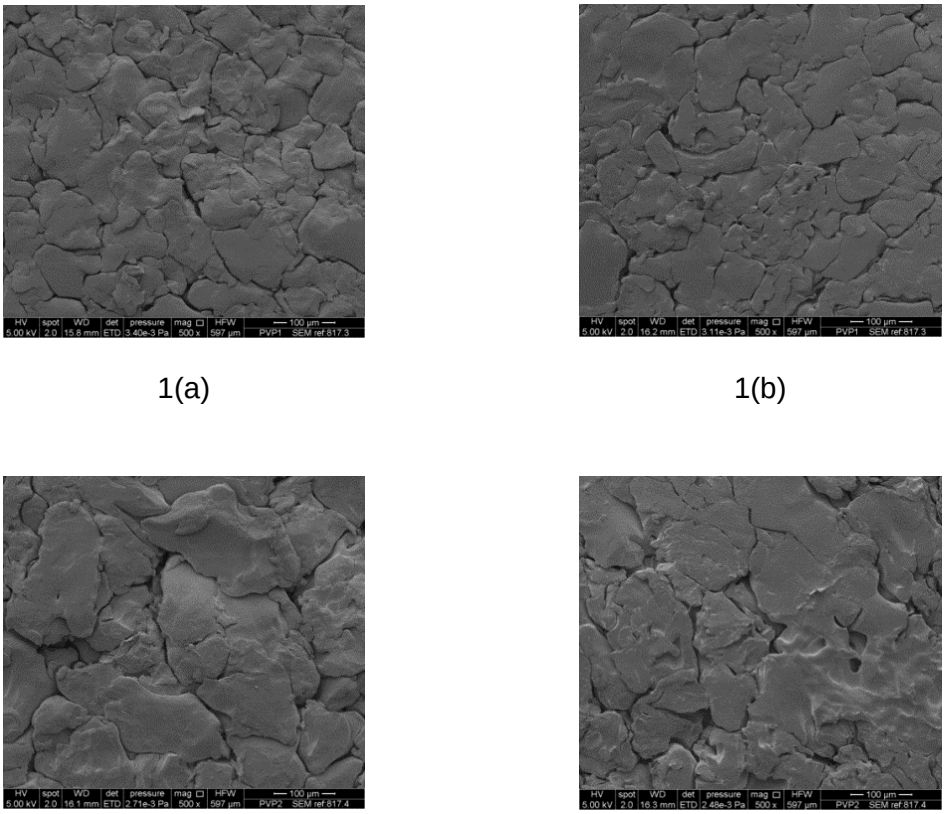

1(a) 1(b)

2(a) 2(b)

Figure 4.5 *SEM images of (1) PVP 90F 125-180 µm mini-tablet and (2) PVP 90F 180-250 µm mini-tablet taken on the cap (a) and the band (b).*

4.3.2.3 SEM images of PEG 6K mini-tablets

From the SEM images, PEG 6K mini-tablets showed the smoothest surface compared to mini-tablets prepared from the other polymers, as shown in ***Figure 4.6***. There is no significant different in the smoothness of the surfaces between mini-tablets made from the two sieve fractions or between the cap and band surfaces. This is most likely to be due to some degree of surface melting during the compression process, as it is well known that the temperature of tablets during compression can reach approximately 60°C, which is similar to the melting point of PEG 6K. This would then lead to the fusing of individual particles and a smoother appearance.

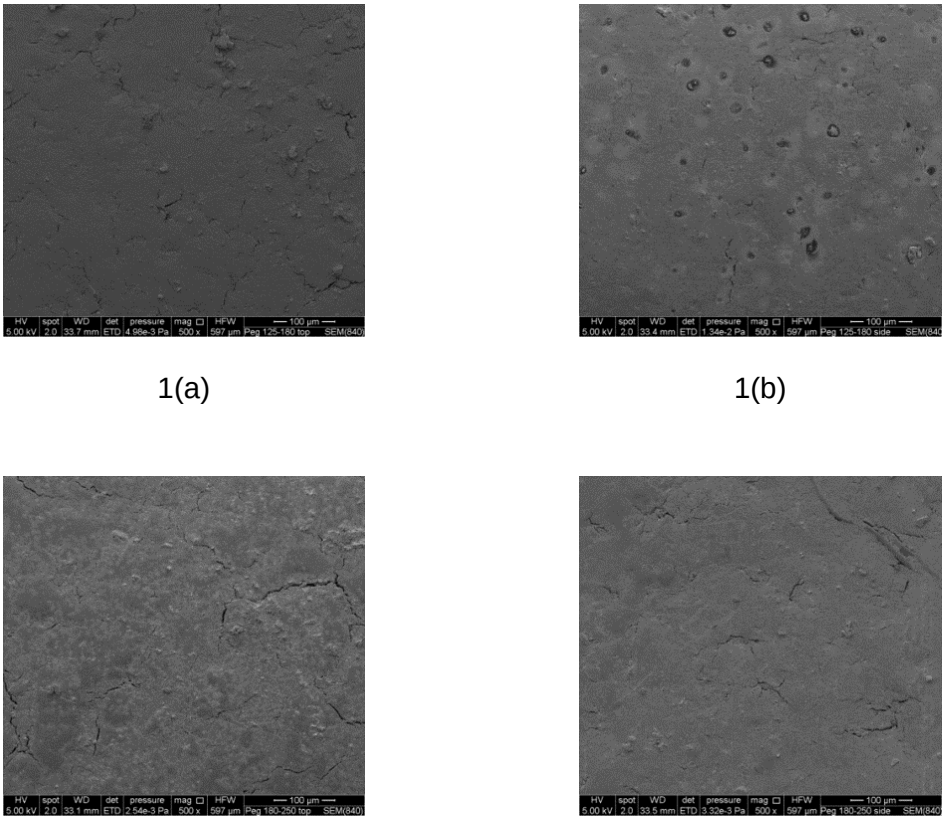

1(a) 1(b)

2(a) 2(b)

Figure 4.6 *SEM images of (1) PEG 6K 125-180 µm mini-tablet and (2) PEG 6K 180-250 µm mini-tablet taken on the cap (a) and the band (b).*

4.3.3 Transition Temperature Microscopy mapping on mini-tablets

Transition temperature microscopy (TTM) mapping is used to make early prediction on the distribution uniformity of drug and excipients by measuring the distribution uniformity of all the materials on the surface of the samples based on their transition temperature. The distribution uniformity of the materials is crucial because it may affect the drug dosage, the physical properties or the dissolution profiles.

Based on the British Pharmacopoiea (2015), the drug content uniformity is assessed by chemical assay of the whole tablet (or mini-tablet in this study). However, this is an averaging test where it takes the whole of the tablet and assesses what is present in the

whole of the tablet. It is very good for checking the dose of the drug, but does not provide any further information. For example, it does not give information about the physical state of the drug (e.g. whether it is in the amorphous or crystalline state) or whether it is evenly distributed throughout the bulk of the tablet or associated with particular regions. The spatial distribution tests will give some physical characterisation data, which may help explain physical stability, chemical reactivity or dissolution profiles. They may also help understand the mixing, flow and segregation process of the powder (i.e. if the surface has a different profile to the original formulation, it may indicate that there is a lack of mixing). If there is more drug on the surface of the mini-tablet than the bulk, it may suggest that it may degrade more quickly than expected if the drug is sensitive to oxidation or light-induced degradation. As mini-tablets have a greater surface area to volume ratio than larger tablets, a different chemical stability profile may possibly be expected, even from the same formulation.

In term of comparability to the other surface techniques, such as Raman spectroscopy, it is just a different analytical approach. Some compounds will be easier to detect by Raman while others are easier to detect by DSC, which is the measurement technique adopted by TTM.

TTM mapping was performed on the top (cap) and side (band) surfaces of representative samples of each mini-tablet formulation (made from both sieve fractions of the polymers). Each of the 121 readings in the 11 × 11 grid was analysed by the TTM software and allocated a colour representing the measured transition temperature according to the colour-temperature scale used (seen on the side bar of the images), using the "colourise" function of the software. The grid was then filled in with the colours to give a visual impression of the distribution of measured transition temperatures across the sample's surface. The data in this section are presented as the coloured grid and as a histogram of transition temperatures measured for each sample. On the colour-

temperature scale used here, purple/blue represent low temperature transitions (25 to circa 75 °C) and orange/red represent the high temperature transitions (circa 225 to 250 °C). For ease of comparison, the temperature scale (x axis) of the histograms has been kept constant for all samples. The mono-component mini-tablets were prepared for this study to eliminate the possibility of misinterpreting the results if several materials were used. The results obtained from the TTM should be representive of the transition temperature from those particular polymers only.

4.3.3.1 TTM analysis of HPMC mini-tablets

The TTM images for HPMC mini-tablets were variable, with a range of apparent transition temperatures being displayed, as shown in ***Figure 4.7***. Based on the MTDSC data generated here, the expected colouration of the grid is green/yellow representing a transition at approximately 190 °C.

Mini-tablet	TTM Map	Histogram
HPMC 125-180 µm (cap)	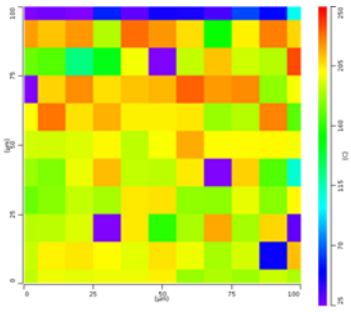	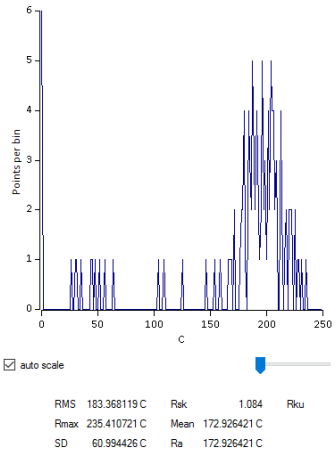

HPMC 125-180 µm (band)

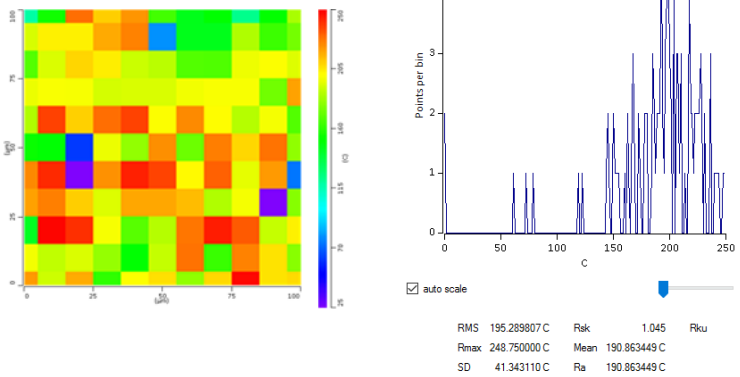

HPMC 180-250 µm (cap)

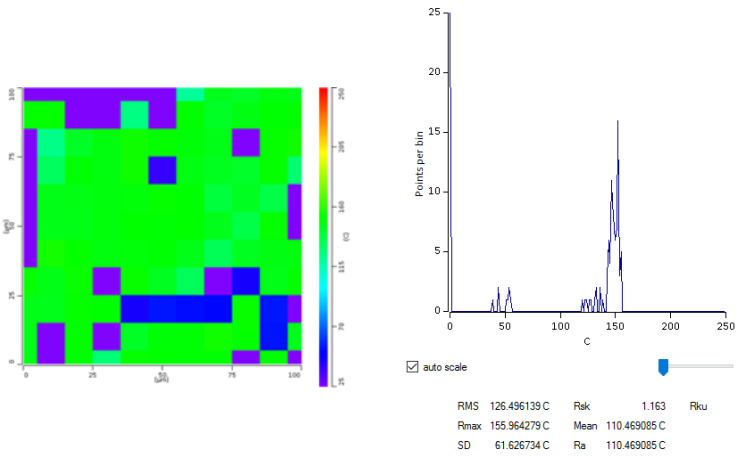

HPMC 180-250 µm (band)

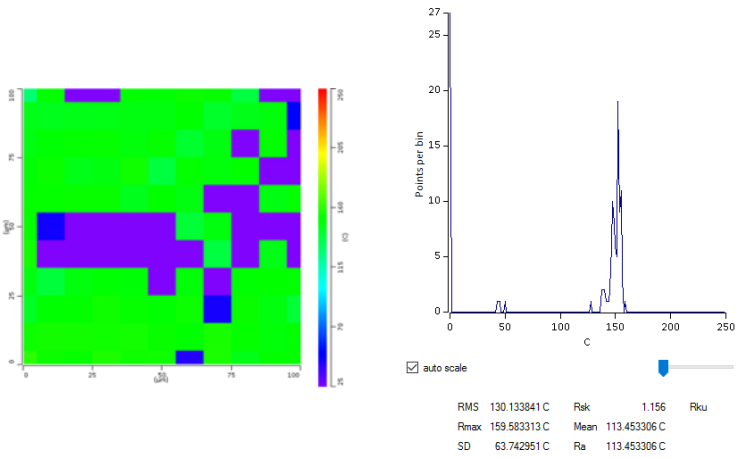

Figure 4.7 *TTM maps and transition temperature histograms of HPMC mini-tablets.*

The TTM results for the mini-tablets prepared from the two particle size distributions seem to be consistently different. HPMC 125-180 µm mini-tablets showed observed transition temperatures on TTM of between 150 and 250 °C, with a maximum occurrence at circa 200 °C, while for the HPMC 180-250 µm mini-tablets, the observed TTM transition temperatures were between 120 and 160 °C with no values near to 200 °C. The results from the smaller particle-size mini-tablets seemed to be in better agreement with the expected values than those from the larger particle-size mini-tablets. Both the histogram and coloured images also showed 0 °C temperature transition values for all samples. This cannot be correct as the probe's heating range is between 25 and 250 °C and hence a 0 °C reading should not be possible. Overall, approximately half the individual readings were incorrect based on the MTDSC data discussed earlier.

4.3.3.2 TTM analysis of PVP 90F mini-tablets

According to the MTDSC data generated earlier, the expected thermal transition of PVP 90F occurs at circa 180 °C, so the TTM grid for the PVP 90F mini-tablets would be expected to show a uniform green colouration. However, the TTM maps and histograms in ***Figure 4.8*** were variable, with a range of apparent transition temperatures being displayed. Readings at 0 °C were observed, similarly to the HPMC mini-tablets. Unlike the HPMC mini-tablet, however, there are no obvious peaks in the histogram that would relate to the T_g observed on MTDSC and transition temperatures were detected across the full experimental temperature range of 25 °C to 250 °C. Again, approximately half the individual readings were incorrect based on the MTDSC data discussed earlier. The TTM maps of the mini-tablet's band (side) were significantly poorer than those taken from the top (cap) of the mini-tablets.

Mini-tablet	TTM Map	Histogram
PVP 90F 125-180 µm (cap)	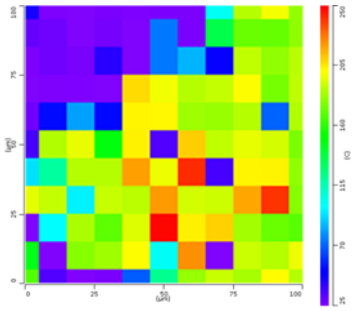	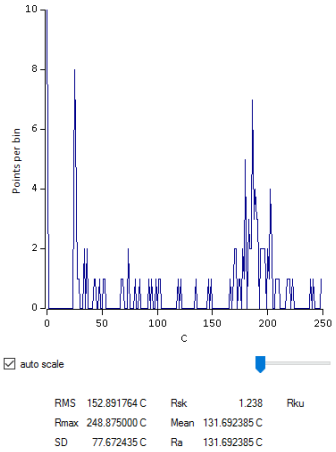
PVP 90F 125-180 µm (band)	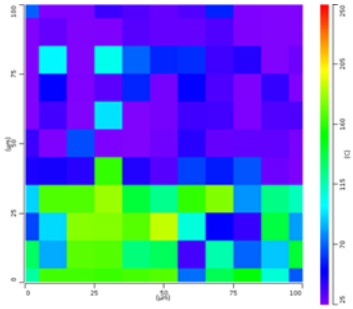	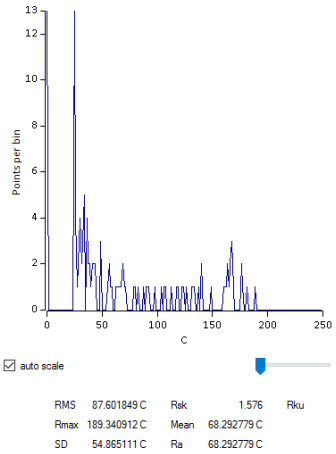
PVP 90F 180-250 µm (cap)	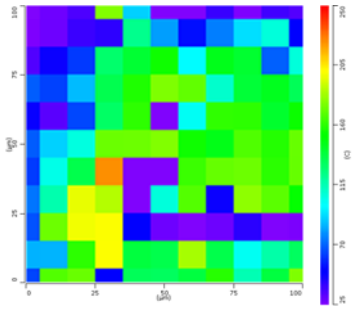	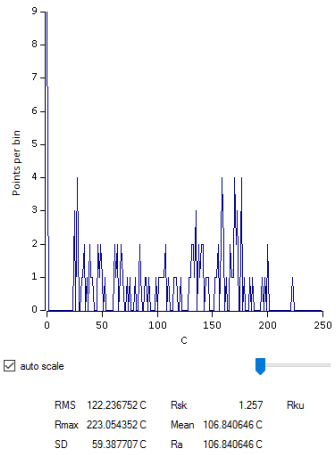

PVP 90F 180-250 µm (band)	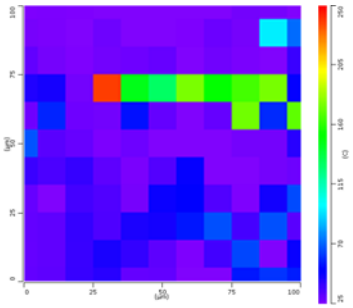	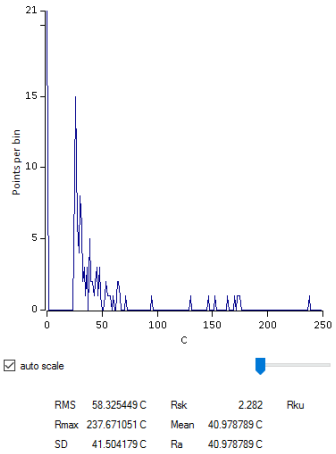

Figure 4.8 *TTM maps and transition temperature histograms of PVP 90F mini-tablets.*

4.3.3.3 TTM analysis of PEG 6K mini-tablets

Figure 4.9 shows the TTM maps and histograms for the PEG 6K mini-tablets. These were very reproducible, giving a predominant purple colouration and a value for the melting point of PEG 6K of circa 31 to 34 °C. There was no difference in the TTM results from any of the samples studied, indicating that neither the particle size of the polymer nor the position on the mini-tablet surface had an effect on the measured transition.

Mini-tablet	TTM Map	Histogram
PEG 6K 125-180 µm (cap)	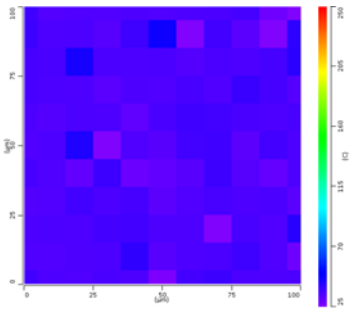	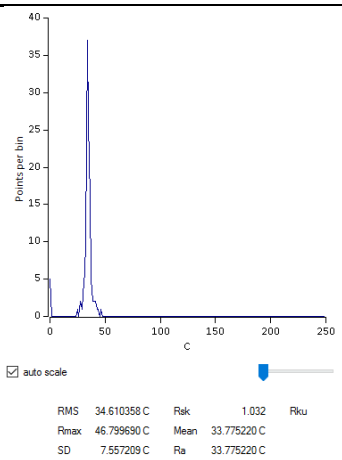

PEG 6K 125-180 µm (band)

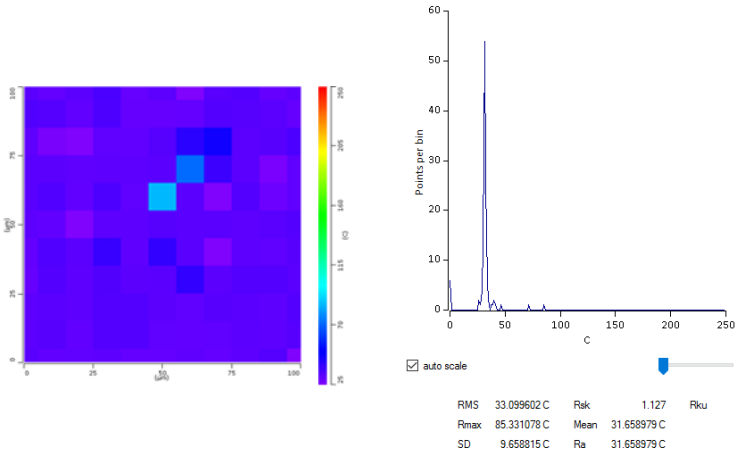

PEG 6K 180-250 µm (cap)

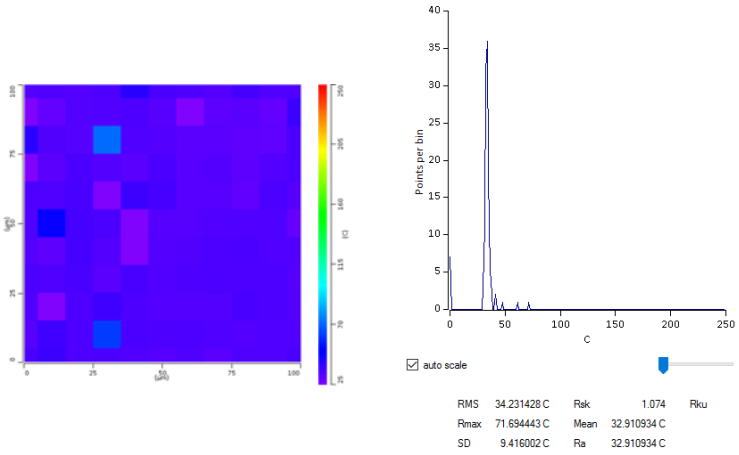

PEG 6K 180-250 µm (band)

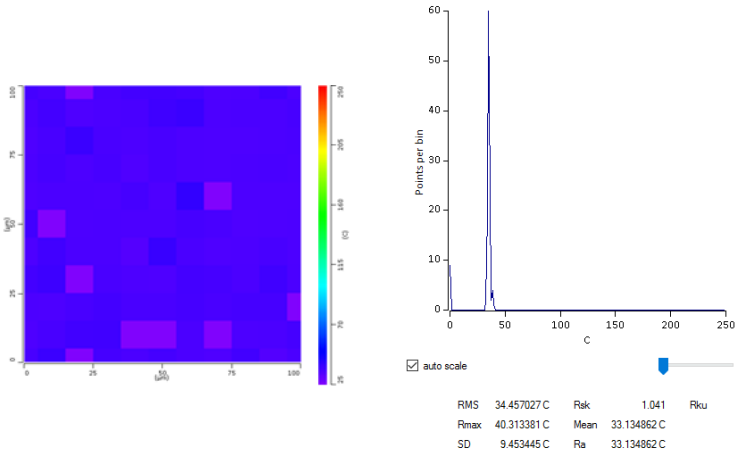

Figure 4.9 *TTM maps and transition temperature histograms of PEG 6K mini-tablets.*

From the TTM histograms, it is suggested that the melting point of the PEG 6K tablet is around 31 to 34 °C. Although the temperature of transition shows consistency, it is lower

that the melting point obtained from MTDSC, which is 59.30 ± 1.38 °C. Such differences have been seen before when comparing (MT)DSC and LTA data and is usually more apparent with low molecular weight compounds than large molecular weight polymers. These differences are thought to arise from pre-melting or surface melting phenomenon during contact of the sample with the heating probe over small surface areas. The heated surface area starts to melt during the heating process before the probe reaches the bulk melting temperature. This causes local disorder and the generation of thin film of liquid on the surface of the material, through which the probe sinks. It is this probe movement that is detected by the instrument (Zhang et al., 2009).

Unfortunately, a number of 0 °C readings were still observed for the PEG 6K mini-tablets. However, at less than 10 readings from 121 points, this is a much lower incidence than was seen with the HPMC or PVP 90F mini-tablets.

4.3.4 Further investigations into the TTM surface analysis of the mini-tablets

The TTM results for the mini-tablets were unexpected in that they showed much greater variability in the measured temperature of transition than would be anticipated. The SEM images of the HPMC, PVP 90F and PEG 6K mini-tablets were compared with the results obtained from the TTM analysis to determine whether the smoothness of the mini-tablets' surface had affected the TTM readings.

The PEG 6K mini-tablets showed smooth surfaces (both cap and band), which was reflected in the more consistent TTM results. HPMC and PVP 90F mini-tablets showed much rougher surfaces, with cracks being visible on the surface of the HPMC mini-tablets and individual original particles being observable on the surface of the PVP 90F mini-tablets. The TTM results for these samples were much more varied. Hence, there seems to be a relationship between the quality of the TTM data and the surface

roughness (or smoothness) of the mini-tablets. Ultimately, the quality of TTM data is dependent on good contact of the probe with the sample surface and this aspect was explored in more detail.

There are three possible ways of the probe making contact with the sample surface, as shown in ***Figure 4.10***.

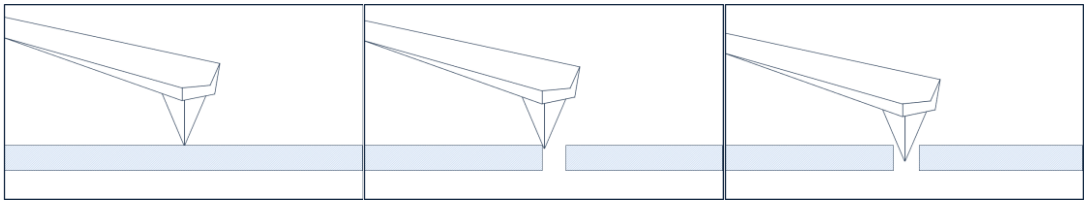

(a) (b) (c)

Figure 4.10 *Three possible ways of the probe contacting the sample surface.*

Theoretically, while running a TTM experiment, the probe will be lowered down and landed directly on the surface, making full contact (***Figure 4.10a***). The probe is then heated and the surface softens at the melting point or glass transition temperature (T_g) of the sample. Probe movement through the softened or molten surface will lead to a measurement reflecting the true nature of the material under study. However, there are two other possible ways of the probe making contact with the sample's surface. If the probe lands on the edge of a particle due to the cracked surface (***Figure 4.10b***), it will make only partial contact which will potentially result in a variable reading as the probe slides down the particle surface during the experiment. If the probe lands between two particles (***Figure 4.10c***), it will make no contact at all and therefore will not be able to detect any temperature of transition, resulting in a "0 °C" reading (***Figure 4.11***).

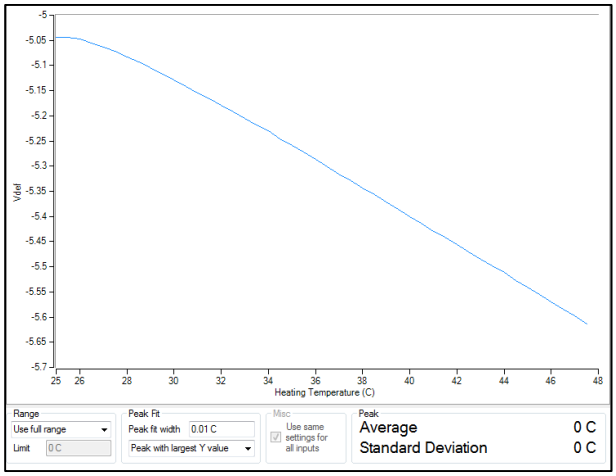

Figure 4.11 *An example of a 0 °C reading from TTM.*

It is thought that the both the "partial contact" and "no contact" modes occurred during the TTM experiments on the HPMC and PVP 90F mini-tablets. This happened because of the very small size of the probe (<30 nm), when compared with the size of the crack on the surface of the compressed tablet, as illustrated in ***Figure 4.12***. Hence, the probe could quite easily slip down the gap between neighbouring particles on the sample surface, leading to a "no contact" experiment and a 0 °C reading. Equally, it is possible that a "partial contact" is made with the probe and the edge of the particle, leading to the probe moving during the experiment and variable results. Overall, therefore, the TTM maps showed a variable transition temperature, even for mono-component systems such as were studied here.

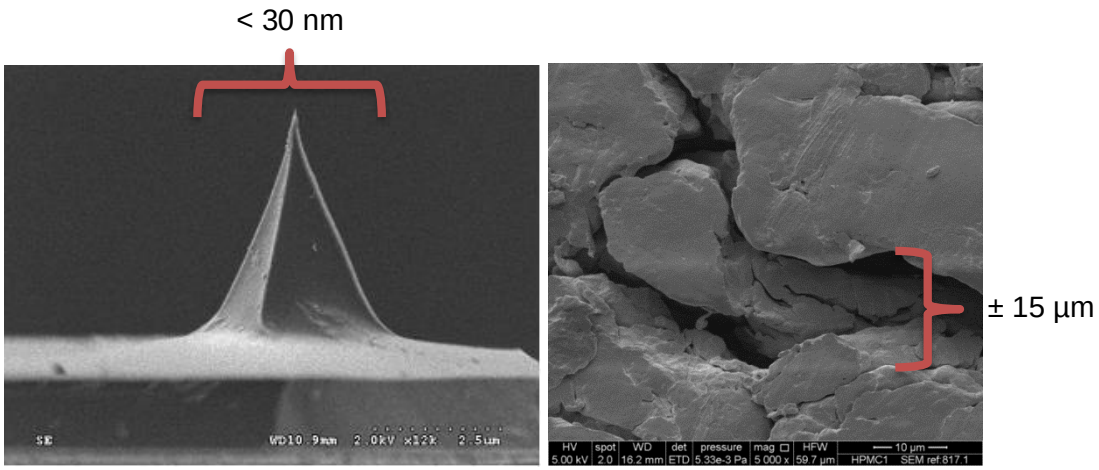

Figure 4.12 *Comparison between (a) the tip radius of the probe (AnasysInstuments) and (b) the gap between neighbouring particles on the HPMC (125-180 µm) mini-tablet surface.*

Another potential issue with the TTM experiment is the ability of the "colourise" function to correct assign a colour to a profile based on the temperature-colour scale being used. Hence, the TTM maps were investigated in detail to compare the colourise images with the actual readings. A TTM result from the HPMC 125-180 µm mini-tablets (band) was chosen for this analysis because this TTM image contained the full range of colours of the temperature-colour scale. Each of the individual readings in this grid was assessed manually to determine the endpoint temperature and to assign an appropriate colour to it based on the temperature-colour scale. This colour was then compared to that assigned by the software. ***Figure 4.13*** shows a range of individual pixels assigned various different colours by the "colourise" software, highlighted by a cross (+), on the TTM grid with their corresponding probe deflection graphs.

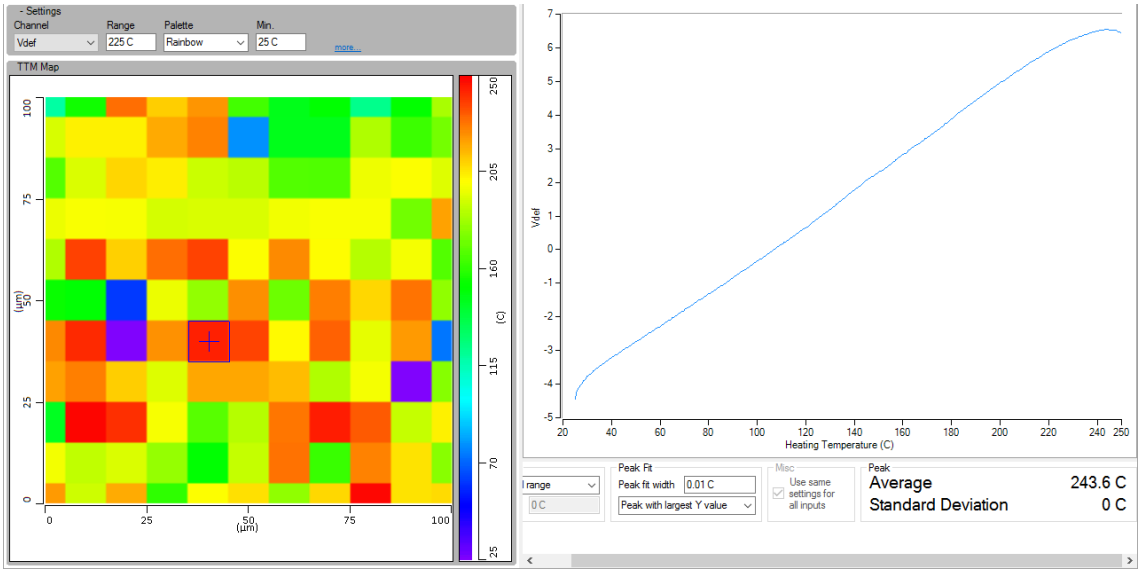
- Settings
Channel
Vdef
Range
225 C
Palette
Rainbow
Min.
25 C
more...
TTM Map
(µm)
(C)
Vdef
Heating Temperature (C)
Peak Fit
Peak fit width
0.01 C
Peak with largest Y value
Misc
Use same settings for all inputs
Peak
Average
243.6 C
Standard Deviation
0 C

(a)

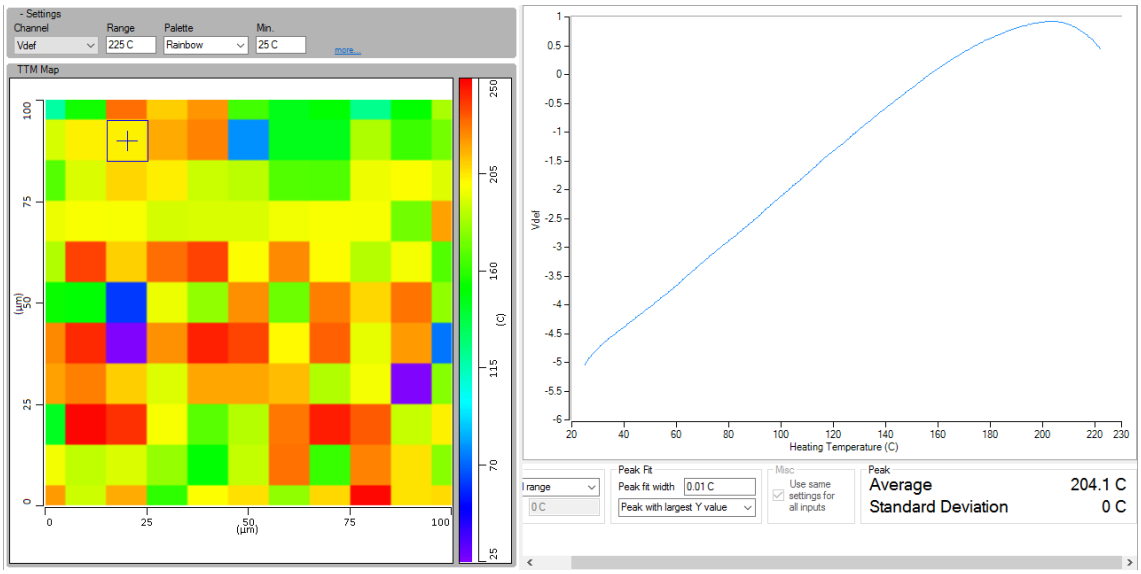
- Settings
Channel
Vdef
Range
225 C
Palette
Rainbow
Min.
25 C
more...
TTM Map
(µm)
(C)
Vdef
Heating Temperature (C)
Peak Fit
Peak fit width
0.01 C
Peak with largest Y value
Misc
Use same settings for all inputs
Peak
Average
204.1 C
Standard Deviation
0 C

(b)

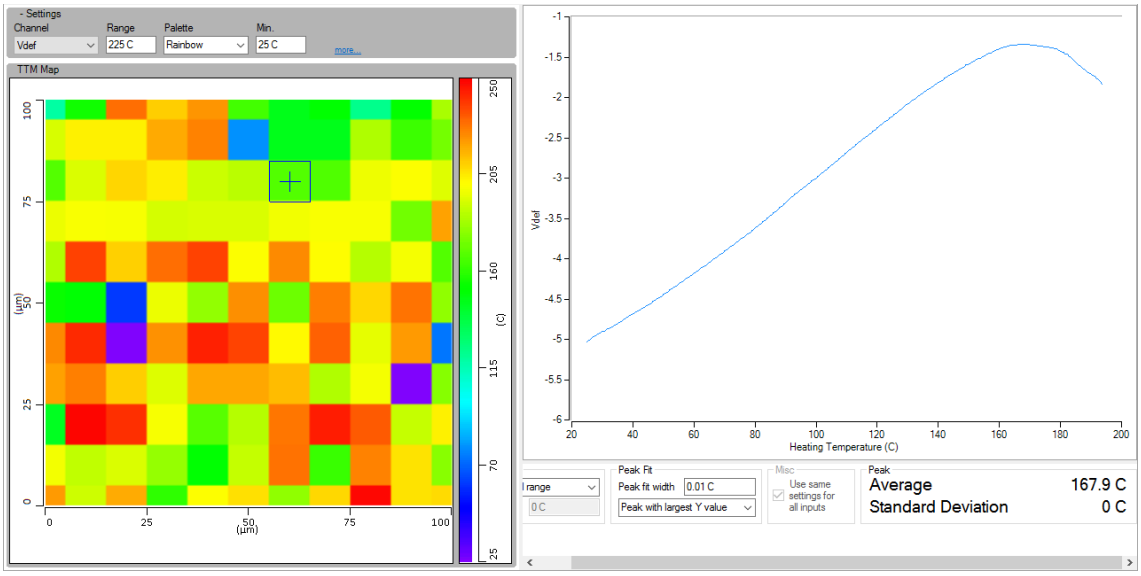
- Settings
Channel
Range
Palette
Min.
Vdef
225 C
Rainbow
25 C
more...
TTM Map
(µm)
(C)
Vdef
Heating Temperature (C)
Peak Fit
Peak fit width
0.01 C
Peak with largest Y value
Misc
Use same settings for all inputs
Peak
Average
167.9 C
Standard Deviation
0 C

(c)

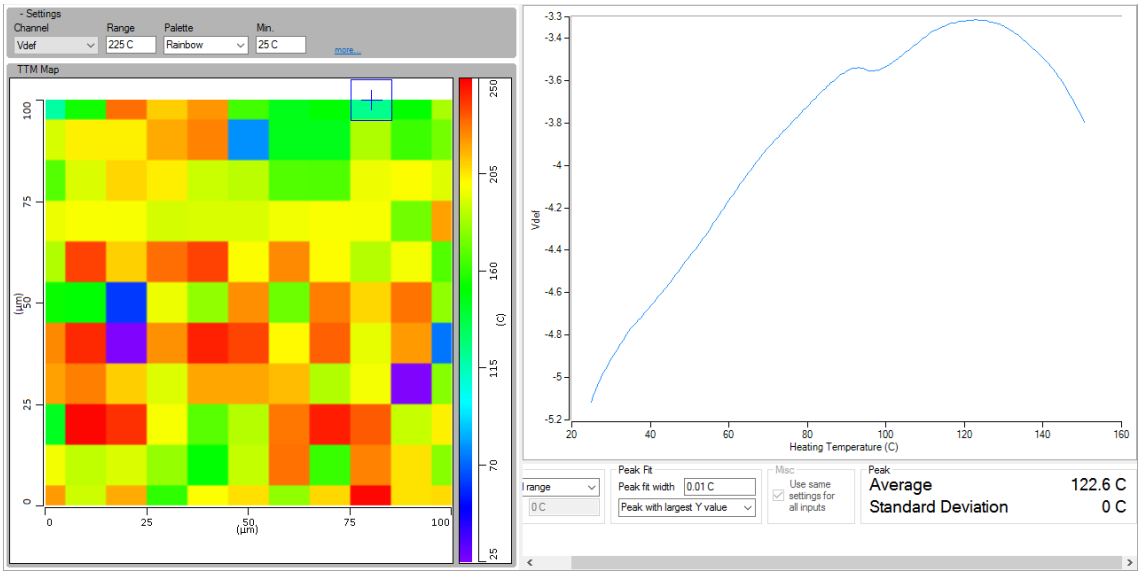
- Settings
Channel
Range
Palette
Min.
Vdef
225 C
Rainbow
25 C
more...
TTM Map
(µm)
(C)
Vdef
Heating Temperature (C)
Peak Fit
Peak fit width
0.01 C
Peak with largest Y value
Misc
Use same settings for all inputs
Peak
Average
122.6 C
Standard Deviation
0 C

(d)

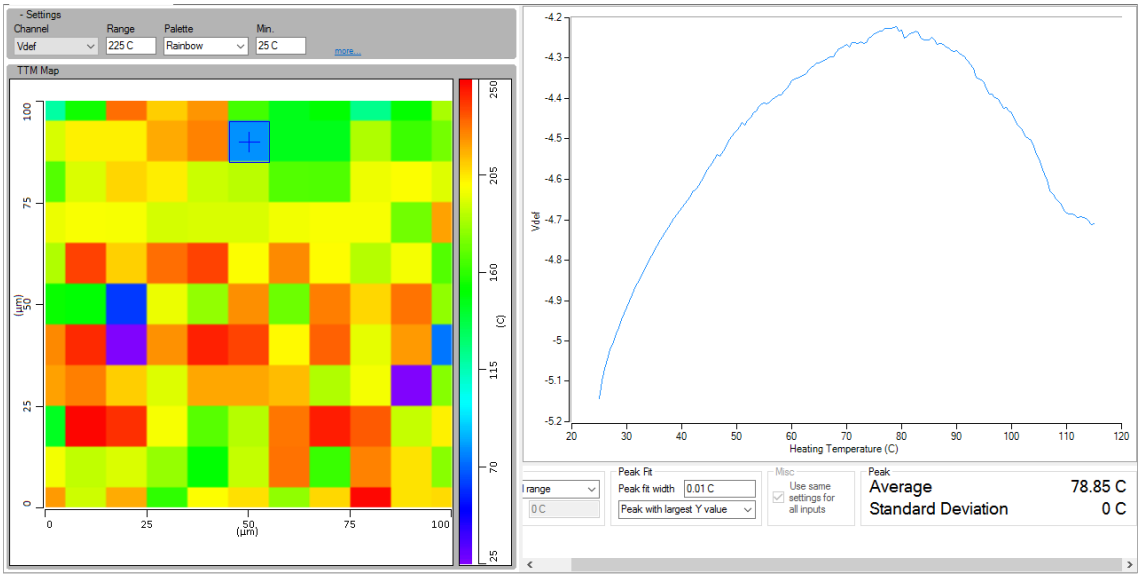

(e)

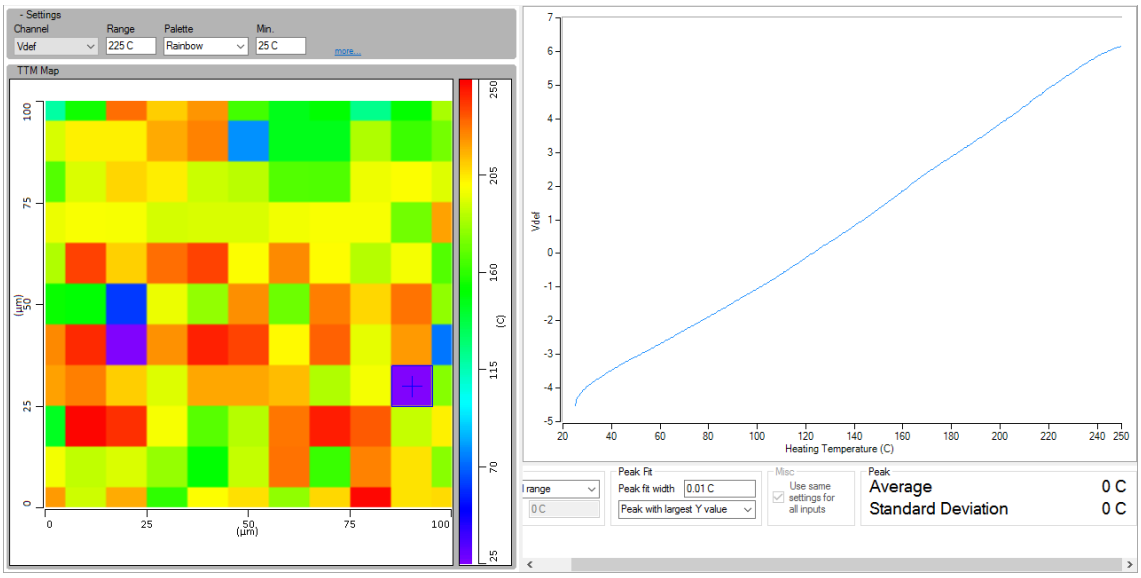

(f)

Figure 4.13 *Comparison between individual TTM pixels with actual readings of probe deflection. (a) = red colour, (b) = yellow colour, (c) = green colour, (d) = pale blue colour, (e) = dark blue colour, and (f) = purple colour*

Based on the results shown in ***Figure 4.13***, it can be concluded that the colours represented in the image tallied with the actual readings, except when poor contact seems to have been made between the probe and the sample, and the probe deflection graph is a straight line with no obvious endpoint. In this case, the software seems to assign either the maximum temperature and a red colouration, or the minimum temperature and a purple colouration. This suggests that the software is working well and the image produced can be trusted, for the intermediate values but not for the extreme values. It is recommended that the individual probe deflection traces are examined in these cases to assess the true results. Ultimately, these "odd" results are probably a combination of the probe landing awkwardly on the junctions between particles or sliding into a gap between particles, and a processing issue for a "non-results" with the "colourise" software.

One of the concerns about using the TTM technique on the surface of a tablet or mini-tablet is the shape of the tablet itself. Reported studies utilising TTM have been on polymer films (Qi et al., 2013, Moffat et al., 2014), which have a naturally flat surface. However, the shape of the cap of the tablet is convex while the band of the tablet is cylindrical, i.e. both are curved from the perspective of the probe. From the results presented earlier, it would appear that the shape of the sample does not affect the efficiency of a TTM reading as long as the probe makes proper contact with the surface.

Up to this point, a few questions still have not been answered regarding the TTM analysis on the surface of the mini-tablets. Even though visible cracks can be seen on the HPMC mini-tablets surface on the SEM image, although not to the naked eye, the surface is still smooth in general. To confirm whether the variable TTM readings were entirely due to the rough areas and cracks on the surface or if there is another contributory factor, TTM analysis was performed on the surface of films made from each of the three polymers individually.

4.3.5 Transition temperature mapping on polymer films

Each of the three polymer films was prepared using the solvent-cast technique. The films were analysed by TTM with the same measurement parameters as the mini-tablets.

4.3.5.1 TTM analysis of HPMC films

The TTM map and histogram for HPMC films in ***Figure 4.14*** showed that 90 out of 121 of the readings were 0 °C readings, with the rest showing the maximum transition temperature.

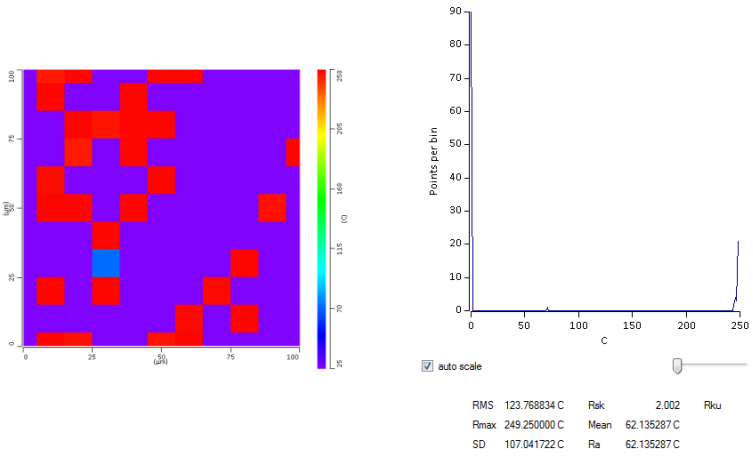

(a) (b)

Figure 4.14 *TTM map and transition temperature histogram of HPMC films.*

TTM analysis on HPMC films therefore displayed a similar but more extreme pattern as seen with the HPMC mini-tablets. Neither sample showed a distinct transition temperature. Since the film surface is smooth and does not have cracks, it is impossible to say that the readings obtained from its TTM analysis were due to improper contact between the probe and sample, although this is unlikely given the smooth nature of the film's surface. ***Figure 4.15*** shows the individual probe deflection graphs for this TTM measurement, suggesting that a proper contact was established on each point, but also that the endpoint could not be determined as the probe keeps heating until it reaches the maximum experimental temperature of 250 °C.

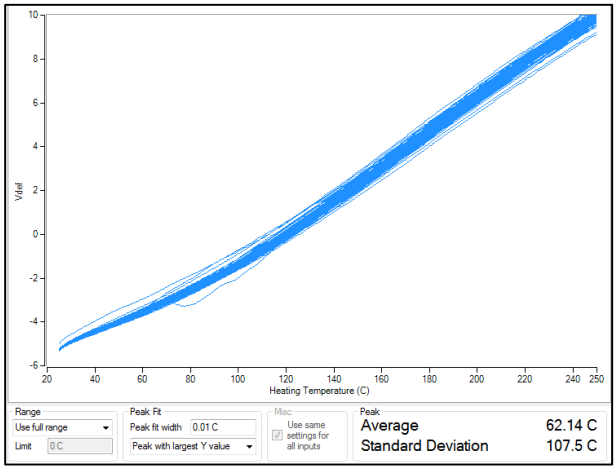

Figure 4.15 *Individual TTM probe deflection graphs for an HPMC film.*

The probable explanation behind this behaviour is that HPMC has a weak and indistinct glass transition. McPhillips et al. (1999) faced a few difficulties while trying to measure T_g of HPMC films using MTDSC, although ultimately they were able to measure it. A large sample size is usually required in order to overcome the issues of measuring a weak transition. In the case of TTM, each point in the measurement will test a very small amount of HPMC which may make it almost impossible to measure the T_g.

4.3.5.2 TTM analysis of PVP 90F films

Based on the TTM map and histogram for PVP 90F mini-tablets, no obvious pattern of transition could be observed. However, PVP 90F films showed a consistent value of the transition temperature, as shown in ***Figure 4.16***.

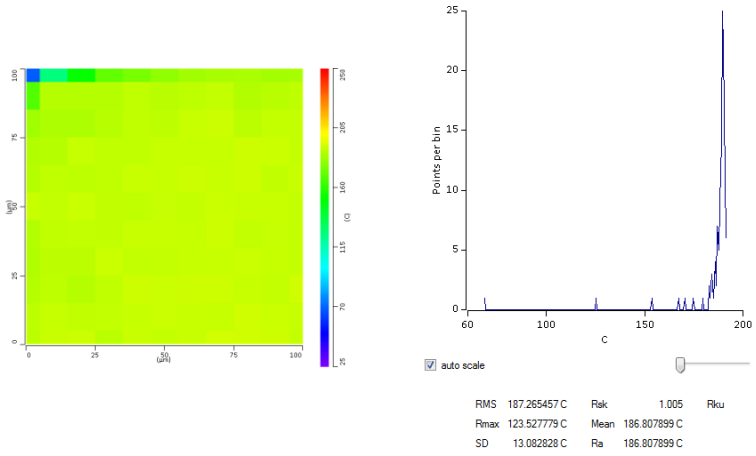

(a) (b)

Figure 4.16 *TTM map and transition temperature histogram of PVP 90F films.*

The T_g measured using MTDSC for the sample of PVP 90F used here is 178.35 ± 0.15 °C. However, the T_g obtained from TTM analysis of the PVP 90F film is 186 °C. The T_g values observed with thermal probe movement measurement, such as TTM, and other thermal measurements, such as (MT)DSC, can differ by up to 20 °C (Royall et al, 2001). This is due to the probe measuring the softening process of the polymer, rather than its actual T_g point (Craig et al., 2002). Hence, the TTM results on the PVP 90F film, with its smooth surface, good probe contact and consistent probe deflection, support the earlier hypothesis that the reason why the measured transition temperature on the surface of PVP 90F mini-tablets was variable was due to the improper contact of the probe on the mini-tablet surface.

4.3.5.3 TTM analysis of PEG 6K films

The results of TTM analysis on PEG 6K films, shown in ***Figure 4.17***, were similar to those of PEG 6K mini-tablets described earlier, as expected, since the surfaces of the mini-tablets are as smooth as that of the films. This means there is no difference in transition temperature between the films and the mini-tablets.

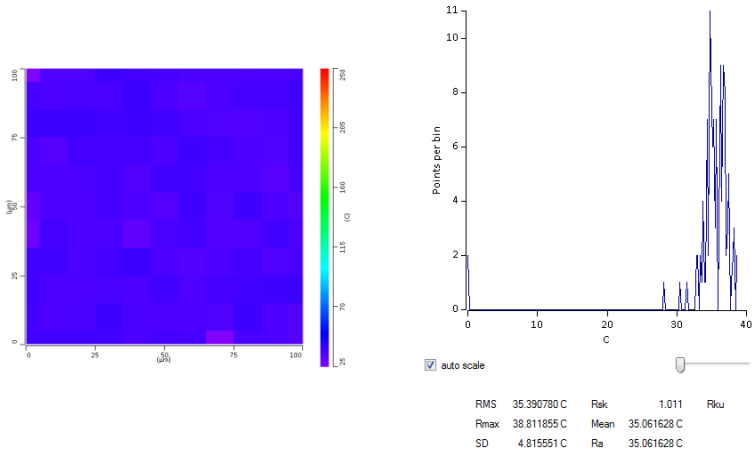

(a) (b)

Figure 4.17 *TTM map and transition temperature histogram of PEG 6K films.*

4.4 GENERAL DISCUSSION

This study sought to understand the factors behind the variable results obtained on the TTM mapping of the drug-loaded mini-tablets seen in **Chapter 3**. TTM maps generated on the surface of samples of the multi-component drug-loaded mini-tablets did not show the expected distribution of components or a reproducible pattern of transitions and one possible explanation was that the surface of the mini-tablets was too rough for the technique. A range of mono-component mini-tablets was made and tested to examine this. SEM images showed that the surfaces of PEG 6K tablets were smooth, due to the tabletting process generating transient temperatures higher than the melting point of PEG 6K. The TTM maps of PEG 6K mini-tablets showed reproducible results, with a sensible value of the melting point of PEG 6K. However, mini-tablets based on both HPMC and PVP 90F were rough, with individual particles being seen and gaps between these particles also being observed. It is thought that as the TTM probe is very small (30 nm), it can easily slip down the side of a particle or into the gap between particles, leading to incomplete or no contact, ultimately resulting in variable and misleading reasons. A comparative study on films prepared from the same polymers supported the

view that the good probe-sample contact was vital in generating reliable data and that the rougher the surface, the less reliable the data generated.

One conclusion from this study would be that a visual surface image should be taken before a TTM study is conducted, to ensure that the probe is landed correctly on a particle, rather than in a gap or on the side of a particle. This is possible with the micro-thermal analysis equipment, as this is based on an atomic force microscope (AFM), with the AFM probe being replaced by the thermal probe. Hence, it is possible to obtain both an AFM image and a thermal image of the same point on the sample's surface. Unfortunately, the TTM equipment (Vesta, Anasys Instruments, USA) is based on a light microscope rather than an AFM, hence the visual image resolution is not sufficient to land the TTM nano-probe in a sufficiently controlled manner.

As this particular study was undertaken to help interpret the unexpected TTM results from Chapter 3, and used mono-component mini-tablets only, it cannot be used as a comparator with the analytical results of the chloramphenicol-loaded mini-tablets. If the surface of the chloramphenicol-loaded mini-tablets can be made to be smooth enough then it would be possible to perform TTM analysis on these tablets and then the results could be compared to the conventional chemical analysis, such as that conducted for the drug content uniformity assessment.

4.5 CONCLUSIONS

TTM can be used to measure the component distribution on the surface of a tablet. However, it is vital to ascertain that the surface is as smooth as possible and that the probe is positioned in the centre of a particle, rather than its edge or in a gap between particles. It is recommended that a topographical image of the sample's surface be acquired prior to TTM analysis to aid in the interpretation of the results and ideally the components used should all have distinct temperature transitions to enable clear differentiation between them.

Chapter 5

Manufacturing Ocular Mini-tablets Using 3D-printing

Manufacturing Ocular Mini-tablets Using 3D-printing

5.1 INTRODUCTION

In Chapter 3, a conventional manufacturing process of direct compression of a powder blend was used to prepare a range of ocular mini-tablets. There are many advantages of using this approach, not least the extensive knowledge within the pharmaceutical industry on tabletting techniques and tabletting machinery. However, there are also potential disadvantages of this approach, such as the need to apply compaction pressures which are too high for tablet punches to withstand and the requirement for the powders to exhibit excellent mixing and flow characteristics.

A novel approach studied in this Chapter is to use 3D-printing techniques in order to prepare mini-tablets. In recent years, 3D-printing has become popular in a range of scientific and artistic endeavours and has started to gain popularity in the pharmaceutical field, as it has the potential to allow bespoke design and manufacture of products, which is not so easy to achieve with conventional manufacturing paradigms (Jonathan and Karim, 2016). To date, there are only a few publications examining the potential for 3D-printing of tablets and they concentrate on conventional, large-sized tablets (Khaled et al., 2014, Wang et al., 2016). Here, the utility of the 3D-printing approach for the manufacture of mini-tablets is explored.

There are a few types of 3D-printer available, but the most popular in the market are fused deposition modelling (FDM) and stereolithography apparatus (SLA) printers. An FDM printer works by heating and extruding filaments and building the object layer by layer. Several studies have been conducted using an FDM printer combined with hot melt extrusion (HME) technique to manufacture films and tablets. For example, Sandler et al. (2014) used HME to prepare drug-loaded extrudates which they then used to 3D-

print with an FDM printer devices which resembled indwelling catheters. A similar approach was adopted by Goyanes et al. (2015) in their preparation of large tablets of different geometrical shapes in order to study the drug release profile.

Meanwhile, an SLA printer uses a photopolymerisation process, in which light catalyses the production of a polymer from a solution of monomer, and uses a laser to cure (polymerise) the photopolymer while shaping it into an object. The SLA technique is also the oldest 3D-printing technique, patented by (Hull, 1986). One common photopolymer used in the SLA approach is polyethylene glycol diacrylate (PEGDA). Hahn et al. (2006a) and Hahn et al. (2006b) used PEGDA with a standard laser jet printer to print hydrogel films. The hydrogel films were used in cell behaviour studies. PEGDA has also been used with a laser printer to manufacture scaffolds for multicellular tissue (Ovsianikov et al., 2010) and aortic valves (Hockaday et al., 2012). The polymer was chosen for those published studies because of its biocompatible properties.

In this chapter, 3D-printing techniques have been used to manufacture ocular mini-tablets. The desired shape of the 3D-printed mini-tablets was the same as that used in Chapter 3 for the compressed powder mini-tablets and was chosen to allow direct comparison to the previous study. The physical properties of the 3D-printed tablets and their corresponding dissolution profiles were characterised to investigate the potential of using this technique as tabletting process.

5.2 METHODOLOGY

5.2.1 Materials

Hydroxypropyl methylcellulose K4M (HPMC) was purchased from The DOW Chemical Company, USA. Polyethylene glycol 6000 (PEG 6K) was purchased from Clariant GmbH, Germany. Polyvinylpyrrolidone 90F, (Kollidon 90F™) (PVP 90F) was provided by BASF The Chemical Company, Germany. Polyethylene oxide 8,000,000 (PEO 8M), chloramphenicol, polyethylene glycol 4000 (PEG 4K), polyethylene glycol diacrylate 700 (PEGDA), phenylbis (2,4,6-trimethylbenzoyl) phosphine oxide (BAPO), sodium bicarbonate and calcium chloride were purchased from Sigma Aldrich, U.K. Sodium chloride was purchased from Fluka Chemie GmbH, Germany. Sodium stearyl fumarate (SSF) was purchased from Tokyo Chemical Industry, Japan. Flexible resin was purchased from Formlabs Inc, USA.

5.2.2 Methods

5.2.2.1 Hot Melt Extrusion

Hot melt extrusion was performed using a Process II parallel twin screw extruder (Thermo Scientific, USA) with a 2 mm nozzle. 15 g of material was extruded per batch. The extrusion parameters were varied, depending on the polymer's melting point or glass transition temperature. The extrusion temperature ranged between 50 and 180 °C with screw speed of 25 rpm.

5.2.2.2 Preparation of photopolymer solutions

Seven solutions were prepared based on formulations shown in ***Table 5.1***. The formulations all contained 100 g PEGDA, 2 g BAPO and 5 g chloramphenicol. Specific formulations also contained one or more of the following materials: 25 mL of H_2O and 25

g of the specified polymer (PEG 6K or PEG 4K). Each formulation was then printed by using a stereolithography 3D-printer.

Table 5.1 *Formulation of photopolymer solutions used for 3D-printing mini-tablets.*

Formula	**Component**					
Name	PEGDA	BAPO	Chl	H_2O	PEG 6K	PEG 4K
Pure	100 g	2 g	5 g	50 mL	-	-
P6K1	100 g	2 g	5 g	25 mL	25 g	-
P6K2	100 g	2 g	5 g	-	25 g	-
P6K3	100 g	2 g	5 g	-	50 g	-
P4K1	100 g	2 g	5 g	25 mL	-	25 g
P4K2	100 g	2 g	5 g	-	-	25 g

* Chl = chloramphenicol

5.2.2.3 3D-printing

The mini-tablets and production mould were designed using Tinkercad (2015), a browser-based 3D design and modelling application, as explained in **Chapter 2**. The design was then saved as an .STL file format and sent to the 3D-printer controller. The printer used to print the mini-tablets and mould is Form 1+ high resolution stereo-lithography printer from Formlabs (USA). The type of material used as printer setting is "flexible" with the highest resolution at 0.05 mm, as explained in **Chapter 2**.

5.2.2.4 Physical characterisation of the 3D-printed mini-tablets

The weight uniformity, measurement of dimensions, crushing strength, friability and moisture uptake methods employed here were described in detail in **Chapters 2** and **3**.

5.2.2.5 Water content

Water content in the 3D-printed mini-tablets was measured by thermogravimetric analysis (TGA). The TGA was equilibrated at 25 °C, heated up to 110 °C at 10 °C/minute and held isothermally for 5 minutes. The percentage of water loss then calculated based on the measured weight changes.

5.2.2.6 Modulated temperature differential scanning calorimetry

Modulated temperature differential scanning calorimetry (MTDSC) was performed using a DSC Q1000 (TA Instruments, USA) over a temperature range of 25 to 200 °C. The method details were described in **Chapter 2**.

5.2.2.7 Visualisation of the photopolymerisation process

Solutions prepared based on ***Table 5.1*** were filled into a polystyrene semi-micro cuvette and the photopolymerisation processes were recorded using a Leica DM2700M microscope (Leica, Germany), a materials microscope with universal LED illumination equipped with digital camera. The capture rate of the video was set at the highest resolution of 1 frame per second (fps). The time taken for the photopolymerisation processes to occur was recorded. Three replicates were performed for each sample.

5.2.2.8 Surface analysis

The surface of the 3D-printed mini-tablets was evaluated by using SEM and TTM techniques as described in **Chapters 2** and **3.**

5.2.2.9 Drug release profile

A modified flow-through dissolution apparatus was used to assess the drug release profile of the mini-tablets as described in **Chapters 2** and **3**. The samples were taken every hour up to 9 hours. The drug release was then quantified spectrophotometrically at 278 nm. At the end of the dissolution test, the remnant mini-tablet was placed into a 20

mL conical test tube containing 15 mL of STF and stirred with a magnetic stirrer. The magnetic stirrer performed the dual functions of stirring the solution while crushing the mini-tablet to facilitate drug extraction. The solution was left for 24 hours before being spectrophotometrically quantified at 278 nm. At least three replicates were made for each formulation.

5.2.2.10 Mathematical modelling for dissolution profile

Zero order kinetics, first order kinetics and the Korsmeyer-Peppas equation were used as mathematical models to determine the dissolution profile statistically. Similarly, the difference (f_1) and similarity (f_2) factors, as proposed by Moore and Flanner (1996), were used to evaluate differences between dissolution profiles. These models are described in **Chapters 2** and **3**.

5.2.2.11 Total drug content

The total drug content in the 3D-printed mini-tablets was determined based on the amount of drug that been released during the dissolution testing and the amount of drug obtained from the remnant tablets as described above.

5.2.2.12 Correlation between vapour sorption and release profile

Graphs of percentage drug release against percentage weight change were plotted to investigate the correlation between the release profiles and vapour sorption, as described in **Chapter 3**.

5.3 RESULTS AND DISCUSSION

5.3.1 Hot Melt Extrusion

The first part of the study was an initial investigation into whether hot melt extrusion (HME) extrudates of the necessary polymers could be made, as filaments are required for the fused deposition modelling (FDM) 3D-printer to work. This type of 3D-printer relies on in-situ melting of the formulation and deposition of a liquid droplet in a pre-defined location. A filament of the formulation is therefore required in order to provide the source of the material and to feed it through the melting and deposition zones of the printer. It is not possible to run this type of 3D-printer without a filament of the material under test. The polymers chosen for this study were assessed as to whether they could be extruded using the HME. If successful, chloramphenicol will be integrated in the polymer. The drug-loaded extrudates would then be used to print ocular mini-tablets by using the FDM 3D-printer.

5.3.1.1 Pure polymer extrusion

The HME used in this study has 8 temperature control points along the barrel that can be controlled individually. However, all extrusion processes performed in this study used the same temperature for all 8 points. Based on data from **Chapter 4**, polyethylene glycol 6000 (PEG 6K) has a melting point at 59.30 ± 1.38 °C. As a starting point, 70 °C was chosen as the heating temperature for this polymer. This temperature was purposely chosen to observe whether extrudates are able to form by heating PEG 6K at a slightly higher temperature than its melting point. Molten PEG 6K was observed dripping from the exit nozzle of the extruder, hence it can be concluded that this temperature (70 °C) is too high a working temperature for PEG 6K and that the molten polymer does not have enough time to cool down and harden into extrudates as it goes through the exit nozzle. The heating temperature then was decreased to 60 °C, at the high end of the melting

point range observed for PEG 6K here. A similar phenomenon to the previous run was observed even though the heating temperature is in PEG 6K melting point range. The heating temperature was still considered too high for PEG 6K to be extruded properly. PEG 6K then was extruded at 55 °C, below the melting point measured here (59.30 ± 1.38 °C), but within the published melting point range for this polymer of 55 to 60 °C (Rowe et al., 2009). Extrudates were obtained at this point as shown in ***Figure 5.1***. The extrudate was slightly brittle and could easily be broken into two. There was no visual evidence of unmelted material on the outside surface of the extrudate, or on the newly created surfaces when the extrudate was snapped into two.

Figure 5.1 *PEG 6K extrudates prepared at 55 °C.*

The heating temperature was further decreased by 5 °C down to 50 °C to observe if PEG 6K is able to be extruded at temperatures lower than its melting point. Unfortunately, at this temperature PEG 6K just moves through the barrel without melting or softening. It was therefore decided that 55 °C is the most successful heating temperature to produce extrudates of PEG 6K.

The attempts to extrude polyethylene oxide 8,000,000 (PEO 8M), hydroxypropyl methylcellulose K4M (HPMC) and polyvinylpyrrolidone 90F (PVP 90F) at temperatures

ranging from 55 °C to 180 °C were not successful. This is because these three polymers all have very high molecular weights, which means they have high viscosity when in the molten state. Polymers with high viscosity are difficult to be extruded and will block the die heater, i.e. the exit nozzle. When this happens, it will cause the pressure in the extruder to increase and the machine will cease to work once the pressure goes above a certain level. Because of that, those three polymers cannot be extruded as they are and need an additional plasticiser to decrease the viscosity. These current observations are in agreement with previous work in this area (Kolter et al., 2012, Ma et al., 2013, Prodduturi et al., 2005). Since PEG 6K is often used in pharmaceutical formulations as a plasticiser, binary combinations of each of those three polymers and PEG 6K were tested.

5.3.1.2 Combination extrusion

Each polymer (HPMC, PEO 8M and PVP 90F) was extruded with PEG 6K in the weight ratios of 3:1, 1:1 and 1:3 (polymer : PEG 6K). The weighed powders (15 g total batch size) were homogenised using a Turbula mixer for 10 minutes. The mixture of PEO 8M and PEG 6K was extruded at temperatures between 55 °C and 80 °C, in 5 °C increments, using the experience of extruding pure PEG 6K and the published melting point of PEO 8M (65 to 70 °C) as a starting point for the temperature selection (Rowe et al., 2009). The first mixture that was studied was the 3:1 ratio. However, this combination could not be extruded even when the heating temperature exceeded the melting point of PEO 8M, due to excessive pressure readings in the barrel of the extruder. According to the study by Pinto et al. (2004) on PEO 301 and PEO 303 with molecular weights of 4 MDa and 7 MDa, respectively, it was not possible to extrude PEO with such high molecular weights at 50 % of the total powder weight when combined with propranolol hydrochloride and lactose. In their study, PEO could only be extruded at a maximum of 40 % of the total weight with the presence of water as a plasticiser. The amount of PEO in the mixture was then decreased to the ratio of 1:1. At 55 °C, the lowest temperature

studied, the mixture was able to be extruded. The appearance of the extrudate was similar to that of PEG 6K alone. Closer inspection showed a few unmelted powder particles, probably PEO 8M, scattered in the extrudate (***Figure 5.2***).

Figure 5.2 *PEO 8M : PEG 6K (1 : 1) extrudate prepared at 55 °C.*

In an attempt to reduce the amount of unmelted solid material, the heating temperature was increased to 60 °C. At this temperature, extrudates were successfully produced, but their surface looked uneven and rough, as shown in ***Figure 5.3***, although there was no obvious powder particles as seen with the extrudates formed at 55 °C. The extrudate was also fragile and could easily be broken into two. When the processing temperature was increased further to 70 °C, the extruder ceased to work because of high pressure readings in the barrel. This is probably because the PEO 8M was predominantly molten at this temperature, which then significantly increased the viscosity of the mixture to above the cut-off point for equipment function.

Figure 5.3 *PEO 8M : PEG 6K (1 : 1) extrudate produced at 60 °C.*

At a process temperature of 80 °C, extrudates could be formed, which is probably due to the increased temperature lowering the viscosity sufficiently to allow the equipment to function. The extrudate obtained was a bit lumpy and felt it rubbery to touch. The colour of the extrudate was also slightly yellowish, unlike previous extrudates, which were white, as shown in ***Figure 5.4***. At this point, processing at 55 °C can be considered to produce the best extrudate for this specific combination of polymers, based on appearance. However, the presence of unmelted PEO 8M in the extrudate indicates that the two polymers do not integrate fully with each other, so the product is not ideal.

Figure 5.4 *PEO 8M : PEG 6K (1 : 1) extrudate produced at 80 °C.*

The amount of PEO 8M in the mixture was further decreased to a 1:3 ratio with PEG 6K. At 55 °C as the processing temperature, the extrudate obtained was similar to the 1:1 extrudate at the same temperature, with a few unmelted PEO 8M polymer particles being observed in the extrudate. A similar phenomena to the 1:1 extrudate was also displayed when the temperature increased to 60 °C. However, when the processing temperature was increased to 70 °C, a lumpy and rubbery extrudate was obtained. The extrudate showed similar appearance to the 1:1 extrudate produced at 80 °C but with a white colour instead of yellowish. Molten polymer could also be observed coming out from the barrel's top opening, as showed in ***Figure 5.5***, and from the nozzle at the beginning of the extrusion. The molten polymer is more likely to be PEG 6K, which has a lower melting point than PEO 8M. A similar conclusion as with the 1:1 formulation can be made for the 1:3 formulation for the best extrudate, based on the appearance, i.e. a processing temperature of 55 °C is best, but some unmixed PEO 8M was still obvious.

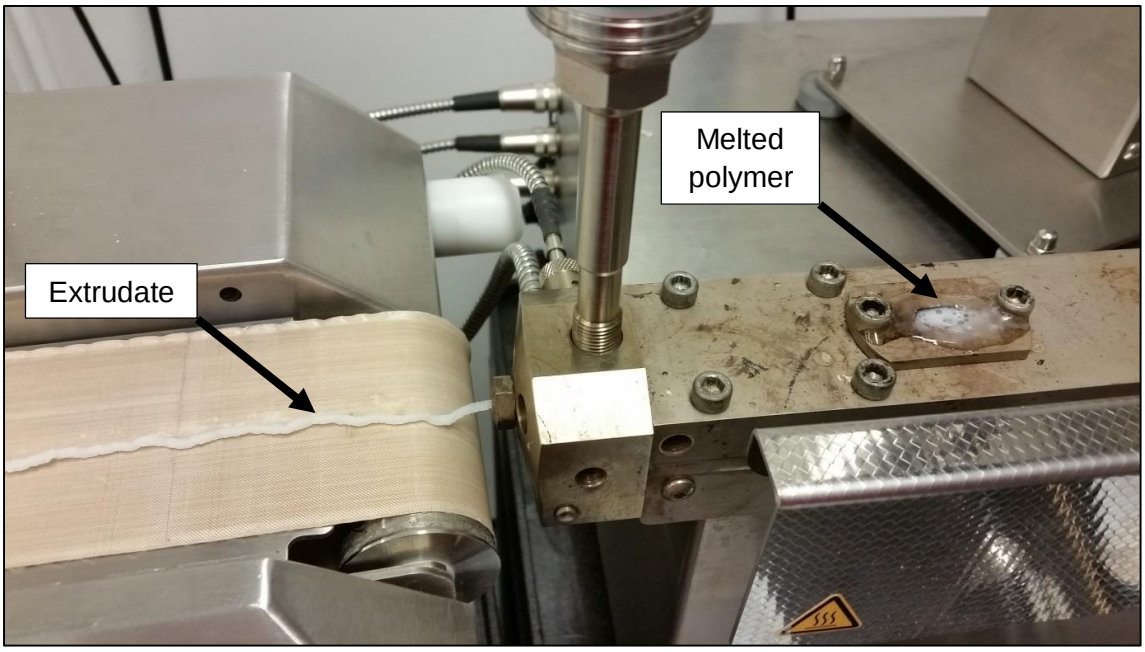

Figure 5.5 *PEO 8M : PEG 6K (1:3) extrudate and melted polymer processed at 80 °C.*

For the combinations of HPMC or PVP 90F with PEG 6K, none of the mixtures were successfully extruded. The mixtures were heated at 160, 170, 175 and 180 °C. A similar scenario was observed for all heating temperatures. Firstly, molten polymer was observed coming out of the nozzle, most likely PEG 6K due to its lower melting point. Then, the polymer started to block the die heater, which caused the extruder to cease to work due to high pressure inside the barrel. The current results therefore agree with the findings of Ma et al. (2013) and Kolter et al. (2012), who concluded that HPMC K4M and PVP 90F cannot be extruded at high concentrations.

Due to unsuccessful extrusion of the desired polymers except PEG 6K, the idea of using extrudates to 3D print the mini-tablets cannot be executed. A different approach was therefore investigated using an SLA 3D printer.

5.3.2 3D Design

5.3.2.1 Manufacturing 3D-printed mini-tablets using a 3D-printed mould

The 3D-printed mini-tablets were designed to be similar in shape with the powder compressed mini-tablets discussed in **Chapter 3**, being cylindrical with 2 mm diameter and 2 mm height. However, the cap surfaces of the 3D-printed mini-tablets were kept flat, compared to the curved surface of the compressed mini-tablets. This is because the flat surfaces design is easier to be 3D-printed than a design with curved top and bottom surfaces. By choosing the similar shape, comparison of the properties and behaviour of the 3D-printed mini-tablets and the compressed powder mini-tablets discussed in **Chapter 3** can be made.

One way of making a 3D-printed product using the stereolithography approach is to use a mould to hold the initial unpolymerised liquid before the photopolymerisation process takes place. The mould determines the overall size and shape of the product, in this

case the 3D-printed mini-tablets. Curing occurs through exposure of the unpolymerised liquid to UV light of the relevant wavelength through the walls of the translucent mould. This approach was investigated initially due to its potential ease of use. Following the design of the 3D-printed mini-tablets described above, a complementary mould was also designed using the Tinkercad software, as described in **Chapter 2**, and consisted of identical matching top and bottom pieces, which would be joined together to form the cavities, into which the unpolymerised liquid would flow. ***Figure 5.6*** illustrates the initial design for the mini-tablets moulds, showing a 3 x 3 grid of nine cavities linked together by channels to allow the movement of the liquid. Three of these channels were then open to the exterior to allow easy input of the unpolymerised liquid. The top and bottom moulds were then successfully printed by using flexible resin (Formlabs, USA).

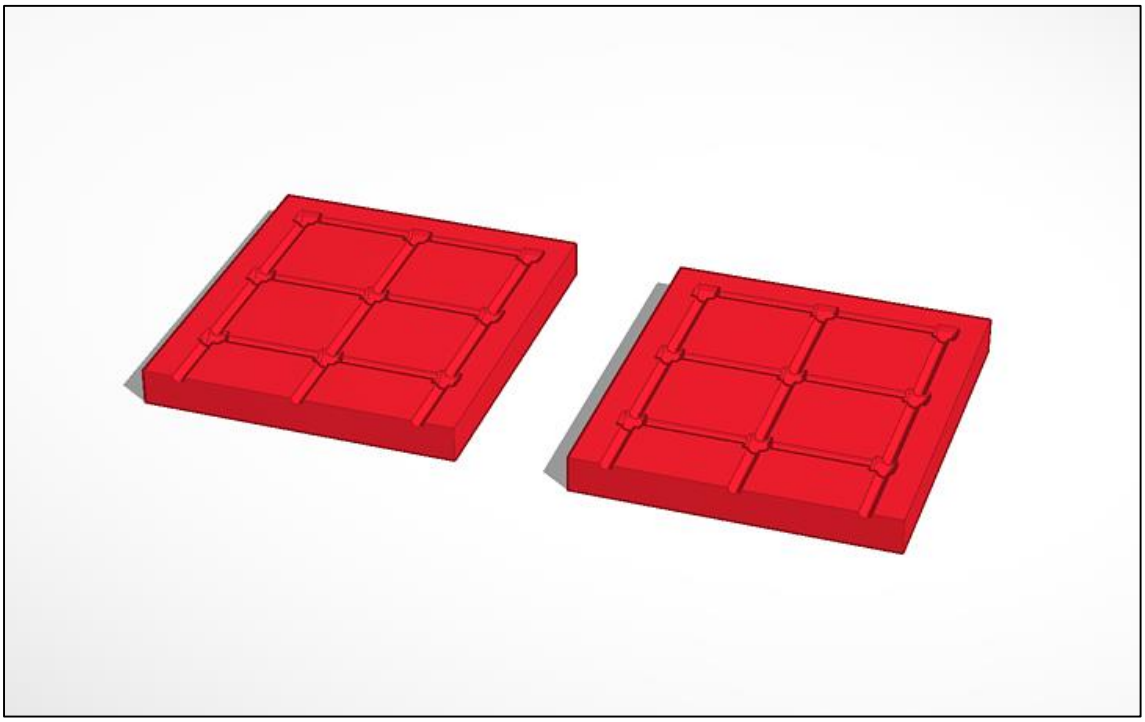

Figure 5.6 *First mould design for the 3-D printed mini-tablets.*

The printed moulds were clipped together and a photopolymer solution made using the "Pure" formulation (consisting of PEGDA, BAPO, chloramphenicol and water, ***Table 5.1***)

was filled into the mould using a syringe. However, there are flaws with this design of the moulds, in that the top and bottom surfaces could not be matched together properly, resulting in solution leaking from the gap between the moulds. To overcome these problems, a simple solution was attempted - to add a tongue-and-groove functionality to the mould (***Figure 5.7***).

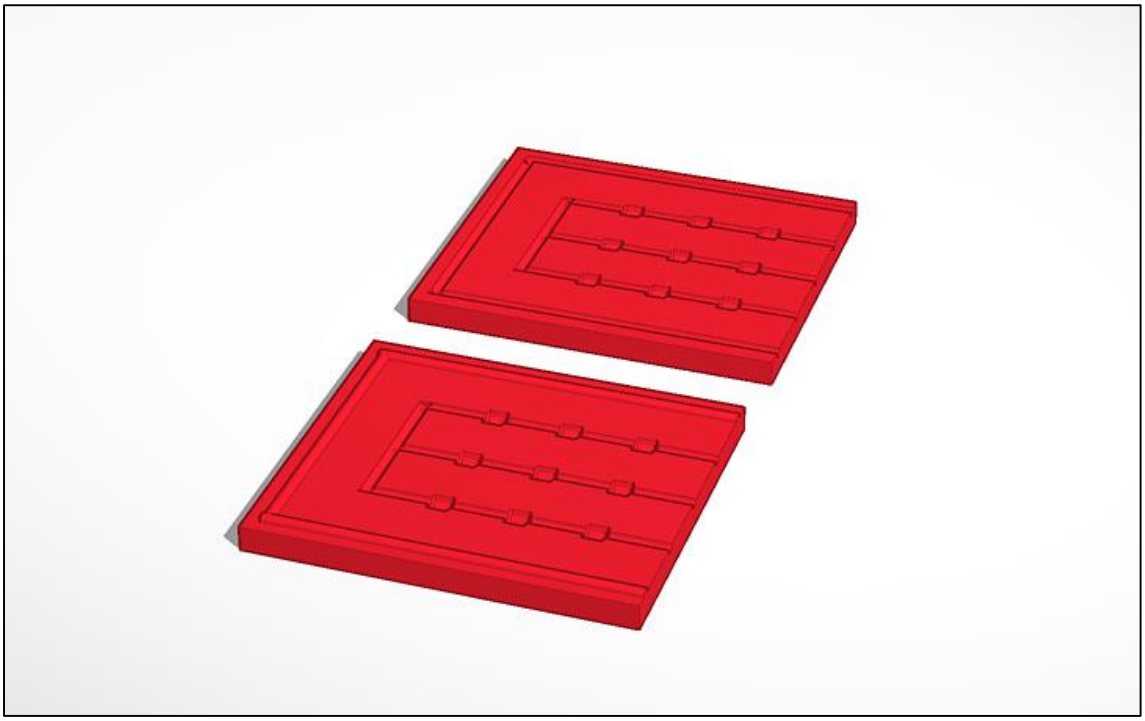

Figure 5.7 *Optimised mould design for the 3D-printed mini-tablets*

By adding a ridge on one side and a hollow on the other side of the moulds, the moulds can be interlocked and this action should solve the problems of connection and leakage. The moulds were printed, assembled and clipped to hold them together. The "Pure" photopolymer solution (as described in ***Table 5.1***) was filled in and exposed to UV-light at 365 nm for a certain time to initiate the photopolymerisation process and cure the polymer producing a solid product.

The effectiveness of the curing process was tested after 5, 15 and 30 minutes. Based on visual observation, the solution had not polymerised and still runny within 5 minutes. After 15 minutes, most of the solution was polymerised but the moulds were glued together and the polymerised mini-tablets broke when the moulds were separated. When the solution was left to cure for 30 minutes, the polymerised mini-tablets dried and crumbled when removed from the mould. The glueing phenomenon was due to a small amount of the formulation leaking out from the channels and forming a thin layer between the top and bottom mould. During the curing process, this thin layer was also exposed to the UV light and was polymerised, effectively making a solid bridge between the top and bottom surfaces of the mould. To attempt to prevent the moulds glueing together after the curing process, a layer of lubricant was added to the mould. The lubricant was sodium stearyl fumarate (SSF), a water-soluble lubricant generally used in conventional powder-based tablet formulations. An aqueous solution of 50 %w/v SSF was applied onto the surface of the mould and left to dry. The moulds then were put together and filled with the "Pure" polymer solution. After 15 minutes of curing, the attempt to split open the moulds was unsuccessful as it was still glued together even with a layer of SSF.

At this point, it seemed that it would be difficult, if not impossible, to manufacture 3D-printed mini-tablets using the mould and UV curing technique. The approach then shifted toward printing the mini-tablets directly onto the platform of stereolithography 3D-printer.

5.3.2.2 Manufacturing 3D-printed mini-tablets using the SLA platform method

As it was not possible to use the mould method of casting and curing the mini-tablets, an alternative method of printing directly onto the platform of the equipment and creating a support was tried. In this case, the support forms part of the design of the product, as described in **Chapter 2**, and once the desired product has been formed, it will need to be

separated from the support. As before, the mini-tablets were designed to match as closely as possible the compressed powder mini-tablets manufactured in **Chapter 3**, and were cylindrical with a 2 mm diameter and 2 mm height. The top and bottom faces were designed to be flat. The support was designed to be a flat base, with "stalks" upon which the mini-tablets themselves would be produced.

An initial batch of 60 mini-tablets was printed using the "flexible" resin (Formlabs, USA) to evaluate the likely outcome of this process. The 3D-printer settings were "flexible" as the material type, "lower" printing resolution (1 mm distance) and 1 mm base thickness with support stalks. ***Figure 5.8*** shows a batch of 3D-printed mini-tablets with the support as the base. Visually, the shape of these 3D-printed mini-tablets was similar to that of the compressed mini-tablets and to the design, indicating that this approach had potential.

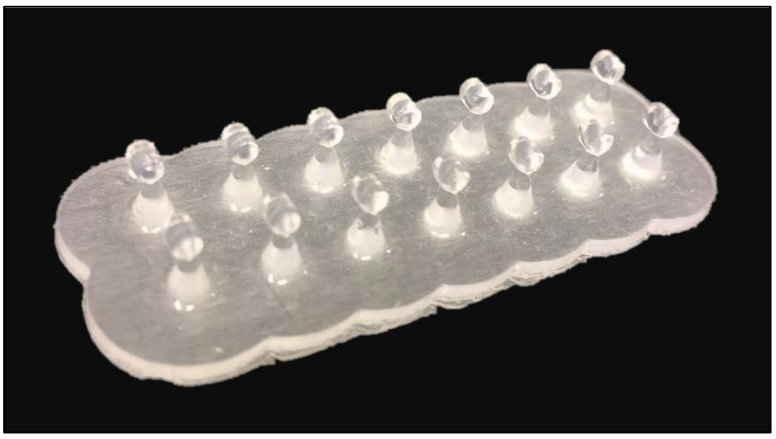

Figure 5.8 *3D-printed mini-tablets prepared from Formlabs (USA) "flexible" resin.*

However, it must be remembered that the "flexible" resin (Formlabs, USA) has been specifically developed for use within the 3D-printing field for solid objects and is not intended to be used as an ingredient in pharmaceutical products. Hence, the further experiments investigating the production settings were conducted using a more pharmaceutically-relevant formulation. A solution similar to the "Pure" formulation (***Table 5.1***) but with only 1 g of BAPO (photoinitiator) was used to optimise the printing settings,

as this concentration of 1 % of this photoinitiator with respect to this photopolymer (PEGDA) was successfully used in published studies (Wang et al., 2016, Chan et al., 2010). The settings that were used were "Clear 02" as the material type, "lower" printing resolution (1 mm distance) and 1 mm base thickness with support stalks, with a batch size of 60 mini-tablets. Although a product was manufactured, the shape of the 3D-printed product was very poor compared to the design, and the support stalks and the mini-tablets cannot be distinguished from each other (***Figure 5.9***).

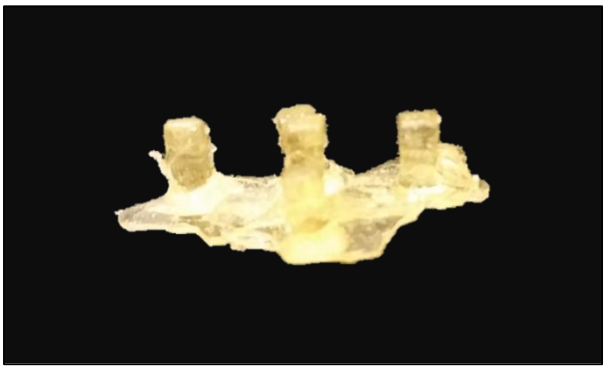

Figure 5.9 *Printed mini-tablets with 1 g of BAPO, "Clear 02" material type, "lower" printing resolution (1 mm distance) and 1 mm base thickness with support as settings.*

The type of material was then changed to "Flexible" keeping the other parameters the same and another batch of mini-tablets cast. The 3D-printed product seems improved and of a better shape (***Figure 5.10***) than the previous setting. However, the shape of mini-tablets still cannot be distinguished from the support stalks.

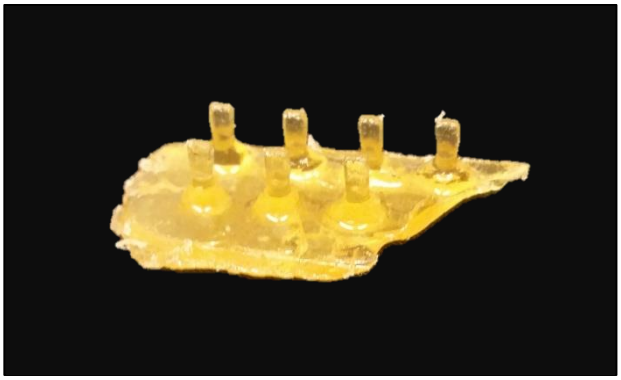

Figure 5.10 *Printed mini-tablets with 1 g of BAPO, "flexible" material type, "lower" printing resolution (1 mm distance) and 1 mm base thickness with support as settings.*

The amount of BAPO then was increased to 2 g, following the "Pure" formulation. The printing resolution was also increased to "medium" level at 0.1 mm distance in order to improve the printing quality. The printed product showed an improvement (***Figure 5.11***) where the shape of mini-tablets can now be distinguished from the support. However, the overall shape was still not as good as that of the mini-tablets printed using the flexible resin. The attempt to increase the printing resolution to the highest level (0.05 mm distance) did not result in any noticeable difference compared with the previous medium resolution, but the highest printing resolution was kept as default setting for the rest of the study.

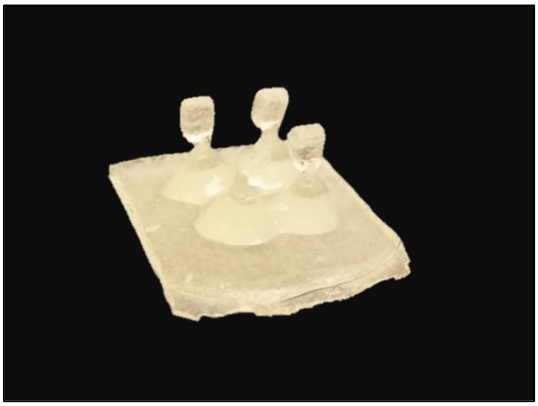

Figure 5.11 *3D-printed mini-tablets with 2 g of BAPO, "flexible" material type, "medium" printing resolution (0.1 mm distance) and 1 mm base thickness with support as settings.*

As this approach of using the support was not entirely successful, a further alternative approach was tested of printing the mini-tablets directly onto the platform without base or support. Recognisable mini-tablets were printed and resembled to some degree the compressed powder mini-tablets from Chapter 3 (***Figure 5.12***). The settings used here, i.e. "flexible" as the material type and "highest" printing resolution (0.05 mm), were chosen as default settings to 3D-print the mini-tablets.

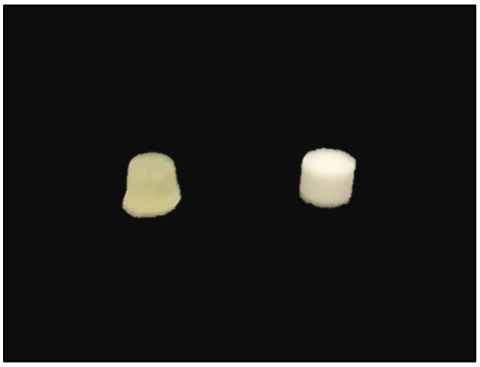

Figure 5.12 *Comparison between 3D- printed (left) and compressed powder (right) mini-tablets.*

PEG 6K was incorporated into the formulation to evaluate the effect on the drug release profile of mini-tablets of the addition of a water-soluble polymer. In order to keep the weight of the formulation constant, 25 g of PEGDA was removed from the formulation and replaced with 25 g of PEG 6K. The printing result was not as expected. "Blob"-shaped mini-tablets with an ill-defined structure were obtained from the printing (***Figure 5.13***).

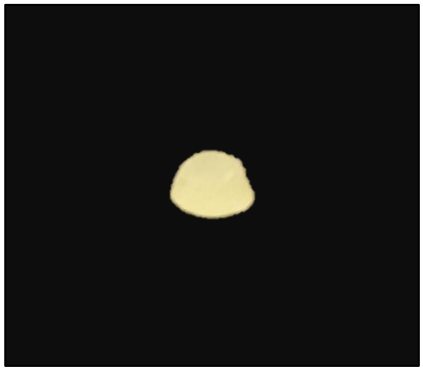

Figure 5.13 *Blob-shaped mini-tablets.*

It is likely that the cause of the poor shape of these mini-tablets is the relative lack of the photopolymer PEGDA, which gives the product its overall structure and rigidity once polymerised. Therefore, the amount of PEGDA was increased to 87.5 g while the volume of water was reduced to 37.5 mL, retaining the 25 g of PEG 6K and maintaining the overall formulation batch weight. The "blob"-shaped mini-tablets were still observed but the shape was better than the previous attempt. By reinstating the PEGDA content to its original value of 100 g and reducing the water volume further to 25 mL, whilst retaining the 25 g of PEG 6K and maintaining the overall formulation batch weight, mini-tablets similar in appearance to the "Pure" formulation were obtained and were deemed suitable for further investigation. This formulation is labelled as P6K1 formulation in ***Table 5.1***.

PEG 6K in the formulation was swapped with HPMC and PVP 90F in order to make a comparison of the effect on drug release from the 3D-printed mini-tablets with different water-soluble polymers and to mirror the formulations used in Chapter 3. Unfortunately, the HPMC formulation coagulated and formed rubbery lumps during the preparation of the solution, so could not be cast. Meanwhile, PVP 90F did not dissolve in the PEGDA solution, so again mini-tablets could not be printed from this formulation.

A batch of 3D printed mini-tablets was prepared using PEG 4K to investigate the effect on the dissolution profile of various molecular weights of PEG. PEG 4K was successfully dissolved in the photopolymer solution and this was able to be printed into mini-tablets. The formulation was labelled as P4K1.

The water was removed from the formulation to evaluate if it has any effect on the polymerisation of the solution and/or the mini-tablets dissolution profiles. Both PEG 6K and PEG 4K, at 25 g, were dissolved in the solutions and their mini-tablets have decent shapes after being printed. PEG 6K and PEG 4K formulations without water were labelled as P6K2 and P4K2 respectively.

The amount of PEG 6K and PEG 4K in the formulations was then increased to 50 g. PEG 6K dissolved in the photopolymer solution and this as then labelled as P6K3. However, some of PEG 4K did not dissolve in the solution. Since PEG 4K is flake-like in appearance, it was ground to increase the surface area to help with the dissolution. This action improved the dissolution of PEG 4K into the photopolymer solution but there was still some undissolved polymer. This mixture was not included in the mini-tablets formulation. Although it would be expected that the PEG 4K should dissolve into the PEGDA and/or water in the photopolymerisation solution to at least the same extent as the PEG 6K as it is chemically identical but with a lower molecular weight, there is an issue in that there is only limited time available for the dissolution process to occur before photopolymerisation starts. For the formulations with increased low molecular weight PEG content, water was removed in order to maintain the same overall formulation weight, which will have had the effect of slowing the dissolution process.

Having undertaken the preliminary investigations into likely printable formulations, at this point, the six formulations in ***Table 5.1*** were 3D-printed and the mini-tablets analysed as described above.

5.3.3 Physical Characterisation

Six tests were performed to evaluate the physical properties of the 3D-printed mini-tablets: weight uniformity, measurement of dimensions, crushing strength, friability, water content and water vapour sorption. ***Table 5.2*** summarises five of these physical characteristics of the 3D-printed mini-tablets. The details of the studies regarding the physical characterisation are discussed in following sections.

Table 5.2 *Summary of the physical characterisation of the chloramphenicol-loaded 3D-printed mini-tablets (mean ± SD).*

Formula *	**Weight (mg) (n=20)**	**Diameter (mm) (n=10)**	**Thickness (mm) (n=10)**	**Friability (%)**	**Crushing strength (N) (n=10)**	**Water Content (%) (n=3)**
Pure	5.66 ± 0.53	2.33 ± 0.07	2.04 ± 0.19	n/a	5.71 ± 2.00	8.52 ± 1.65
P6K1	12.25 ± 0.93	2.58 ± 0.10	2.74 ± 0.11	n/a	24.18 ± 5.72	3.68 ± 0.10
P6K2	18.84 ± 1.19	2.74 ± 0.11	3.35 ± 0.25	n/a	22.55 ± 2.95	1.70 ± 0.01
P6K3	25.60 ± 1.48	2.86 ± 0.09	4.12 ± 0.21	n/a	19.79 ± 2.01	0.89 ± 0.02
P4K1	10.82 ± 0.62	2.53 ± 0.07	2.30 ± 0.20	n/a	20.65 ± 1.67	5.61 ± 0.57
P4K2	36.76 ± 1.60	2.97 ± 0.09	4.69 ± 0.22	n/a	9.67 ± 1.71	1.75 ± 0.04

* n/a = not applicable

* Refer to ***Table 5.1*** for full details of the formulations.

5.3.3.1 Weight uniformity

The weight of the 3D-printed mini-tablets ranged between 5.66 ± 0.53 mg for the "Pure" formulation and 36.76 ± 1.60 mg for the P4K2 formulation, as shown in ***Table 5.2***. As discussed in **Chapter 3** for the compressed powder mini-tablets, although the BP weight uniformity specification technically does not apply to products where the individual weights are less than 40 mg, the criteria were applied here as product weight variability is a good indication of whether the product and process are appropriate and useable pharmaceutically. ***Table 5.3*** shows the weight measurements of twenty 3D-printed mini-tablets randomly chosen from each formulation. Black type denotes tablets that directly passed the BP weight uniformity specification (i.e. tablets with weights showing less than 10 % deviation from the mean), red type denotes tablets that show between 10 and 20 % deviation from the mean value, and blue type denotes tablets that show greater than 20 % deviation from the mean value.

Of the six formulations studied, only P4K2 passed the BP specification directly with all 3D-printed mini-tablets showing weights with less than 10 % deviation from the mean. P4K1 and P6K2 passed when the allowance of two tablets out of 20 showing between 10 and 20 % deviation from the mean weight was taken into account. The "Pure", P6K1 and P6K3 mini-tablets all had more than two individual mini-tablet weights that showed between 10 and 20 % deviation from the mean values, and the "Pure" formulation has one tablet where the deviation from the mean was greater than 20 %. These three batches of mini-tablets would not comply with the BP standard for weight variation.

"Pure" 3D-printed mini-tablets have the lowest mean weight of all the mini-tablets formulations studied here. The weight of mini-tablets increased substantially with the addition of 25 g of low molecular weight PEG and removal of 25 mL water (P6K1 and P4K1 mini-tablets), in that the weight was roughly double that of the "Pure" formulation,

Table 5.3 *Weight uniformity of the chloramphenicol-loaded 3D-printed mini-tablets.*

Mini-tablets	Pure* (mg)	P6K1* (mg)	P6K2* (mg)	P6K3* (mg)	P4K1* (mg)	P4K2* (mg)
1	5.77	12.86	18.28	24.03	10.38	36.79
2	5.92	12.44	19.08	25.79	11.21	39.18
3	5.86	12.22	17.11	26.75	11.88	36.62
4	5.24	13.31	18.00	28.20	10.33	37.55
5	6.86	10.92	21.34	26.99	10.98	34.49
6	5.97	12.75	18.16	22.64	10.17	35.78
7	5.25	13.34	18.76	24.70	9.99	37.10
8	6.04	12.99	19.23	25.46	11.22	36.74
9	6.21	11.39	19.19	24.64	10.68	34.45
10	5.33	12.89	20.09	26.90	11.09	35.44
11	5.48	12.41	17.12	25.12	9.55	35.75
12	4.74	12.31	18.24	22.99	11.31	35.58
13	5.49	11.70	19.23	25.79	11.06	39.64
14	4.96	12.51	18.95	24.73	10.08	35.12
15	4.98	13.82	17.91	26.10	10.61	34.80
16	6.57	10.41	18.74	27.80	11.66	37.90
17	5.65	10.43	21.20	25.37	11.25	37.48
18	5.82	12.39	18.97	24.64	10.47	38.86
19	5.69	11.69	20.04	27.23	11.60	39.12
20	5.39	12.16	17.20	26.08	10.78	36.73
Mean (mg)	5.66	12.25	18.84	25.60	10.82	36.76
SD (mg)	0.53	0.93	1.19	1.48	0.62	1.60
RSD (%)	9.37	7.57	6.29	5.77	5.70	4.36

* Refer to ***Table 5.1*** for full details of the formulations.

and was further increased with the removal of water from the starting formulations (P6K2, P6K3 and P4K2 mini-tablets). This may be due in part to the densities of the low molecular weight PEGs being higher than that of water. Both PEG 6K and PEG 4K are reported to have densities of 1.080 g/cm^3 while water density is 1.000 g/cm^3 (Rowe et al., 2009). If the overall size of the 3D-printed mini-tablets remained the same, an increase of roughly 8 % in their weight would be expected if all the water in the formulation was replaced by PEG 4K or PEG 6K. However, this argument does not directly explain all of the differences in weight observed between the various batches, and it must be noted that the heavier mini-tablets were also visibly larger than their smaller counterparts, as discussed below.

5.3.3.2 Mini-tablets dimensions

The diameter and thickness of 10 mini-tablets randomly chosen from each formulation were measured, as showed in ***Table 5.4***. The results show that the diameter of the 3D-printed mini-tablets ranged from 2.33 ± 0.07 mm for the "Pure" formulation to 2.97 ± 0.09 mm for the P4K2 formulation, while the observed thickness values were between 2.04 ± 0.19 mm for the "Pure" formulation and 4.69 ± 0.22 mm for the P4K2 formulation. "Pure" mini-tablets therefore displayed the lowest values for both the diameter and thickness measurements while the P4K2 mini-tablets showed the highest values for both measurements, which is consistent with the weight data presented above. Based on the mean values and the RSD values (ranging between 2.85 and 3.90 %), the diameters of the 3D-printed mini-tablets were reasonably consistent, both between formulations and within individual formulations. In all cases, though, the mean value was greater than the original design feature of a diameter of 2 mm. The thickness values were much more varied than the diameters, both between batches and within a batch, with RSD values ranging between 3.90 % and 9.40 %.

Table 5.4 *Diameter (D) and thickness (T) of chloramphenicol-loaded 3D-printed mini-tablets.*

Mini-tablets	**Pure***		**P6K1***		**P6K2***		**P6K3***		**P4K1***		**P4K2***	
	D (mm)	T (mm)	D (mm)	T (mm)	D (mm)	T (mm)	D (mm)	T (mm)	D (mm)	T (mm)	D (mm)	T (mm)
1	2.32	1.75	2.45	2.73	2.73	3.47	2.96	3.97	2.49	2.31	2.99	5.05
2	2.23	1.91	2.66	2.92	2.92	3.23	2.92	3.80	2.70	2.69	2.95	4.46
3	2.38	2.26	2.37	2.81	2.81	3.60	2.80	4.35	2.48	2.21	2.96	4.47
4	2.29	1.92	2.63	2.88	2.88	3.73	2.84	4.34	2.59	2.10	2.93	4.80
5	2.43	2.05	2.59	2.71	2.71	3.53	3.01	3.99	2.53	2.56	2.74	4.51
6	2.38	2.15	2.61	2.68	2.68	3.51	2.84	4.03	2.47	2.00	3.04	4.48
7	2.38	1.75	2.56	2.67	2.67	3.03	2.80	4.48	2.46	2.45	2.98	4.91
8	2.21	2.25	2.70	2.53	2.53	3.41	2.75	4.02	2.53	2.20	3.09	4.88
9	2.34	2.06	2.69	2.74	2.74	2.99	2.93	4.28	2.45	2.27	2.99	4.84
10	2.35	2.29	2.53	2.68	2.68	3.02	2.75	3.91	2.56	2.22	3.03	4.45
Mean (mm)	2.33	2.04	2.58	2.74	2.74	3.35	2.86	4.12	2.53	2.30	2.97	4.69
SD (mm)	0.07	0.19	0.10	0.11	0.11	0.25	0.09	0.21	0.07	0.20	0.09	0.22
RSD (%)	2.85	9.40	3.88	3.90	3.90	7.54	2.99	5.21	2.86	8.67	2.99	4.70

* Refer to ***Table 5.1*** for full details of the formulations.

There was a general trend towards increasing thickness and diameter with increasing weight, as shown in ***Figure 5.14***. While this in itself may not be surprising (a larger mini-tablet would be expected to be heavier), it does raise some issues about control during the 3D-printing process, as the same mini-tablet design and print parameters were used for all batches, and the bulk of the material (PEGDA, BAPO, chloramphenicol) was also the same for all six batches.

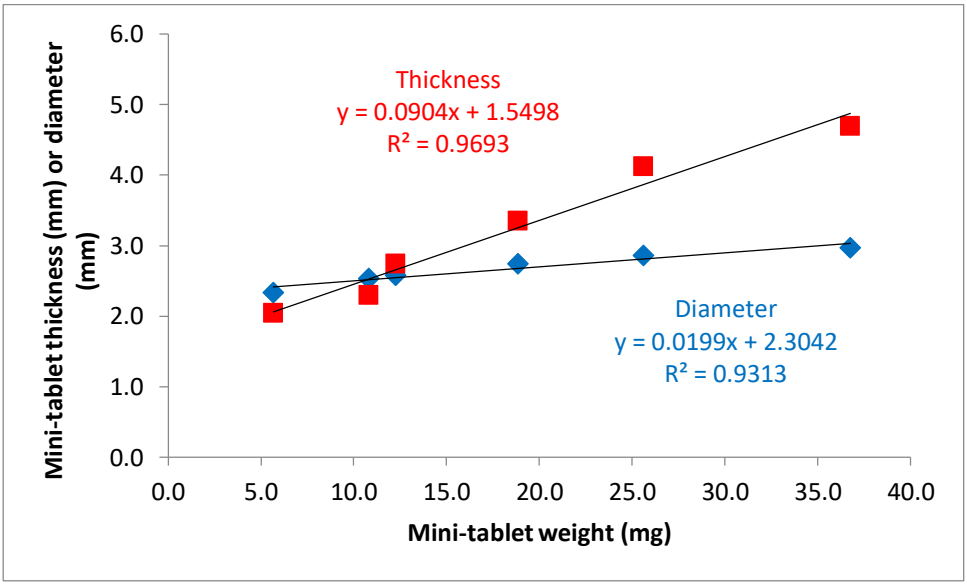

Figure 5.14 *The relationship between chloramphenicol-loaded 3D-printed mini-tablet weight, thickness and diameter.*

5.3.3.3 Crushing strength

Table 5.5 shows the crushing strength measurements of 10 mini-tablets randomly selected from each formulation. The mean crushing strength of the mini-tablets varied between 5.71 ± 2.00 N for the "Pure" formulation and 24.18 ± 5.72 N for the P6K1 formulation. The crushing strength showed a complex relationship with the formulation variables, and may also have been influenced by varying weight and shape of the mini-tablets. Generally, the crushing strength increased with the addition of the low molecular weight PEGs, but decreased with the elimination of water from the formulations.

Table 5.5 *Crushing strength of the chloramphenicol-loaded 3D-printed mini-tablets.*

Mini-tablets	Pure* (N)	P6K1* (N)	P6K2& (N)	P6K3* (N)	P4K1* (N)	P4K2* (N)
1	5.31	13.81	23.70	19.02	22.50	12.91
2	3.34	23.09	26.05	17.01	21.39	8.44
3	4.54	31.86	24.35	19.06	20.18	9.86
4	4.49	17.16	22.68	23.70	18.91	7.69
5	6.48	23.29	26.23	18.66	17.26	9.82
6	6.15	26.20	21.61	21.53	20.35	7.74
7	4.14	29.59	24.48	21.28	22.75	9.41
8	9.16	30.52	19.03	20.68	20.14	11.88
9	8.98	22.29	19.37	17.69	21.76	10.40
10	4.53	24.01	18.01	19.24	21.28	8.59
Mean (N)	5.71	24.18	22.55	19.79	20.65	9.67
SD (N)	2.00	5.72	2.95	2.01	1.67	1.71
RSD (%)	34.96	23.67	13.07	10.14	8.08	17.69

* Refer to ***Table 5.1*** for full details of the formulations.

This can be observed from the crushing strength values of "Pure"" mini-tablets compared to the matching pairs of P6K1/P6K2 and P4K1/P4K2 mini-tablets (P6K1 and P4K1 both contained 25 g of the relevant PEG and 25 mL of water, whereas P6K1 and P4K1 both contained 25 g of the relevant PEG and no water). The crushing strength values increased from 5.71 ± 2.00 N for "Pure" mini-tablets to 24.18 ± 5.72 N and 20.65 ± 1.67 N for P6K1 and P4K1 mini-tablets, respectively, and then dropped to 22.55 ± 2.95 N for the P6K2 mini-tablets and more dramatically to 9.67 ± 1.71 N for the P4K2 mini-tablets. Doubling the amount of PEG 6K in the formulation reduced the crushing strength still further.

The crushing force is a useful measure to evaluate a specific batch of tablets or mini-tablets against a pre-defined specification, but it is dependent on the size and shape of the material being tested, so for comparative purposes between formulations, the tensile strength is a better measure as it accounts for dimensions. The mean tensile strength of the mini-tablets was calculated as follows, assuming a perfect cylindrical shape, with the data being summarised in ***Table 5.6***:

$$\sigma = \frac{2P}{\pi DT} \qquad \text{Eq. 5.1}$$

σ = Tensile strength

P = Fractural loading (crushing strength)

D = Diameter

T = Thickness

The calculated values of tensile strength were different for the different batches, suggesting a formulation effect on this parameter. There appeared to be a general trend towards decreasing tensile strength with increasing weight, as shown in ***Figure 5.15***. The one formulation that did not follow this general trend was the "Pure" formulation.

Table 5.6 *Tensile strength of chloramphenicol-loaded 3D-printed mini-tablets.*

	Pure* **(N)**	**P6K1*** **(N)**	**P6K2*** **(N)**	**P6K3*** **(N)**	**P4K1*** **(N)**	**P4K2*** **(N)**
Mean thickness (mm)	2.04	2.74	3.35	4.12	2.30	4.69
Mean diameter (mm)	2.33	2.58	2.74	2.86	2.53	2.97
Mean crushing strength (N)	5.71	24.18	22.55	19.79	20.65	9.67
Mean tensile strength (MPa)	0.76	2.18	1.56	1.07	2.26	0.44

* Refer to ***Table 5.1*** for full details of the formulations.

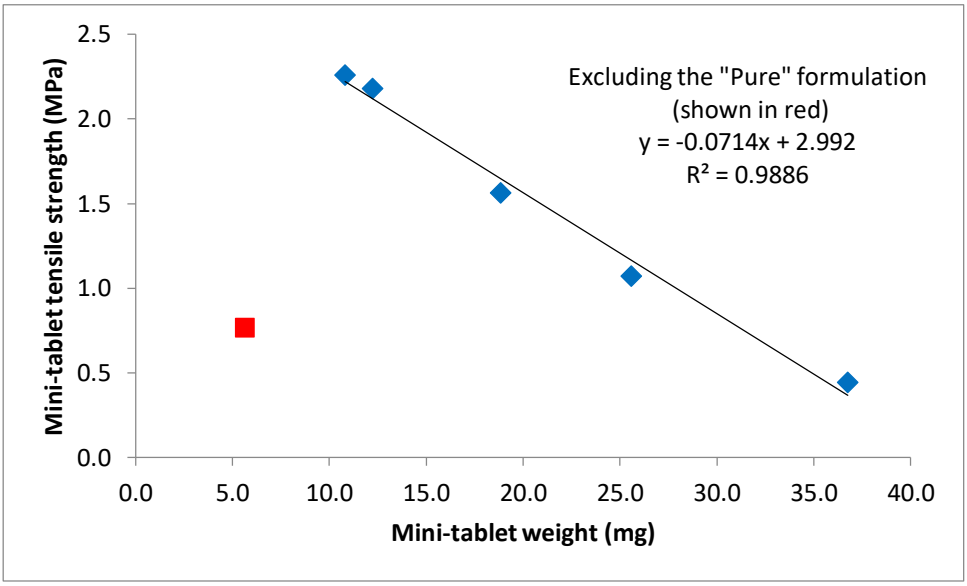

Figure 5.15 *The relationship between chloramphenicol-loaded 3D-printed mini-tablet weight and tensile strength.*

5.3.3.4 Friability test

No friability test results were obtained because the mini-tablets stuck to the surface of friability tester drum and each other during the test procedure. The test is therefore considered invalid for these 3D-printed mini-tablets. There are a few implications of stickiness for the 3D-printed product in terms of pharmaceutics and clinical applications. A sticky product would be difficult to pack as it may stick on the packaging machine and not properly fill in the packet. It may also keep sticking on the patient's finger and may not stick onto the eye during the application. A layer of anti-adherent applied after processing can possibly be used to overcome the stickiness of the mini-tablets. However, it may interfere with the friability test results as the weight changes measured might be coming from the loss of dust associated with the anti-adherent layer. Alternatively, it may be possible to incorporate an anti-adherent into the printing formulation.

5.3.3.5 Water content

The water content of the 3D-printed mini-tablets was assessed after manufacture by TGA. "Pure" mini-tablets showed the highest water content of all the formulations. This would be expected due to the high quantity of water used in the “Pure” formulation. Meanwhile, P6K3, P6K2 and P4K2 mini-tablets showed low levels of water content, again expected as no water was added to these formulations. The water found in these mini-tablets could have arisen from low amounts of adsorbed water in the formulation ingredients or absorption from the atmosphere after manufacture. P6K1 and P4K1 showed intermediate levels of water in the final mini-tablets, as expected from the intermediate levels of water in the initial formulation.

These results therefore seem logically to be following the amount of water added into the formulation. However, closer inspection found that the amounts of water in the mini-

tablets are lower than the initial percentage of water in the formulation, as shown in ***Table 5.7***. It can be concluded that there is water loss during the printing process.

Table 5.7 *Comparison of the water content in the initial (pre-printing) formulation and the chloramphenicol-loaded 3D-printed mini-tablets (mean ± SD, n=3).*

Formula*	Water content in formulation (%)	Water content in the mini-tablets (%)
Pure	31.85	8.52 ± 1.65
P6K1	15.92	3.68 ± 0.10
P6K2	0	1.70 ± 0.01
P6K3	0	0.89 ± 0.02
P4K1	15.92	5.61 ± 0.57
P4K2	0	1.75 ± 0.04

* Refer to ***Table 5.1*** for full details of the formulations.

5.3.3.6 Vapour sorption

The moisture uptake tests were performed over 24 hours at a relative humidity level of 95.0 ± 1.0 %, the highest humidity level that can be acquired by the DVS equipment. The percentage weight changes were plotted against time as shown in ***Figure 5.16*** to evaluate the vapour sorption of each mini-tablet formulation.

“Pure” mini-tablets showed the lowest changes in weight, roughly 30 % only at equilibrium, which was reached after approximately 5 hours. The rate of moisture uptake over the first 4 hours was highest for the “Pure” formulation and the P4K1 formulation. P6K3 mini-tablets displayed the highest weight changes; slightly above 50 % at equilibrium. The rest of mini-tablets showed similar intermediate values of around 35 to 40 %.

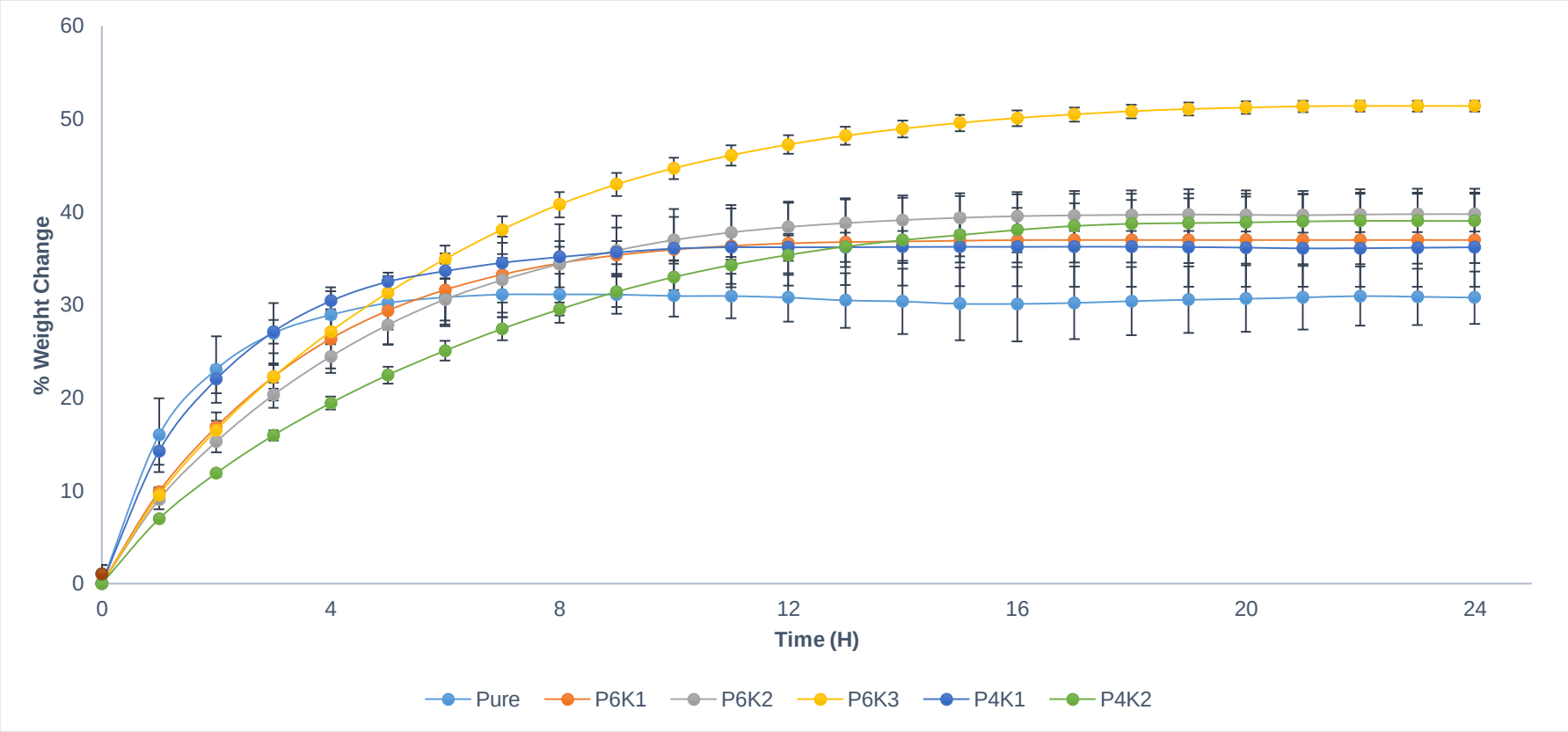

Figure 5.16 *Moisture uptake of the chloramphenicol-loaded 3D-printed mini-tablets* (mean ± SD, n=3)*

* Refer to ***Table 5.1*** for full details of the formulations.

From the graph, it can be concluded that by adding low molecular weight PEG polymers in the formulations, the mini-tablets can retain more vapour/water. P6K1, P6K2 and P6K3 all showed a lower initial rate of moisture uptake than the “Pure” formulation and a longer time until equilibrium was reached (approximately 15 hours for P6K1 and P6K2 and 20 hours for P6K3). The equilibrium moisture increased with increasing PEG 6K content, to approximately 37 to 40 % for P6K1 and P6K2, which initially contained 25 g of PEG 6K, and to approximately 51 % for P6K3, which initially contained 50 g of PEG 6K. There was limited effect of the initial presence of water in the formulations in that P6K1 and P6K2 showed very similar responses throughout this part of the study. P4K1 and P4K2 showed different initial rates of moisture uptake, but both showed similar equilibrium values of moisture content to P6K1 and P6K2, suggesting that the final moisture content is dependent on the added quantity of PEG in the initial formulation. There did not seem to be a relationship between residual moisture content in the mini-tablets and water vapour uptake in the DVS study.

5.3.4 MTDSC

MTDSC was used to try to assess whether the polymer existed in an amorphous, crystalline or semi-crystalline state in the 3D-printed mini-tablets and in which form the drug was present. The raw materials were therefore assessed as well as the final products. ***Figure 5.17*** shows the MTDSC profile of chloramphenicol, following a heat-cool-heat cycle. Chloramphenicol demonstrates a melting point of 149.22 ± 1.32 °C and a glass transition temperature (Tg) of 32.68 ± 0.34 °C. PEG 4K and PEG 6K showed melting points of 60.71 ± 0.50 and 59.30 ± 1.38 °C °C, respectively, but no obvious Tg in the temperature range studied. ***Figure 5.18*** shows the MTDSC profiles of PEG 6K and PEG 4K. PEGDA and BAPO were not studied by MTDSC as raw materials, as they would not exist in this same state after the photopolymerisation process.

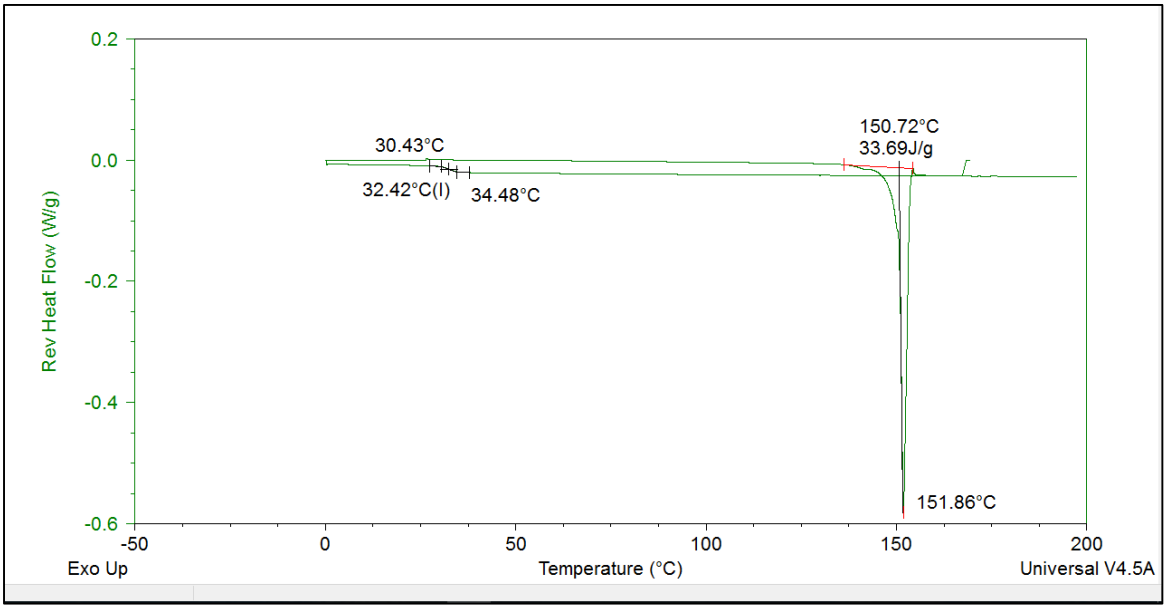

Figure 5.17 *A representative MTDSC trace of chloramphenicol.*

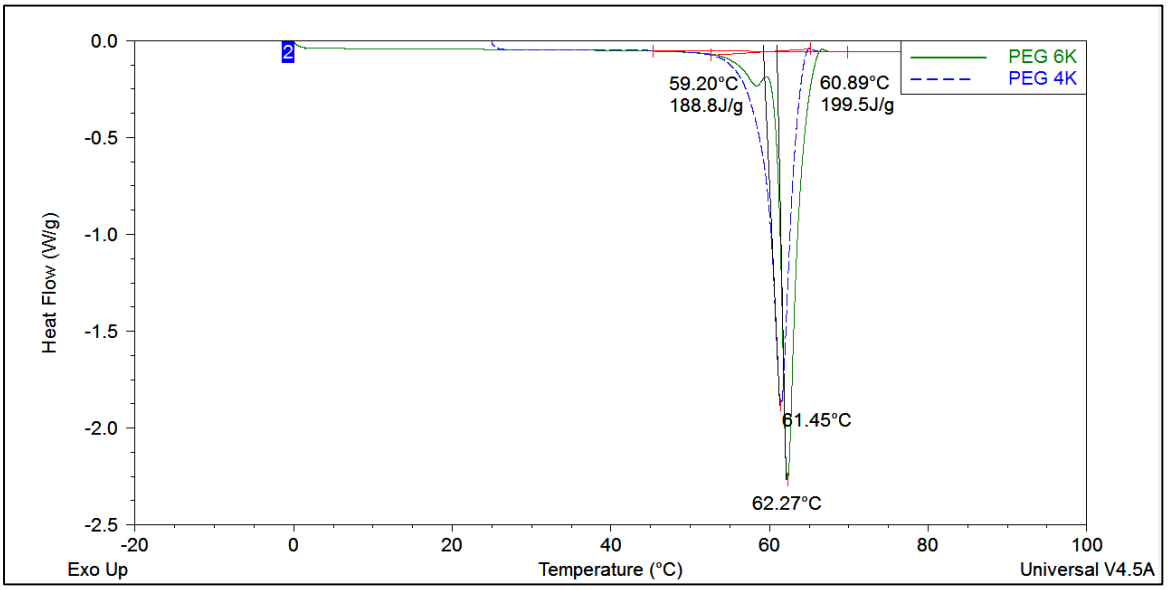

Figure 5.18 *Representative MTDSC traces of PEG 6K and PEG 4K.*

Figures 5.19 and ***5.20*** show MTDSC profiles of all mini-tablets. ***Table 5.8*** shows a summary of the MTDSC behaviour of chloramphenicol, the low molecular weight PEGs and the 3D-printed mini-tablets.

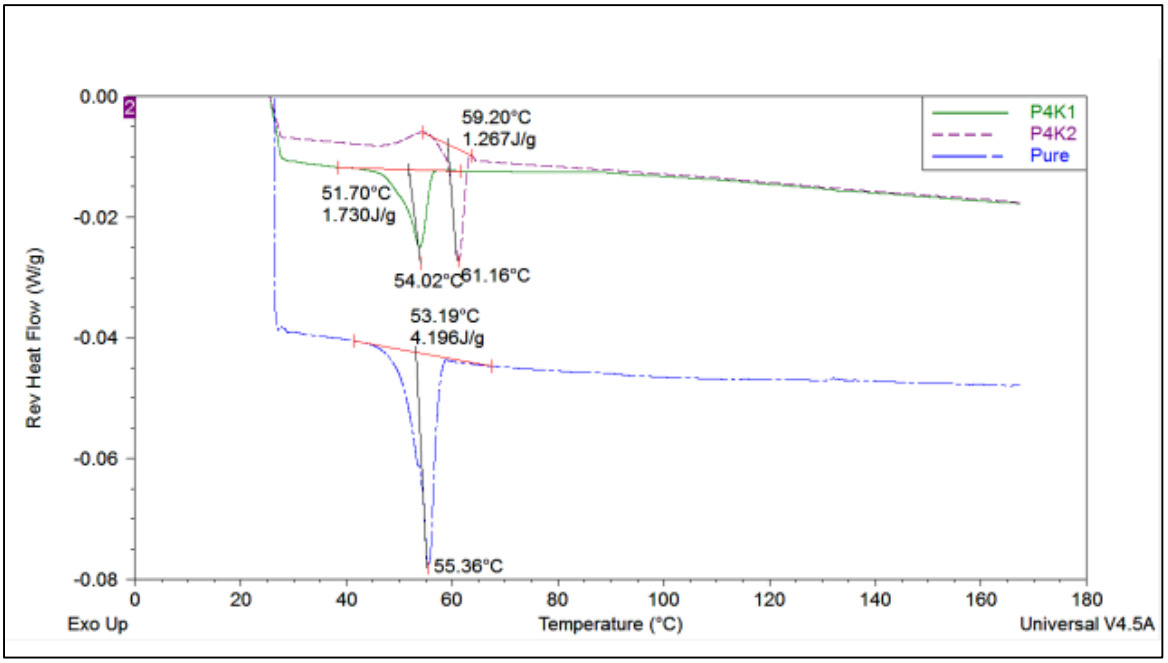

Figure 5.19 *Representative MTDSC profiles of "Pure", P4K1 and P4K2 mini-tablets.*

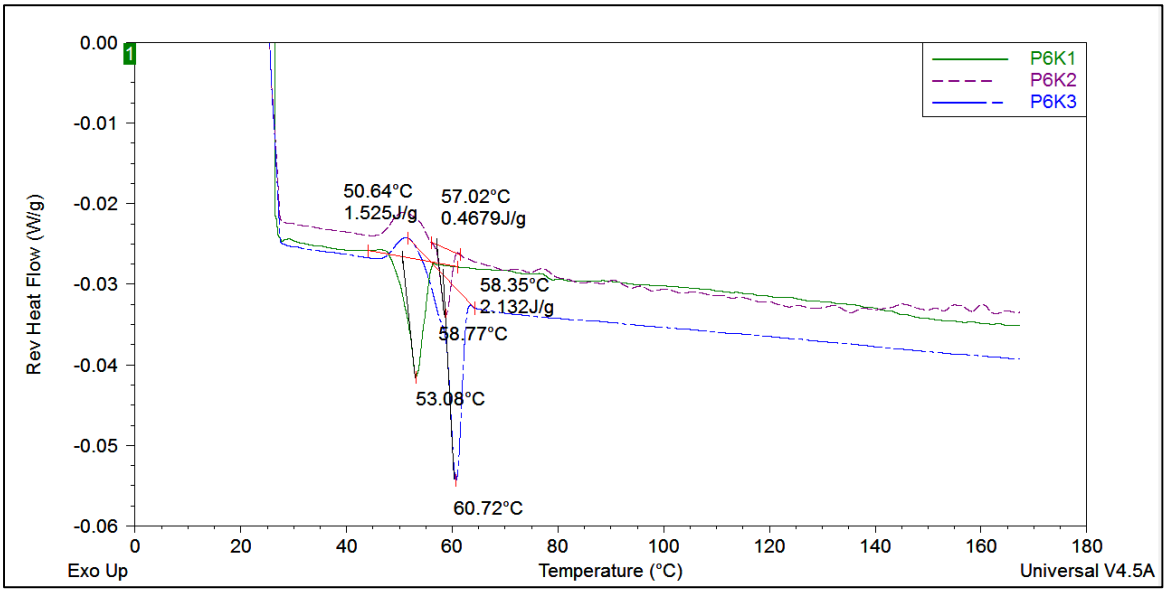

Figure 5.20 *Representative MTDSC profiles of P6K1, P6K2 and P6K3 mini-tablets.*

Table 5.8 *Summary of the thermal behaviour of the drug, excipients and chloramphenicol-loaded 3D-printed mini-tablets (n=3).*

Compound*	**Melting Temperature (°C) (mean ± SD)**	**Glass Transition Temperature (°C) (mean ± SD)**
Chloramphenicol	149.22 ± 1.32	32.68 ± 0.34
PEG 6K	59.30 ± 1.38	n/o
PEG 4K	60.71 ± 0.50	n/o
Pure	55.39 ± 1.91	n/o
P6K1	51.79 ± 1.62	n/o
P6K2	55.40 ± 1.82	n/o
P6K3	57.17 ± 2.09	n/o
P4K1	51.01 ± 5.11	n/o
P4K2	58.38 ± 1.20	n/o

* n/o = not observed

* Refer to ***Table 5.1*** for full details of the formulations.

Based on the MTDSC results, the presence of the low molecular weight PEGs and water in the formulations influenced the melting temperature of the 3D-printed mini-tablets. The “Pure” mini-tablets melting temperature was 57.50 ± 1.85 °C, while the P6K1 and P4K1 mini-tablets (the original formulations contained 25 g of the relevant PEG and 25 mL of water) displayed melting points which were approximately 4 °C lower, at circa 53 °C. In comparison to the P6K1 and P4K1 formulations, the melting point of the 3D-printed mini-tablets increased after water was removed from the formulations (P6K2 and P4K2) to be more similar to the "Pure" formulation.

There was no evidence of a melting peak or a glass transition attributed to chloramphenicol in the 3D-printed mini-tablets. There are several possible explanations for this. If chloramphenicol was present in the amorphous state, it may not be easily

detectable as the glass transition is relatively small and may be lost in the MTDSC baseline. However, in the temperature region that chloramphenicol's glass transition would be expected, the baseline was expanded to allow easier visualisation and no glass transition was observed. Hence, it is unlikely that the chloramphenicol is present in the amorphous state. If chloramphenicol is present in the crystalline state, then it would be expected to show a melting point, but if all other components had melted whilst chloramphenicol was still solid, then it would probably dissolve into the molten liquid, rather than remain as a solid. In this case, a melting peak would not be observed. Finally, the drug may exist in micro- or nano- crystalline deposits, which would have been as difficult to detect as the macro-crystalline system would be. Similarly, a separate melting peak was not observed for either PEG 4K or PEG 6K, but as their melting points are so similar to that of the "Pure" mini-tablets, which don't contain either of the low molecular weight PEGs, then it would be expected for the mixed systems that a broad, combined melting endotherm would be expected.

5.3.5 Observation of the photopolymerisation process

The photopolymerisation processes were monitored using a light microscope equipped with a digital camera. The times for the polymerisation processes to occur have been recorded based on visual observation, as shown in ***Table 5.9***. The endpoint of the photopolymerisation process was determined as when the solution ceased to “move” because of its change in state from liquid to solid. Three replicates were performed for each formulation. All formulations used for mini-tablet production were studied, along with a "Pure" formulation without water, in order to determine if the water content affected the photopolymerisation process directly.

Table 5.9 *Polymerisation length of time process (n=3).*

Formula*	**Time (minutes) (mean ± SD)**
Pure	13.99 ± 1.55
Pure without H_2O	6.59 ± 1.16
P6K1	1.58 ± 0.18
P6K2	1.63 ± 0.28
P6K3	1.60 ± 0.20
P4K1	4.14 ± 0.47
P4K2	1.28 ± 0.23

* Refer to ***Table 5.1*** for full details of the formulations.

The light intensity that was used to observe and polymerise the solution was different, depend on the individual solution. The light intensity had to be adjusted in this way to allow the light to pass through the solution so the polymerisation process could be observed. “Pure”, “Pure” without water and P4K1 formulation were translucent solutions, so the light intensity used was level 2. Meanwhile, the rest of the formulations displayed cloudy solutions under the microscope, although they were clear visually to the naked eye, so the light intensity had to be increased to level 8. Based on the observed results, the polymerisation was faster with the reduction (P4K1, circa 4 minutes) or total absence ("Pure" without water, circa 6.5 minutes) of water from the initial formulation ("Pure", circa 14 minutes). This is probably because the addition of water in the formulation diluted the PEGDA and BAPO solution. However, the addition of PEG 4K also decreased the polymerisation time (P4K1 compared to the "Pure" formulation).

All solutions observed with the higher light intensity showed very similar polymerisation times, which is probably a reflection of the light intensity used rather than as a result of formulation changes. According to Nomoto et al. (1994), generally for

photopolymerisation processes, the higher the light intensity, the faster the curing process. There was an obvious difference between the matched pair of P4K1 and P4K2 formulations: P4K1 was polymerised after approximately 4 minutes, noticeably slower than the P4K2 formulation which required approximately 75 seconds. However, this is more likely to be attributable to the different light intensities used rather than a formulation difference. This investigation was somewhat inconclusive, due to the need to vary the light intensity in order to study the photopolymerisation process. However, it should be noted that during the actual 3D-printing process of the mini-tablets, the light intensity was kept constant for all formulations.

5.3.6 Surface analysis

The surface images of mini-tablets were captured using SEM. ***Figure 5.21*** shows the collective SEM images of mini-tablets. All the 3D-printed mini-tablets had an uneven and rough surface, with the "Pure" mini-tablets showing the most regular surface. The P6K1 and P4K1 mini-tablets look similar with small spikes covering the surface. P6K2, P6K3 and P4K2 mini-tablets have the roughest surface. There are a few lumps that can be observed on P6K2 and P6K3 mini-tablets surfaces and a large crater on the surface of the P4K2 mini-tablets. It was initially intended to study the surface of the 3D-printed mini-tablets with transition temperature microscopy (TTM) to assess the distribution of materials across the surface, in the same manner as had been conducted for the compressed powder mini-tablets. However, the tip of the TTM probe stuck to the mini-tablet's sticky surface during the analysis, and broke. Therefore, the TTM study was halted, as it was apparent that the 3D-printed mini-tablets are too sticky and their surfaces are too rough for the delicate (and expensive) TTM probes to cope with.

Pure

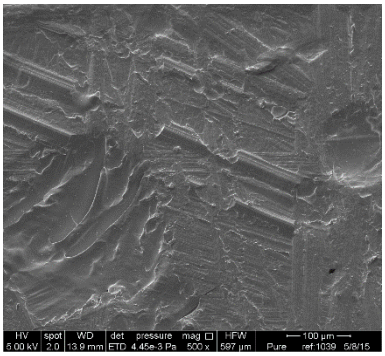

P6K1

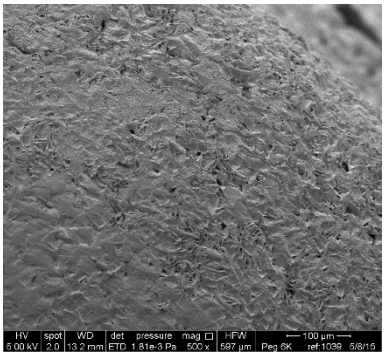

P6K2

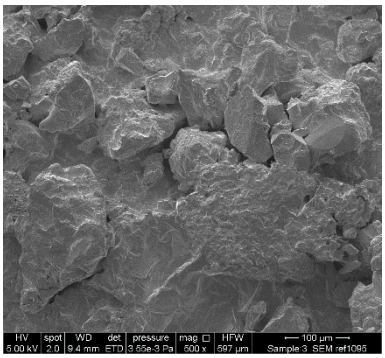

P6K3

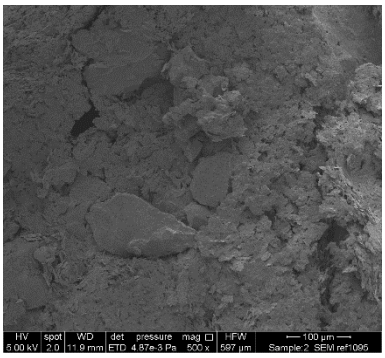

P4K1

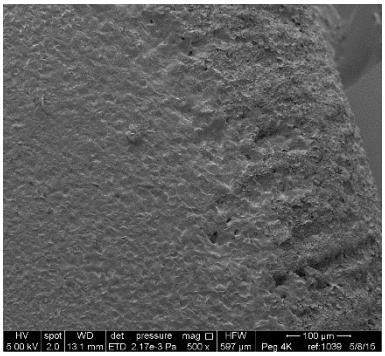

P4K2

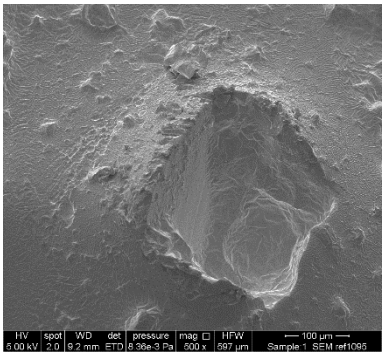

Figure 5.21 *SEM images of the chloramphenicol-loaded 3D-printed mini-tablets. Scale bar = 100 µm.*

5.3.7 Drug release profile

The drug release profiles from the 3D-printed mini-tablets were obtained using the same dissolution test as for the compressed powder mini-tablets in Chapter 3. The same flow-through dissolution apparatus was used, with STF as the dissolution medium. Samples were taken hourly within a 9-hour total time frame and the drug content quantified spectrophotometrically at 278 nm. The amount of drug remaining undissolved at this point was quantified as described earlier in this Chapter and was used to determine the % released at each timepoint. ***Figure 5.22*** shows the drug release profiles for all six 3D-printed mini-tablet batches.

"Pure" and P6K1 mini-tablets showed the lowest percentage drug release at the end of 9 hours of dissolution test, with both formulations showing approximately 47 % release at 9 hours. The two formulations based on PEG 4K showed the highest total drug release, with circa 80 % release at 9 hours. The Pure formulation showed a different dissolution profile to the others, with an initial fast release rate for the first three hours, then appearing to plateau after 7 hours. All the other batches continued to release drug throughout the full 9 hours of the dissolution test and the differences between them were related to speed and extent of drug release rather than the dissolution profile shape.

PEG 4K and PEG 6K were added to the formulation in order to act as pore formers in the insoluble PEGDA/BAPO matrix. In the dissolution experiment, it was expected that the low molecular weight PEGs would dissolve into the STF, creating pores through which the STF could move, dissolving the drug in situ and allowing the drug to diffuse out into the bulk fluid for detection. As PEG 4K has a lower molecular weight than PEG 6K, it would be expected to dissolve faster itself, thus promoting a faster general release rate of the drug. On the other hand, the pores formed by the heavier PEG 6K would be expected to be larger, so would promote greater drug release.

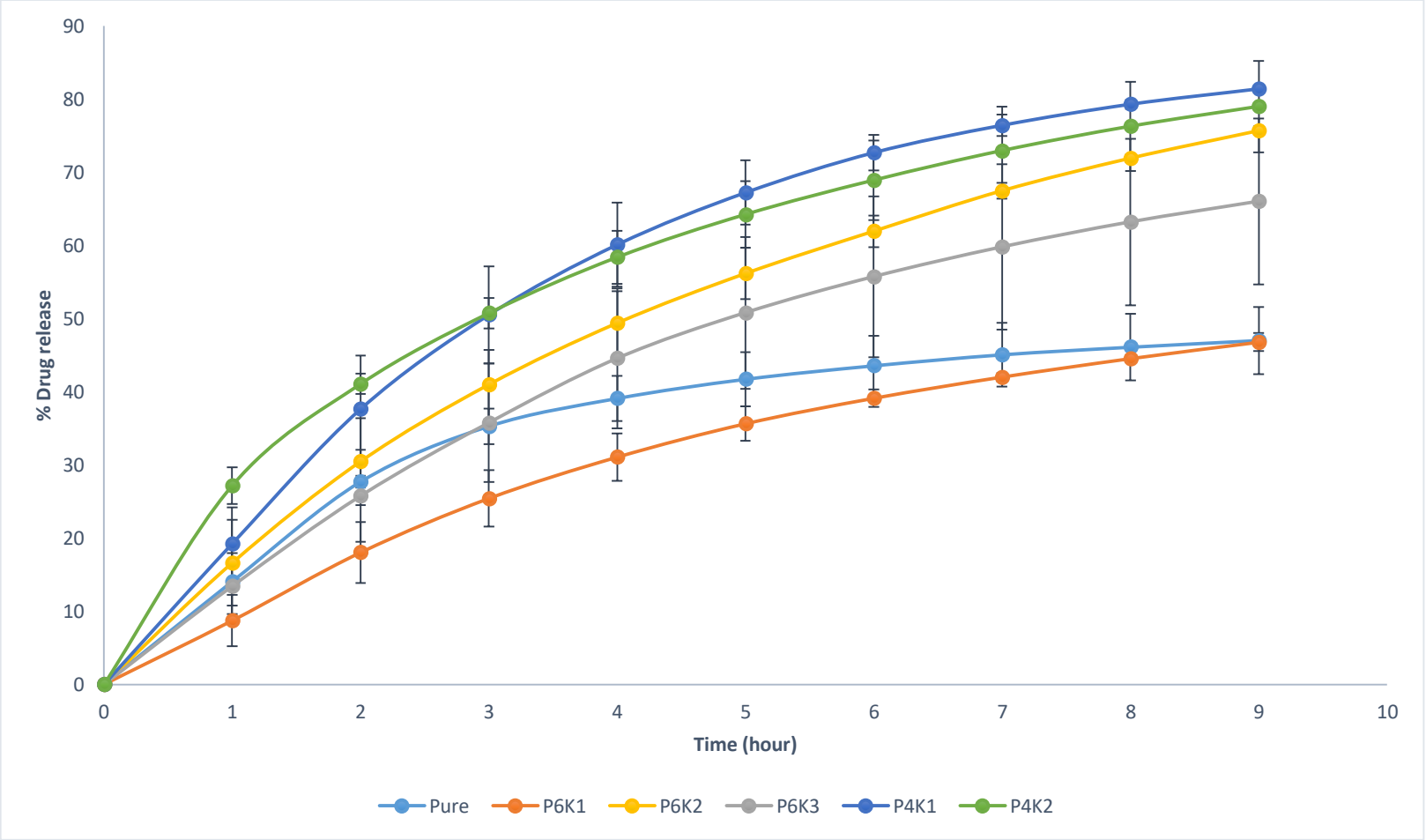

Figure 5.22 *Drug release profiles of the chloramphenicol-loaded 3D-printed mini-tablets (mean ± SD, n=3)*

* Refer to ***Table 5.1*** for full details of the formulations.

From ***Figure 5.22***, it is obvious that the presence of PEG 4K in the formulation (P4K1 and P4K2) did lead to substantially enhanced drug dissolution at all timepoints compared to the "Pure" formulation. However, there was no apparent difference in the drug release profiles of P4K1 and P4K2, except at 1 hour where P4K2 showed a higher amount released than P4K1, suggesting that the presence or absence of water in the initial formulation mix had no significant effect on the behaviour of the 3D-printed mini-tablets. A different relationship was observed for the PEG 6K formulations in comparison to the "Pure" formulation. P6K1 (25 g of PEG 6K and 25 mL of water) showed a slower but steadier drug release than the "Pure" formulation, which was not expected. Removing the water from the initial formulation (P6K2) increased the rate and extent of drug release compared to both the "Pure" mini-tablets and the P6K1 mini-tablets. Increasing the PEG 6K content further (P6K3) seemed to have a detrimental effect on the rate and extent of drug release.

5.3.7.1 Mathematical modelling for dissolution profile

The dissolution profiles were modelled mathematically in the same manner as the compressed powder mini-tablets discussed in Chapter 3. ***Table 5.10*** shows the coefficient of determination (r^2), the release rate constants (k_0, k_1 *and* k_{KP}), and the diffusional exponent (n) values for the release profiles of the 3D-printed mini-tablets. Green values indicated the best fitting model.

Table 5.10 *Mathematical fitting parameters for the dissolution profiles from the chloramphenicol-loaded 3D-printed mini-tablets.*

Mini-tablet*	Zero Order		First Order		Korsmeyer-Peppas		
	r^2	k_0	r^2	k_1	r^2	k_{KP}	n
Pure	0.5674	6.6996	0.7110	0.0880	0.9022	17.29	0.5110
P6K1	0.8881	6.0679	0.9951	0.0780	0.9728	10.07	0.7468
P6K2	0.8819	9.7524	0.9963	0.1610	0.9870	18.21	0.6791
P6K3	0.8803	8.6215	0.9807	0.1296	0.9788	15.05	0.7180
P4K1	0.7876	11.0900	0.9788	0.2041	0.9580	22.46	0.6406
P4K2	0.6852	10.7420	0.9536	0.1890	0.9890	28.75	0.4820

* Refer to ***Table 5.1*** for full details of the formulations.

As expected from visual inspection of the dissolution profiles, none of the formulations showed a good fit to the zero order model. The "Pure" mini-tablets fitted best to the Korsmeyer-Peppas model, although as the r^2 value was only 0.9022, this was not a perfect fit. The P6K1, P6K2, P6K3 and P4K1 formulations were best fitted to a first-order process if all data points were included. If only the data up to approximately 60 % drug release were included, then these formulations were best fitted to the Korsmeyer-Peppas model. P4K2 fitted best with the Korsmeyer-Peppas model irrespective of whether the full or truncated data set was used. In each case where the Korsmeyer-Peppas model was used, the exponent n took values between 0.5 and 1, suggesting an "anomalous" drug release profile. In such cases, there are multiple factors governing the release pattern, such as polymer relaxation and diffusion, as suggested by Peppas et al (1989). For the formulations studied here, the governing factors are likely to be dissolution of the added low molecular weight PEG, diffusion of the drug throughout the pores created by the dissolution of the PEG, and a degree of swelling that may occur with the insoluble PEGDA/BAPO matrix on prolonged exposure to aqueous fluid.

The dissolution profiles of the 3D-printed mini-tablets were compared pair-wise using the f_1 difference and f_2 similarity factors. These results are summarised in ***Table 5.11***, with green text indicating that the two formulations have similar dissolution profiles and red text indicating that the profiles are dissimilar. As expected, the two formulations based on PEG 4K were deemed to be similar in this exercise. The P6K2 and P6K3 mini-tablets were similar in their profiles, but both were deemed to be different to the P6K1 profile. The "Pure" formulation was similar only to the P6K1 formulation.

Table 5.11 *Difference (f_1) and similarity (f_2) factors for the dissolution profiles of chloramphenicol-loaded 3D-printed mini-tablets.*

	Pure	**P6K1**	**P6K2**	**P6K3**	**P4K1**	**P4K2**
Pure		f_1 = 14 f_2 = 60	f_1 = 28 f_2 = 38	f_1 = 19 f_2 = 47	f_1 = 38 f_2 = 27	f_1 = 37 f_2 = 32
P6K1	f_1 = 14 f_2 = 60		f_1 = 38 f_2 = 34	f_1 = 30 f_2 = 42	f_1 = 47 f_2 = 27	f_1 = 46 f_2 = 28
P6K2	f_1 = 28 f_2 = 38	f_1 = 38 f_2 = 34		f_1 = 12 f_2 = 59	f_1 = 14 f_2 = 53	f_1 = 13 f_2 = 55
P6K3	f_1 = 19 f_2 = 47	f_1 = 30 f_2 = 42	f_1 = 12 f_2 = 59		f_1 = 24 f_2 = 41	f_1 = 23 f_2 = 43
P4K1	f_1 = 38 f_2 = 27	f_1 = 47 f_2 = 27	f_1 = 14 f_2 = 53	f_1 = 24 f_2 = 41		f_1 = 5 f_2 = 70
P4K2	f_1 = 37 f_2 = 32	f_1 = 46 f_2 = 28	f_1 = 13 f_2 = 55	f_1 = 23 f_2 = 43	f_1 = 5 f_2 = 70	

* Refer to ***Table 5.1*** for full details of the formulations.

5.3.7.2 Drug loading

All the 3D-printed mini-tablets showed higher than expected drug content, as shows in ***Table 5.12***. The results obtained ranged from 113 to 129 % of expected. According to BP specifications, the formulations would be considered uniform if not more than 1 individual drug content value were outside the limit of 85 to 115 % and none outside 70 to 130 % of the average content. However, this specification relates to data for 10 tablets tested where in this case, they were only being done with 3 tablets. The red type indicates the values that deviated outside the range of 85 to 115 % but within the 70 to 130 % range compared to the average for both the actual content and drug loading. Blue type indicates the values that deviated outside of the range of 70 to 130 %. Based on the results, Pure, P6K2, P4K1 and P4K2 mini-tablets passed the BP

specifications. Meanwhile, P6K1 and P6K3 showed more than 1 value that is outside the 70 to 130% range which mean they fail the test.

Table 5.12 *Chloramphenicol loading in the 3D-printed mini-tablets compared to the chloramphenicol amount in the formulation (n=3).*

Polymer	Tablet weight (µg)	Drug content (µg)	Mean (µg)	SD (µg)	Drug content (%)	Mean (%)	SD (%)
Pure	5.71	0.24	0.22	0.02	4.20	3.83 (3.18)	0.33
	5.68	0.21			3.70		
	5.57	0.20			3.59		
P6K1	11.00	0.44	0.47	0.08	4.00	3.90 (3.18)	0.83
	13.24	0.40			3.02		
	11.99	0.56			4.67		
P6K2	19.95	0.94	0.91	0.03	4.71	4.81 (3.79)	0.14
	18.13	0.90			4.96		
	18.72	0.89			4.75		
P6K3	27.10	1.30	1.05	0.26	4.80	4.12 (3.18)	0.69
	23.14	0.79			3.41		
	25.60	1.06			4.14		
P4K1	9.15	0.34	0.36	0.03	3.72	3.62 (3.18)	0.11
	9.99	0.35			3.50		
	10.71	0.39			3.64		
P4K2	35.15	1.73	1.74	0.12	4.92	4.59 (3.79)	0.40
	39.05	1.62			4.15		
	39.51	1.86			4.71		

* Refer to ***Table 5.1*** for full details of the formulations.

** Values in () showed the percentage of chloramphenicol based on the formulations.

The high drug loading is highly possibly due to the water loss during the printing process as mentioned previously. Since the amount of water in the final mini-tablets was reduced compared to the starting formulation, the percentage of drug content based on the formulation would have changed to compensate. However, there is no easy correlation between the water content measured in the mini-tablets and the drug content calculated here, so there this cannot explain fully the discrepancy.

5.3.7.3 Correlation between vapour sorption and release profile

As with the compressed powder mini-tablets, the dissolution profiles and the water sorption profiles look similar and hence a correlation between the two was investigated. ***Figure 5.23*** shows the correlation graphs between these two profiles for the six formulations of 3D-printed mini-tablets. All the formulations showed a good correlation between the water uptake and drug release, although there were some subtle differences between the batches. Those batches with added PEG 6K (i.e. P6K1, P6K2, and P6K3) appeared to show a linear relationship between drug release and water uptake, beginning at the start of the experiment, with limited differences between these three batches. This probably reflects the pore formation in the 3D-printed mini-tablets which occurs due to the dissolution of the low molecular weight PEG. The two batches based on PEG 4K (P4K1 and P4K2) also showed a linear relationship between drug release and water uptake, but were different in whether they showed a lag time or not. The "Pure" mini-tablet formulation appeared to show drug release occurring before any water uptake started, but a linear relationship thereafter. All the graphs showed p values lower than 0.0001. These indicate that there are significant correlation between two profiles since the *p* value is smaller than 0.05 (Seltman, 2015).

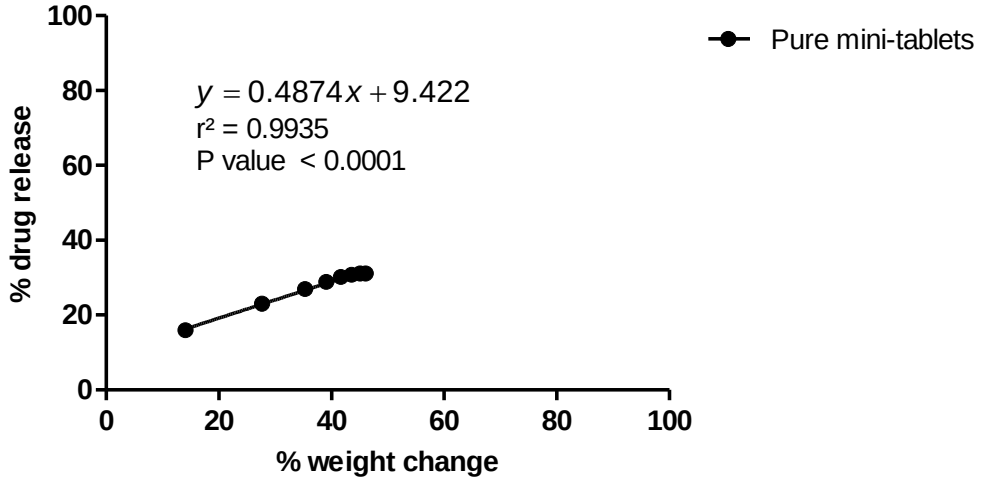
Pure mini-tablets
$y = 0.4874x + 9.422$
r² = 0.9935
P value < 0.0001
% drug release
% weight change
0
20
40
60
80
100

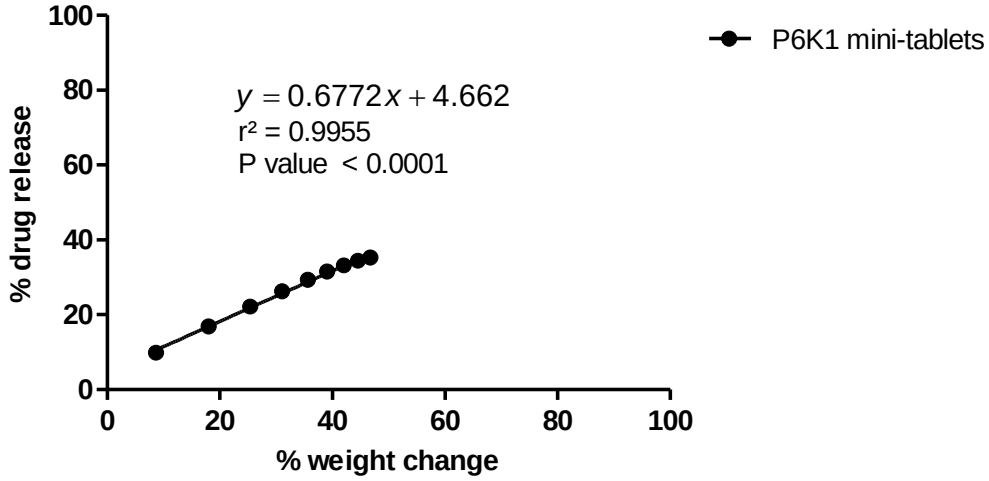
P6K1 mini-tablets
$y = 0.6772x + 4.662$
r² = 0.9955
P value < 0.0001
% drug release
% weight change
0
20
40
60
80
100

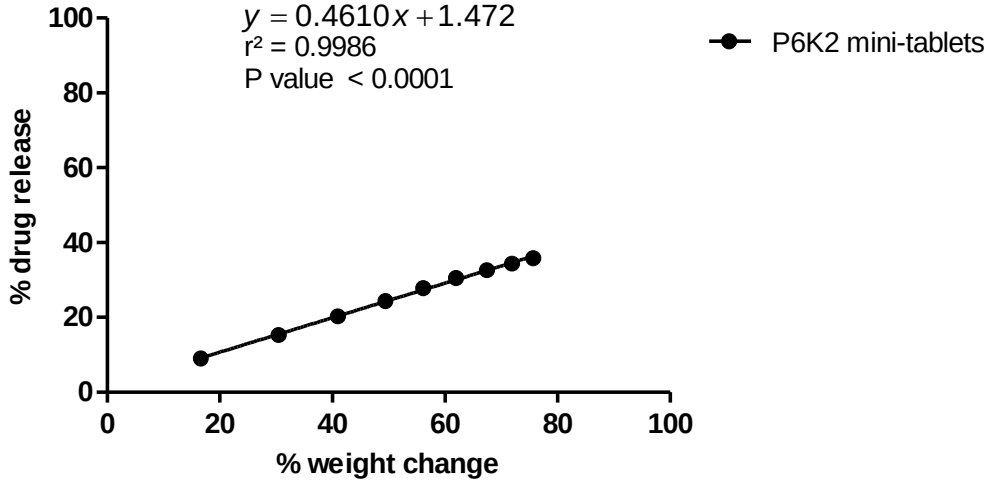
P6K2 mini-tablets
$y = 0.4610x + 1.472$
r² = 0.9986
P value < 0.0001
% drug release
% weight change
0
20
40
60
80
100

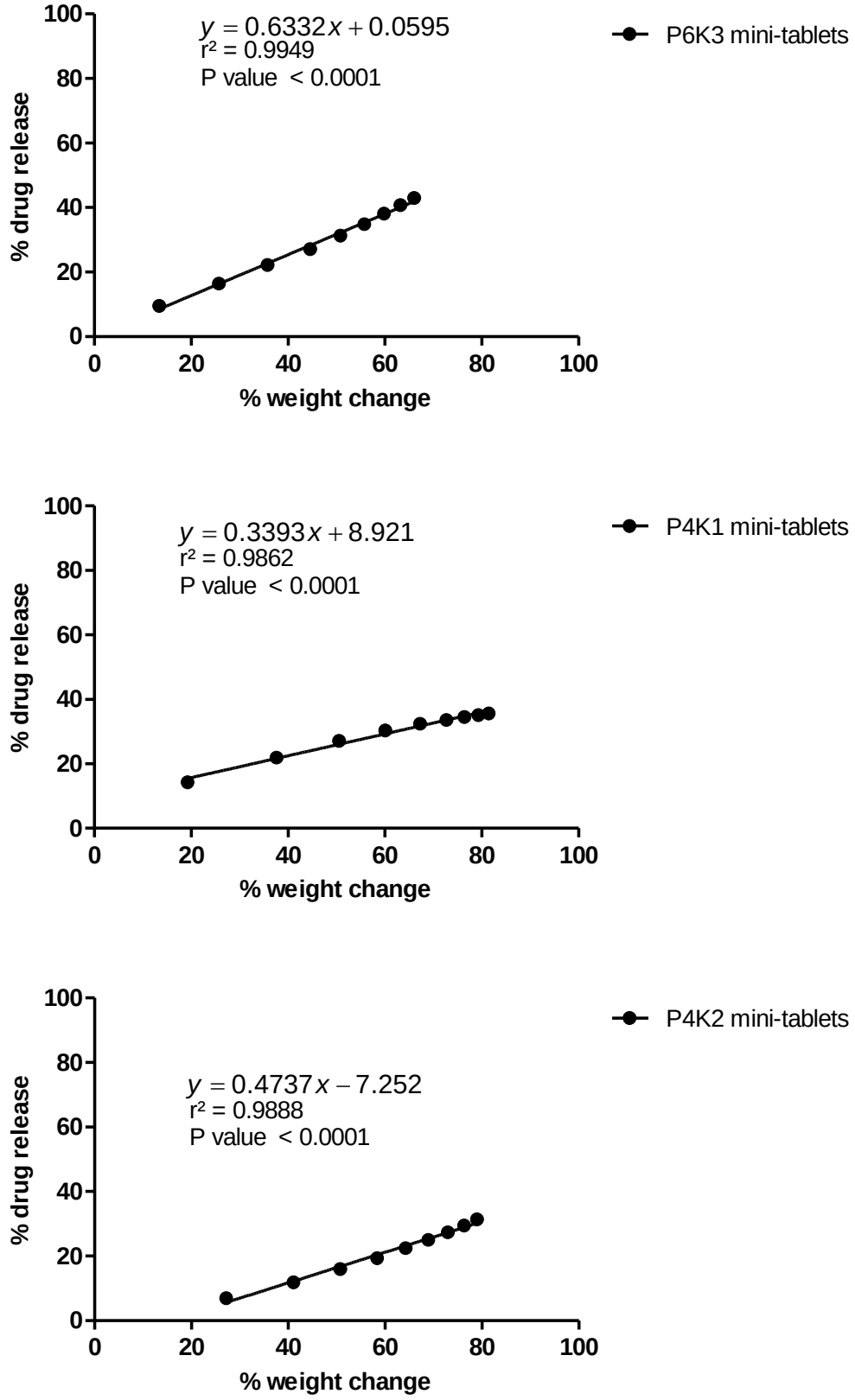

Figure 5.23 *Correlation between drug release profile and vapour sorption of the chloramphenicol-loaded 3D-printed mini-tablets.*

5.4 GENERAL DISCUSSION

The current study was an initial investigation into whether various 3D printing techniques could be used to prepare mini-tablets suitable for a range of purposes, specifically here for ocular drug delivery. Recently, a 3D-printed tablet product (Spritam™ from Aprecia Pharmaceuticals) has been granted marketing approval by FDA. The tablets were printed using a solid, free-form fabrication (SFF) technique. This technique creates a 3D object by printing fluid droplets using the drop-on-demand print head into selected areas of deposited layers of powder. A few layers were printed to produce the tablets (Yoo et al., 2015).

In this study, two different types of 3D-printers with different printing techniques were used. It was not possible to use the more common fused deposition model (FDM) of 3D-printing (similar to the SFF technique used to manufacture the Spritam™ tablets) as this requires a filament of the relevant formulation to be manufactured to use as a stock material for the actual printing process. Unfortunately, the polymers initially selected for investigation, to match the compressed powder mini-tablets studied earlier, could not be extruded to make a suitable filament. The focus of the study then switched to stereolithography techniques for 3D-printing, using a base material which could be photopolymerised by exposure to light. PEGDA was chosen as the photopolymerisable substrate, as it has been used before successfully to produce 3D-printed material, albeit not for pharmaceutical use (Hockaday et al., 2012, Ovsianikov et al., 2010). Its chemistry is well understood and therefore it provided a platform upon which to build a formulation strategy. As well as investigating the ability of the stereolithography approach for manufacturing mini-tablets, by adjusting the level of low molecular weight polymeric additives in the base formulation, the effect of these on the behaviour of the product could be evaluated. The design process for the mini-tablets was simple and

straightforward, using freely-available software to design the size and shape of the mini-tablets and to guide the 3D-printing process. Production of the mini-tablets was not as straightforward as their design, in that it was not possible to cast the mini-tablets using a mould system, due to leakage and the photopolymerised material acting as a glue between the mould surfaces and the mini-tablets, preventing them being released from the mould at the end of the photopolymerisation period. It was also not possible to 3D-print the mini-tablets using a scaffold structure, as was the original intention and possible with the "flexible" resin manufactured by Formlabs (USA) for use as a design trial material and hence the mini-tablets were 3D-printed directly onto the platform of the 3D-printer.

Six batches of mini-tablets were 3D-printed, varying the formulation in terms of added low molecular weight polymer and water, and characterising their physical and drug release behaviour. The mini-tablets showed quite substantial differences in their physical dimensions (thickness and diameter) and weight, indicating that the control parameters of the 3D-printing process need investigating to determine how to ensure that the product matches the design. The weight variability of the 3D-printed mini-tablets was not as good as would be hoped, with only three of the six batches passing the BP weight uniformity specification. Fine-tuning the production control parameters of the 3D-printing process would be expected to have a direct beneficial effect on this quality control aspect. During the 3D-printing process, water was lost from the formulation, and understanding this evaporation process in more detail may also help to design formulations and 3D-printing processes which will lead to higher quality and more reproducible products.

As a potential drug delivery vehicle, it is important to understand and characterise the drug release behaviour of the 3D-printed mini-tablets. The dissolution profiles could be modelled using either first-order kinetics or the Korsmeyer-Peppas equation. In the

latter case, the release exponent (n) indicated that the release profile was "anomalous". In some respects, this is to be expected, as the 3D-printed mini-tablets are not water-soluble, so will not erode in the same way as the compressed powder mini-tablets did, so drug dissolution will be reliant on diffusion of the dissolution medium (in this case STF) into the bulk of the mini-tablet by diffusion through pores either naturally occurring or created by dissolution of water-soluble additives such as the low molecular weight PEGs. The linear relationship between water vapour uptake and drug release suggests that movement of water and hydration of the mini-tablet is important in controlling the drug release pattern. It was interesting to note that the "Pure" formulation appeared to reach a dissolution plateau after 7 hours testing and circa 47 % drug release. This may be a reflection of the internal structure of these mini-tablets, such as pore size and tortuosity, and warrants further investigation to fully understand the factors which determine this plateau effect. Addition of PEG 4K or PEG 6K generally increased the dissolution rate, except for the P6K1 formulation, which unexpectedly showed an initial slower rate than the "Pure" formulation. All formulations with additives shown a drug release profile which was incomplete but still ongoing when the dissolution experiment was terminated after 9 hours. Further studies into how to control the drug release behaviour with alternative additives would be useful. Ideally, a slower and more zero-order release rate would be required for treatment with a non-biodegradable drug delivery device, such as these mini-tablets. Alternatively, a biodegradable drug delivery device would be ideal and would require the patient only to insert it and not to have to remove it at the end of its useful life.

Table 5.13 below summarises whether the 3D-printed mini-tablet batches would pass the initial target specifications presented in **Chapter 1** and whether they would be considered for further development.

Table 5.13 *Summary of the analytical tests of the 3D-printed mini-tablets in comparison to the initial target values.*

Attribute	Target	Pure	P6K1	P6K2	P6K3	P4K1	P4K2
Drug content	5 % w/w = 0.5 mg	No	No	No	No	No	No
	Meets BP specifications for content uniformity	Yes	Yes	Yes	Yes	Yes	No
Weight	10 mg	No	No	No	No	Yes	No
	Meets BP specifications for weight uniformity	No	No	Yes	No	Yes	Yes
Hardness	5 to 15 N	No	No	No	No	No	Yes
Thickness	2 mm	Yes	No	No	No	No	No
Diameter	2 mm	No	No	No	No	No	No
Friability	Meets BP specifications for friability	N/A	N/A	N/A	N/A	N/A	N/A
Dissolution profile	Zero order	No	No	No	No	No	No
	24 hours release, i.e. 4.17 % per	No	Possibly	No	Possibly	No	No

	hour						
Development potential		Possibly	Possibly	Possibly	Possibly	Possibly	Possibly
Comments		For all formulations: - Dissolution profile needs to be altered and extended. - Factors controlling the final drug loading need to be investigated (e.g. evaporation of water). - Factors controlling the size and shape of the product need to be investigated (e.g. laser strength).					

5.5 CONCLUSIONS

Based on the results of this investigative study, it can be concluded that it is plausible to use specific 3D-printing techniques to manufacture mini-tablets, such as stereolithography, although there is much work to be done to fully understand the 3D-printing process and the factors which govern product quality. The drug release rate was altered by the presence of water-soluble additives, suggesting that the basic framework of PEGDA/BAPO could be used as a basis for much formulation design work in order to tailor the drug release rate to that desired to treat the particular disease state under study.

Chapter 6

Design and Manufacture of Customised Ocular Inserts and Corresponding Flow-through Dissolution Apparatus Using 3D-printing Techniques

Design and Manufacture of Customised Ocular Inserts and Corresponding Flow-through Dissolution Apparatus Using 3D-printing Techniques

6.1 INTRODUCTION

The possibility of using 3D-printing techniques to manufacture mini-tablets for ocular treatment was studied and discussed in Chapter 5. Since the shape of the samples produced with these techniques can easily be reconfigured, it is a good idea to broaden the current studies towards using different shapes and hence different drug delivery methods. Thus, ocular inserts were made using the 3D-printing technique.

Ocular inserts are one of the drug delivery methods that have been used in ocular treatment but are less commonly used than eye drops. The inserts can be either soluble (erodible) or insoluble. Insoluble inserts would be expected to give a controllable, pre-determined rate of drug release, possibly with zero-order kinetics. The disadvantage of insoluble inserts is the need for removal from the eye once the drug is fully dissolved (Saettone and Salminen, 1995). Despite this disadvantage, insoluble inserts are one of the most effective ways of providing ocular treatment. This is because inserts increase the overall local drug bioavailability and efficiency due to prolongation of contact time and controlled drug release. The inserts can also reduce the potential drug systemic adverse effects and administration frequency (Rawas-Qalaji and Williams, 2012).

There are a few studies published on erodible inserts. Most of these inserts are in the form of compressed tablets (Di Colo et al., 2001, Di Colo et al., 2002) and mini-tablets (El-Gawad et al., 2012, Weyenberg et al., 2006, Weyenberg et al., 2004, Weyenberg et al., 2003, Weyenberg et al., 2005, Bozdag et al., 2010, Ceulemans et al., 2001). These inserts would absorb water when in contact with tear fluid and then form a gel into which

the drug would dissolve and diffuse through in order to provide a slow release profile. The quoted studies were mostly focused on investigating the release profiles of the inserts by manipulating the composition of the excipients, particle sizes and compression forces. The inserts used in these studies would normally be intended to be placed at the eye conjunctival fornix or cul-de-sac.

Bioerodible inserts were also studied by several researchers. Aburahma and Mahmoud (2011) studied bioerodible inserts manufactured using a film-casting method. These inserts were tested to treat glaucoma in rabbits' eyes after being placed in the cul-de-sac. A more invasive insert, known as the OphthaCoil, was developed using a short coil of thin stainless steel wire as the device core which was coated with bioerodible drug-loaded hydrogel and then inserted into the fornix. However, the coil needed to be removed once the hydrogel was completely dissolved (Pijls et al., 2007, Pijls et al., 2005).

Although several studies have been performed on the formulation of ocular inserts, none of the inserts were customised based on the shape of the patient's eye or used 3D-printing techniques in their manufacture. In this chapter, ocular inserts resembling scleral shields were designed based on actual human data, i.e. the shape of a subject's eye, and manufactured using a 3D-printing technique. The flow-through dissolution apparatus used in **Chapters 3** and **5** could not be used here as the insert was too large to fit into the dissolution chamber. Hence, a customised flow-through dissolution cell was designed for these inserts and produced using the same 3D-printing technique. The drug release profiles from the inserts were studied and compared with the profiles from the 3D-printed mini-tablets generated in **Chapter 5**.

The same 3D-printing formulations were used in this part of the study as before, in order

to enable comparisons with the previous Chapter. Additionally, a starting point of ocular coverage of the inserts was selected, of 1/8th of the eye's surface, in order to assess whether or not the SLA approach of 3D-printing these shaped inserts is feasible. As this is an exploratory study into the feasibility of producing such an insert, the weight of the insert cannot be predicted at the outset and hence the actual drug content is also not directly predictable. However, compliance with BP specifications for weight uniformity and drug content uniformity would be required.

The target product profile of the chloramphenicol-loaded 3D-printed inserts is given in ***Table 6.1*** below.

Table 6.1 Ideal product profile of the chloramphenicol-loaded 3D-printed inserts.

Attribute	**Specification detail**
Drug content	5.0 % w/w
	Meets BP specifications for content uniformity
Weight	Meets BP specifications for weight uniformity
Dimensions	Crescent-shaped
	Height, width and depth: to cover 1/8th of the eye surface
	Thickness 1 mm
Dissolution profile	Zero order over 5 days, i.e. 20 % per day, or 0.83 % per hour

6.2 METHODOLOGY

6.2.1 Materials

Polyethylene glycol 6000 (PEG 6K) was provided by Clariant GmbH, Germany. Chloramphenicol, polyethylene glycol 4000 (PEG 4K), polyethylene glycol diacrylate 700 (PEGDA), phenylbis (2,4,6-trimethylbenzoyl) phosphine oxide (BAPO), sodium bicarbonate and calcium chloride were purchased from Sigma Aldrich, U.K. Sodium chloride was obtained from Fluka Chemie GmbH, Germany. Flexible resin was purchased from Formlabs Inc (USA). Polylactic acid (PLA) 1.75 mm white filament was purchased from 3DFilaPrint, UK.

6.2.2 Methods

6.2.2.1 Preparation of photopolymer solutions

Three photopolymer solutions were prepared matching the formulations used in **Chapter 5**, as shown in ***Table 6.2***. The formulations generally contained 100 g of PEGDA, 2 g of BAPO, 5 g of chloramphenicol (Chl) and 25 mL of water. Specific formulations also contained 25 g of a low molecular weight polymer or an additional 25 mL of water. These solutions were used to manufacture the ocular inserts.

Table 6.2 *List of polymer solutions used for manufacturing the ocular inserts.*

Name	**Component**					
	PEGDA	BAPO	Chl	H_2O	PEG 6K	PEG 4K
Pure	100 g	2 g	5 g	50 mL	-	-
P6K1	100 g	2 g	5 g	25 mL	25 g	-
P4K1	100 g	2 g	5 g	25 mL	-	25 g

6.2.2.2 3D-printing

6.2.2.2.1 Magnetic resonance imaging

A Magnetic Resonance Imaging (MRI) image was provided by a colleague in the UCL School of Pharmacy, based on his own head scan. The colleague gave permission for his MRI scan to be used in this project. The MRI image obtained was in several 2D images, called slices. These images were analysed by using InVesalius (2016), a free software that generates 3D images based on the MRI slices, as described in **Chapter 2**.

6.2.2.2.2 3D design

Following analysis of the shape of the eye from the MRI scan, a matching ocular insert was designed using Tinkercad (2015), a free browser-based 3D design and modelling application. The design processes were the same as used for the 3D-printed mini-tablets and were explained in **Chapter 2**. The model designs were saved in .STL file format and then uploaded to the 3D-printers for the printing process. The design for the flow-through dissolution cell was finalised after the shape of the inserts had been defined, using the design processes described above.

6.2.2.2.3 3D-printing

For the printing process two different 3D-printers were used. A fused deposition modelling (FDM) MakerBot Mini Replicator printer (MakerBot, USA) was used to print the prototype design of the customised flow-through dissolution cell and a stereolithography apparatus (SLA) FormLabs 1+ printer (Formlabs, USA) was used to print the finalised design. For the ocular inserts, only the SLA printer was used. The printing settings used were similar to those used to 3D-print the mini-tablets in **Chapter 5**. Fifteen inserts printed for each batch.

6.2.2.3 Physical characterisation of the inserts

6.2.2.3.1 Weight uniformity

Ten ocular inserts were chosen randomly and weighed individually. The mean and standard deviation were calculated based on the data obtained.

6.2.2.3.2 Surface area

In order to determine the surface areas of ocular inserts, ten inserts from each formulation were selected randomly. The height, width and depth of the inserts were measured using a digital calliper (Mitotoyo, Japan). The STL format files for the ocular inserts from Section 6.2.2.2.3 were uploaded to Netfabb (2016). This software can be used to edit, repair and analyse STL format files. The surface areas of the inserts were calculated using this software, by editing the inserts dimensions based on the measurements, as explained in **Chapter 2**.

6.2.2.3.3 Thickness swelling test

Three inserts were chosen randomly from each formulation. The thickness of the inserts were measured using a digital calliper (Mitotoyo, Japan). Each insert was placed into a 20 mL sample tube containing 10 mL simulated tear fluid (STF). The samples were left for one hour before the thickness was re-measured. The mean and standard deviation of the percentage thickness swelling were calculated based on the data obtained.

6.2.2.4. Drug release profile

The customised flow-through dissolution apparatus was used to assess the drug release profile of the ocular inserts. The 3D-printed dissolution apparatus made in section 6.2.2.2.2 was attached to a peristaltic pump with the dissolution medium flowing through at a rate of 50 µL/min to be consistent with the dissolution method used in **Chapter 5**. In

this study, STF was used as the dissolution medium. STF consists of sodium bicarbonate 0.2 % w/w, calcium chloride 0.008 %w/w and sodium chloride 0.67 %w/w at pH 7.4, based on the STF formulation suggested by Marques et al. (2011). Samples were taken every hour up to 9 hours and then at 24, 48, 72 and 96 hours. The drug content in the samples was quantified spectrophotometrically at 278 nm, as in the analysis of the mini-tablets in **Chapters 3** and **5**. The remnant ocular inserts then were crushed and dissolved in STF with the amount of drug remaining being quantified as above. Three replicates were performed for each formulation.

6.2.2.4.1 Mathematical modelling of the dissolution profile

Zero order kinetics, first order kinetics and the Korsmeyer-Peppas equation were used as mathematical models to determine the dissolution profiles of the 3D-printed ocular inserts statistically. Similarly, the difference (f_1) and similarity (f_2) factors, as proposed by Moore and Flanner (1996), were used to evaluate any differences between the dissolution profiles of the 3D-printed ocular inserts and the corresponding 3D-printed mini-tablets. These models are described in **Chapter 2, 3** and **5**.

6.3 RESULTS AND DISCUSSION

6.3.1 Measurement of eye dimensions

The inserts and the customised flow-through dissolution cell were designed based on MRI images. ***Figure 6.1*** shows selected MRI images from three different angles based on human axial, sagittal and coronal planes. The axial, or transverse, images are horizontal slices through the body, beginning at the bottom and moving through to the top of the body. The sagittal images are vertical slices through the body, beginning at the left hand side and moving to the right hand side. Finally, the coronal images are vertical slices through the body, beginning at the front and moving to the back of the body.

The dimensions of the eye were measured by using InVesalius (2016) as described above. In particular, as the eye is a three-dimensional structure, measurements in the x, y and z directions are all required. Here, the x axis reflects the horizontal distance across the eye from left to right and is obtained from the axial and coronal images. The y axis reflects the vertical distance across the eye from bottom to top and is obtained from the sagittal and coronal images. The z axis reflects the horizontal distance across the eye from front to back and is obtained from the sagittal and axial images. This is summarised in ***Figure 6.2***. There are three different colours of lines drawn on the MRI images in ***Figure 6.1***, representing the measurements in the three dimensions and utilising the colour scheme shown in ***Figure 6.2***.

Anatomical plane	MRI image
Axial	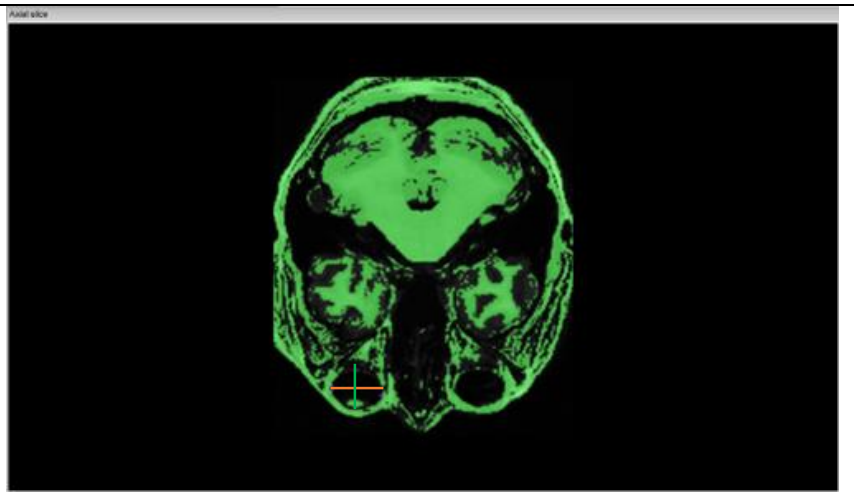
Sagittal	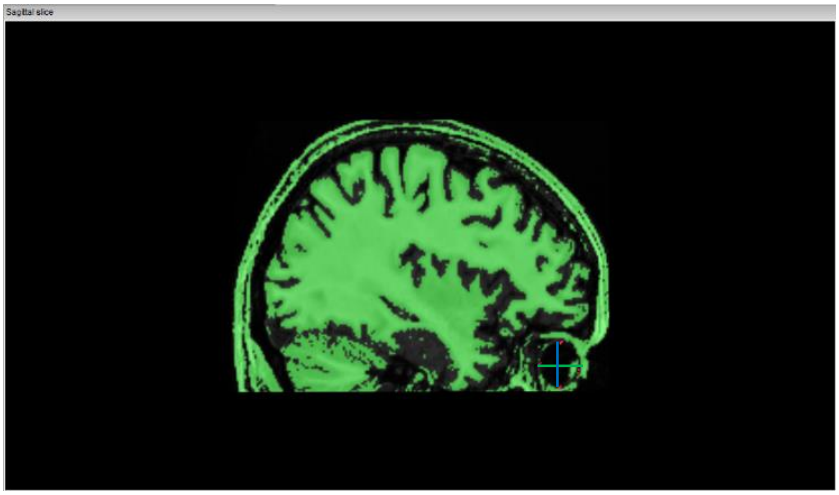
Coronal	

Figure 6.1 *MRI images from the three different anatomical planes.*

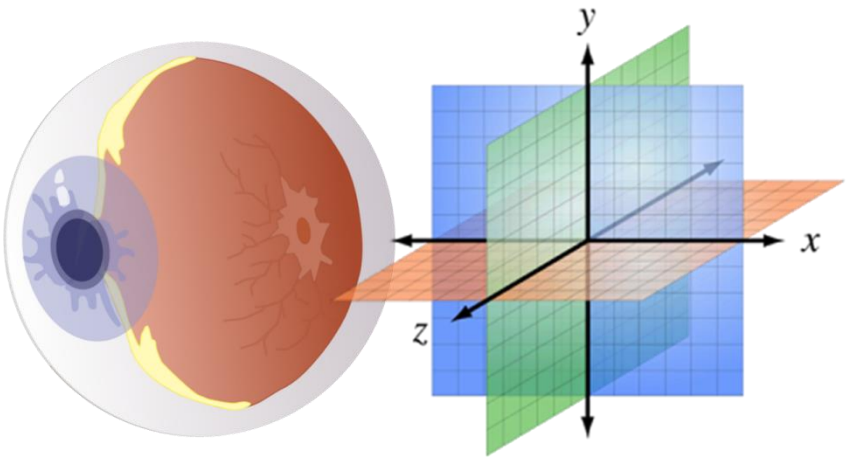

Figure 6.2 *The x-, y- and z-axes of the eye.*

Figure 6.1 shows the MRI slices at the point where the maximum dimensions of the eye in all three directions can be measured. ***Table 6.3*** shows the triplicate measurements of each of these lines, with the global mean (i.e. the mean value summarising all the readings from both the relevant MRI slices) of the maximum dimensions of the eye being shown in ***Table 6.4***.

Table 6.3 *Line measurements on each anatomical plane of the MRI images in* ***Figure 6.1****.*

Reading	Axial (mm)		Sagittal (mm)		Coronal (mm)	
	x-axis	z-axis	z-axis	y-axis	x-axis	y-axis
1	26.72	19.80	19.50	22.99	26.79	21.73
2	26.16	20.66	19.98	22.15	26.07	21.04
3	25.49	20.64	19.84	22.17	25.38	20.99
Mean	26.12	20.37	19.77	22.44	26.08	21.25
STD	0.62	0.49	0.25	0.48	0.71	0.41

Table 6.4 *Measurement of the eye's maximum dimensions, taken from the MRI images in* ***Figure 6.1*** *(n=3).*

Axis	Length (mm) (mean ± SD)
x-axis	26.10 ± 0.59
y-axis	21.85 ± 0.48
z-axis	20.07 ± 0.76

According to Bekerman et al. (2014), the dimensions of the eye in healthy human adults range between 20.9 and 27.1 mm for the coronal axis, 20.5 mm and 26.4 mm for the sagittal axis and 19.9 mm and 26.2 mm for the axial axis when measured across the external surface of the sclera. The study could not find any significant difference in eye dimensions between subjects of different gender, age or race, or between left and right eyes in the same subject.

The coronal, sagittal and axial measurements mentioned in their study are equivalent to the x-, y- and z-axis measurements generated here. Based on these results, the eye dimensions measured from the current MRI scans were overall within the range for normal adult humans. However, the x-axis measurement was near to the higher end of the normal range while for the y-axis and the z-axis, the measurements were close to the lower end of the range, suggesting that the subject of the current study had eyes that were more elongated (x-axis), flatter (y-axis) and narrower (z-axis) than the "average" adult human.

6.3.2 Design and 3D-printing of the Ocular Inserts

The ocular inserts were designed based on the MRI images discussed above and to mimic the shape and structure of the subject's eye. The administration of these would

into eye "sac" between the bulbar conjunctiva and palpebral conjunctiva (***Figure 6.3***). This will allow the insert to be relatively easily inserted and removed from the eye after the treatment is accomplished. The shape chosen for the inserts was crescent-shape, as it fits well with the eye shape and can easily be placed in the sac, which make it an ideal shape for the inserts. The inserts also need to be thin since there is not much gap between the eye lid and eye surface. The dimensions of the ocular inserts were designed based on the measurements of this particular patient's eye. In this study, the inserts' dimensions were chosen as 8.30 mm height (y-axis), 24.80 mm width (x-axis), 7.22 mm depth (z-axis) and 1.00 mm thickness with surface area (including the top and bottom surfaces) of 4.72 cm^2. The inserts as designed would cover roughly $1/8^{th}$ of the whole eye surface area. ***Figure 6.4*** illustrates the design and measurements of the ocular insert.

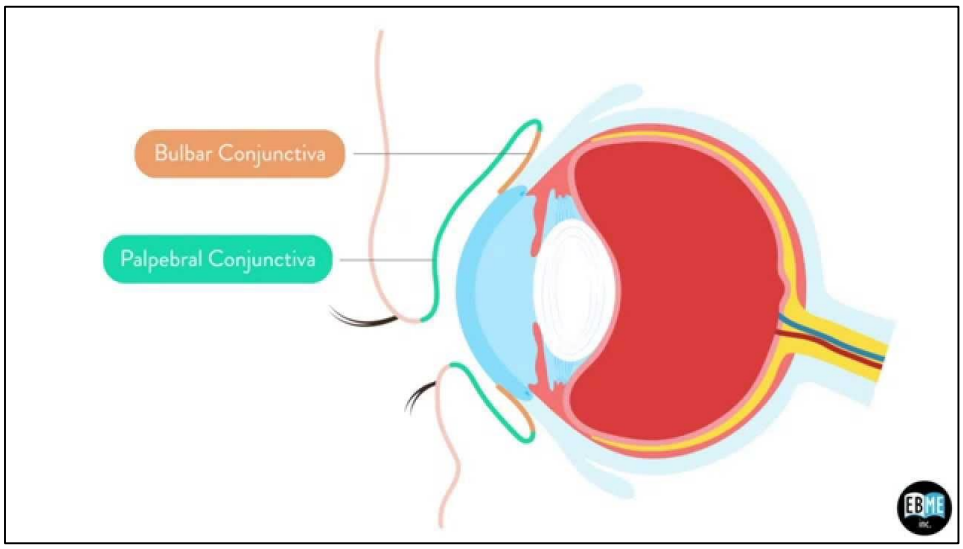

Figure 6.3 *Anatomy of bulbar conjunctiva and palpebral conjunctiva.*

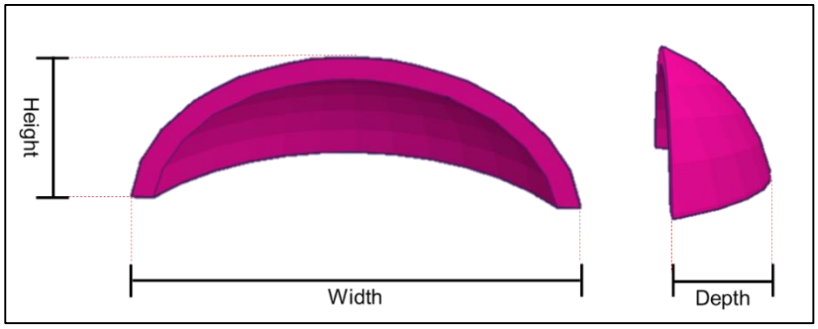

Figure 6.4 *3D image of the design of the ocular inserts with 8.30 mm height, 24.80 mm width, 7.22 mm depth and 1.00 mm thickness*.

A similar approach was taken to the refining the manufacturing process of the 3D-printed ocular inserts as was used for the 3D-printed mini-tablets in **Chapter 5**. Initial experimentation was performed using the flexible resin (Formlabs, USA) to assess whether the procedure was viable or not, and these inserts are described as "model" inserts to distinguish them from the inserts that were later 3D-printed using the photopolymer formulations listed in ***Table 6.2***, which are denoted "sample" inserts.

The model inserts were originally designed to be 3D-printed with a support, so a prototype was printed using the SLA printer using the following settings: "flexible" material type, "highest" printing resolution (0.05 mm distance) and 1 mm base thickness with support. This was successful when the flexible resin (Formlabs, USA) was used. However, due to the problems faced when attempting to 3D-print the PEGDA-based mini-tablets with supports in **Chapter 5**, it was decided to try to print the model inserts directly onto the platform surface, using the same material type and printing resolution settings. Again, this was successful for the flexible resin-based inserts. ***Figure 6.5*** shows an image of the model inserts 3D-printed both with and without support. In both cases, the model insert closely resembled the design specification, giving confidence that this approach of preparing inserts was viable.

Figure 6.5 *3D-printed model ocular insert with support (left) and without support (right).*

Following the procedure used with the 3D-printed mini-tablets in **Chapter 5**, all the sample inserts were printed directly onto the platform surface, using the three formulations listed in ***Table 6.2*** and the same settings as for the model inserts. ***Figure 6.6*** shows images of representative sample inserts from the three formulations. To the naked eye, the sample inserts looked similar overall to the model inserts, but the sample inserts seemed thicker than the model inserts, even though they were printed using the same settings and design. This observation is discussed in more detail later in this Chapter.

The 3D-printed "Pure" inserts were yellowish in colour. The shape seemed uniform for the whole batch of 15 inserts, the texture was slightly flexible and the surface was smooth and sticky. P6K1 inserts were paler in colour than the "Pure" inserts. Again, the texture of the P6K1 inserts was slightly flexible with a smooth surface and the shape seemed uniform for the whole batch. However, their surfaces were covered with a thin layer of white powder, possibly PEG 6K. The powder was easily removed by wiping it off with a tissue and instantly dissolved when in contact with water. The occurrence of a layer of white powder was not observed with the corresponding 3D-printed mini-tablets from **Chapter 5**. For the P4K1 formulation, the inserts were beige in colour and displayed similar texture and uniformity to the P6K1 inserts. All inserts were similar in colour to the 3D-printed mini-tablets with the same formulations from **Chapter 5**.

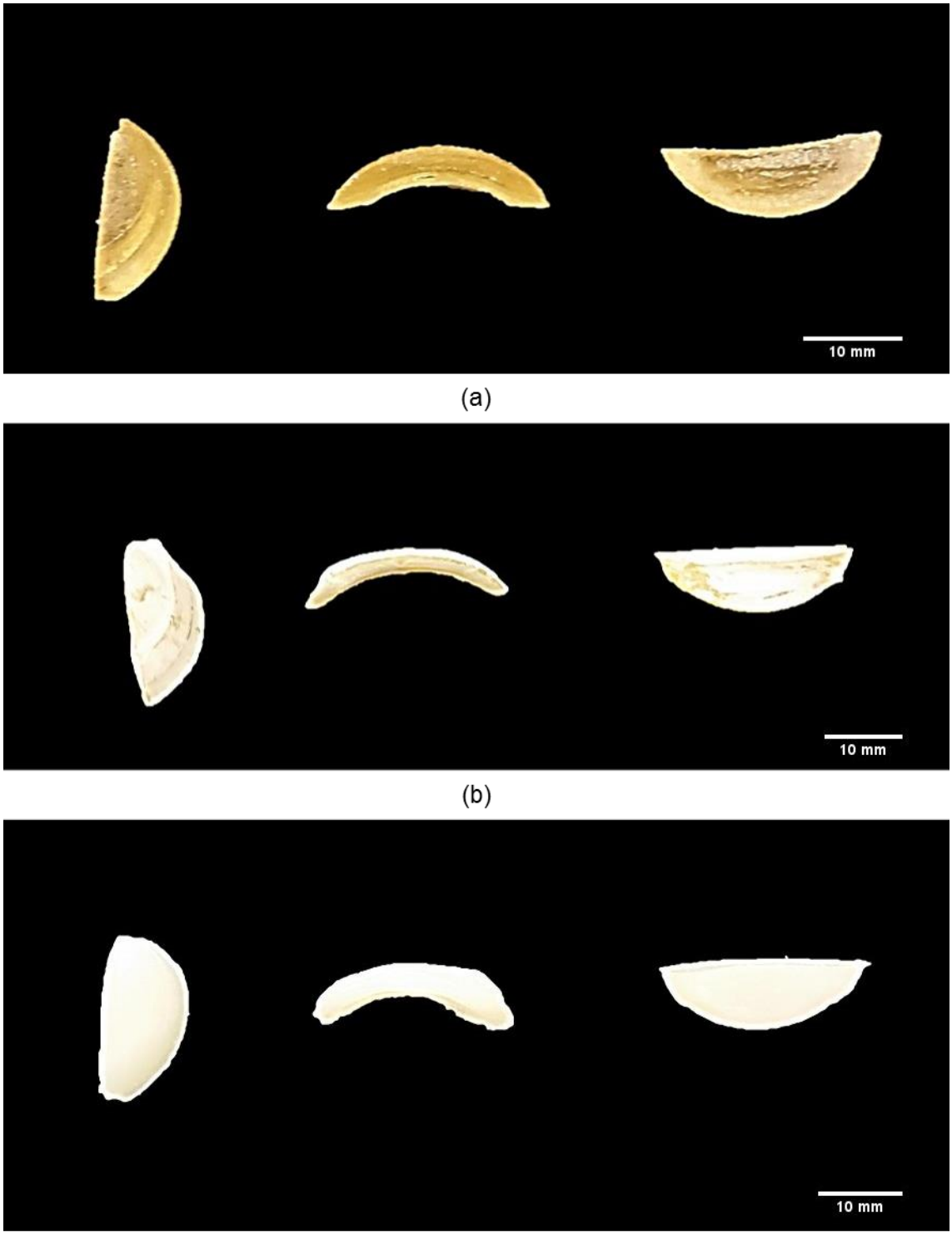

Figure 6.6 *Images of (a) "Pure", (b) P6K1 and (c) P4K1 chloramphenicol-loaded 3D-printed inserts from three different angles.*

6.3.3 Design and 3D-printing of the customised flow-through dissolution cell

Normally, dissolution studies are performed using either a conventional large-volume dissolution bath or a flow-through dissolution apparatus. However, these dissolution methods do not necessarily represent the actual dissolution process which is likely to take place on the surface of the human eye. There are a few factors that can affect the dissolution profiles on the human eye such as the composition of the tear fluid, flow rate and eye shape. Previous dissolution methods, for example the flow-through apparatus with a small sample chamber, were able to mimic the tear fluid composition and have an appropriately low flow rate but could not replicate the eye shape. The eye shape is crucial in ocular treatment with inserts, since everyone has different eye shape and size and it would be expected that contact between the insert and the surface of the eye would be necessary for dissolution to occur. There is the additional factor of size of the inserts, in that the inserts studied here are too large for the flow through cell using for the mini-tablets.

The customised flow-through dissolution cell was designed based on the measurement of eye dimensions and the size of the ocular insert. The shape of the eye was reconstructed by using Tinkercad software. The first prototype design of the dissolution cell consisted of an upper and a lower part, which would then be assembled by screwing the two parts together using bolts and nuts, as indicated in ***Figure 6.7***.

In the lower part, the 3D shape of the eye was re-created using the full x-axis and y-axis dimensions and approximately half the z-axis dimension. This was because the insert would be placed only over approximately 1/8th of the eye, rather than totally surrounding the eye, and the local dissolution of the drug from the insert was the important factor to study. The "eye" part of the design stands proud of the flat surface of the mould.

Surrounding this is an evenly-sized raised ridge, which would allow interlocking with the top part of the dissolution cell. The upper part itself was effectively a mirror image of the lower part, consisting of an eye-shaped hollow and a surrounding channel into which the ridge on the lower part would fit. Once assembled, there would be a 2 mm gap between the upper and lower parts of the cell. This 2 mm gap was to allow the insert (design thickness 1 mm) to be placed inside the dissolution cell with sufficient space to allow the dissolution medium to pass over the inserts. The design of the lower part of the dissolution cell included a small horizontal channel from the exterior to the 2 mm gap to enable the dissolution fluid to be pumped in one side and collected on the other.

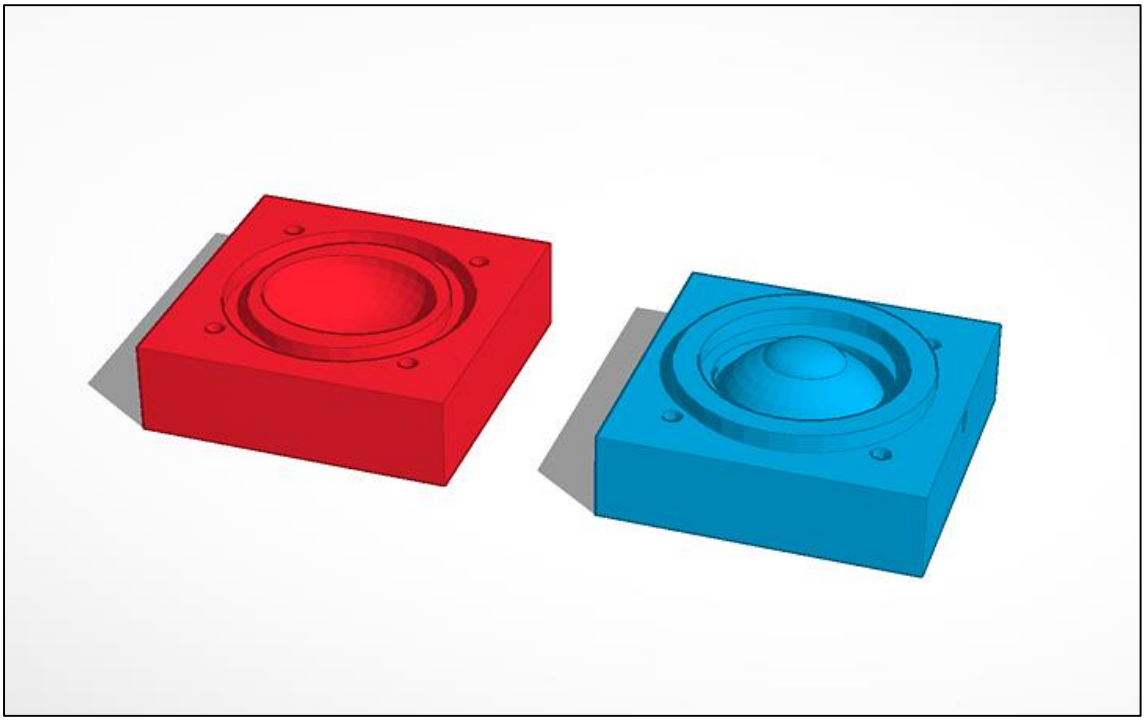

Figure 6.7 *The first prototype of the customised flow-through dissolution cell consisted of upper (red) and lower (blue) parts.*

The dissolution cell prototypes were printed using the FDM printer with a polylactic acid (PLA) filament because it is more cost effective compared to the SLA printer. However, a significant problem associated with this approach was discovered after the two

components of the dissolution cell were printed. Following the design, the lower part was built with a ridge to fit with the recess in the upper part and seal the dissolution cell with the aim of preventing leakage of the dissolution medium during the dissolution process. Unfortunately, the upper part did not fit with the lower part, so therefore the cell could not be sealed, as shown in ***Figure 6.8***.

During the 3D-printing process, the PLA filament undergoes heating and melting at the point where the deposition of the polymer onto the mould occurs. It is actually droplets of liquid that are deposited, which then solidify and build up the 3D construct. If there is any movement of liquid away from the exact deposition site, this will result in a broadening of the element being printed and the product not being an exact match to the original design. In the present case, the issue will be exacerbated as two 3D-printed surfaces need to interact for the dissolution cell to seal correctly. It is likely that the ridge on the lower part of the cell will expand to be wider than it should be and the recess in the top part will be narrower than it should be as material on its edges will expand into this space. Only a small amount of movement in either or both of the parts would be sufficient to prevent the ridge and recess interlocking and cause the dissolution cell to leak.

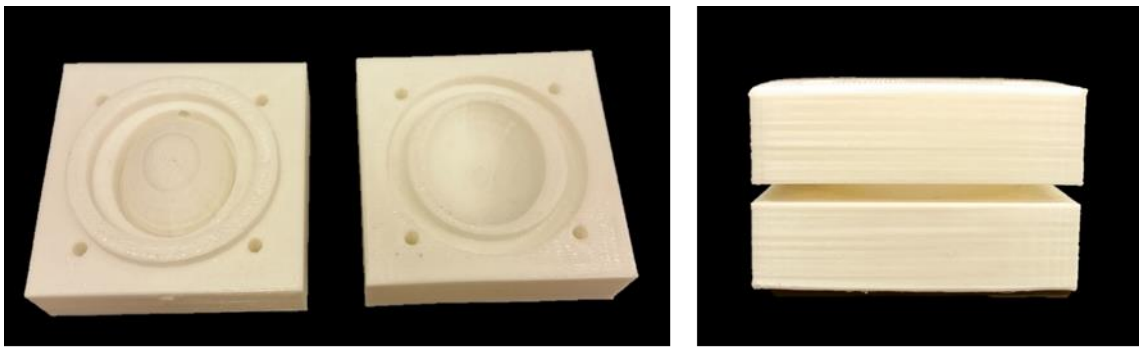

Figure 6.8 *(a) 3D-printed lower (left hand side) and upper (right hand side) parts of the customised dissolution cell prototype and (b) both parts when put together.*

Obviously, the two components of the dissolution cell need to fit properly in order to prevent the dissolution medium from leaking during the experiment. To attempt to overcome this problem, the ridge was removed from the design of the lower part of the cell, leaving it flat in this zone. The top part of the cell was kept the same with the recess, but this was now to be filled with a rubber O-ring, so that when the two parts of the cell were affixed to each other, the O-ring would form the seal between the two surfaces and preventing dissolution fluid loss. ***Figure 6.9*** shows the two components separately and sealed together to make the dissolution cell.

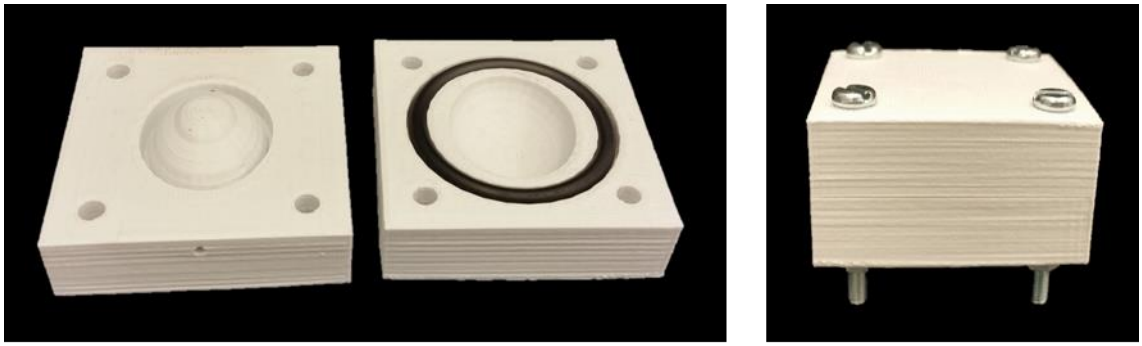

Figure 6.9 *(a) 3D-printed lower (left hand side) and upper (right hand side) parts of the dissolution cell prototype with the rubber ring and without ridge or recess and (b) the successfully assembled prototype with bolts and nuts.*

The design without the ridge was chosen as the final design for the dissolution cell and printed using the SLA printer with flexible resin (Formlabs Inc., USA). The SLA printer was used to print the final design because this printer is capable of printing the product more accurately, based on the design measurement from the 3D software. The flexible resin was used to provide a translucent dissolution cell, so that the dissolution experiment could be monitored visually. Two metal tubes with 1 mm inner diameter were attached and glued to the dissolution medium inlet and outlet. These were to make it

easier to connect the dissolution cell to the peristaltic pump and to collect the dissolution samples. ***Figure 6.10*** shows the final 3D-printed customised dissolution cell ready before use. The dissolution medium inlet and outlet were positioned across the eye shape to mimic the tear flow in human eye which is excreted from the tear duct and then spread across the eye surface.

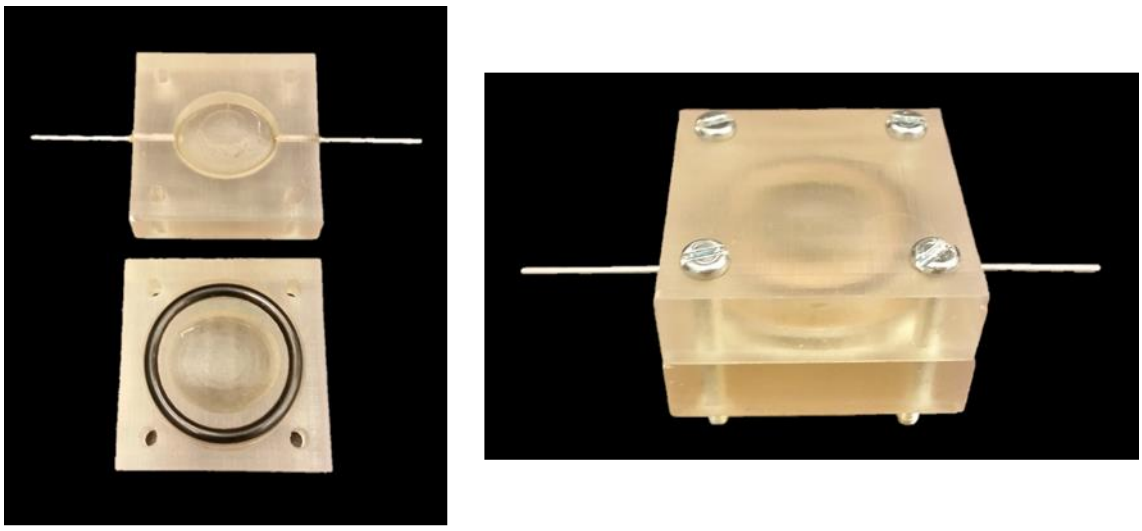

(a) (b)

Figure 6.10 *(a) The lower (top) and upper (bottom) parts of the final 3D-printed customised dissolution cell and (b) the successfully assembled prototype with bolts and nuts.*

6.3.4 Physical characterisation of the 3D-printed ocular inserts

6.3.4.1 Weight Uniformity

The weight uniformity of the inserts was measured by individually weighing ten inserts that were randomly chosen. The mean and standard deviation of the readings were then calculated, as shown in ***Table 6.5***. Although these inserts would not necessarily be subject to the BP weight uniformity guidelines, and the batch size of 15 inserts is lower than the 20 units that are required for the BP analysis, the general specification for this

attribute was applied to assess the manufacturing reproducibility of the inserts. As the inserts are greater than 250 mg in weight, 5 % deviation from the mean is used as the criterion for assessing whether the batch met the BP specifications or not. In ***Table 6.5***, black type denotes inserts that directly passed the BP weight uniformity specification (i.e. inserts with weights showing less than 5 % deviation from the mean), red type denotes inserts that show between 5 and 10 % deviation from the mean value, and blue type denotes inserts that show greater than 10 % deviation from the mean value.

Table 6.5 *Weight uniformity data for chloramphenicol-loaded 3D-printed ocular inserts.*

Insert	Pure* (mg)	P6K1* (mg)	P4K1* (mg)
1	540.53	497.71	539.89
2	494.94	516.82	553.62
3	479.48	537.63	619.78
4	500.34	519.19	511.56
5	492.20	502.23	634.67
6	434.46	477.25	613.84
7	519.83	490.47	624.88
8	446.27	502.15	568.41
9	475.25	507.27	575.04
10	431.20	517.67	545.89
Mean	481.45	506.84	578.76
SD	35.95	16.96	42.20
RSD (%)	7.47	3.35	7.29

* Refer to ***Table 6.2*** for full details of the formulations.

The "Pure" formulation and the P6K1 formulation were not statistically significantly different in weight, but the P4K1 formulation was statistically significantly different

($p<0.05$) to both of the other formulations. The 3D-printed mini-tablets studied in **Chapter 5** also showed differences in weight between formulations, in that the "Pure" formulation was significantly lower in weight than all other formulations, and the P6K1 and P4K1 3D-printed mini-tablets were significantly different ($p<0.05$) to each other. However, in that case the P6K1 3D-printed mini-tablets were heavier than the P4K1 3D-printed mini-tablets, whereas for the 3D-printed ocular inserts, the relationship was inversed.

Based on the summary values, the P6K1 formulation was the most reproducible in terms of weight with an RSD value of 3.35 %. Both the "Pure" formulation and the P4K1 showed similar higher variability (RSD values of 7.47 % and 7.29 %, respectively), although the actual weights were quite dissimilar between the batches. Using the BP weight uniformity specifications as a guide, only the P6K1 inserts would pass, and only then if the "2 out 20 showing deviation between 5 and 10 % of the mean" could be taken to be "2 out of 10". Both the "Pure" and the P4K1 inserts would fail this specification.

The slightly higher weights of individual inserts, and hence the high variability, may have been caused, at least in part, by the excessive areas that look like a "skirt" around the inserts, as shown in ***Figure 6.11***. This "skirt" was a by-product created during the curing process of the inserts. After the 3D-printing process was complete, the platform was lifted from the formulation solution in the resin tank. One or more droplets of the formulation solution were adsorbed to the surface of the inserts. During the curing process, these residues were photopolymerised and cured, creating the "skirt".

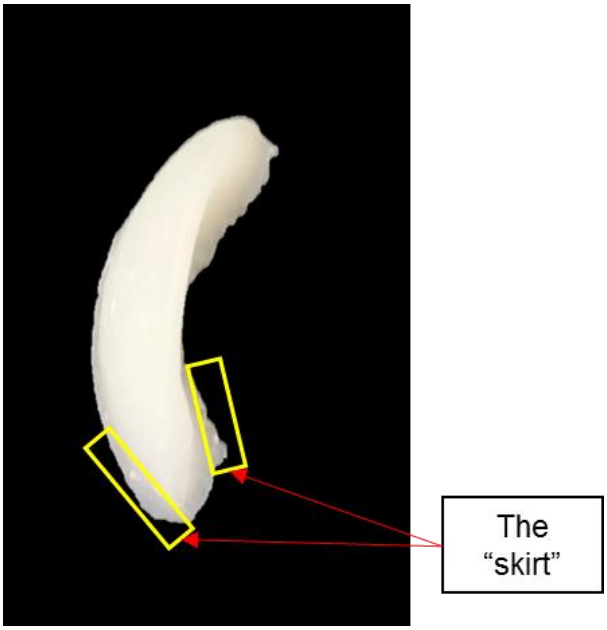

Figure 6.11 *The "skirt" around the inserts*

6.3.4.2 Dimensions

The ocular inserts were crescent-shaped, close to being a quarter-sphere. Since the inserts' shape was irregular, it is difficult to calculate the surface area using standard surface area (cubic, sphere, pyramid etc.) formulae. Because of that, Netfabb software was used to determine the surface area of the inserts. To use the software, the height, width and depth of the 3D-printed inserts need to be measured. A digital calliper was used for that purpose. The inserts' dimensions on the software were then re-adjusted using these readings and the surface areas were then calculated, as summarised in ***Table 6.6***.

Table 6.6 *Summary of the design parameters and actual dimensional data for chloramphenicol-loaded 3D-printed ocular inserts (mean ± SD) (n=10).*

Inserts	Height (mm)	Width (mm)	Depth (mm)	Surface area (cm^2)
Design	8.30	24.80	7.22	4.72
Pure*	8.32 ± 0.16	22.59 ± 0.26	6.72 ± 0.20	4.22 ± 0.09
P6K1*	8.71 ± 0.38	26.13 ± 0.30	8.16 ± 0.09	5.43 ± 0.13
P4K1*	8.01 ± 0.36	23.80 ± 0.28	8.23 ± 0.43	4.80 ± 0.18

* Refer to ***Table 6.2*** for full details of the formulations.

Based on the results, the P4K1 inserts were the closest to the design in term of the mean surface area and width. Meanwhile, the mean values of the height and depth of the "Pure" inserts were the closest to the design, as shown in green type in ***Table 6.6***. P6K1 inserts displayed higher mean values for all measurements and calculated surface area, indicating the P6K1 inserts were printed larger than the model.

Tables 6.7, 6.8 and ***6.9*** show the individual dimensional data for ten inserts from each of the three different batches. Overall, the "Pure" formulation was the most consistent, with very low RSD values for all measurements. Both the P6K1 and P4K1 inserts showed much more variability in the height dimension and the P4K1 inserts also showed higher variability in the depth dimension.

Overall, it was apparent that the inserts had not been 3D-printed exactly as the original design. This is probably due to the printing settings used to manufacture the inserts, in that the pre-installed printing settings on the software were meant for commercialised resin specifically developed for 3D-printing, e.g. the flexible resin used in the prototyping exercise. However, the settings chosen for this study was the best settings possible for these formulations, as discussed in **Chapter 5** for the 3D-printed mini-tablets. This is an

area which needs some attention if this technology is to be used successfully for pharmaceutical products.

Table 6.7 *Measured dimensions and calculated surface areas of chloramphenicol-loaded 3D-printed "Pure"* inserts.*

Insert	Height (mm)	Width (mm)	Depth (mm)	Surface area (cm^2)
1	8.42	21.98	6.82	4.18
2	8.28	22.57	6.82	4.23
3	7.98	22.86	6.46	4.06
4	8.55	22.47	6.93	4.34
5	8.26	22.38	6.89	4.21
6	8.38	22.72	6.87	4.30
7	8.30	22.78	6.55	4.18
8	8.28	22.79	6.88	4.28
9	8.54	22.71	6.62	4.28
10	8.24	22.65	6.40	4.10
Mean	8.32	22.59	6.72	4.22
SD	0.16	0.26	0.20	0.09
RSD (%)	1.92	1.15	2.98	2.13

* Refer to ***Table 6.2*** for full details of the formulations.

Table 6.8 *Measured dimensions and calculated surface areas of chloramphenicol-loaded 3D-printed P6K1* inserts.*

Insert	Height (mm)	Width (mm)	Depth (mm)	Surface area (cm^2)
1	8.97	26.66	8.26	5.66
2	8.41	26.27	8.13	5.33
3	9.37	25.56	8.03	5.53
4	8.15	26.08	8.27	5.25
5	9.16	25.89	8.08	5.53
6	8.84	26.00	8.19	5.46
7	8.51	26.00	8.13	5.32
8	8.50	26.39	8.27	5.43
9	8.72	26.17	8.23	5.46
10	8.46	26.24	8.04	5.31
Mean	8.71	26.13	8.16	5.43
SD	0.38	0.30	0.09	0.13
RSD (%)	4.36	1.15	1.10	2.39

* Refer to ***Table 6.2*** for full details of the formulations.

Table 6.9 *Measured dimensions and calculated surface areas of chloramphenicol-loaded 3D-printed P4K1* inserts.*

Insert	Height (mm)	Width (mm)	Depth (mm)	Surface area (cm^2)
1	7.63	23.50	7.76	4.46
2	7.59	24.04	8.47	4.77
3	7.85	24.29	8.35	4.86
4	8.22	23.64	7.72	4.67
5	7.93	23.62	8.56	4.85
6	8.53	23.47	8.53	5.02
7	8.02	23.66	7.55	4.55
8	7.88	23.88	8.61	4.89
9	7.81	24.17	8.73	4.96
10	8.67	23.71	7.98	4.93
Mean	8.01	23.80	8.23	4.80
SD	0.36	0.28	0.43	0.18
RSD (%)	4.49	1.18	5.22	3.75

* Refer to ***Table 6.2*** for full details of the formulations.

6.3.5 Drug release profile

The dissolution studies on the inserts could not be conducted using the same flow-through dissolution system as used in **Chapters 3** and **5**, because the inserts were too large to fit into the 200 µL chamber. Hence, a flow-through cell based on the shape of the subject's eye was designed and manufactured as described earlier in this Chapter. The remainder of the experimental set-up was the same as used previously, i.e. it was simply that the sample casket that was connected to the peristaltic pump was replaced with the 3D-printed customised dissolution cell. The inserts were placed and sealed inside the dissolution cell, as shown in ***Figure 6.12***. The cell was sealed to ensure that the dissolution medium did not leak during the test. The dissolution cells were translucent, which made it possible to observe the sample inside.

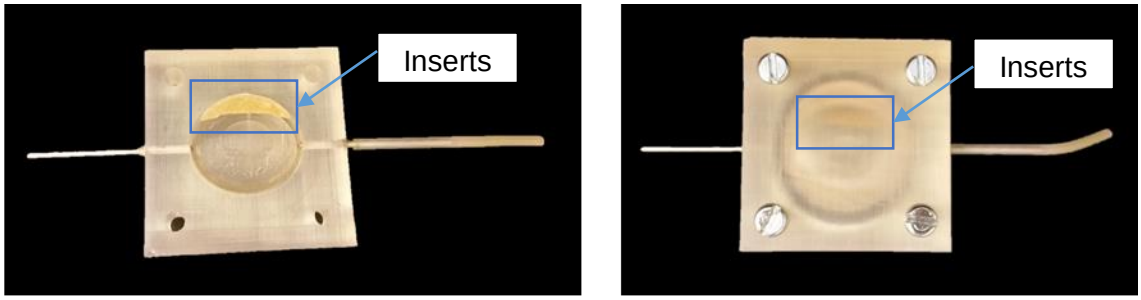

Figure 6.12 *Sample placement inside the 3D-printed customised dissolution cell. (a) The insert was placed on the lower part and (b) the two parts were held together by bolts and nuts.*

The complete dissolution system was assembled as shown in ***Figure 6.13***. The dissolution medium was kept at 34.0 ± 1.0 °C to mimic the temperature of normal human eye which is 34.0 ± 0.5 °C (Fujishima et al., 1996). The medium then was pumped through the dissolution cell using the peristaltic pump at the rate of 50 µL/minute. This rate was chosen in order to obtain sufficient amount of sample to be analysed using a UV/Vis spectrophotometer at 278 nm and to provide a comparison to the dissolution data

generated in **Chapters 3** and **5**. The sample was collected at the dissolution cell outlet using a 15 mL vial, every hour up to 9 hours and then at 24, 48, 72 and 96 hours.

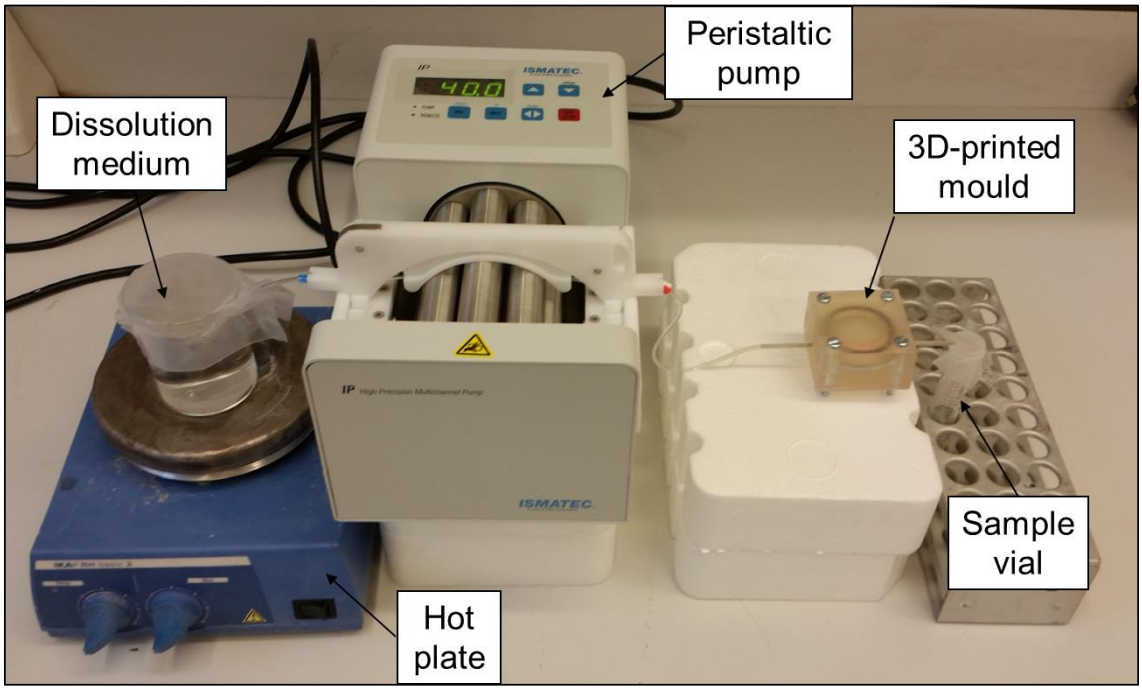

Figure 6.13 *Customised ocular flow-through dissolution apparatus.*

The data obtained from the dissolution tests were plotted graphically as percentage of drug release against time, as shown in ***Figure 6.14***. Three replicates were generated for each formulation.

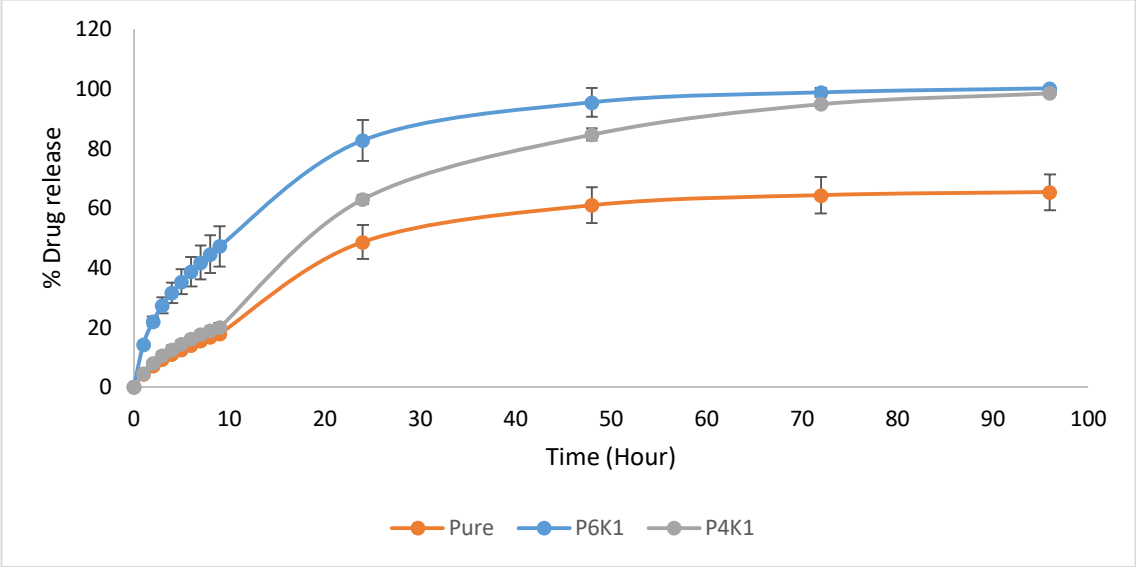

Figure 6.14 *Drug release profile from chlorampenicol-loaded "Pure", P4K1 and P6K1 inserts (n=3).*

Based on ***Figure 15***, all formulations displayed slow release profiles, but there were some obvious differences between the three formulations. The rank order of release was "Pure" (slowest rate and lowest total % drug released), P4K1 (intermediate rate but complete drug release), P6K1 (fastest rate and complete drug release).

The "Pure" inserts released the drug up to the 72 hours timepoint before the release profile started to plateau. Over the first 9 hours the "Pure" inserts released only circa 20 % of the drug. There then appeared to be a slight disconnect between the results for the inserts at 9 hours and 24 hours, i.e. the profile is not completely smooth, which is probably a consequence of the long-time gap (overnight) between these samples. Drug release continued after 24 hours until a plateau was reached at circa 65 % drug release at 72 hours.

Similar behaviour was observed with the P4K1 inserts, in that over the first 9 hours of the study only circa 20 % of the drug was released. Again, there was a disconnect between the results at 9 hours and 24 hours, but drug release continued thereafter until the drug was completely released after 96 hours.

Meanwhile, the P6K1 inserts released the drug at a higher rate than the other formulations up to 24 hours, before the release rate started to slow down significantly. Drug release from these inserts was essentially complete after 72 hours of the dissolution test.

6.3.5.1 Mathematical modelling of the drug release profiles

As discussed in **Chapters 3** and **5** for the compressed powder and 3D-printed mini-tablets, three mathematical models of release kinetics were used to evaluate the drug release profiles: first order kinetics, zero order kinetics and the Korsmeyer-Peppas equation. For the first and zero order kinetics, data were analysed up to approximately 85 % of release profile. Meanwhile, for the Korsmeyer-Peppas analysis, the values were analysed up to approximately 60 % of the fractional release. In case of the release profile plateauing before reaching the 100 %, the values were analysed up to the point before it plateaued. ***Table 6.10*** shows the coefficient of determination (r^2), release rate constant ((k_0, k_1 *and* k_{KP})) and the diffusional exponent (n) values for the release profiles of the 3D-printed ocular inserts. Green values indicated the best fitting model. ***Table 6.11*** shows a similar analysis but using data from the first 9 hours of the experiment only, in order to facilitate comparison with the 3D-printed mini-tablets, discussed later in this Chapter.

Table 6.10 *Mathematical modelling parameters for drug release from chloramphenicol-loaded 3D-printed ocular inserts - full profile.*

Mini-tablet	Zero Order		First Order		Korsmeyer-Peppas		
	r^2	k_0	r^2	k_1	r^2	k_{KP}	n
Pure*	0.8688	1.4945	0.9581	0.0215	0.9869	4.1678	0.7032
P6K1*	0.6006	4.3318	0.9805	0.0748	0.9982	14.7008	0.5406
P4K1*	0.9311	1.9898	0.9874	0.0384	0.9717	4.3017	0.768

* Refer to ***Table 6.2*** for full details of the formulations.

Table 6.11 *Mathematical modelling parameters for drug release from chloramphenicol-loaded 3D-printed ocular inserts - 9 hours only.*

Mini-tablet	Zero Order		First Order		Korsmeyer-Peppas		
	r^2	k_0	r^2	k_1	r^2	k_{KP}	n
Pure*	0.8966	2.2454	0.9242	0.0243	0.9992	4.5136	0.633
P6K1*	0.7962	6.1315	0.9086	0.0788	0.9970	14.7567	0.5373
P4K1*	0.8962	2.5444	0.9261	0.0279	0.9950	4.8477	0.665

* Refer to ***Table 6.2*** for full details of the formulations

Over the full dissolution profile, the "Pure" and P6K1 inserts were best modelled with the Korsmeyer-Peppas equation, with n values of 0.7032 and 0.5406, respectively. This values indicate an "anomalous" mechanism of dissolution, whereby multiple factors are involved in the controlling the drug release pattern. The dissolution profile of the P4K1 inserts was best fitted with a first order profile. Although it is obvious from ***Figure 6.15***, that the drug release profiles are different, this was confirmed by examination of the similarity factors (f_2) which were < 50 for all paired comparisons.

When only the first 9 hours of the dissolution profile were considered, all three formulations showed excellent fitting to the Korsmeyer-Peppas equation, with $r^2 \geq 0.9950$, and n values of 0.6330, 0.5373 and 0.665 for the "Pure", P6K1 and P4K1 inserts, respectively, indicating an "anomalous" control process. In this timeframe, the "Pure" and P4K1 inserts had similar dissolution profiles (f_2 = 85) whereas the P6K1 inserts still showed f_2 < 50 for comparisons with the other inserts.

6.3.5.2 Comparison between the 3D-printed mini-tablets and 3D-printed ocular inserts

The drug release profiles of matched pairs of 3D-printed mini-tablets and ocular inserts were compared in order to investigate if their different size and shapes played essential roles in their release profiles, since both the ocular inserts and mini-tablets were 3D-printed using the same formulations. The comparison was performed over the first 9 hours only, as this was the duration of the release testing for the 3-D printed mini-tablets and the timepoints at which the dissolution samples were taken were the same for both the 3-D printed mini-tablets and the 3D-printed ocular inserts.

Figures 6.15, 6.16 and 6.17 compare the drug release profiles of the two product types for the "Pure", P6K1 and P4K1 formulations, respectively.

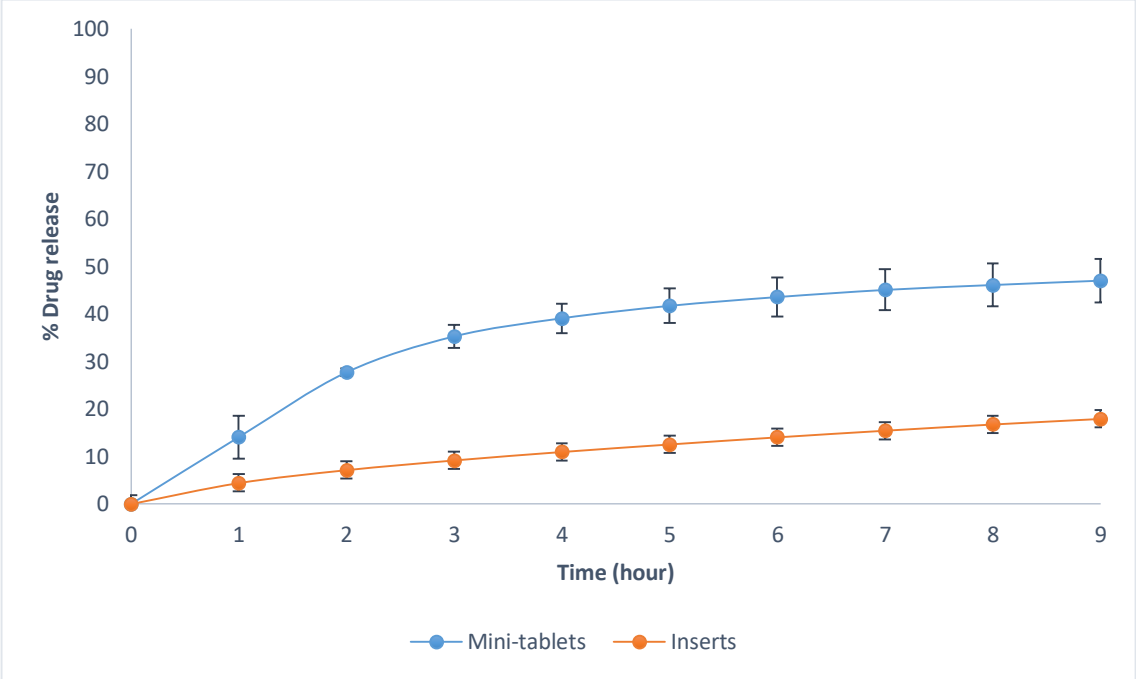

Figure 6.15 *Drug release profiles from the chloramphenicol-loaded "Pure" formulations (n=3).*

The drug release from the "Pure" 3D-printed mini-tablets appeared to plateau after 7 hours, with only minimal drug release being observed thereafter. The inserts showed a similar type of profile, but the time taken to reach the plateau was much longer at 72 hours. Both product types showed incomplete dissolution, with circa 20 % and 65 % drug release for the inserts at 9 hours and 96 hours respectively, and circa 47 % drug release for the mini-tablets at 9 hours. The two drug release profiles were clearly different over the first 9 hours, reinforced by examination of the f_1 and f_2 difference and similarity factors, as summarised in ***Table 6.12***. These results suggest that the dimensions and surface area of the product may play a role in controlling the dissolution rate for this particular formulation.

Meanwhile, the profiles of the P6K1 inserts and mini-tablets were very similar and overlapped from the 3 hour timepoint to the 9 hour timepoint, when the dissolution experiment for the mini-tablets was terminated. Given these profiles, it would be expected that the mini-tablet would have continued to release the drug until complete release was observed, rather than plateauing as was the case with the "Pure" formulation. The inserts' profile over this 9-hour period fitted better to the Korsmeyer-Peppas equation (anomalous dissolution), whereas the mini-tablets' profile fitted better to first-order kinetics, which is probably a consequence of the slight differences at the very early timepoints (1 hour and 2 hours). For the P6K1 formulation, therefore, it would appear that there was little effect of the product dimensions on the release profile. The f_1 and f_2 difference and similarity factors, as summarised in ***Table 6.12***, support this conclusion.

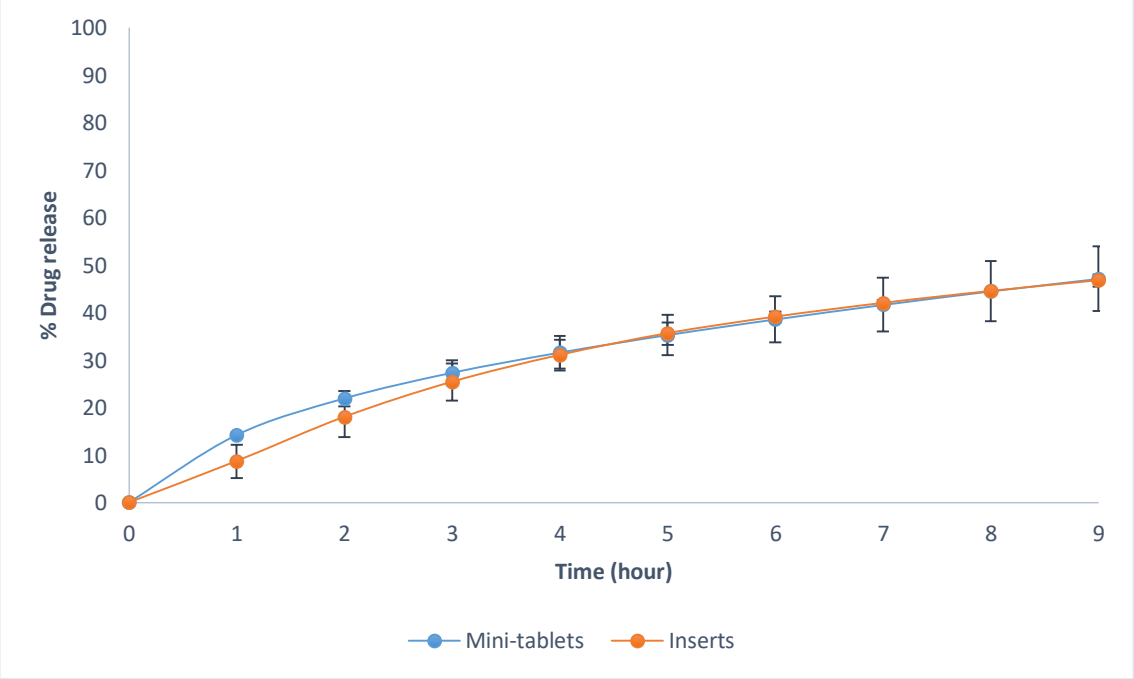

Figure 6.16 *Drug release profiles from the chloramphenicol-loaded P6K1 formulation (n=3).*

The behaviour of the P4K1 products displayed a similar pattern to that of the "Pure" products, in that there was a substantial difference between the drug release profiles of the inserts and the mini-tablets, with that of the inserts being significantly slower than the mini-tablets over the first 9 hours. The P4K1 mini-tablets had released circa 80 % of the drug at 9 hours when the experiment was terminated, and would be expected to show complete drug release at longer time periods. The P4K1 inserts had only released circa 20 % of the drug at 9 hours, although complete drug release was observed at 96 hours. Evaluation of the f_1 and f_2 difference and similarity factors (***Table 6.12***), confirm that the profiles are dissimilar. Similarly to the "Pure" formulation, it would appear that there was an effect of the product dimensions for this particular formulation.

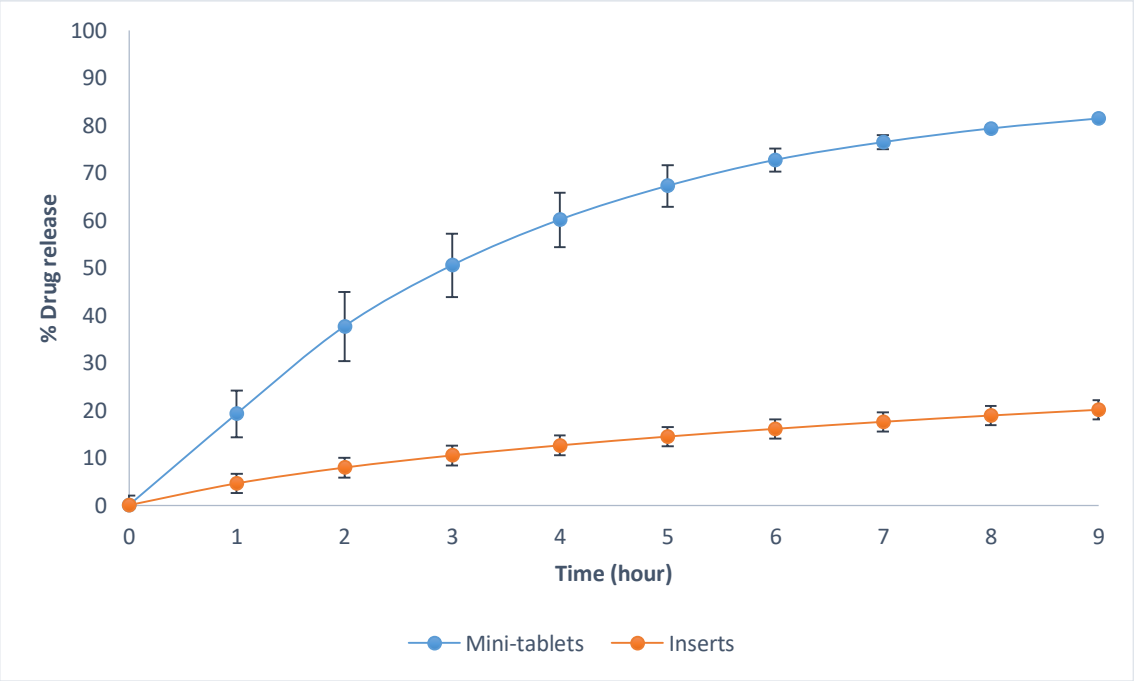

Figure 6. 17 *Drug release profiles from the chloramphenicol-loaded P4K1 formulations (n=3).*

Table 6.12 *Difference and similarity factors between chloramphenicol-loaded ocular inserts and 3D-printed mini-tablets.*

Formulation	Difference Factor (f_1)	Similarity Factor (f_2)
Pure*	68	29
P6K1*	5	80
P4K1*	77	15

* Refer to ***Table 6.2*** for full details of the formulations.

6.3.5.3 Evaluation of the thickness and swelling behaviour of the 3D-printed ocular inserts

The dissolution behaviour of the 3D-printed inserts was unexpected, particularly when compared to the 3D-printed mini-tablets of the same formulation, and hence was investigated further. One possibility is that the physical dimensions of the inserts resulted in contact with both the upper and lower surfaces of the dissolution cell, preventing the dissolution medium flowing easily across the surface of the insert and reducing the amount of drug dissolved. The gap between the lower and upper parts of the dissolution cell when they were put together was 2 mm and the design thickness of the inserts was 1 mm, hence there should have been plenty of clearance. However, if the thickness of the insert was greater than 2 mm, it would be expected that contact to both surfaces would arise. Therefore, the central thickness of ten randomly-selected inserts was measured to investigate this issue, and the results are presented in ***Table 6.13***.

Table 6.13 *The thickness values of the chloramphenicol-loaded 3D-printed ocular inserts.*

Reading	Pure*	P6K1*	P4K1*
1	2.64	1.78	1.88
2	2.44	1.80	2.36
3	1.80	1.60	1.74
4	2.47	1.88	2.18
5	2.48	1.80	2.35
6	1.70	1.75	2.41
7	1.83	1.90	1.97
8	1.83	1.73	1.74
9	2.33	1.78	1.85
10	1.85	1.82	1.78
Mean	2.14	1.78	2.03
SD	0.36	0.08	0.27
RSD (%)	16.82	4.49	13.30

* Refer to ***Table 6.2*** for full details of the formulations.

It can be seen immediately from ***Table 6.14*** that all of the inserts were significantly thicker than the design specification of 1 mm. The values of insert thickness that were lower than 2 mm (the width of the gap in the dissolution cell design) are highlighted in green while red is used for values equal to or higher than 2 mm. The mean thickness of the "Pure" inserts was 2.14 ± 0.36 mm, with a large range of individual values from 1.70 mm to 2.64 mm. Closer inspection showed that the thickness values seemed to fall into two groups, with half of the readings being much higher than 2 mm and the other half being much lower than 2 mm. When these two subsets of data are analysed separately, the variability within each subset is much lower, with the means, SD and

RSD values being 1.80 mm, 0.06 mm and 3.32 % for those inserts thinner than 2mm, and 2.47 mm, 0.11 mm and 4.50 % for those inserts thicker than 2 mm, respectively. These two subsets of thickness data were shown to be statistically significant ($p < 0.001$).

A similar pattern was displayed by the P4K1 inserts. The mean thickness was 2.03 ± 0.27 mm, with a range of individual values between 1.74 mm and 2.41 mm. Four of the readings were much higher than 2 mm and 6 readings were much below 2 mm. When these two subsets of data are analysed separately, the variability within each subset is much lower, with the means, SD and RSD values being 1.83 mm, 0.09 mm and 4.97 % for those inserts thinner than 2mm, and 2.33 mm, 0.10 mm and 4.31 % for those inserts thicker than 2 mm, respectively. These two subsets of thickness data were also shown to be statistically significant ($p < 0.001$).

Meanwhile, all the P6K1 inserts had thickness readings that were lower than 2 mm, with a mean of 1.78 ± 0.08 mm and a range of 1.60 mm to 1.90 mm. The RSD value for the thickness of the P6K1 inserts was 4.49 %, similar to the RSD values of the subsets of data for the other two formulations discussed above.

If the thickness values of all 10 of the P6K1 inserts are compared to the values of the thinner "Pure" and P4K1 inserts, then there is no significant differences ($p > 0.1$) between them. Examination of the weight variability data in ***Table 6.5*** shows that the P6K1 inserts are more consistent in weight than the "Pure" or P4K1 inserts, which may be related to the variability in the thickness data. Together, this suggests the 3D-printing process was reasonably well controlled in terms of product thickness, but that there was a systematic issue causing some thicker inserts to be printed and an underpinning issue that even the "thin" inserts are almost twice as thick as the design

specification of 1 mm. This warrants further investigation.

With respect to the dissolution studies on the inserts using the customised dissolution cell, since all the P6K1 inserts had thickness values that were less than 2 mm, it would be expected that the dissolution medium would be able to flow across the inserts in the manner intended and that the "correct" dissolution profile would be obtained. If the inserts are greater than 2 mm in thickness, it would be expected that the dissolution cell could not be closed. However, such a problem was not identified during the dissolution experiments on the "Pure" and P4K1 inserts, possibly in part because the inserts are slightly flexible and may have deformed sufficiently to allow the dissolution cell components to be screwed together. Additionally, the possibility of choosing for the dissolution tests the inserts that were thinner than 2 mm was roughly 50 %, so it is possible that all dissolution experiments were conducted on "thin" inserts.

However, based on the drug release profiles, both the "Pure" and P4K1 inserts showed slower release rates than the mini-tablets of the same formulations from **Chapter 5**, whereas the P6K1 inserts and mini-tablets gave the same drug release profiles. Overall, the error bars for the inserts' dissolution data were small, indicating all replicates displayed similar results, suggesting that the inserts studied in each batch were of similar thickness. A plausible explanation of why the "Pure" and P4K1 inserts behaved differently is these inserts swelled during the dissolution test. To investigate this, three inserts from each formulation were chosen randomly. The thickness of the inserts was measured with a digital calliper before the test. The inserts then were placed into a 20 mL tube sample containing 10 mL of STF and were completely submerged. The thickness of the inserts was re-measured after one hour. ***Table 6.14*** shows the readings for all the inserts.

Based on these results, the "Pure" and P4K1 inserts had significantly swollen after one hour of soaking, with thickness increments of 14.29 ± 1.46 % and 7.83 ± 1.22 %, respectively. However, for P6K1 inserts, a very small percentage increment was displayed by only one of the samples, with no change being observed for the other two inserts tested. This increment is so small that it is likely to be insignificant experimentally. Therefore, even if the "Pure" and P4K1 inserts chosen for the dissolution test were thinner than 2 mm, it is likely that they would swell more than 2 mm within one hour of the dissolution test. This would then result in the insert pushing against both the top and bottom of the dissolution cell gap and reducing the flow of dissolution fluid across its surfaces, with a consequent decrease in the amount of drug that could be dissolved from the inserts. The dissolution profile measured would be slower than would normally be expected. As the dissolution chamber used for the mini-tablets had a volume of 200 µL (equivalent to 200 mm^3), and the 3D-printed mini-tablets had a maximum calculated volume of circa 35 mm^3, any swelling during the test is unlikely to have a significant effect on the results, such that a "true" dissolution profile would be measured.

Table 6.14 *The thickness and swelling data of chloramphenicol-loaded 3D-printed ocular inserts.*

Inserts	**Initial (mm)**	**Final (mm)**	**Difference (%)**	**Mean ± SD of the difference (%)**
Pure*	2.42	2.77	14.46	14.29 ± 1.46
	1.98	2.29	15.66	
	2.43	2.74	12.76	
P6K1*	1.60	1.60	0.00	0.37 ± 0.64
	1.80	1.82	1.11	

	1.77	1.77	0.00	
P4K1*	1.80	1.95	8.33	7.83 ± 1.22
	2.33	2.48	6.44	
	1.95	2.12	8.72	

* Refer to ***Table 6.2*** for full details of the formulations.

Taken together, these results provide an explanation of why the dissolution rates for both the "Pure" and P4K1 inserts were slower than the mini-tablets from the same formulations. Since the P6K1 inserts did not swell and the thickness of the inserts were less than 2 mm, a "true" dissolution profile could be obtained. The drug release for the inserts and mini-tablets from P6K1 formulation showed identical profiles. Perhaps surprisingly, this is to be expected as the surface area to volume ratios are approximately the same for the two product types.

6.3.5.4 Content uniformity

According to BP specifications, the formulations would be considered uniform if not more than 1 individual drug content value were outside the limit of 85 to 115 % and none outside 70 to 130 % of the average content. However, these specifications were for 10 dosages while in this study, only 3 dosages were used. ***Table 6.15*** shows the content uniformity for the ocular inserts. All formulations were between 85 and 115 % which complied the BP standards. The percentage of drug in the inserts were similar with the percentage of drug content in **Chapter 5** from the same formulations.

Table 6.15 *Content uniformity for the ocular inserts.*

Polymer	Weight (µg) (Mean ± SD)	Drug content (µg)	Mean (µg)	SD (µg)	Drug content (%)	Mean (%)	SD (%)
Pure	481.45 ±	18.53	18.29	0.28	3.85	3.80	0.06
	35.95	18.37			3.82		
		17.98			3.73		
P6K1	506.84 ±	19.54	19.79	0.25	3.86	3.91	0.05
	16.96	20.03			3.95		
		19.81			3.91		
P4K1	578.76 ±	21.40	21.07	0.30	3.70	3.64	0.05
	42.20	20.98			3.62		
		20.83			3.60		

* Refer to ***Table 6.2*** for full details of the formulations.

6.4 GENERAL DISCUSSION

In this Chapter, the potential of 3D-printing to manufacture customised ocular inserts and corresponding flow-through dissolution cells was investigated. A colleague in the UCL School of Pharmacy kindly gave permission for an MRI scan of his head to be used as a basis for designing a customised ocular insert specifically for one individual. The MRI data were analysed with InVesalius (2016) in order to recreate the shape of this individual's eye. Following analysis of the dimensions of the eye, Tinkercad software was used to design an ocular insert to match the shape of the eye, the same software having been used to design the 3D-printed mini-tablets studied in **Chapter 5**.

As observed in **Chapter 5**, it was possible to 3D-print the prototype ocular inserts using flexible resin (Formlabs, USA), either with a support or directly onto the platform. Such model inserts showed a good correlation to the initial design of the inserts. Three formulations based on PEGDA and used to 3D-print mini-tablets in **Chapter 5** were selected to create the sample ocular inserts for analysis: "Pure", with no added low molecular weight PEG, and P6K1 and P4K1, where an equal amount of low molecular weight PEG (6000 or 4000) is added to the formulation. It was possible to 3D-print these ocular inserts directly onto the platform, i.e. without a support. However, as seen with the 3D-printed mini-tablets, the 3D-printed ocular inserts were larger than the initial design in all four dimensions (height, width, depth and thickness), with an inconsistent effect of varying the formulation on each of these parameters, i.e. the rank order of the variation from the design measurement was not the same for each parameter. Of particular concern, the thickness of even the thinnest ocular insert was almost twice that of the design (1 mm). Interestingly, and perhaps worryingly, the "Pure" and P4K1 inserts seemed to fall into two groups when the thickness was evaluated, with the variability within each group being reasonable, whereas the P6K1 inserts were

consistently "thin".

The difference in 3D-printing behaviour of the model and sample inserts in most likely due to the fact that the 3D-printer is designed to be used with commercially-available (from the same company) resins and all the printing parameters are set up to maximise printing efficiency with those materials. The 3D-printer is not optimised to be used with the PEGDA-based formulations studied here, and the settings used to 3D-print the mini-tablets and inserts were the best possible under the circumstances. This aspect of the 3D-printing control needs to be investigated further and improved (or at least understood), as it is vital for pharmaceutical products that the final product is identical to the design and the products are consistent in appearance and performance. A high degree of product variability, such as was seen with the thickness of the inserts, is unacceptable pharmaceutically.

A customised flow-through dissolution cell was successfully developed, matching both the subject's eye and the ocular insert. Such a dissolution cell was necessary as the ocular insert was too large to fit into the dissolution chamber used to assess the drug release profile of the mini-tablets in **Chapters 3** and **5**. This dissolution cell was manufactured using the flexible resin (Formlabs, USA) to maximise the efficiency of printing. An additional advantage is that this resin is translucent, so it is possible to observe the insert in situ once placed in the dissolution cell and to monitor the dissolution experiment.

Dissolution studies on the 3D-printed ocular inserts suggested that the drug release pattern is governed by the Korsmeyer-Peppas equation, with values of the exponent n suggesting "anomalous" diffusion. "Anomalous" kinetics indicate that there is more than one factor governing the release of the drug from the product. In the case of the

inserts, this is likely to be a combination of diffusion of water into pores within the insert matrix to dissolve the drug, dissolution of the low molecular weight PEG from the matrix creating more pores, and the continual flow of dissolution medium across the surface of the insert. The actual dissolution results were unexpected and further investigation suggested that some of the inserts absorbed water during the initial stage of the dissolution experiment, swelling to a such a degree that they made contact with both the top and bottom surfaces of the dissolution cell, which resulted in lower contact between the insert and the dissolution fluid and hence lower total dissolution than would be expected. The P6K1 inserts were consistently thinner than the other two batches and also did not swell when submerged in STF, leading to a "correct" dissolution profile being observed. Overall, the dissolution profile from the P6K1 inserts was essentially indistinguishable from that of its counterpart mini-tablets, probably as ultimately the surface area to volume ratios are similar for the two product shapes. The P4K1 and P6K1 inserts swelled significantly during the 1 hour STF submersion test, so even if "thin" inserts were selected for the dissolution test, they would have swollen during the test, making the results inconclusive. Hence, it was not surprising that the inserts of these two formulations showed different dissolution behaviour to the equivalent mini-tablets.

Table 6.16 below summarises whether the 3D-printed ocular inserts would pass the initial target specifications presented earlier in this Chapter and whether they would be considered for further development.

Table 6.16 *Summary of the analytical tests of the chloramphenicol-loaded 3D-printed ocular inserts in comparison to the initial target values.*

Attribute	**Target**	**Pure**	**P6K1**	**P4K1**
Drug content	5.0 % w/w	No	No	No
	Meets BP specifications for content uniformity	Yes	Yes	Yes
Weight	Meets BP specifications for weight uniformity	No	Yes	No
Dimensions	Height	Yes	No	No
	Width	No	No	Yes
	Depth	Yes	No	No
	Thickness 1 mm	No	No	No
Dissolution profile	Zero order 5 days release, i.e. 20 % per day	No	No	No
Development potential		Possibly	Possibly	Possibly
Comments		For all formulations: Dissolution profile needs to be altered and extended Factors controlling the final drug loading need to be investigated (e.g. evaporation of water). Factors controlling the size and shape of the product need to be investigated (e.g. laser strength).		

6. 5 CONCLUSIONS

This Chapter used the novel approach of combining MRI scans and 3D-printing to design, manufacture and test customised ocular inserts with a matching customised flow-through dissolution cell. Overall, it can be concluded that this approach was successful, in that both the inserts and the dissolution cell were 3D-printed. Some issues were identified, such as the difference in the product's dimensions compared to the design specification, which are related to the control of the 3D-printer and choice of formulation, and which need to be overcome if this technology is to be developed further for pharmaceutical use.

Chapter 7

Overall Discussion, Conclusions and Future Work

Overall Discussion, Conclusions and Future Work

7.1 Concluding Remarks

The work in this thesis covers the general area of ocular formulation. In particular, it includes a study into some of the manufacture and characterisation issues related to "normal", compressed powder mini-tablets. Additionally, the novel approach of 3-D printing mini-tablets and customised ocular inserts was investigated, along with the development of matching customised dissolution cell. From the data presented in this thesis, this novel approach shows promising results although further work is required to fully exploit this technology.

The particle size distribution of the powders is significant for the manufacture of tablets generally and is especially important for mini-tablets. One initial finding for the manufacturing process was that the lowering cam on the tablet press needs to be removed when very small tablets are being produced. The lowering cam is a feature on the Riva Piccola press and exists to pull down the lower punch slightly after die filling to prevent loss of powder from the surface of the die during rotation. However, due to the design of the underside of the mini-tablet dies, this can result in loss of powder through the small gap between the die and the punch. It is recommended, therefore, that the design of very small tablet dies and the presence of a lowering cam on a tablet press are considered together when developing a manufacturing process for mini-tablets.

In **Chapter 3**, the effect of particle size on the physical characteristics of the compressed powder mini-tablets and the drug release profiles were investigated. Mini-tablets could be manufactured from both particle size distributions of all polymers studied, although PVP 90F gave very weak mini-tablets and would not be recommended as the bulk

component in a mini-tablet formulation. There were some subtleties in the properties of the mini-tablets between the two particle size distributions, such as the crushing strength results, but these could probably be manipulated by changing the compression parameters - in this study they were kept constant to reduce the number of experimental parameters. All mini-tablets showed similarity in the drug release profiles between the two sieve fractions except PEO 8M. A direct linear correlation between water sorption and drug release profiles was observed once dissolution had commenced. There were some subtle differences at the start of the process between formulations based on the different polymers, due to the time required for the polymer to show sufficient levels of hydration before the drug release started.

At least 85 % of drug was released within 9 hours of dissolution test except PEO 8M 125-180 µm, which showed a slower release profile. HPMC, PEG 6K and PVP 90F mini-tablets were best described either first order kinetics or Korsmeyer-Peppas, since the correlation values (r^2) were similar. Meanwhile, PEO 8M mini-tablets were best described by zero order kinetics. In conclusion, with the exception of PEG 8M, the particle size distribution of the bulk polymer did not seem to have a serious effect on the characteristics and behaviour of the mini-tablets, as long as it was kept within the overall range of 125 to 250 µm.

The work performed in this chapter examined the role of powder particle size in the behaviour of mini-tablet formulations, which has not been explored in the literature previously, and has highlighted some areas for consideration for other workers in this field in terms of the range of particle sizes recommended to be used for mini-tablet development. As the intention was not to fully define one ideal formulation and manufacturing process, but to compare how different polymers affected the behaviour of the mini-tablets, the specific compaction parameters used were kept constant throughout

the study to allow for easier comparison. This has left some room for some improvement in the production of specific formulations. ***Table 3.14*** summarised the development potential of the formulations studied. Particular areas of concern were the tablet weight and by extension the drug content within the mini-tablets, although it has to be noted that the majority of mini-tablet batches met the BP specifications for uniformity of weight and content (when assessed in comparison to the mean values rather than the target values). The dissolution profiles of the PEG 6K-based and PVP-based mini-tablets were zero-order as required, but the drug release did not extend for the intended 24 hours. It is possible that experimentation with different (higher) molecular weights of these polymers, or a suitable mixture of them, may prolong the release profile and this should be investigated further. The HPMC-based formulation probably needs additives in order to make it give a zero-order drug release profile.

Examining the correlation between water sorption using DVS and drug release is a novel approach to the characterisation of prolonged-release mini-tablets and has not been reported in the literature before. This may give some insights into the mechanisms of drug release from the various formulations of mini-tablets and is likely to be more representative of an *in vivo* situation as the mini-tablet is stationary in the DVS, as would be the case once inserted in to the ocular pocket. This technique may also be a useful approach to predicting drug release under different physiological conditions. For example, where a patient suffers from dry eye conditions or a reduced generation of tear fluid, there may be a prolonged initial hydration period with the HPMC-type mini-tablets with no drug release and possibly a slower release rate thereafter, whereas with the PEG-type formulations, it may be expected that the delay in the initiation of drug release would be shorter or even negligible, although a slower release profile may be seen due to the relative lack of tear fluid. This could easily be investigated using the DVS system as the humidity of the chamber is easily varied and controlled. Similarly, the correlation

between drug release and water sorption profiles may give insights into how a formulation may be manipulated to improve the dissolution rate, for example adding pore formers (such as NaCl) may be expected to change the behaviour of the HMPC-type formulations but not that of the PEG-type formulations.

Following on the irregular results obtained in Transition Temperature Microscopy (TTM) in **Chapter 3**, further study was undertaken in **Chapter 4** to assess the ability of TTM to cope with surfaces of varying smoothness. Mono-component mini-tablets of three different polymers (HPMC, PEG 6K and PVP 90F) with two sieve fractions (125-180 µm and 180-250 µm) were prepared by compression. PEG 6K mini-tablets had very smooth surfaces as seen on scanning electron microscopy (SEM) images, due to some surface melting during the compression process, itself due to the low melting point of PEG 6K (circa 60 °C). The TTM images for PEG 6K mini-tablets were consistent, with a sensible value for the melting point being observed. Mini-tablets of HPMC and PVP 90F showed rough surfaces and inconsistent TTM data, with a range of transition temperatures being displayed.

These inconsistent results are thought to be due to inconsistent contact of the probe with the sample's surface. If the probe makes contact directly with a particle, the results are reliable. If, however, the probe lands on the edge of a particle or in the gap between particles, the results are inconsistent. This is compounded by the software applying a variable analysis to such data. It is recommended that all probe deflection graphs are examined individually in a TTM map, rather than relying on the software to provide the interpretation of the results. It is also recommended that the surface of the sample be examined closely before a TTM mapping experiment is started, to ensure that measurement is viable. Unfortunately, with the current experimental set-up, it is not possible to generate a topology map of the sample before acquiring the transition map,

although this would be the obvious solution to this problem, allowing the probe to be positioned during on a particle rather than at its edge or in a gap between particles. This investigation was undertaken to attempt to explain the unexpected results from the initial TTM studies in **Chapter 2** and to continue the work conducted in the research group on the utility of the TTM technique for complex pharmaceutical systems. The overall aim of the development work on TTM is to allow it to be applied to sample surfaces, generating extra information that cannot easily be obtained from the analysis of whole samples, such as whether there is a surface excess of any specific component or in which physical state a material exists. This information is complementary to that obtained from the whole tablet, averaging studies and may help interpret dissolution and stability data.

Unconventional methods of manufacturing mini-tablets using 3D-printing techniques were studied in **Chapter 5**. The first attempt of manufacturing 3D-printed mini-tablets was by combining hot melt extrusion (HME) with fused deposition modelling (FDM) 3D-printing, as a polymer-based filament (acquired from the HME) is required for the FDM process to work. Attempts were made to extrude HPMC, PEG 6K, PEO 8M and PVP 90F based on their transition temperatures. However, only PEG 6K was able to be extruded. The attempts to integrate PEG 6K in other polymers as a plasticiser showed minimal success with PEO 8M, but no success with HPMC and PVP 90F. Due to unsuccessful extrusion of the desired polymers except PEG 6K, the idea of using extrudates to 3D print the mini-tablets cannot be executed and hence this approach was abandoned. This work was conducted with the intention of expanding the range of polymers demonstrated to be useable for FDM printing, as only a very limited range of polymers have been used in the past, most studies utilising PLGA as the carrier polymer due to its suitable melting and setting properties. The polymers studied in this work were all pharmaceutically acceptable and have been used for many years in a range of

pharmaceutical products. However, as demonstrated here, this was not possible with these specific polymers and further materials should be investigated for their potential.

The alternative approach of stereolithography (SLA) was investigated, whereby a photopolymerisation process is used to "cure" a monomer solution into a polymer which can take on and maintain a pre-designed 3D shape. The photopolymer used here was PEGDA, as it has been used successfully previously, albeit for non-pharmaceutical use. Initially, the use of a casting mould to provide the 3D shape was investigated. Mini-tablets moulds were designed using Tinkercad software based on the mini-tablets shape from **Chapter 3** and 3D-printed using an SLA printer and used to cast the mini-tablets. Unfortunately, this approach was not successfully, as the light-induced curing process for the mini-tablets resulted in the moulds and mini-tablets being glued together.

The photopolymer was then printed directly on the platform using SLA printer. The printing settings were optimised along with the photopolymer formulations. The final settings were set to print the mini-tablets directly on the platform without support and using flexible as material type at the highest resolution. The mini-tablets formulations were based on PEGDA as photopolymer, BAPO as photoinitiator and chloramphenicol as a model drug with addition of PEG 6K, PEG 4K and/or water. Based on the physical characterisations, the mini-tablets showed quite substantial differences in their physical dimensions and weight in which only three of the six batches passing the BP weight uniformity specification. The drug release profiles indicated that the mini-tablets better fit either first order kinetics or Korsmeyer-Peppas equation. In the latter case, the release exponent (n) indicated that the release profile was "anomalous". Addition of the low molecular weight PEGs as pore formers increased the drug dissolution rate from the 3D-printed mini-tablets. The linear relationship between water vapour uptake and drug

release suggests that movement of water and hydration of the mini-tablet is important in controlling the drug release pattern.

The implications of the work presented in **Chapter 5** are that the novel approach of using SLA 3D-printing of mini-tablets has potential, but there are several areas which require further investigation. ***Table 5.13*** summarises the performance of the 3D-printed mini-tablets against the pre-determined performance indicators. As can be seen, the product did not behave quite as intended. The variability in the physical characteristics of the 3D-printed mini-tablets such as weight, thickness and diameter, are concerning, as these will result in differences in drug loading and hence therapeutic effect, and also potentially the drug release profile. This variability was seen both between formulations and, more worryingly, within a batch of the same formulation. The most likely cause of this is the printing settings used, which are optimised for the use of commercial resins, rather than the photopolymer used here, so this is an area of obvious future work. However, even if the print settings are not completely optimised, it would be expected that the reproducibility of the product, especially within a batch, would be better than was observed. There is probably a lower "limit of production" in terms of the size of an article that can be printed reproducibly using the SLA 3D-printing technique and it is likely that the 2 mm diameter and thickness mini-tablets are below this lower limit of production leading to the variability seen in mini-tablet dimensions and hence weight and drug content. It is worth noting at this point that the vast majority of 3D-printing activities reported in both scientific studies and more artistic-based studies concern larger structures, and not small products the size of mini-tablets. There are no published studies (September 2016, Web of Science) on 3D-printing of mini-tablets. The factors governing the deposition of the material at each layering stage need to fully understood in order to assess whether this SLA method really is appropriate for the production of mini-tablets.

The drug release profile from the 3D-printed mini-tablets was interesting in that the "pure" formulation, i.e. the one that contained only the structuring polymer and not the pore formers, showed a maximum drug release of approximately 47 % and appeared to reach a plateau after about 6 hours. Conversely, the formulations with the pore formers showed much higher drug release, which was still ongoing when the experiment was terminated after 9 hours. The data for the "pure" formulation were unexpected in that full drug dissolution would be expected over time, even if the profile was very slow, rather than the obvious plateauing that was observed here. This suggests that the internal micro-structure of the mini-tablet is controlling the movement of the water into the mini-tablet and the drug (in solution) out of the mini-tablet. In these experiments, approximately half of the drug was being retained within the tablet matrix, suggesting that there was some impedance to the movement of the water into the mini-tablet. Factors such as pore size and pore tortuosity need to be investigated further to fully understand this process, and additional experimental investigations as to whether there is indeed a dry part of the mini-tablet during the dissolution process need to be undertaken.

A limited number of experimental variables were explored in this work and it would be useful in future to extend this work to include different pore formers and different drugs, if the same structuring polymer system is used and to try to improve the intra-batch reproducibility and to understand the factors that affect that process. One major issue is the use of the PEGDA / BAPO system. This was chosed deliberately as it has been used in the literature for SLA 3D-printing and this was a proof-of-principle investigation into whether it is possible to 3D-print mini-tablets. The concept was proven to be sound, in that recognisable mini-tablets were produced, which showed some pharmaceutical functionality. However, PEGDA is not biodegradable so would not be suitable for use in a real-life situation, as the mini-tablet ghost would need to be removed at the end of its

therapeutic life. An immediate need to take the field further is to develop a photo-polymerisable biodegradable polymer which can then be used to provide the mechanical construct for the mini-tablets. Similarly, the BAPO used here as a photo-polymerisation photo-initiator should be replaced with a more biocompatible compound. If a suitable polymer and initiator system can be developed, then there is great potential for the use of 3D-printed mini-tablets, both for ocular use and more general pharmaceutical use, if the reproducibility issues discussed earlier are overcome.

Chapter 6 extended the study from **Chapter 5** by developing customised ocular inserts based on an individual subject's eye. The dimensions of subject's eye were measured based on an MRI image supplied with permission by the subject. Inserts, similar to scleral shields, were designed using Tinkercad software based on these dimensions to specifically cover approximately 1/8th of the external surface of the eye. This use of an MRI scan to develop a customised 3D-printed pharmaceutical product is a really exciting development in personal therapy and has many potential applications other than the one explored here. To date, there have been no literature reports (September 2016, Web of Science) on using MRI scans in this manner. The actual process of analysing the MRI data files and generating the image to be printed is relatively straightforward and uses freely-available software.

Three formulations ("Pure", P6K1 and P4K1) from **Chapter 5** were 3D-printed into inserts using an SLA printer based on settings used in that chapter. ***Table 6.16*** summarises the performance of the 3D-printed ocular inserts against the pre-determined performance indicators. All the 3D-printed ocular inserts showed dimensions that were larger than the initial design with an inconsistent effect of varying the formulation on each of the parameters. Again, this is most probably because the 3D printer is designed for commercially-available resins rather than the photopolymer and formulations used here

and again suggests that this is an area for further work. As discussed before with the 3D-printed mini-tablets, this issue of consistency of printing requires further work before the technology can be fully developed towards a useful pharmaceutical product. Additionally, the biocompatibility of the polymer and initiator needs to be improved. However, if a biodegradable polymer is developed, this is likely to have an effect on the rate and extent of drug release and this would need extensive investigation.

Since the flow-through dissolution apparatus used in **Chapters 3** and **5** could not be used here due to the inserts' shape and size, a customised dissolution cell was designed based specifically on the subject's eye shape and individualised insert shape. This was relatively easy to design and 3D-print. Using the customised dissolution cell and the same control parameters as in **Chapter 3** and **5** (flow rate, dissolution fluid, etc.) the dissolution profile of the inserts was studied over 96 hours. During the dissolution process, it became apparent that the inserts swelled during the test. This swelling was compounded by the fact that the inserts were thicker than the design, so after swelling they contacted both surfaces of the dissolution cell resulting in unusually slow dissolution profiles being generated. The dissolution profiles of each inserts fit better with Korsmeyer-Peppas equation, with values of the exponent n suggesting "anomalous" diffusion. 3D-printed mini-tablets and inserts prepared from the P6K1 formulation showed identical profiles, whereas the inserts made from the "Pure" and P4K1 formulation showed slower profiles than the 3D-printed mini-tablet counterparts, but this is probably a consequence of the swelling behaviour of the inserts in the dissolution cell.

The use of the individual's MRI scan to develop firstly a personalised drug delivery device and secondly a matching personalised dissolution chamber is very exciting and has not been reported before. Typically, drug release profiles from solid ocular formulations are obtained using a flow-through cell similar to that described in the BP

2016 as Apparatus IV. The BP 2016 method, however, is a general method applicable to all solid products and the volume of the cell is in the order of 8 mL with a minimum flow rate of the dissolution fluid of 4 mL/minute. This is not very representative of the *in vivo* ocular situation, so systems based on Apparatus IV but with smaller chambers and lower flow rates have been used, such as the one used here in Chapters 3 and 5 for the mini-tablets (courtesy of Professor Steve Brocchini). Additionally, Hou et al. (2014) have developed a system for use with intra-vitreal inserts based on the volume of the vitreous humour and the vitreal fluid turnover rate in rabbits. Awwad et al. (2015) have proposed a novel two compartment system which also considers the flow of fluid from the posterior section of the eye to the anterior section and have suggested that this may be used to aid in initial drug pharmacokinetic studies. Such systems give a reasonably good first-line approach to the *in vivo* case for both anterior segment application of a small medicated product (e.g. mini-tablets) and in-dwelling posterior segment products (e.g. small inserts), as in both cases the pharmaceutical product is essentially stationary but surrounded by ocular fluid and with only limited fluid flow across its surface. However, none of these systems are suitable for assessing the drug release behaviour of larger in-dwelling products such as the ocular inserts resembling scleral shields produced in this work, as there are too large to fit into the dissolution chambers. Additionally, in the *in vivo* situation, these inserts would have limited room for movement or for fluid to flow across their surfaces, so simply covering the insert with an appropriate dissolution medium, as has been used in the past for the study of medicated contact lenses, would not be a good method. Hence, the 3D-printed personalised dissolution chamber used here is a step forward in the development of rationally-designed dissolution methodology. More work is obviously required to fully validate this approach, including examining a range of products of different dimensions, loaded with various drugs and varying the flow rate of the dissolution medium. Ultimately, comparisons to *in vivo* release studies would be

required to fully establish this type of system as a tool to be used in routine product development.

Overall, the work presented in **Chapter 6** suggest that there is great potential for the use of 3D-printed personalised pharmaceutical products. Here, ocular inserts were studied based on the MRI image of an individual subject, but the same approach could be taken for any device where personalisation would be useful. Additionally, the MRI images were used to design an individualised dissolution cell for use with the customised ocular inserts and constructed using 3D-printing techniques. Again, the same approach could be taken to the development of customised analytical equipment for all devices.

However, there are some drawbacks to the 3D-printing approaches. FDM requires a filament to be produced initially, which reduces the number and type of polymers that can be used to prepare the final product. The SLA approach is useful but requires much further study into the control systems used to ensure that the correct product is made reproducibly. Small changes in product dimensions may not be serious in some applications, but pharmaceutical products have very tight specifications and a requirement for high consistency, and hence the level of reproducibility seen here is not sufficient. PEGDA and BAPO are not the most pharmaceutically-acceptable photopolymer and photoinitiator, so an area of future work would be to develop more pharmaceutically-acceptable compounds.

Summarising as a whole the work presented in this thesis, it can be concluded that mini-tablets are more easily produced using conventional tabletting technology rather than the SLA 3D-printing technique, as the compressed powder mini-tablets were more uniform and reproducible than the 3D-printing ones. However, conventional tabletting has been used for several decades whereas 3D-printing is still in its infancy and there is a lot of

development work required. This thesis has highlighted that precision 3D-printing is challenging and that there may very well be a lower limit of size of product or detail that can be printed using the SLA technique. Even using the FDM technique to prepare the customised dissolution cell highlighted some issues in terms of how the molten material spread during deposition, leading to the same concerns about precision.

The most original part of the thesis was the use of the MRI head scan to allow the development of a personalised ocular insert (scleral shield) and matching customised dissolution chamber. This work demonstrated that this was indeed possible with easily available software and equipment and opens the way to future developments in this area.

7.2 Future Work

Based on the studies conducted in this thesis, some areas that would benefit from further investigation are listed below.

1. The TTM technique could be developed by investigating how the probe penetrates through gaps in a sample's surface and what effect this has on the results generated. The hypothesis behind this is that the results obtained in **Chapter 4** could be explained if the probe did not make adequate contact with the samples' surface. A TTM based on larger probes would be useful as well, as this may help in eliminating the variability inherent in using the nano probes on uneven surfaces, as it would be expected to be less sensitive to particle and gap dimensions. Here the rationale is that a larger probe would lead to more "averaging" of the measured results, albeit still on a sub-micron level. Ultimately, for TTM to be useful as an analytical technique, the results need to be reliable and accurate. If so, TTM can give a measure of the

drug and excipients distribution across the sample's surface. Taken together with the bulk analytical content uniformity and dissolution results, this could help understand a product's performance, particularly for systems which have a high surface area to volume ratio such as mini-tablets.

2. The quality of 3D-printed samples printed using the SLA printer needs to be improved, in terms of the closeness of the match to the original design and the reproducibility within and between batches. An intensive study on the 3D-printer settings for each individual formulation may help elucidate the level of control possible with the current commercial printers. Improving the understanding of the factors controlling the 3D-printing process will lead to better products and may help in the rational design of SLA 3D-printed products, e.g. by reducing the amount of fine detail needed on a product.

3. Further studies into how to control the drug release behaviour of the 3D-printed products with alternative additives would be useful. Ideally, a slower and more zero-order release rate would be required for treatment with a non-biodegradable drug delivery device, such as the mini-tablets. The hypothesis here is that the water-soluble pore formers will dissolve from the insoluble matrix, leading to ingress of water and hence drug dissolution. Varying the levels of these pore formers will allow different release rates to be designed.

4. A biodegradable drug delivery device would be ideal and would require the patient only to insert it and not to have to remove it at the end of its useful life. A biodegradable and biocompatible photo-polymer and photo-initiator would both be required to make a fully biodegradable drug delivery device. Such chemical, if

developed, would need to be tested for general and ocular toxicity before being used in a clinical situation.

5. An investigation into patient perspectives regarding ocular treatments in general and mini-tablets and inserts in particular would be required. Most of the published work on ocular therapy has considered the technical aspects, rather than the patient aspects, and it is well known that people are squeamish about their eyes, so may be less willing to accept novel ocular devices than novel systems intended for other routes of administration. Patients' opinions on the shape, size and feel of the samples as well as their general willing ness to use them would be very useful in taking this field further.

References

ABURAHMA, M. H. & MAHMOUD, A. A. 2011. Biodegradable Ocular Inserts for Sustained Delivery of Brimonidine Tartarate: Preparation and In Vitro/In Vivo Evaluation. *AAPS PharmSciTech,* 12**,** 1335-1347.

AGRAWAL, R. & NAVEEN, Y. 2011. Pharmaceutical Processing - A Review on Wet Granulation Technology. *International Journal Of Pharmaceutical Frontier Research,* 1**,** 65-83.

ALLEN, N. S. 1996. Photoinitiators for UV and visible curing of coatings: Mechanisms and properties. *Journal of Photochemistry and Photobiology A: Chemistry,* 100**,** 101-107.

ANASYSINSTUMENTS. *Therma-Lever™ Probes. Probes for sub-100nm Localized Thermal Analysis* [Online]. Available: http://www.anasysinstruments.com/nano-TAprobes.pdf.

ANDERSON, N. H., BAUER, M., BOUSSAC, N., KHAN-MALEK, R., MUNDEN, P. & SARDARO, M. 1998. An evaluation of fit factors and dissolution efficiency for the comparison of in vitro dissolution profiles. *Journal of pharmaceutical and biomedical analysis,* 17**,** 811-822.

ANDERSON, S. 2005. *Making Medicines: A Brief History of Pharmacy and Pharmaceuticals*, Pharmaceutical Press.

ARAYICI, Y. 2007. An approach for real world data modelling with the 3D terrestrial laser scanner for built environment. *Automation in Construction,* 16**,** 816-829.

ARıCı, M. K., ARıCı, D. S., TOPALKARA, A. & GÜLER, C. 2000. Adverse effects of topical antiglaucoma drugs on the ocular surface. *Clinical & Experimental Ophthalmology,* 28**,** 113-117.

AULTON, M. E. & TAYLOR, K. M. 2013. *Aulton's pharmaceutics: the design and manufacture of medicines*, Elsevier Health Sciences.

AWWAD, S., LOCKWOOD, A., BROCCHINI, S. & KHAW, P. T. 2015. The PK-Eye: A Novel In Vitro Ocular Flow Model for Use in Preclinical Drug Development. *Journal Of Pharmaceutical Sciences*, 104, 3330–3342.

BATTERBURY, M., BOWLING, B. & MURPHY, C. 2009. *Ophthalmology: An Illustrated Colour Text*, Elsevier/Churchill Livingstone.

BECHGAARD, H. & NIELSEN, G. H. 1978. Controlled-Release Multiple-Units and Single-Unit Doses a Literature Review. *Drug Development and Industrial Pharmacy,* 4**,** 53-67.

BEKERMAN, I., GOTTLIEB, P. & VAIMAN, M. 2014. Variations in Eyeball Diameters of the Healthy Adults. *Journal of Ophthalmology,* 2014**,** 5.

BLEY, O., SIEPMANN, J. & BODMEIER, R. 2009. Characterization of Moisture‐Protective Polymer Coatings Using Differential Scanning Calorimetry and Dynamic Vapor Sorption. *Journal of Pharmaceutical Sciences,* 98**,** 651-664.

BOZDAG, S., WEYENBERG, W., ADRIAENS, E., DHONDT, M. M., VERGOTE, V., VERVAET, C., DE PRIJCK, K., NELIS, H. J., DE SPIEGELEER, B., LUDWIG, A. & REMON, J. P. 2010. In vitro evaluation of gentamicin- and vancomycin-containing minitablets as a replacement for fortified eye drops. *Drug Dev Ind Pharm,* 36**,** 1259-70.

BRITISH PHARMACOPOIEA. 2015. *British Pharmacopoeia 2016*, Stationery Office.

BROWN, C. K., FRIEDEL, H. D., BARKER, A. R., BUHSE, L. F., KEITEL, S., CECIL, T. L., KRAEMER, J., MORRIS, J. M., REPPAS, C., STICKELMEYER, M. P., YOMOTA, C. & SHAH, V. P. 2011. FIP/AAPS joint workshop report: dissolution/in vitro release testing of novel/special dosage forms. *AAPS PharmSciTech,* 12**,** 782-94.

BUCKTON, G. & DARCY, P. 1995. The use of gravimetric studies to assess the degree of crystallinity of predominantly crystalline powders. *International Journal of Pharmaceutics,* 123**,** 265-271.

BÜHLER, V. 2008. *Kollidon® - Polyvinylpyrrolidone excipients for the pharmaceutical industry,* Ludwigshafen, Germany, BASF The Chemical Company.

ÇELIK, M. 2016. *Pharmaceutical Powder Compaction Technology, Second Edition*, CRC Press.

CEULEMANS, J., VERMEIRE, A., ADRIAENS, E., REMON, J. P. & LUDWIG, A. 2001. Evaluation of a mucoadhesive tablet for ocular use. *J Control Release,* 77**,** 333-44.

CHAN, V., ZORLUTUNA, P., JEONG, J. H., KONG, H. & BASHIR, R. 2010. Three-dimensional photopatterning of hydrogels using stereolithography for long-term cell encapsulation. *Lab on a Chip,* 10**,** 2062-2070.

CHEONG, L., HENG, P. & WONG, L. 1992. Relationship Between Polymer Viscosity and Drug Release from a Matrix System. *Pharmaceutical Research,* 9**,** 1510-1514.

CHOKSHI, R. & ZIA, H. 2004. Hot-melt extrusion technique: A review. *Iranian Journal of Pharmaceutical Research,* 3**,** 3-16.

CHUA, C. K., LEONG, K. F. & LIM, C. S. 2003. *Rapid Prototyping: Principles and Applications*, World Scientific.

COOPER, G. & NEGRUSZ, A. 2013. *Clarke's Analytical Forensic Toxicology*, Pharmaceutical Press.

COSTA, P. & SOUSA LOBO, J. M. 2001. Modeling and comparison of dissolution profiles. *European Journal of Pharmaceutical Sciences,* 13**,** 123-133.

CRAIG, D. Q. & READING, M. 2006. *Thermal analysis of pharmaceuticals*, CRC press.

CRAIG, D. Q. M. & NEWTON, J. M. 1991. Characterisation of polyethylene glycols using differential scanning calorimetry. *International Journal of Pharmaceutics,* 74**,** 33-41.

CRAIG, D. Q. M. 1990. Polyethyelene Glycols and Drug Release. *Drug Development and Industrial Pharmacy,* 16**,** 2501-2526.

CRAIG, D. Q., KETT, V. L., ANDREWS, C. S. & ROYALL, P. G. 2002. Pharmaceutical applications of micro-thermal analysis. *J Pharm Sci,* 91**,** 1201-13.

CRUMP, S. S. 1992. Apparatus and method for creating three-dimensional objects. Google Patents.

CUCHIARA, M. P., ALLEN, A. C. B., CHEN, T. M., MILLER, J. S. & WEST, J. L. 2010. Multilayer microfluidic PEGDA hydrogels. *Biomaterials,* 31**,** 5491-5497.

DAI, X., MOFFAT, J. G., WOOD, J. & READING, M. 2012. Thermal scanning probe microscopy in the development of pharmaceuticals. *Advanced Drug Delivery Reviews,* 64**,** 449-460.

DANA, S. F., NGUYEN, D.-V., KOCHHAR, J. S., LIU, X.-Y. & KANG, L. 2013. UV-curable pressure sensitive adhesive films: effects of biocompatible plasticizers on mechanical and adhesion properties. *Soft Matter,* 9**,** 6270-6281.

DANESH, A., CHEN, X., DAVIES, M. C., ROBERTS, C. J., SANDERS, G. H., TENDLER, S. J., WILLIAMS, P. M. & WILKINS, M. J. 2000. The discrimination of drug polymorphic forms from single crystals using atomic force microscopy. *Pharm Res,* 17**,** 887-90.

DE BRABANDER, C., VERVAET, C., FIERMANS, L. & REMON, J. P. 2000. Matrix mini-tablets based on starch/microcrystalline wax mixtures. *International Journal of Pharmaceutics,* 199**,** 195-203.

DI COLO, G., BURGALASSI, S., CHETONI, P., FIASCHI, M. P., ZAMBITO, Y. & SAETTONE, M. F. 2001. Gel-forming erodible inserts for ocular controlled delivery of ofloxacin. *International Journal of Pharmaceutics,* 215**,** 101-111.

DI COLO, G., ZAMBITO, Y., BURGALASSI, S., SERAFINI, A. & SAETTONE, M. F. 2002. Effect of chitosan on in vitro release and ocular delivery of ofloxacin from erodible inserts based on poly(ethylene oxide). *International Journal of Pharmaceutics,* 248**,** 115-122.

EGERTON, R. 2011. *Physical Principles of Electron Microscopy: An Introduction to TEM, SEM, and AEM*, Springer US.

EL-GAWAD, A. E.-G. H., SOLIMAN, O. A., BARKER, S. A. & GIRGIS, G. N. 2012. Formulation and Evaluation of Gel Forming Ocular Minitablets Containing Piroxicam. *British Journal of Pharmaceutical Research,* 2.

FEI, T., XIAODING, X., TING, D., MIAO, Y., XIANZHENG, Z. & JIAWEI, W. 2012. Fabrication of positively charged poly(ethylene glycol)-diacrylate hydrogel as a bone tissue engineering scaffold. *Biomedical Materials,* 7**,** 055009.

FINI, A., BERGAMANTE, V., CESCHEL, G. C., RONCHI, C. & DE MORAES, C. A. F. 2008. Fast dispersible/slow releasing ibuprofen tablets. *European Journal of Pharmaceutics and Biopharmaceutics,* 69**,** 335-341.

FOLLONIER, N. & DOELKER, E. 1992. Biopharmaceutical comparison of oral multiple-

unit and single-unit sustained-release dosage forms. *STP Pharma Sciences,* 2**,** 141-155.

FORMLABS. 2016. Available: http://formlabs.com/support/software/install-preform-software/.

FOTAKI, N. 2011. Flow-Through cell apparatus (usp apparatus 4): operation and features. *Dissolution Technol,* 18**,** 46-49.

FOTAKI, N., BROWN, W., KOCHLING, J., CHOKSHI, H., MIAO, H., TANG, K. & GRAY, V. 2013. Rationale for selection of dissolution media: three case studies. *Dissolution Technologies,* 20**,** 6-14.

FUJISHIMA, H., TODA, I., YAMADA, M., SATO, N. & TSUBOTA, K. 1996. Corneal temperature in patients with dry eye evaluated by infrared radiation thermometry. *The British Journal of Ophthalmology,* 80**,** 29-32.

GAISFORD, S., KETT, V. & HAINES, P. 2016. *Principles of Thermal Analysis and Calorimetry: 2nd Edition*, Royal Society of Chemistry.

GHEBRE-SELASSIE, I. 1994. *Multiparticulate Oral Drug Delivery*, Taylor & Francis.

GILL, P., SAUERBRUNN, S. & READING, M. 1993. Modulated differential scanning calorimetry. *Journal of thermal analysis,* 40**,** 931-939.

GOYANES, A., ROBLES MARTINEZ, P., BUANZ, A., BASIT, A. W. & GAISFORD, S. 2015. Effect of geometry on drug release from 3D printed tablets. *International Journal of Pharmaceutics,* 494**,** 657-663.

HAHN, M. S., MILLER, J. S. & WEST, J. L. 2006a. Three-Dimensional Biochemical and Biomechanical Patterning of Hydrogels for Guiding Cell Behavior. *Advanced Materials,* 18**,** 2679-2684.

HAHN, M. S., TAITE, L. J., MOON, J. J., ROWLAND, M. C., RUFFINO, K. A. & WEST, J. L. 2006b. Photolithographic patterning of polyethylene glycol hydrogels. *Biomaterials,* 27**,** 2519-2524.

HAMMICHE, A., READING, M., POLLOCK, H., SONG, M. & HOURSTON, D. 1996. Localized thermal analysis using a miniaturized resistive probe. *Review of Scientific*

Instruments, 67**,** 4268-4274.

HERRMANN, K.-H., GÄRTNER, C., GÜLLMAR, D., KRÄMER, M. & REICHENBACH, J. R. 3D printing of MRI compatible components: Why every MRI research group should have a low-budget 3D printer. *Medical Engineering and Physics,* 36**,** 1373-1380.

HOCKADAY, L. A., KANG, K. H., COLANGELO, N. W., CHEUNG, P. Y. C., DUAN, B., MALONE, E., WU, J., GIRARDI, L. N., BONASSAR, L. J., LIPSON, H., CHU, C. C. & BUTCHER, J. T. 2012. Rapid 3D printing of anatomically accurate and mechanically heterogeneous aortic valve hydrogel scaffolds. *Biofabrication,* 4**,** 035005.

HÖLZER, A. W. & SJÖGREN, J. 1979. Evaluation of sodium stearyl fumarate as a tablet lubricant. *International Journal of Pharmaceutics,* 2**,** 145-153.

HOU H, NIETO A, MA F, FREEMAN WR, SAILOR MJ, CHENG L. 2014. Tunable sustained intravitreal drug delivery system for daunorubicin using oxidized porous silicon. *J Control Release*, 178, 46–54.

HUBBARD, A. T. 1995. *The Handbook of Surface Imaging and Visualization*, Taylor & Francis.

HULL, C. W. 1986. Apparatus for production of three-dimensional objects by stereolithography. Google Patents.

HUMMERT, C., LUCKAS, B. & SIEBENLIST, H. 1995. Determination of chloramphenicol in animal tissue using high-performance liquid chromatography with a column-switching system and ultraviolet detection. *Journal of Chromatography B: Biomedical Sciences and Applications,* 668**,** 53-58.

INVESALIUS. 2016. Available: http://svn.softwarepublico.gov.br/trac/invesalius.

JAMES, B. 2012. *Lecture Notes: Ophthalmology*, Wiley.

JONATHAN, G. & KARIM, A. 2016. 3D printing in pharmaceutics: A new tool for designing customized drug delivery systems. *International Journal of Pharmaceutics,* 499**,** 376-394.

KENNING, N. S., FICEK, B. A., HOPPE, C. C. & SCRANTON, A. B. 2008. Spatial and temporal evolution of the photoinitiation rate for thick polymer systems illuminated by

polychromatic light: selection of efficient photoinitiators for LED or mercury lamps. *Polymer International,* 57**,** 1134-1140.

KHALED, S. A., BURLEY, J. C., ALEXANDER, M. R. & ROBERTS, C. J. 2014. Desktop 3D printing of controlled release pharmaceutical bilayer tablets. *International Journal of Pharmaceutics,* 461**,** 105-111.

KHAN, F., LI, M. & SCHLINDWEIN, W. 2013. Comparison of In Vitro Dissolution Tests for Commercially Available Aspirin Tablets. *Dissolution Technologies,* 20**,** 48-58.

KJOLLER, K., ROSE, J. & SAHAGIAN, K. 2010. Transition Temperature Microscopy: Nanoscale Thermal Analysis for Micron- and Submicron-Scale Devices. Available: http://www.americanlaboratory.com/913-Technical-Articles/598-Transition-Temperature-Microscopy-Nanoscale-Thermal-Analysis-for-Micron-and-Submicron-Scale-Devices/ [Accessed 28 May 2016].

KJOLLER, K., SAHAGIAN, K., GOTTHARD, D., KURTZ, A., PRATER, C., SHETTY, R. & READING, M. 2012. Transition temperature microscopy. Google Patents.

KOLTER, K., KARL, M. & GRYCZKE, A. 2012. *Hot-melt extrusion with BASF pharma polymers,* Ludwigshafen, Germany, BASF SE.

KORSMEYER, R. W., GURNY, R., DOELKER, E., BURI, P. & PEPPAS, N. A. 1983. Mechanisms of solute release from porous hydrophilic polymers. *International Journal of Pharmaceutics,* 15**,** 25-35.

LAFERRIERE, C. I. & MARKS, M. I. 1982. Chloramphenicol: properties and clinical use. *Pediatr Infect Dis,* 1**,** 257-64.

LEIBOWITZ , H. M. 2000. The Red Eye. *New England Journal of Medicine,* 343**,** 345-351.

LENNARTZ, P. & MIELCK, J. B. 1998. Minitabletting: improving the compactibility of paracetamol powder mixtures. *International Journal of Pharmaceutics,* 173**,** 75-85.

LOBOVSKY, M., FERGUSON, I., RECHES, Y. & LIVINGSTON, J. 2014. 3d printer with self-leveling platform. Google Patents.

LOPES, C. M., LOBO, J. M. S., PINTO, J. F. & COSTA, P. 2006. Compressed mini-tablets

as a biphasic delivery system. *International Journal of Pharmaceutics,* 323**,** 93-100.

LUDWIG, A. & VAN OOTEGHEM, M. 1992. Influence of viscolysers on the residence of ophthalmic solutions evaluated by slit lamp fluorophotometry. *STP Pharma Sciences,* 2**,** 81-87.

LUO, X. P., SILIKAS, N., ALLAF, M., WILSON, N. H. F. & WATTS, D. C. 2001. AFM and SEM study of the effects of etching on IPS-Empress 2TM dental ceramic. *Surface Science,* 491**,** 388-394.

MA, D., DJEMAI, A., GENDRON, C. M., XI, H., SMITH, M., KOGAN, J. & LI, L. 2013. Development of a HPMC-based controlled release formulation with hot melt extrusion (HME). *Drug Dev Ind Pharm,* 39**,** 1070-83.

MADAN, S. & MADAN, S. 2012. Hot melt extrusion and its pharmaceutical applications. *Asian Journal of Pharmaceutical Sciences,* 7**,** 123-133.

MANIRUZZAMAN, M., BOATENG, J. S., SNOWDEN, M. J. & DOUROUMIS, D. 2012. A review of hot-melt extrusion: Process technology to pharmaceutical products. *ISRN Pharmaceutics,* 2012**,** 1-9.

MARQUES, M. R. C., LOEBENBERG, R. & ALMUKAINZI, M. 2011. Simulated biological fluids with possible application in dissolution testing. *Dissolution Technologies,* 18**,** 15-28.

MCPHILLIPS, H., CRAIG, D. Q., ROYALL, P. G. & HILL, V. L. 1999. Characterisation of the glass transition of HPMC using modulated temperature differential scanning calorimetry. *Int J Pharm,* 180**,** 83-90.

MOFFAT, J. G., QI, S. & CRAIG, D. Q. 2014. Spatial characterization of hot melt extruded dispersion systems using thermal atomic force microscopy methods: the effects of processing parameters on phase separation. *Pharm Res,* 31**,** 1744-52.

MOORE, J. W. & FLANNER, H. H. 1996. Mathematical comparison of dissolution profiles. *Pharma Tech,* 20**,** 64-74.

MORTAZAVI, S. A., JAFFARIAZAR, Z. & DAMERCHELI, E. 2010. Formulation and *In-Vitro* Evaluation of Ocular Ciprofloxacin-Containing Minitablets Prepared with Different

Combinations of Carbopol 974P and Various Cellulose Derivatives. *Iranian Journal of Pharmaceutical Research,* 9**,** 107-114.

MORTAZAVI, S. A., JAFFARIAZAR, Z. & DAMERCHELI, E. 2010. Formulation and *In-Vitro* Evaluation of Ocular Ciprofloxacin-Containing Minitablets Prepared with Different Combinations of Carbopol 974P and Various Cellulose Derivatives. *Iranian Journal of Pharmaceutical Research,* 9**,** 107-114.

MUNDAY, D. L. 1994. A Comparison of the Dissolution Characteristics of Theophylline from Film Coated Granules and Mini-Tablets. *Drug Development and Industrial Pharmacy,* 20**,** 2369-2379.

NEMIR, S., HAYENGA, H. N. & WEST, J. L. 2010. PEGDA hydrogels with patterned elasticity: Novel tools for the study of cell response to substrate rigidity. *Biotechnology and Bioengineering,* 105**,** 636-644.

NETFABB. 2016. Available: http://www.netfabb.com/ [Accessed 01 May 2016].

NICULA, R. 2002. *Introduction to differential scanning calorimetry,* Rostock University.

NOMOTO, R., UCHIDA, K. & HIRASAWA, T. 1994. Effect of Light Intensity on Polymerization of Light-cured Composite Resins. *Dental Materials Journal,* 13**,** 198-205,272.

NUNN, T. & WILLIAMS, J. 2005. Formulation of medicines for children. *Br J Clin Pharmacol,* 59**,** 674-6.

OLMEDILLA, B., GRANADO, F., BLANCO, I. & VAQUERO, M. 2003. Lutein, but not α-tocopherol, supplementation improves visual function in patients with age-related cataracts: a 2-y double-blind, placebo-controlled pilot study. *Nutrition,* 19**,** 21-24.

OVSIANIKOV, A., GRUENE, M., PFLAUM, M., KOCH, L., MAIORANA, F., WILHELMI, M., HAVERICH, A. & CHICHKOV, B. 2010. Laser printing of cells into 3D scaffolds. *Biofabrication,* 2**,** 014104.

OWEN, T. 2000. *Fundamentals of Modern UV-visible Spectroscopy: Primer*, Agilent Technologies.

PATEL, A., CHOLKAR, K., AGRAHARI, V. & MITRA, A. K. 2013a. Ocular drug delivery systems: An overview. *World journal of pharmacology,* 2**,** 47-64.

PATEL, A., SAHU, D., DASHORA, A., GARG, R., AGRAVAL, P., PATEL, P., PATEL, P. & PATEL, G. 2013b. A review of hot melt extrusion technique. *international Journal of Innovative Research in Science, Engeenering and Technology,* 2**,** 2194-2198.

PATEL, P. S., RAVAL, J. P. & PATEL, H. V. 2010. Review on the pharmaceutical applications of hot melt extruder. *Asian Journal of Pharmaceutical and Clinical Research,* 3**,** 80-83.

PERKAMPUS, H. H., GRINTER, H. C. & THRELFALL, T. L. 2013. *UV-VIS Spectroscopy and Its Applications*, Springer Berlin Heidelberg.

PIJLS, R. T., CRUYSBERG, L. P. J., NUIJTS, R. M. M. A., DIAS, A. A. & KOOLE, L. H. 2007. Capacity and tolerance of a new device for ocular drug delivery. *International Journal of Pharmaceutics,* 341**,** 152-161.

PIJLS, R. T., SONDERKAMP, T., DAUBE, G. W., KREBBER, R., HANSSEN, H. H. L., NUIJTS, R. M. M. A. & KOOLE, L. H. 2005. Studies on a new device for drug delivery to the eye. *European Journal of Pharmaceutics and Biopharmaceutics,* 59**,** 283-288.

PINTO, J. F., WUNDER, K. F. & OKOLOEKWE, A. 2004. Evaluation of the potential use of poly(ethylene oxide) as tablet- and extrudate-forming material. *AAPS PharmSci,* 6**,** 17-26.

PIVSA-ART, W., FUJII, K., NOMURA, K., ASO, Y., OHARA, H. & YAMANE, H. 2016. The effect of poly(ethylene glycol) as plasticizer in blends of poly(lactic acid) and poly(butylene succinate). *Journal of Applied Polymer Science,* 133**,** n/a-n/a.

PRODDUTURI, S., MANEK, R. V., KOLLING, W. M., STODGHILL, S. P. & REPKA, M. A. 2005. Solid-state stability and characterization of hot-melt extruded poly(ethylene oxide) films. *Journal of Pharmaceutical Sciences,* 94**,** 2232-2245.

PUBCHEM. 2016. *National Center for Biotechnology Information* [Online]. PubChem Compound Database. Available: https://pubchem.ncbi.nlm.nih.gov/compound/5959 [Accessed 15 April 2016].

QI, S., MOFFAT, J. G. & YANG, Z. 2013. Early Stage Phase Separation in Pharmaceutical Solid Dispersion Thin Films under High Humidity: Improved Spatial Understanding Using Probe-Based Thermal and Spectroscopic Nanocharacterization Methods. *Molecular Pharmaceutics,* 10**,** 918-930.

RAUWENDAAL, C. 2001. *Polymer Extrusion*, Hanser.

RAWAS-QALAJI, M. & WILLIAMS, C. A. 2012. Advances in ocular drug delivery. *Curr Eye Res,* 37**,** 345-56.

READING, M., LUGET, A. & WILSON, R. 1994. Modulated differential scanning calorimetry. *Thermochimica Acta,* 238**,** 295-307.

REPKA, M. A., BATTU, S. K., UPADHYE, S. B., THUMMA, S., CROWLEY, M. M., ZHANG, F., MARTIN, C. & MCGINITY, J. W. 2007. Pharmaceutical Applications of Hot-Melt Extrusion: Part II. *Drug Development and Industrial Pharmacy,* 33**,** 1043-1057.

REPKA, M. A., MAJUMDAR, S., BATTU, S. K., SRIRANGAM, R. & UPADHYE, S. B. 2008. Applications of hot-melt extrusion for drug delivery. *Expert Opin Drug Deliv,* 5**,** 1357-1376.

RITGER, P. L. & PEPPAS, N. A. 1987. A simple equation for description of solute release II. Fickian and anomalous release from swellable devices. *Journal of Controlled Release,* 5**,** 37-42.

RODRÍGUEZ-LLAMAZARES, S., RIVAS, B. L., PÉREZ, M. & PERRIN-SARAZIN, F. 2012. Poly(ethylene glycol) as a compatibilizer and plasticizer of poly(lactic acid)/clay nanocomposites. *High Performance Polymers,* 24**,** 254-261.

ROWE, R. C., SHESKEY, P. J., QUINN, M. E. & ASSOCIATION, A. P. 2009. *Handbook of Pharmaceutical Excipients*, Pharmaceutical Press.

ROYALL, P. G., KETT, V. L., ANDREWS, C. S. & CRAIG, D. Q. M. 2001. Identification of Crystalline and Amorphous Regions in Low Molecular Weight Materials Using

Microthermal Analysis. *The Journal of Physical Chemistry B,* 105**,** 7021-7026.

SAETTONE, M. F. & SALMINEN, L. 1995. Ocular inserts for topical delivery. *Advanced Drug Delivery Reviews,* 16**,** 95-106.

SANDLER, N., SALMELA, I., FALLARERO, A., ROSLING, A., KHAJEHEIAN, M., KOLAKOVIC, R., GENINA, N., NYMAN, J. & VUORELA, P. 2014. Towards fabrication of 3D printed medical devices to prevent biofilm formation. *International Journal of Pharmaceutics,* 459**,** 62-64.

SANDLER, N., SALMELA, I., FALLARERO, A., ROSLING, A., KHAJEHEIAN, M., KOLAKOVIC, R., GENINA, N., NYMAN, J. & VUORELA, P. 2014. Towards fabrication of 3D printed medical devices to prevent biofilm formation. *International Journal of Pharmaceutics,* 459**,** 62-64.

SELTMAN, H. J. 2015. *Experimental design and analysis,* Pennsylvania, USA, Carnegie Mellon University.

SHEOKAND, S., MODI, S. R. & BANSAL, A. K. 2014. Dynamic Vapor Sorption as a Tool for Characterization and Quantification of Amorphous Content in Predominantly Crystalline Materials. *Journal of Pharmaceutical Sciences,* 103**,** 3364-3376.

SIEPMANN, J. & PEPPAS, N. A. 2001. Modeling of drug release from delivery systems based on hydroxypropyl methylcellulose (HPMC). *Advanced Drug Delivery Reviews,* 48**,** 139-157.

SINTZEL, M. B., BERNATCHEZ, S. F., TABATABAY, C. & GURNY, R. 1996. Biomaterials in ophthalmic drug delivery. *European journal of pharmaceutics and biopharmaceutics,* 42**,** 358-374.

SKOOG, D. A., HOLLER, F. J. & CROUCH, S. R. 2007. *Principles of Instrumental Analysis*, Thomson Brooks/Cole.

SMITH, B. T. 2015. *Remington Education: Physical Pharmacy*, Pharmaceutical Press.

STOLTENBERG, I. & BREITKREUTZ, J. 2011. Orally disintegrating mini-tablets (ODMTs)--a novel solid oral dosage form for paediatric use. *Eur J Pharm Biopharm,* 78**,** 462-9.

SUNGTHONGJEEN, S., PUTTIPIPATKHACHORN, S., PAERATAKUL, O., DASHEVSKY, A. & BODMEIER, R. 2004. Development of pulsatile release tablets with swelling and rupturable layers. *Journal of Controlled Release,* 95**,** 147-159.

SZCZERBA, R. J. 2015. FDA Approves First 3-D Printed Drug. Available: http://www.forbes.com/sites/robertszczerba/2015/08/04/fda-approves-first-3-d-printed-drug/#6e4dfa992c8a [Accessed 29 May 2016].

THOMSON, S. A., TULEU, C., WONG, I. C., KEADY, S., PITT, K. G. & SUTCLIFFE, A. G. 2009. Minitablets: new modality to deliver medicines to preschool-aged children. *Pediatrics,* 123**,** e235-8.

THOORENS, G., KRIER, F., LECLERCQ, B., CARLIN, B. & EVRARD, B. 2014. Microcrystalline cellulose, a direct compression binder in a quality by design environment—A review. *International Journal of Pharmaceutics,* 473**,** 64-72.

TINKERCAD. 2015. Available: https://www.tinkercad.com/.

TISSEN, C., WOERTZ, K., BREITKREUTZ, J. & KLEINEBUDDE, P. 2011. Development of mini-tablets with 1mm and 2mm diameter. *Int J Pharm,* 416**,** 164-70.

TÖRMÄLÄ, P. 1974. Determination of glass transition temperature of poly(ethylene glycol) by spin probe technique. *European Polymer Journal,* 10**,** 519-521.

TUERK, J., REINDERS, M., DREYER, D., KIFFMEYER, T. K., SCHMIDT, K. G. & KUSS, H.-M. 2006. Analysis of antibiotics in urine and wipe samples from environmental and biological monitoring—Comparison of HPLC with UV-, single MS- and tandem MS-detection. *Journal of Chromatography B,* 831**,** 72-80.

VERHOEVEN, J., SCHAEFFER, R., BOUWSTRA, J. A. & JUNGINGER, H. E. 1989. The physico-chemical characterization of poly (2-hydroxyethyl methacrylate-co-methacrylic acid: 2. Effect of water, PEG 400 and PEG 6000 on the glass transition temperature.

Polymer, 30**,** 1946-1950.

WANG, J., GOYANES, A., GAISFORD, S. & BASIT, A. W. 2016. Stereolithographic (SLA) 3D printing of oral modified-release dosage forms. *International Journal of Pharmaceutics,* 503**,** 207-212.

WATSON, D. G. 2012. *Pharmaceutical Analysis: A Textbook for Pharmacy Students and Pharmaceutical Chemists*, Elsevier Health Sciences UK.

WEYENBERG, W., BOZDAG, S., FOREMAN, P., REMON, J. P. & LUDWIG, A. 2006. Characterization and in vivo evaluation of ocular minitablets prepared with different bioadhesive Carbopol-starch components. *Eur J Pharm Biopharm,* 62**,** 202-9.

WEYENBERG, W., VERMEIRE, A., D'HAESE, E., VANHAELEWYN, G., KESTELYN, P., CALLENS, F., NELIS, H. J., REMON, J. P. & LUDWIG, A. 2004a. Effect of different sterilisation methods on the properties of bioadhesive powders and ocular minitablets, and clinical evaluation. *Eur J Pharm Sci,* 23**,** 77-87.

WEYENBERG, W., VERMEIRE, A., DHONDT, M. M., ADRIAENS, E., KESTELYN, P., REMON, J. P. & LUDWIG, A. 2004b. Ocular bioerodible minitablets as strategy for the management of microbial keratitis. *Invest Ophthalmol Vis Sci,* 45**,** 3229-33.

WEYENBERG, W., VERMEIRE, A., REMON, J. P. & LUDWIG, A. 2003. Characterization and in vivo evaluation of ocular bioadhesive minitablets compressed at different forces. *J Control Release,* 89**,** 329-40.

WEYENBERG, W., VERMEIRE, A., VANDERVOORT, J., REMON, J. P. & LUDWIG, A. 2005. Effects of roller compaction settings on the preparation of bioadhesive granules and ocular minitablets. *Eur J Pharm Biopharm,* 59**,** 527-36.

WU, C.-Y. & SEVILLE, J. P. K. 2009. A comparative study of compaction properties of binary and bilayer tablets. *Powder Technology,* 189**,** 285-294.

YEE, C. S. 2013. *The Development of PVP-based Solid Dispersions using Hot Melt Extrusion for the Preparation of Immediate Release Formulations.* Degree of Doctor Philosophy, University of East Anglia.

ZHANG, J., BUNKER, M., CHEN, X., PARKER, A. P., PATEL, N. & ROBERTS, C. J. 2009. Nanoscale thermal analysis of pharmaceutical solid dispersions. *International Journal of Pharmaceutics,* 380**,** 170-173.